CARDIFF UNIVERSITY

PRIFYSGOL CAERDY�

पद्माक्षी सरस्वती बालाजी प्रसन्न

DEDICATED TO MY GRANDFATHER
THE LATE MR WAMAN RAO DESHMUKH
AND
DESHMUKH FAMILY

UMI Number: U584903

UMI

Dissertation Publishing

ProQuest

Voltage Harmonics Analysis and Efficiency of Three-Phase Induction Motor with change in Coil Pitch of the Stator Winding

By

Ram Raghotham Rao Deshmukh

A thesis submitted to Cardiff University in candidature for the degree of Doctor of Philosophy

October, 2006

Wolfson Centre for Magnetics

Cardiff School of Engineering

Cardiff University

DECLARATION

This work has not previously been accepted in substance for any degree and is not being concurrently submitted in candidature for any degree.

Signed.. (candidate)

Date...

STATEMENT 1

This thesis is the result of my own investigations, except where otherwise stated.

Other sources are acknowledged by footnotes giving explicit references. A bibliography is appended.

Signed.. (candidate)

Date...

STATEMENT 2

I hereby give consent for my thesis, if accepted, to be available for photocopying and inter-library loan, and for the title and summary to be available to outside organisation.

Signed.. (candidate)

Date...

NB: *Candidates on whose behalf a bar on access has been approved by the University, should use the following version of Statement 2.*

I hereby give consent for my thesis, if accepted, to be available for photocopying and for inter-library loans **after expiry of a bar on access approved by the University of Wales on the special recommendation of the Constituent Institution/University concerned.**

Signed.. (candidate)

Date...

ACKNOWLEDGEMENTS

SUMMARY

Variable speed drives employing induction motors have been widely used in industry for decades. Today there is a continually increasing demand for more precise and flexible speed control usually with close attention to energy efficiency. The inverter is used because of its reliability, flexibility and relatively low cost. However its output a.c. voltage is not sinusoidal so the core losses in the induction motors consequently increase. This research is centred on the design and testing of the stator winding configuration of three phase induction motors with various coil pitches and measure the dynamic performance under sinusoidal and PWM supplies.

Measurements were carried out to determine the behavior of harmonic losses and the efficiency of four identical three-phase 746 W induction motors with stator coil pitches of 180°, 160°, 140° and 120°. The motors were fed from either a three-phase inverter or a three-phase sinusoidal voltage supply. The switching frequency was varied from 4 kHz to 16 kHz and the modulation frequency was varied between 30 Hz to 60 Hz. Simulations were carried out using OPERA 2D software under sinusoidal voltage supply.

The phenomenon of chording by $1/n^{th}$ of pole pitch to suppress the nth harmonic was particularly followed by motors with 120° and 160° coil pitches under sinusoidal voltage supply. This phenomenon was also followed by 120°, 140° and 160° coil pitch motors under PWM voltage supply at all the switching frequencies and modulation frequencies. The motor with 120° coil pitch showed a drastical increase in the lower order voltage harmonic components with simulation under sinusoidal supply when compared to full pitch motor.

The total voltage harmonic distortion due to the third, fifth and ninth harmonics was less for the motor with 120° coil pitch under PWM voltage at higher switching frequencies and under over modulation condition. The efficiency of the same motor was higher at full load and over loads under all the switching frequencies and modulation frequencies. The measurement results and discussion enable motor manufacturers to consider 120° coil pitch motor under PWM voltage supply and 160° coil pitch motor under sinusoidal voltage supply for the 746 W induction motors as

the increase in the efficiencies were 12% and 5% respectively when compared to full pitch motor.

CONTENTS

CHAPTER 1

AIMS OF THE INVESTIGATION

Electric motors are major users of electricity in industrial plant and commercial premises throughout the world. In industrialised countries about one-third of all primary energy is converted into electricity. Of this, about two-third is converted back into mechanical energy by motors of different types. The largest part is absorbed by a.c. induction motors in the power range 1-100 kW. Motor efficiency is therefore an important economic factor. By adopting energy efficient systems, the UK could save more than 24 billion kWh each year [1.1]. In environmental terms, this equates to a 12 million tonne (100 million tonne in Europe) reduction in CO_2 emissions and a total environmental saving to society of £480 millions per year in the UK [1.2]. To improve motor efficiency, engineers focus on five types of losses: stator resistance loss, rotor resistance loss, core loss (iron loss), friction and windage loss, and stray load loss [1.3].

Induction motor losses can be reduced by changing the design of the motor; changing the shape of the stator and rotor slot, number of stator slots, material of the stator and rotor, thickness of lamination etc. One of the important methods that can also have major impact of the losses is the air-gap flux density. This can be improved by changing the stator winding design.

The winding of a motor conveys electrical energy to the stator, and is concerned with emf induction and the development of magneto-motive force (mmf). When excited the phase winding combination should produce an mmf that is, as far as possible, sinusoidally distributed in the air gap. Rotating machines are considered as a source of voltage harmonics [1.4, 1.5] because the winding are embedded in slots and the mmf can never be considered sinusoidal. In most drives, pulse width modulation (PWM) inverters are employed to supply the voltage to the induction motors and this supply contains various voltage harmonics. Despite the number of such drives in operation,

the harmonic loss dependence on stator winding designs and change in efficiency is not well understood.

Lap, wave, and concentric coils constructions are employed for polyphase induction motor. The concentric winding is most frequently used in stators, while the wave winding is usually preferred for the rotors of wound-rotor machines. The lap winding is not used frequently as it cannot be done with automatic winding machines.

This project is concerned with the measurement of lower order voltage harmonics and efficiency of the 746 W, three-phase induction motor. The purpose is to identify the shortcomings of the conventional winding design under PWM voltage supply and to design the stator windings by short pitching of the stator coils (lap windings) to lower the losses due to harmonics so as to increase the efficiency of the motor.

The main aims of the investigation can be summarised as follows:

a) To study the lower order voltage harmonics of the short chorded three-phase induction motor under sinusoidal voltage supply by 2D simulation.

b) To design three induction motor with different coil pitches of the stator windings.

c) To study the lower order voltage harmonics and efficiency of the short-chorded three-phase induction motor under sinusoidal voltage supply experimentally.

d) To characterise the influence of short pitching of the stator coils of induction motors on the lower order voltage harmonics and the efficiency under PWM voltage supply with various switching frequencies and modulation frequencies.

REFERENCES FOR CHAPTER 1

[1.1] "Energy Efficient Motor Driven Systems-Report", The Motor Challenge Programme, European Copper Institute, Belgium, April 2004

[1.2] M. Spear, "Efficient Savings-Report", Process Engineering, Environment Energy Efficiency Magazine, June 2004

[1.3] R.E. Hanitsch, "Novel soft and hard magnetic material improve energy efficiency", ELECTROMOTION 7, pp. 81-88, 2000

[1.4] A. J Moses, J. Leicht, F. Anayi, "Analysis of magnetic properties of electrical steels in stator cores of inverter fed motors", 'Proc. of 7th Int. workshop on 1 & 2 dimensional magnetic measurement and testing, Ludenschied, Germany, PTB-E-81, pp. 37-45, 2003

[1.5] W.M. Grady, W.H. Kersting, D. Osborn, N.R. Prasad, S.O. Ranade, H.A. Smolleck, "Power Factor Correction and Power System Harmonics", Spring Short Course Series on Electric Power System Harmonics, New Mexico, USA, 1993

CHAPTER 2

THE FUNDAMENTALS OF INDUCTION MOTORS

2.1 General introduction

Three-phase induction motors are widely used in industry. About 95% of all drive sources today rely on induction motors. They are available in a wide range of power rating, from a fraction of watts to tens of megawatts. Squirrel cage induction motors are most popular. This is because there is only an insulated winding in the stator and the rotor winding simply is made up of solid and cast high conductivity bars. For this reason induction motor are very sturdy and their reliability is very high.

The history of the induction motor is most interesting. In 1888 the rotating magnetic field, as it is understood today, was discovered independently by Ferraris and Tesla by using two coils set at right angles and supplied with two identical sinusoidal currents displaced 90° in time. At that time, as mentioned by Chapman [2.1] and Hawary [2.2], a paper was presented by Tesla in which the basic principle of a two-phase motor was described.

115 years ago, as mentioned by Hawary [2.2] and Say [2.3], Dobrowolsky suggested the structure of a squirrel cage for the rotor and a three-phase distributed winding for the stator. Since then, the improvement in the quality of electric steels, construction, insulation and the rotor bar casting technique have progressed steadily. However, until the 1970s, because electricity was so inexpensive, only a minor attempt was directed towards increasing the efficiency of motors and the main effort was oriented to reducing the cost and designing smaller motor for a constant power output. As a result, a 100 hp motor in 1974 has same physical size as a 7.5 hp motor of 1897. [2.1]

For a given desired power output and speed, the best approach for the designer to follow would seem to be to build a machine that could take up as little space as

practicable, have a small mass, and be inexpensive to make. Unfortunately, as the size of a machine decreases, its power loss per unit area goes up which leads to higher operating cost. It is usual, therefore, to trade off size and design for a minimum total cost, i.e. the sum of manufacturing and operating costs, and a minimum power loss. The trade off also presumes that the material and dimensions for the electrical and structural parts are chosen such that the electric intensity in the insulation, stresses and strains, and especially temperature are within prescribed limits.

Since the increase in oil prices caused electricity prices to go up, efforts has been put into designing more efficient motors and the life time operating cost of the motor has become more important.

Reducing copper losses by using more copper in the stator winding, utilizing high grade electric steel with low hysteresis losses, increasing the length of the rotor and stator to reduce the magnetic flux density in the air gap, using thin insulated lamination with very high internal resistivity to reduce the eddy current loss and several other techniques are used to reduce the lifetime operating cost of a motor. Beside these, as the cooling air is made to circulate by the rotating parts of machine, more steel is used in the stator, allowing a greater amount of heat transfer out of the motor.

2.2 Fundamental Introduction

All electromagnetic machines can be related to three-phase principle, namely those of induction, interaction and alignment. [2.3]

2.2.1 Induction

The essential for the production of an electromotive force by magnetic means are electric and magnetic circuits, mutually linked. Summation of all products of magnetic flux with complete turns of electric circuit gives the total flux linkages ψ. If ψ is made to change, an emf is induced in the electric circuit. The emf exists only while change is

taking place, and the magnitude of its time integral is equal to the change of linkages, so that

$$\int e \bullet dt = -\psi \ \text{ or } \ e = -d\psi / dt \qquad (2.1)$$

The direction of emf is such as to oppose the change. For engineering purposes this is used in the form of equation 2.2.

$$e = N(d\phi / dt) \qquad (2.2)$$

where all N turns link to the flux and the result is a linkage $\psi = N\phi$. The flux Φ may be resolved into a useful or working component and a non-useful or leakage component. [2.3]

Change of linkage in a coil may occur in three ways:
   (1) Supposing the flux is constant, the coil may move through it.
   (2) Supposing the coil is stationary with respect to the flux, the flux may vary in magnitude.
   (3) Both the changes may occur together i.e. the coil may move through a time varying flux.

In (1) the flux cutting rule can be applied, and the emf in a single conductor of length l calculated from the rate at which it cuts across a magnetic field of the uniform density B when moving at a speed v in a direction at right angle to the direction of flux: then

$$e = Blv \qquad (2.3)$$

This is the motional emf always associated with the conversion of energy between mechanical and electric forms. [2.3]

2.2.2 Interaction

When a current i lies in and perpendicular to a magnetic field of density B over active length l, a mechanical force

$$f_e = Bli \qquad (2.4)$$

is developed on it in a direction perpendicular to both current and field. In figure 2.1 (a), B represents the flux density of an undisturbed field. Introduction of a conductor carrying current imposes a corresponding field component, developing the resultant in (b). In the neighborhood of the conductor the resultant density is greater than B on one side and less than B on the other; provided that increase on one side has the same magnitude as reduction on the other, the force on the conductor is given in equation (4).[2.3]
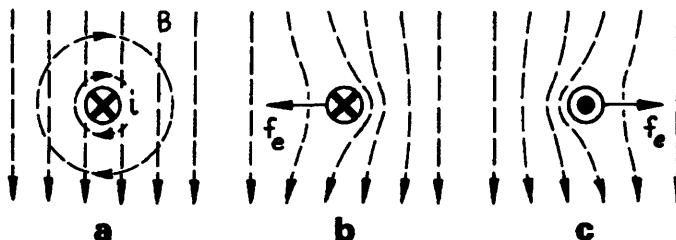
Figure 2.1 (a) Flux density of an undisturbed field, (b) Flux density with current carrying conductor in positive direction and (c) Flux density with current carrying conductor in negetive direction

2.2.3 Alignment

Pieces of high permeability material (e.g. steel) in an ambient low permeability medium (e.g. air) in which the magnetic field is established, experience a mechanical force tending to align them with the field direction in such a way as to minimize the reluctance of the system. [2.3]

2.3 Left hand rule for motors

The relationship between the directions of voltage (or current) applied, the magnetic field, and the motion of conductor may be expressed by Fleming's left hand rule. If the left hand is held so that the thumb, forefinger, and middle finger are all at right angle with each other as shown in figure 2.2, the thumb will indicate the direction of motion of the conductor through the magnetic field, the forefinger will indicate the direction of the magnetic lines of forces, and the middle finger will indicate the direction of induced voltage. [2.4]
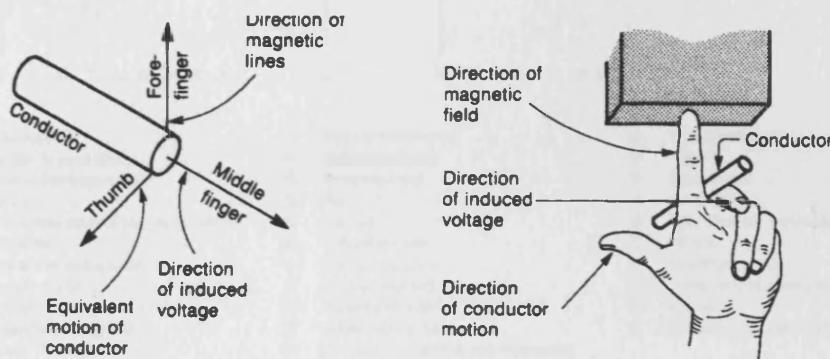
Figure 2.2 Fleming's Left hand rule [2.4]

2.4 Motors

All induction motors consists of two major sections. One is the stator, which is stationary and produces the magnetic field and the second is the rotor, which rotates to, gives the mechanical output. Apart from these main parts that help to build the induction motor there are many other parts, which constitutes a motor. Figure 2.3 shows the components that make up a typical small or a medium size induction motor. [2.5]

1	Grease nipple	13	Endplate (non-drive end)	25	Internal bearing cap
2	Alternative flange endplate	14	External bearing cap	26	Felt seal
3	Alternative face flange endplate	15	V-ring rubber seal	27	Drive end shaft
4	Shaft key	16	Fan	28	Die cast rotor
5	Terminal block with terminals, nuts and washers	17	Fan cowl	29	Stator frame, core and winding
6	Terminal box	18	V-ring rubber seal	30	Felt seal
7	Terminal cover sealing gasket	19	External bearing cap	31	Internal bearing cap
8	Terminal box cover	20	Endplate (drive end)	32	Internal circlip for retaining bearing
9	Cable gland	21	External circlip retaining bearing on shaft	33	Ball bearing
10	Terminal box sealing gasket	22	Grease retaining disc	34	External circlip retaining bearing on shaft
11	Eye bolt	23	Corrugated disc spring for preloading bearing		
12	Grease retaining disc	24	Ball or roller bearing		

Figure 2.3 Components of induction motor [2.5]

2.5 The principles of induction motor

The basis of the three phase induction motor is for the stator winding to produce a continuously rotating field in the iron and air gap and for this to induce currents in the rotor conductors such as to generate a torque which will make the rotor turn and allow the electrical power supplied to the stator to be converted into a rotational mechanical energy which can be drawn from the motor shaft. [2.6]

2.6 The stator

The stationary part of the induction motor, the stator, is a cylindrical structure, usually a stack of lamination of good electric steel that contains carefully insulated copper windings. The shape of the teeth in the laminations has an important effect upon the operating performance of the motor as well as problem of installing the winding; this feature is given the designer's special attention. Figure 2.4 shows two shapes of the teeth employed. With the open slot, winding coils can be formed and insulated completely before they are inserted into the core; moreover, windings are reasonably accessible when individual coils must be replaced or serviced in the field. With the open slot, however, iron is removed from that portion of magnetic circuit near the air-gap, where it contributes greatly to good motor performance; this means that easier manufacturing and servicing conditions are attained with some sacrifice in the performance. The partially closed slots, on the other hand makes winding somewhat more difficult because the coil must be tapped and insulated after they are placed in the core. Also, since coils usually have several turns of wires, the winding procedure requires that individual conductor be fed into slots between the narrow openings formed by overhanging teeth. The latter design does, nevertheless, have the advantage that iron is provided in the magnetic circuit where it is most useful; for motors of equal output and performance, this makes it possible to have a core that is shorter axially than one with the open slots. [2.7]

(a) Open slots.   (b) Partly closed slots.
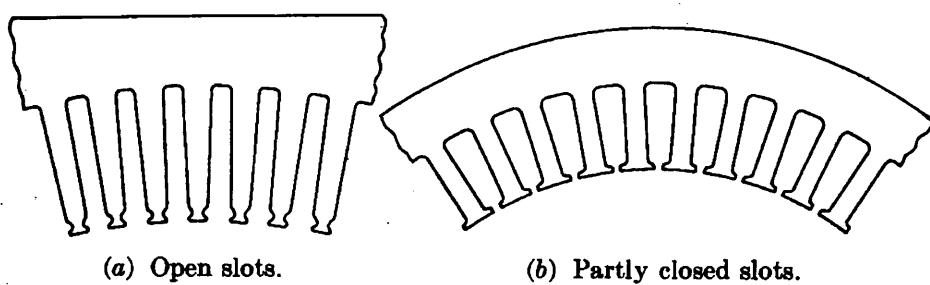
Figure 2.4 (a) Open slots (b) Partly closed slots [2.7]

The stator winding can be of various designs but the essence of all of them is that each winding occupies two, 60 electrical degree section of the iron periphery, these two sections, being separated by 180 electrical degrees. The three phase windings are then arranged in the sequence as shown in figure 2.5, the sequence of the physical winding corresponding to the sequence of rotation of the voltage vector applied to the phases. Figure 2.6 shows the arrangement of a typical single layer stator windings to demonstrate how such winding are arranged in practice. This diagram shows a two-pole section of the stator flattened out for clarity. With more pole pairs in the stator this sequence is repeated with the coils of each phase usually being connected in series. [2.6]

The aim of the stator winding is to produce a field flux, which rotates smoothly around the air gap so as to induce voltages and current into the rotor conductors. The voltage induced in the armature winding is given by

$$E_s = 4.44 f \phi N K_d K_p \qquad (2.5)$$

Where E_s is the voltage induced in the stator winding per phase, V, f is the supply frequency, Hz, ϕ is the flux per pole, Wb, N is the number of stator winding turns in series per phase, K_d is the winding distribution factor and K_p is the pitch factor. [2.8]

The distribution factor K_d, simply put, accounts for the fact that all coils in a group are not centered on the group. Pitch factor K_p, is the factor by which short pitching each coil of lap winding reduce the back emf. [2.11]

If such a winding as shown in figure 2.6 is supplied with three phase currents, displace by 120 electrical degree and changing sinusoidally in time, then just two flux poles of opposite polarity are produced which will move along the winding and hence rotate in the air gap space, at a speed dependent on the cyclic frequency of the currents. [2.6]
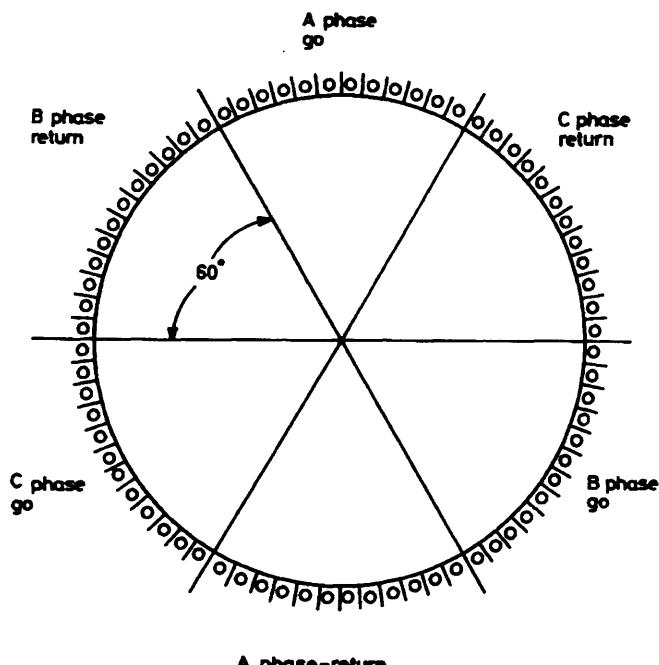
Figure 2.5 Two-pole stator winding space allocation [2.6]
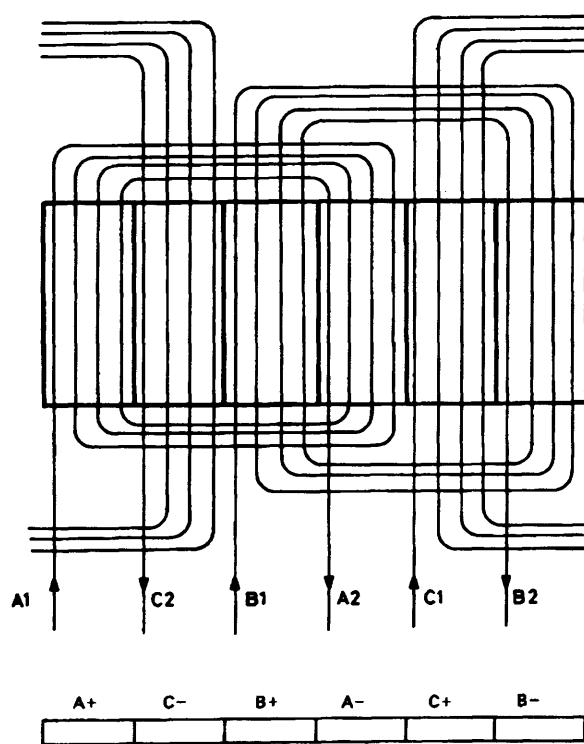
Figure 2.6 Typical Stator Winding [2.6]

To understand this very key feature of the AC motor it should be appreciated that the magneto-motive force (MMF) or ampere-turns produce by each phase winding is trapezoidal in shape, with the magnitude of the MMF being dependent on the level of the current flowing in the winding. Figure 2.7 shows the MMF's produced by the individual phase windings and the total summation of the three, at one instant in time when the phase currents are as shown. The three winding therefore produces a single pair of flux poles. [2.6]
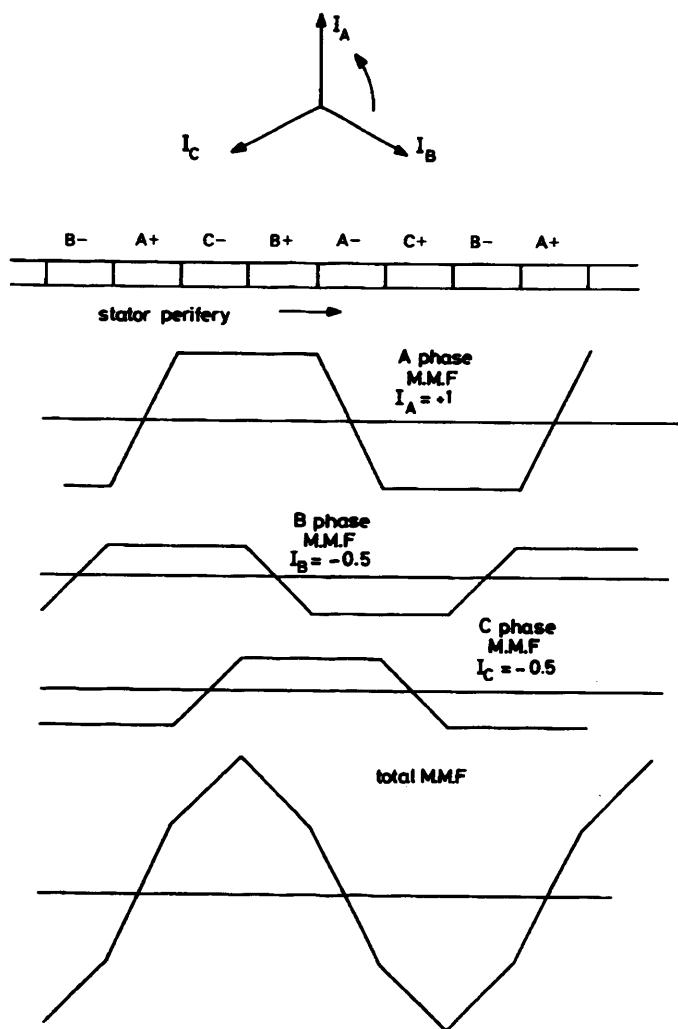
Figure 2.7 Stator MMF waveform at A-Phase due to current I_A, B-Phase due to current I_b, C-Phase due to current I_c, and the total MMF. [2.6]

2.7 The rotating magnetic field

The pattern of flux produce in an ideal four-pole motor supplied from a balanced three phase source is as shown in the figure 2.8(a) at successive instant of times. The term 'four-pole' reflects that the fact that the flux leave the stator from two N pole, and returns at two S pole. If the variation of air gap flux density with respect to the distance round the stator is plot, at each of the three instants of time, the patterns obtained is shown in figure 2.8(b). The first feature is that the radial flux density varies sinusoidally in space. There are two N and two S peaks, but the transition from N to S occurs in smooth sinusoidal way, giving rise to the term 'flux wave'. The distance from the centre of one N pole to the distance of the adjacent S-pole is called the pole pitch. Figure 2.8(b) shows that after one quarter of a cycle of the main frequency, the flux wave retains its original shape, but has moved a round the stator by half a pole pitch while after half a cycle it has rotated by full pole pitch. The patterns are plotted at the intermediate times, progressed smoothly, advancing at a uniform rate of two pole-pitches per cycle of the main frequency. The term 'travelling flux wave' is thus an appropriate one to describe the air-gap field. [2.9]

The general expression for the speed of the field N_S is given by equation 2.6.

$$N_s = \frac{120f}{p} \qquad (2.6)$$

where p is the pole number.

(a)

(b)
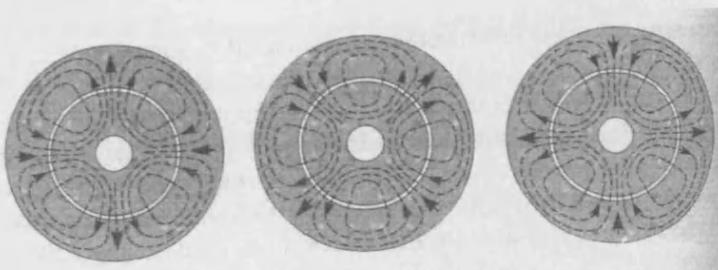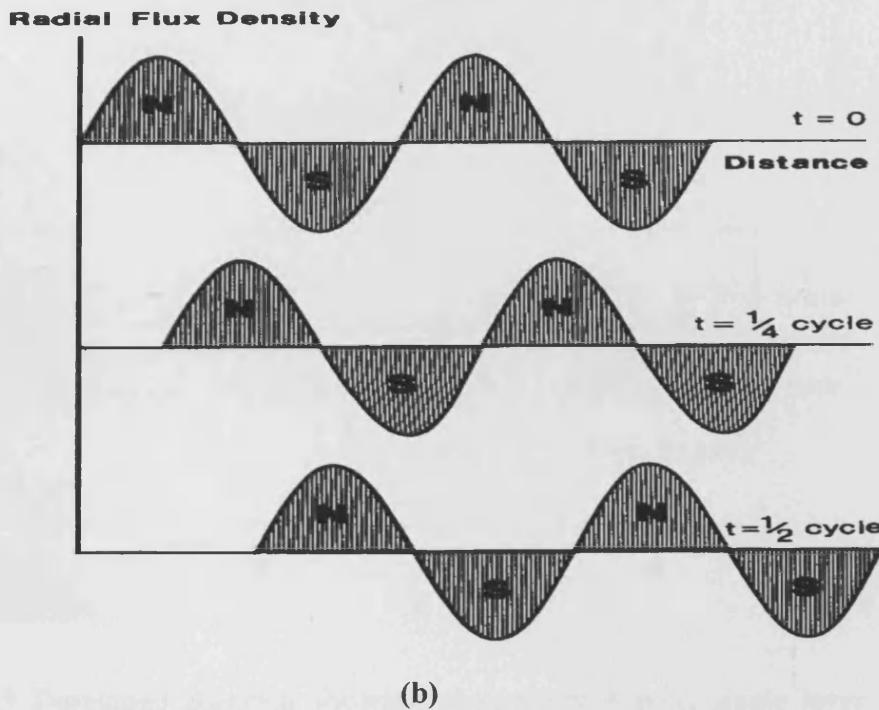
Figure 2.8 (a) Flux pattern in a 4 pole induction motor at 3 successive instant of time, each one quarter of cycle apart; (b) radial flux density distribution in air gap at 3 instant shown in figure (a) with distance in radians [2.9]

Figure 2.9 shows the arrangement with four numbers of poles, the air gap field shown by only two flux lines per pole for the sake of clarity is uniform between each go (positive current direction) and return (negative current direction) coil side. The air gap flux is rectangular, whereas it is deserved to be sinusoidal. It can be improved by adding more coils in the adjacent slots, as shown in figure 2.10. All the coils have the same number of turns and carry the same current. The addition of the extra slightly displaced coils give rise to the stepped waveform of the MMF and air gap flux density shown in figure 2.10. It is still not sinusoidal, but is much better than the original rectangular shape. It can be remarkably close to the sinusoidal pattern, especially when 'two layer' windings are used. [2.9]
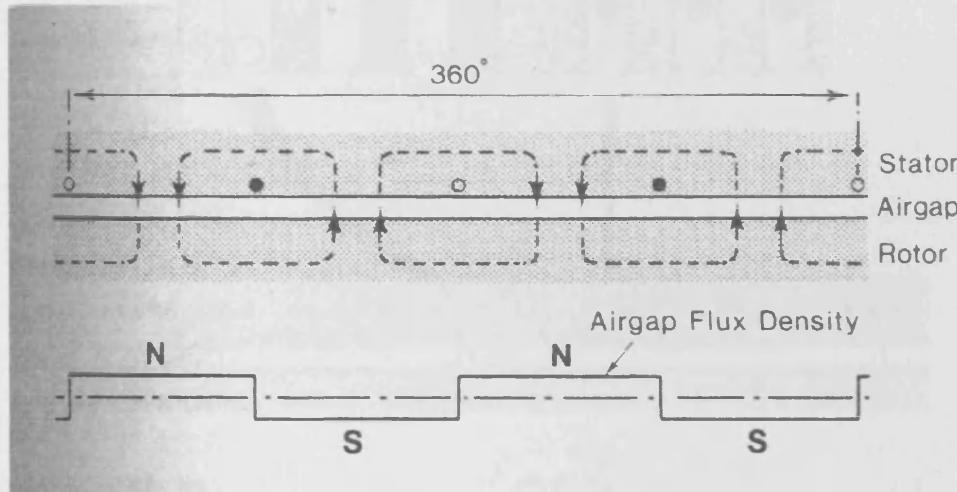
Figure 2.9 Developed diagram showing elementary 4 pole, single layer stator winding consisting of 4 conductor spaced by 90°. The 'go' side of each conductor (shown o) carries current positive current at the instant shown, while the return side is shown as dark dot carries negative current [2.9]
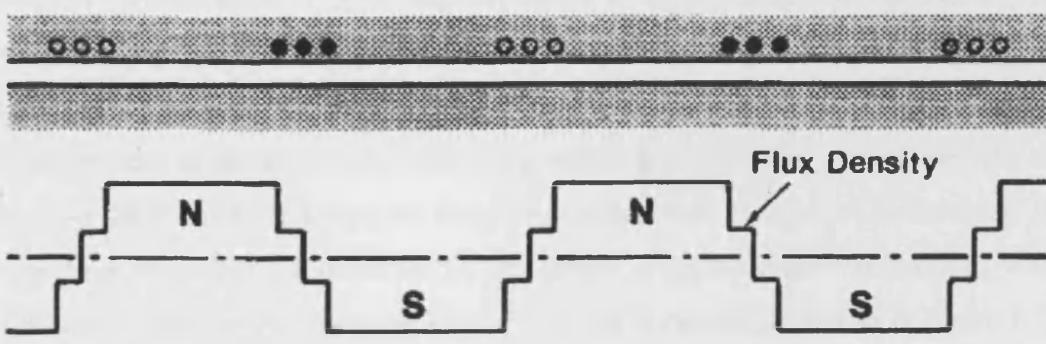
Figure 2.10 Developed diagram showing flux density produced by one phase of a single layer winding having three slots per phase [2.9]
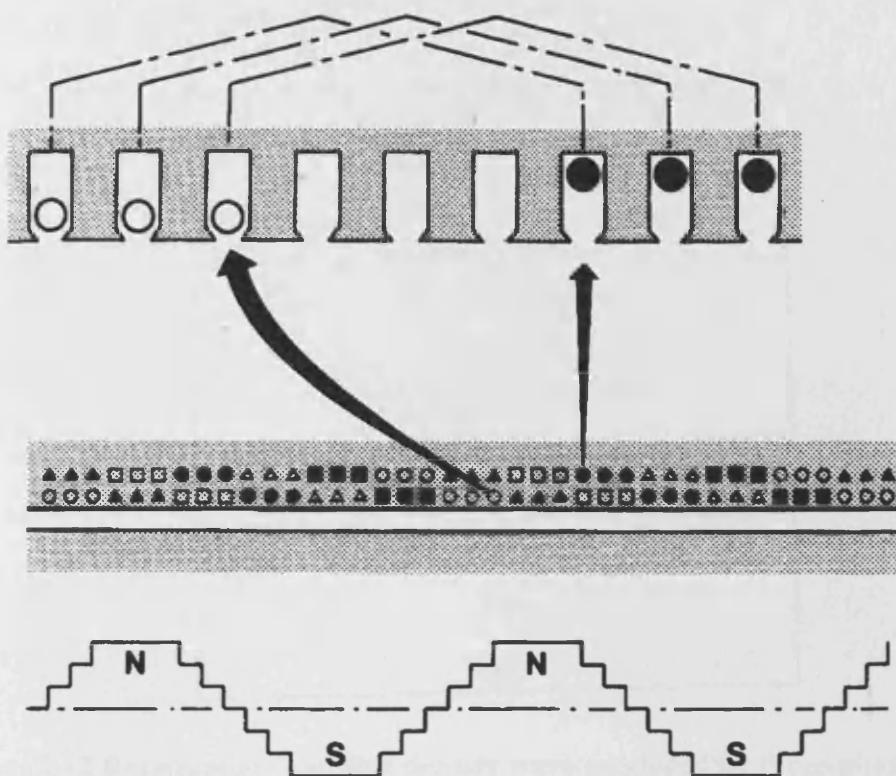
Figure 2.11 Developed diagram showing layout of winding [2.9]

Figure 2.11 shows the developed diagram layout of the winding in a 3 phase, 4- pole, two layer induction motor, together with a flux density wave produce by one phase acting alone. The three phases are represented by circles, triangles, and squares, the go and return sides of the coils being shown by outline and the solid symbol respectively. The upper detail shows how the coil sides form upper and lower layers in the slots. The figure shows that the field produced by one phase is approximately sinusoidal. When the resultant field for the complete 4-pole winding is plotted as shown in figure 2.11, for three discrete times during one complete cycle, the patterns shown in figure 2.12 is obtained. [2.9]
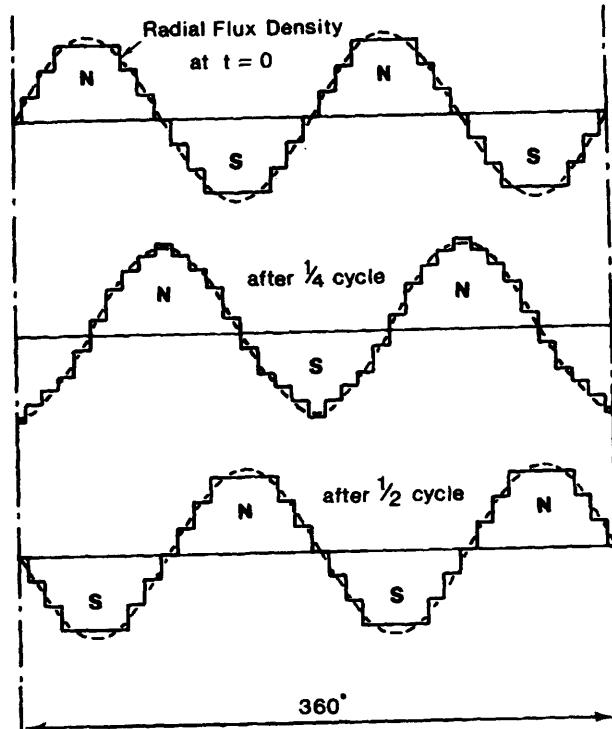
Figure 2.12 Resultant air-gap flux density wave produced by three-phase winding, at three successive instants in time [2.9]

2.8 Main (air-gap) flux, leakage flux and magnitude of rotating flux wave

Broadly speaking the motor designer shapes the stator and rotor teeth to encourage as much as possible of flux produced by the stator to pass through the rotor teeth, so that before completing its path back to the stator it is fully linked with the rotor conductors. In practice the vast majority of the flux produced by the stator is indeed main or mutual flux. But there is some flux, which bypasses the rotor conductors, linking only with the stator winding. This is known as stator leakage flux. Similarly, not all the flux produce by the rotor currents links the stator, but some (the rotor leakage flux) links only the rotor conductor. This leakage flux reflects the prominent part played by the associated leakage reactance in equivalent circuit models of the induction motor. [2.9]

If an alternating voltage, V, is applied to the stator winding then an alternating emf E is induced. The emf is proportional to B and to f

$$E \propto B \, f \qquad (2.7)$$

and $$V \approx E \qquad (2.8)$$

So by combining the above equations equation 2.9 can be derived

$$B = k.\frac{V}{f} \qquad (2.9)$$

k depends upon the number of turns per coil, the number of coil per phase and the distribution of the coils. [2.9]

Equation 2.9 shows that if the supply frequency is constant, the flux in air gap is directly proportional to the applied voltage, or in other words the voltage sets the flux. If the frequency is changed (in order to increase or decrease the speed of rotation of field), the voltage needs to be changed in proportion, if the magnitude of the flux to be constant. [2.9]

The reluctance will be dominated by the air gap, and the magnitude of the magnetising current will therefore depend mainly on the width of the air gap. The magnetising current increases with increase in the air gap. Since the magnetising current contributes to the stator copper losses, but not the useful power, the air gap should be as small as possible, so induction motors usually have the smallest air gap, which is consistent with providing the necessary mechanical clearance. [2.9]

The stator is connected to a three-phase supply to set up, a sinusoidally-distributed and radially-directed rotating magnetic flux in air gap. The speed of rotation of the field is directly proportional to frequency of supply, and inversely proportional to number of

poles. The magnitude of the flux wave is proportional to the applied voltage, and inversely proportional to the frequency. [9]

When the rotor circuit are ignored (i.e. under no load condition), the real power drawn from the mains is small, but the magnetising current itself can be quite large, giving rise to a significant reactive power demand from the mains.

2.9 The rotor

Two types of rotor are used in the induction motors. In both the rotor 'iron' consist of a stack of steel laminations with evenly-spaced slots punched around the circumference. The cage rotor is by far the most common. Each rotor slot contains a solid conductor bar and all the conductor are physically and electrically joined together at each end of the rotor by conducting 'end rings' as shown in figure 2.13. The conductor may be of copper, in which case the end rings are brazed on. The rotor cage comprises permanently short-circuited conductor bars, so no external control can be exercised over the resistance of the rotor circuit once the rotor has been assembled. This is the drawback avoided in second type of rotor, which is known as the 'wound rotor' or 'slip ring' type as shown in figure 2.14. In the wound rotor, the slots accommodate a set of three phase windings similar to those on the stator. The winding are connected in star, with their other ends connected to three slip rings. In particular the resistance of each phase of the rotor circuit can be increased by adding external resistance, as indicated in figure 2.14. [2.9]
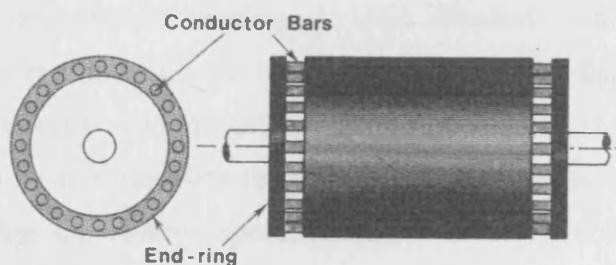
Figure 2.13 Cage rotor construction [2.9]
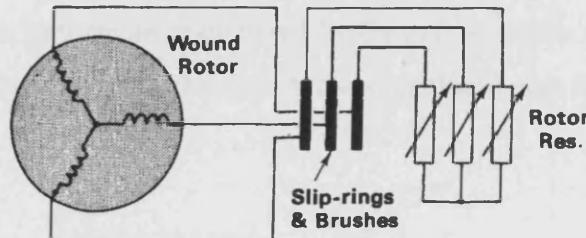
Figure 2.14 Wound rotor, showing slip ring and brushes to provide connection to an external (stationary) 3-phase resistance [2.9]

2.10 Slip

The behavior of the rotor depends very much on its relative velocity with respect to the rotating field. If the rotor is stationary, the rotating field will cut the rotor conductor at synchronous speed, thereby inducting a high emf in them. On the other hand, if the rotor were running at synchronous speed, its relative velocity with respect to field would be zero, and no emf's would be induced in the rotor conductors. The relative velocity between the rotor and the field is known as the slip.

$$s = \frac{(Ns - N)}{Ns} \qquad (2.10)$$

where Ns is the synchronous speed of the field and N is the rotor speed. [2.9]

2.11 Rotor induced e.m.f., current and torque

When the rotor is at stand still, the rotating flux caused by the stator induced emf's in the rotor conductor and as rotor winding are short circuited, significant current are caused to flow. The rate at which the rotor conductor cuts the flux and hence their induced emf's are directly proportional to slip. The frequency of rotor emf is also directly proportional to slip, since the rotor effectively slides with respect to the flux-wave, and the higher the relative speed, the more times in a second each rotor conductor is cut by a N and S pole. At synchronous speed (s=0) the frequency is zero, while at standstill (s=1) the rotor frequency is equal to the supply frequency. The relationship is as shown in figure 2.15. [2.9]

Since the entire rotor bars are short-circuited by the end rings, the induced voltage will drive current along the rotor bars, the current forming closed path through the end rings as shown in figure 2.16. [2.9]
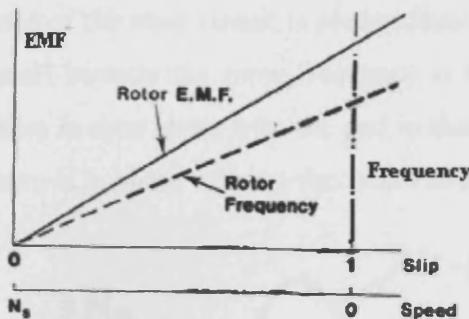
Figure 2.15 Variation of rotor induced e.m.f. and frequency with speed and slip [2.9]
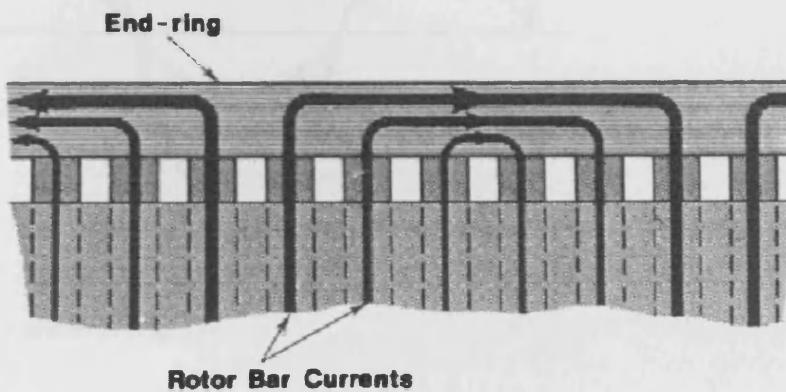
Figure 2.16 Instantaneous sinusoidal patterns of rotor current in the rotor bars and end rings. Only one pole pitch is shown, but the pattern is repeated [2.9]

In figure 2.16, the lines representing the currents in the rotor bars have drawn so that their width is proportional to the instantaneous current in the bars. The axial currents in the rotor bars will interact with the radial flux wave to produce the driving torque to the motor, which will act in the same direction as the rotating field, the rotor being dragged along by the field. [2.9]

2.11.1 Rotor currents and torque-small slip

When the slip is small the frequency of induce emf is also very low. At these low frequencies the impedance of the rotor circuit is predominantly resistive, the inductive reactance being very small because the rotor frequency is low. The current in each rotor conductor is therefore in time phase with the emf in that conductor, and the rotor current wave, which in turn is in phase with the flux wave as shown in the figure 2.17.
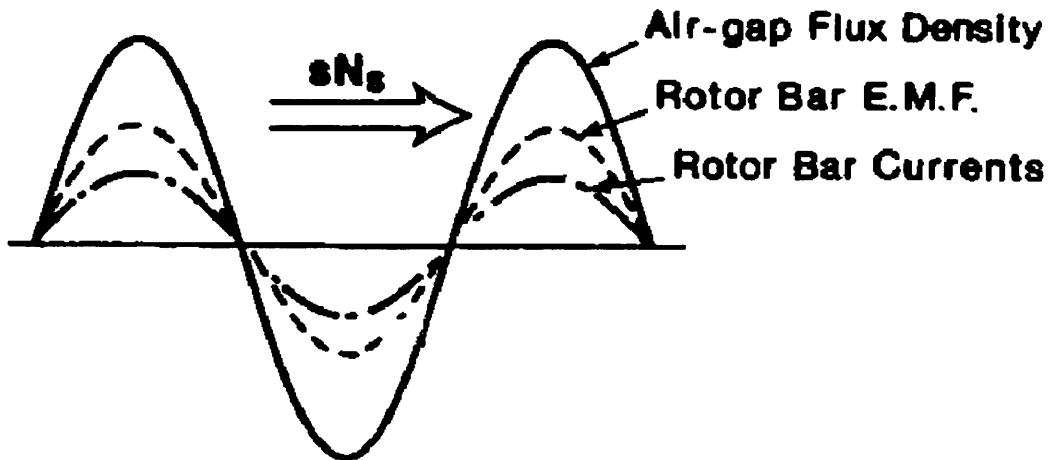
Figure 2.17 Pattern of air-gap density, induced e.m.f. and current in cage rotor bars at low values of slip [9]

So the torque is therefore given by:

$$\tau = kBI_r \qquad (2.11)$$

where I_r denotes the rotor current. [2.9]

The equation above shows that the torque is proportional to slip. This relates to low value of slip only. [2.9]

If the motor is unloaded, it will need very little torque to keep running, so an unloaded motor will run with very small slip at just below the synchronous speed, as shown at point 'A' in figure 2.18. When load is increased, the rotor slows down and the slip

increases, thereby inducing more emf and current, and thus more torque as point 'B' in figure 2.18.

Induction motors are usually designed so that their full load torque is developed for small values of slip. At the full load slip the rotor conductor carry safe maximum continuous current, and if the slip is higher, the rotor will begin to overheat. This over load region is shown by the dotted line in figure 2.18. [2.9]
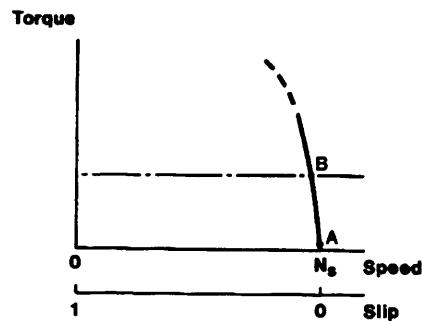
Figure 2.18 Torque-speed relationships for low value of slip [2.9]

2.11.2 Rotor currents and torque-large slip

As the slip increases, the rotor emf and the rotor frequency both increase in direct proportional to slip. At the same time the rotor inductive reactance, which is negligible at low slip (low rotor frequency), begins to be appreciable in comparison with the rotor resistance. At high values of slip, the rotor current also lags behind the rotor emf because of inductive reactance. This space lag is shown in figure 2.19. The unwelcome space-lag can be allowed by modifying the equation (2.11), to obtain more general equation of torque as

$$\tau = kBI_r Cos\phi_r \qquad (2.12)$$

where Φ_r is angle of space lag

For most cage rotors, as the slip increases the term $Cos\phi_r$ reduces more quickly than the current (I_r) increases; so that some slip between 0 and 1 the developed torque reaches the maximum value. This is illustrated in the figure 2.20. The peak torque actually occur at a slip at which the rotor inductive reactance is equal to the rotor resistance, so the motor designer can position the peak torque at any slip by varying the reactance to resistance ratio. [2.9]
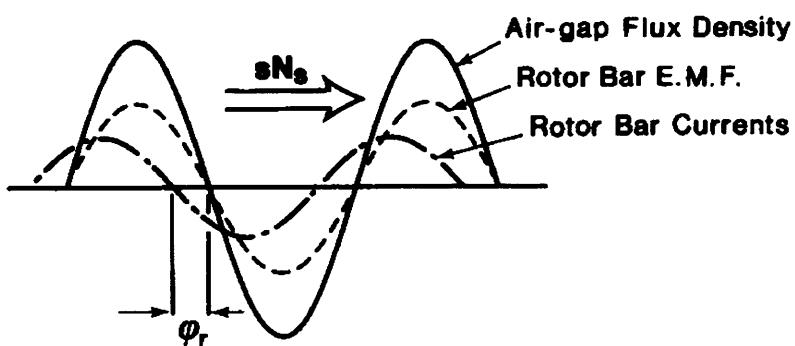
Figure 2.19 Pattern of air gap flux density, induced emf and current in cage rotor bars at high values of slip [2.9]
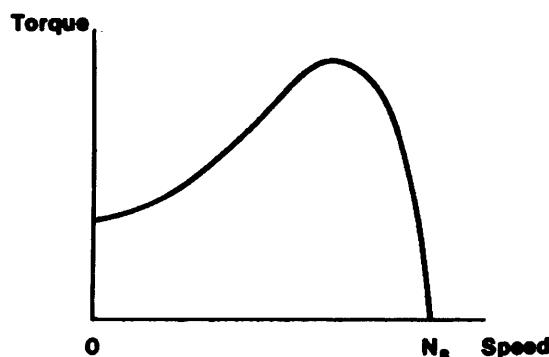
Figure 2.20 Typical complete torque-speed characteristic for cage induction motor [2.9]

2.11.3 Reduction of flux by rotor current

When rotor current is negligible (s≈0), the emf that the rotating fields induce in the stator winding is very nearly equal to the applied voltage. A reactive current (which is

termed as magnetizing current) flows into the winding, to set up the rotating flux. Any slight tendency for the flux to fall is immediately detected by a corresponding slight reduction in emf, which is reflected in a proportionately large increase in magnetizing current, which thus opposes the tendency for the flux to fall. Exactly same mechanism comes into play when the slip increases from zero, and the rotor currents are induced. The rotor current wave gives rise to rotor MMF wave, which rotates at slip speed (S N_s) relative to the rotor. But the rotor is rotating at the speed of (1-S) N_s, so that when viewed from the stator, the rotor MMF rotates at synchronous speed. The rotor MMF wave would, if unchecked, causes its own rotor flux wave, rotating at synchronous speed in the air gap, in the same way as the stator magnetizing current originally set the flux wave. The rotor flux wave would oppose the original flux wave, causing the resultant wave to reduce. [2.9]

However, as soon as the resultant flux begins to fall, the stator emf reduces, there by admitting more current to the stator winding, and increasing its MMF. The extra stator MMF produced by the large increase in stator current effectively cancels the MMF produced by the rotor currents, leaving the resultant MMF (and hence the rotating flux wave) virtually unchanged. [2.9]

The flux will be constant when the slip is very small but if the slip is high then the leakage fluxes assume a much greater importance than under normal low slip condition. So at high slip the flux is not constant. [2.9]

2.12 The equivalent circuit of the induction motor

The equivalent circuit diagram of induction motor is as shown in figure 2.21.
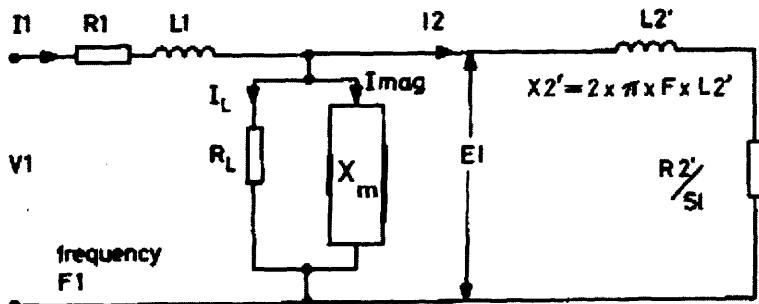
Figure 2.21 Induction motor single-phase equivalent diagram [2.2]

In which $R1$ is the stator resistance per phase

$R2'$ is the rotor resistance per phase referred to the stator

$L1$ is the stator leakage inductance per phase

$L2'$ is the rotor leakage inductance referred to the stator

The losses in the magnetic circuit (the iron losses) are represented by the presence of resistor R_L and the magnetizing impedance X_M dictating the magnetizing current I_{mag} is shown connected across the transformer primary. [2.6]

In the figure the total mechanical output to the rotor shaft (including the friction and windage losses) is t given by $(I_L)^2 \times R_2'((1 - S_1)/S_1)$

2.13 Motor power losses

2.13.1 Copper losses

The electrical winding of a motor always have a finite resistance and this cause power losses $I_1^2 R_1$. The value of the winding resistance will increase with temperature. The above approach of using the total RMS value of the current will be satisfactory in most circumstances but if more precision is required it is necessary to consider any harmonic content in the current more thoroughly. Due to frequency dependent skin effect the

current tends to concentrate in the outer layers of the conductor and the resistance of winding increases with frequency. The more accurate way of assessing the losses in this case is to sum up the individual I^2R values for each harmonic contained in the total current. [2.6]

2.13.2 Iron losses

In motor operation, the flux in the core of the motor will be reversed and this causes a loss of energy called hystersis loss. Its value depends on the quality of iron used, the value of the flux density over which it is being used and the frequency of operation. [6]

For a particular iron circuit study shows that the hystersis loss is given by

$$P_h = K_h f B^x \qquad (2.13)$$

Where K_h is the material constant which depends on core material and x is dependent on the quality of the iron and which normally varies between 1.5 and 2.5. [2.6]

The iron losses also contain another component, an eddy current loss due to induced currents in the iron. In order to reduce this loss to relative small proportions AC magnetic circuit are laminated using thin insulated sheets. There will be an eddy current loss and for a specific iron circuit this loss is given by

$$P_e = K_e (f B t)^2 \qquad (2.14)$$

where K_e is proportionality constant and t is the lamination thickness.

2.13.3 Friction losses and windage losses

In general the power losses in the bearings will vary in direct proportion to the speed of the motor. Windage losses are caused by the fan mounted on the rotor for cooling purposes and by the rotation of the motor itself. The power loss caused by the windage

will be proportional to the cube of rotor speed [2.6]. The friction and windage losses accounts for 10% of the total losses.

2.13.4 Stray losses

Apart from all the above losses there are other losses which will occur and which are harder to estimate. To be accounted for here are

1. No-load losses in the rotor teeth because of the stator slot opening modulation of the fundamental flux density.
2. Load losses in the rotor teeth because of stator zigzag mmf and
3. No-load losses in the rotor body (if exists) due to stator slot opening modulation of the fundamental flux density. [2.10]

These losses have somewhat different character from the other miscellaneous losses. They show drag on the rotor, so their power is subtracted from the mechanical output of the machine. The first and third are very closely related so they are taken first. The stator slot openings 'modulate' the space fundamental magnetic flux density. The amplitude of the magnetic field disturbance is given by

$$B_H = B_r \times (2/\Pi) \times Sin(\theta_D / 2) \qquad (2.15)$$

Where B_r is radial flux density; θ_D is slot-opening angle (relative to slot pitch).

In fact the flux disturbance is really in the form of two travelling waves, one going forward and one backward with respect to stator. [2.10]

The zigzag order current harmonics in the stator will produce the magnetic field in the air gap, which will drive magnetic losses in the teeth of the rotor. This is a bit different from the modulation of the space fundamental produce be the stator slot openings.

Although the harmonic order is be same, the spatial orientation will be different and will vary with load current. [2.10]

REFERENCES FOR CHAPTER 2

[2.1] S. J. Chapman, "Electric machinery fundamentals", Mc Graw-Hill Book Company, 1987

[2.2] M. E. Hawary, "Principle of electric machines with power electronics applications, Prentice Hall International edition, 1986

[2.3] M. G. Say, "Alternating current machine", Longman Scientific and Technical, fifth edition, 1983

[2.4] A. J. Pansini, "Basic of electric motors", Pennwell publishing company, Second edition, 1996

[2.5] D. G. Searle, "European electric motors drive and controls", Roles publishing, 1997

[2.6] D. Finney, "Variable frequency AC motor drive system", Peter Peregrinus Ltd., London, 1991

[2.7] C. S. Siskind, "Induction motors single-phase and polyphase", Mc Graw-Hill Book Company, 1958

[2.8] E. S. Hamdi, "Design of small electrical machines", John Wiley and Sons Ltd., 1994

[2.9] A. Hughes, "Electric motors and drives fundamentals, types and applications", Butterworth-Heinemann Ltd., Second edition, 1993

[2.10] H. W. Beaty, J. L. Kirtley, "Electric motor handbook", Peter Peregrinus Ltd., London, 1999

[2.11] G. W. Wakileh, "Harmonics in rotating machines", Electrical Power System Research, Vol. 66, pp. 31-37, 2003

CHAPTER 3

DRIVES AND INVERTERS

3.1 Introduction

A combination of power electronic system such as voltage controller and an electric motor with the associated control mechanism is referred as variable speed drive. In an A.C. type variable speed drive the supply to an induction motor is controlled by an ac voltage controller, a cycloconverter, or an inverter to achieve prescribed speed for a given load.

The choice of the power semiconductor driving system depends on the type of available power supplies and load characteristics.

3.2 Adjustable speed induction motor drives

The speed of an induction motor driving a mechanical load with a given torque-speed characteristic can be controlled by controlling either its synchronous speed or the rotor slip. For a fixed number of stator poles, the synchronous speed is controlled by varying the supply frequency. The slip of the rotor under load is controlled by regulating either the stator voltage or current. [3.1]

Schemes of adjustable speed drives for an induction motor can be classified as shown in figure 3.1.

Adjustable speed drive

Stator control   slip power, rotor control

Constant frequency Variable frequency   Kramer drive   Scherbius drive
variable voltage   variable voltage

DC link conversion   Cycloconverter drive

Voltage fed inverter   Current fed inverter

Square wave   PWM inverter
Inverter
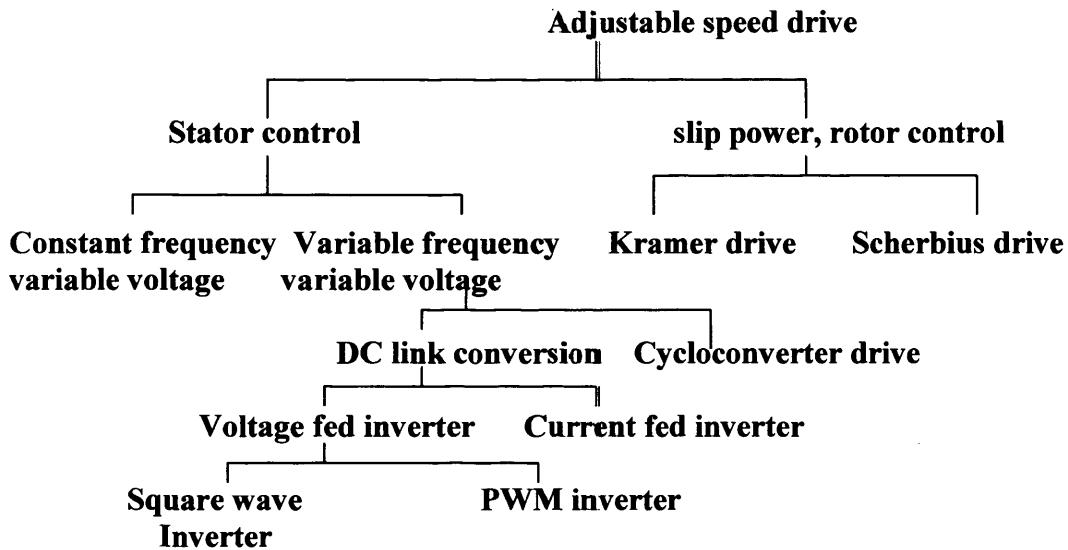
Figure 3.1 Classification of adjustable speed induction motor drives [3.1]

3.3 Variable voltage, constant frequency drives

In this method the voltage applied to the stator winding is controlled while maintaining the frequency of the supply unchanged. The drive is applicable for medium power levels such as pumps and blower type loads. This method is simple and economical for the control of squirrel cage class D type induction motor with high slip. The performance of the drive is poor since line currents carry more harmonics and the drive has a poor power factor. [3.1]

3.4 Variable voltage, variable frequency drives

It is reasonable to expect improved performance of adjustable speed drives if a variable frequency stator supply is employed. The air gap flux is directly proportional to the stator-applied voltage and inversely proportional to the frequency. A reduction in supply frequency to achieve speed control below synchronous speed will be associated with an increase in the air gap flux if the applied voltage is maintained at rated value. [3.1]

To avoid saturation due to increase flux, variable frequency drives employ a variable voltage as well, with the object of maintaining an acceptable air gap flux level. This concept is generally as referred as constant v/f control and is used in drives employing squirrel-cage induction motor of all classifications. [3.1]

In figure 3.2 a family of torque speed characteristics of a three-phase induction motor. The angular speed ω_{so} corresponds to rated frequency operation. The speed at maximum torque for rated voltage and frequency defines the division of the speed range into constant Volts/HZ region to the left and the constant voltage variable frequency region to the right. [3.1]
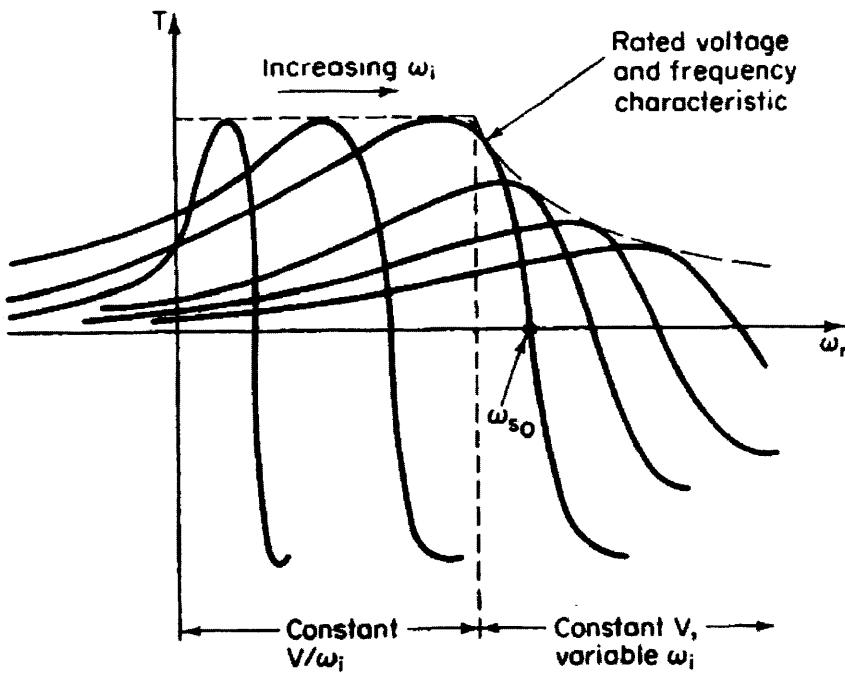
Figure 3.2 Torque-speed characteristics with variable frequency condition for an induction motor [3.1]

3.5 DC link converter drive

Adjustable speed drive of an ac motor requiring variable voltage-variable frequency from a fixed frequency-fixed voltage supply can be designed using an intermediate dc link. Here ac power is converted to dc output of a rectifier and is fed through a dc link to the three-phase inverter connected to the motor stator terminal to provide the required variable frequency supply. [3.1] Figure 3.3 shows some different dc link converter schemes.
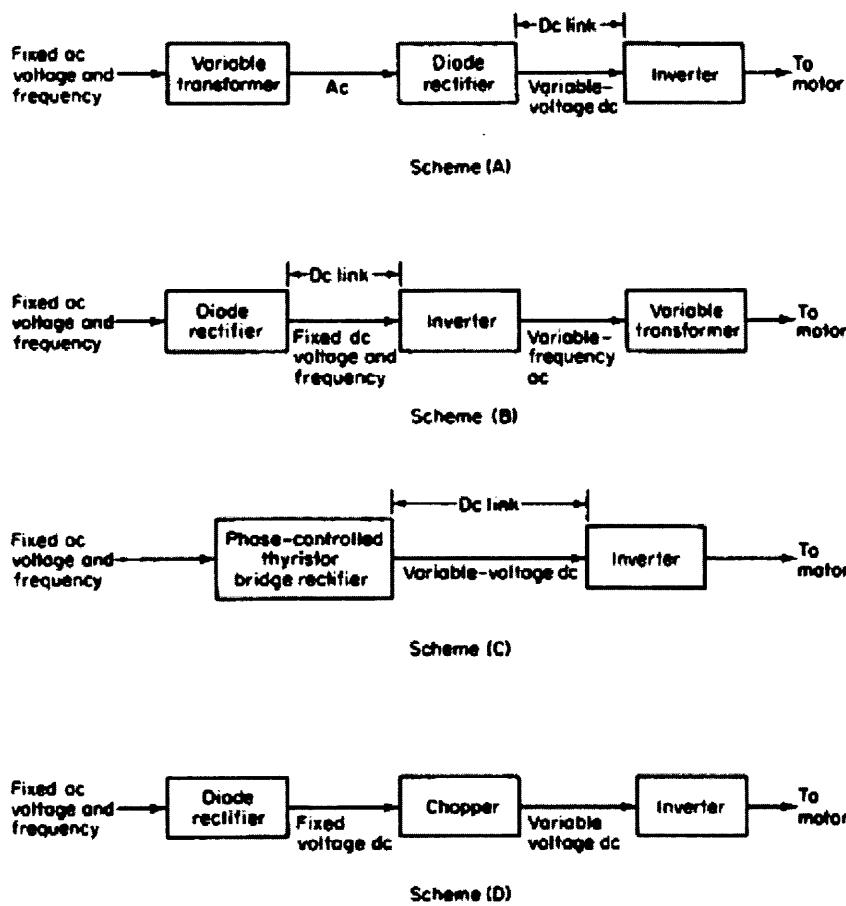
Figure 3.3 Square wave dc link converter drives [3.1]

In all the above schemes the inverter provides adjustable frequency. The voltage levels are adjusted externally to the inverter by a variable transformer. In schemes (a) and (b) three phase diode rectifiers are employed. In scheme (a) fixed ac is fed to the transformer whose ratio is controlled as a function of the desired output. The variable ac voltage is then fed to a rectifier. The rectifier variable output is injected into the inverter. The inverter output is of variable magnitude and frequency. [3.1]

Scheme (b) differs from scheme (a) in that the output of the inverter is of variable frequency but fixed voltage. The desired variable voltage is achieved by using an intermediate variable transformer between the inverter output terminals and the motor stator terminal. [3.1]

In scheme (c), a phase controlled thyristor bridge rectifies the incoming ac voltage to variable dc voltage while maintaining the desired voltage to frequency ratio. No transformers are involved in these schemes.

In scheme (d) the thyristor bridge rectifier of scheme (c) is replaced by a cascade of a diode rectifier bridge and a chopper to provide the variable dc input to the inverter. The voltage supply to the ac motor's stator terminals is a square wave of adjustable voltage and frequency.

A more attractive arrangement uses a pulse width modulation inverter (PWM), which provides both frequency and voltage control with the same set of thyristors. The output of a PWM inverter is a series of adjustable width pulses, which provides for an adjustable rms voltage supply. The dc supply to the inverter is furnished by a diode rectifier bridge as shown in figure 3.4.

```
Fixed ac                 Diode                    PWM        To
voltage and  ----->    rectifier              inverter ---> motor
frequency                        Fixed-
                                 voltage dc
```
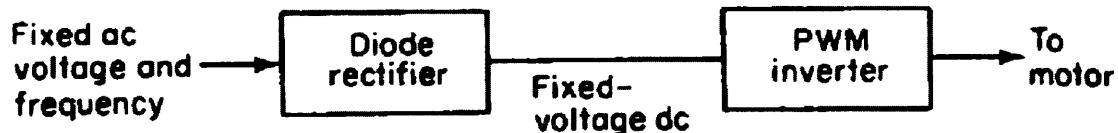
Figure 3.4 PWM inverter dc link converter supply [3.1]

In this dc link inverter voltage and current fed drives are used.

3.5.1 Voltage fed inverter drive

* Low slip motors are used in this type are resulting in improved efficiencies. Desired voltage-frequency and torque-frequency characteristics are shown in figure 3.5.
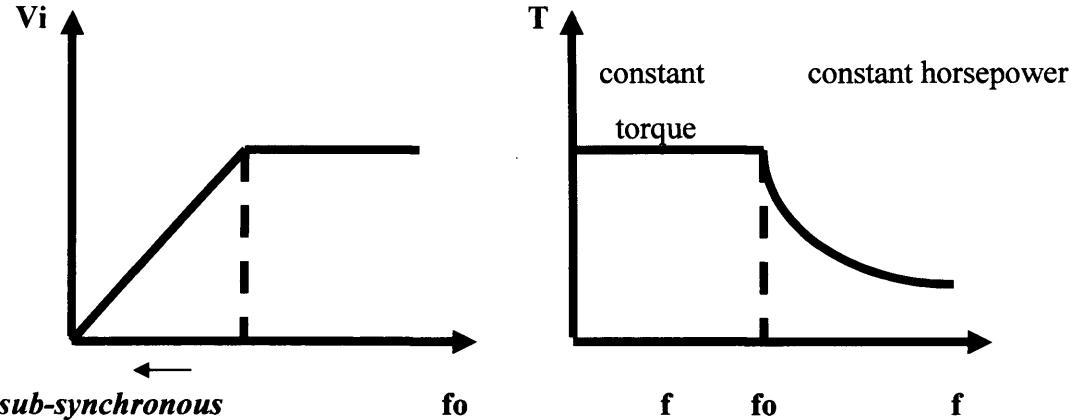
Figure 3.5 Voltage-Frequency and Torque-Frequency relation of an induction motor drive [3.1]

In the sub-synchronous region voltage/frequency is constant, resulting in a constant torque output. For frequency above rated value the voltage is maintained constant, resulting in constant horsepower operation. At low frequency, the resistance effect dominates that of the leakage reactance and additional voltage is impressed to compensate for this effect. [3.1]

The two main classes of voltage fed inverter drives are the square wave inverter and the PWM inverter drive.

3.5.1.1 Square wave inverter drive

A square wave inverter ac motor drive is shown in figure 3.6. It is referred to as a voltage fed since the capacitor C provides low Thevenin's impedance to the inverter. The inverter voltage waves are not affected by the load. Voltage fed square wave drives are employed in low to medium power application. [3.1]
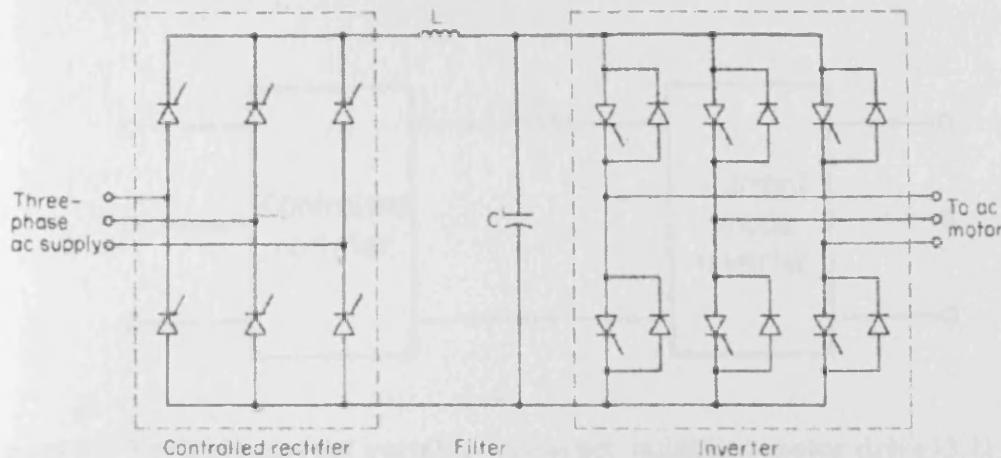
Figure 3.6 Voltage fed square inverter ac motor drive [3.1]

3.5.1.2 PWM inverter drives

The controlled rectifier shown in figure 3.6 can be replaced by an uncontrolled diode rectifier in an uncontrolled dc link voltage. At the same time the inverter is controlled using a pulse width modulation strategy to provide variable frequency, variable voltage output. [3.1]

PWM voltage control is applicable in constant torque region, whereas in the constant power region the inverter operation is identical to a square wave drive. An important advantage of the PWM inverter drive is that a number of inverter drives can be supplied through a dc bus at the output of a single uncontrolled rectifier. The drive can be made uninterruptible for possible ac line failure by switching in a standby battery in the dc link. The detail explanation of PWM is given in section 3.8.

3.5.2 Current fed inverter

A current fed inverter ac motor drive shown in figure 3.7. The differences between a voltage fed inverter drive and the current fed inverter drive are that in the latter a capacitor C in the voltage fed inverter is absent and the inductor is large enough so that the dc link presents a constant regulated dc current to the inverter. This type of drive is used with individual motors in medium to high power ranges, which have some minimum load present at all times. [3.1]
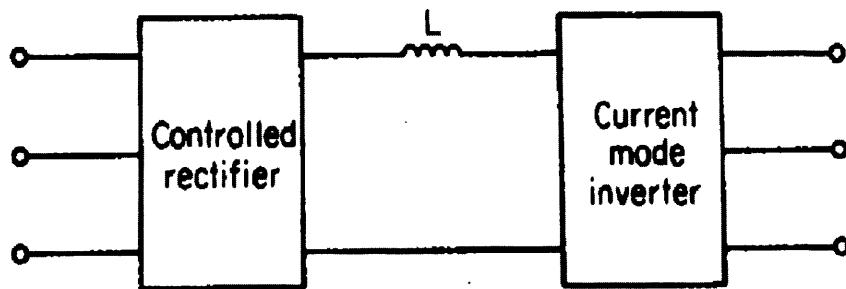
Figure 3.7 Variable current variable frequency induction motor drive [3.1]
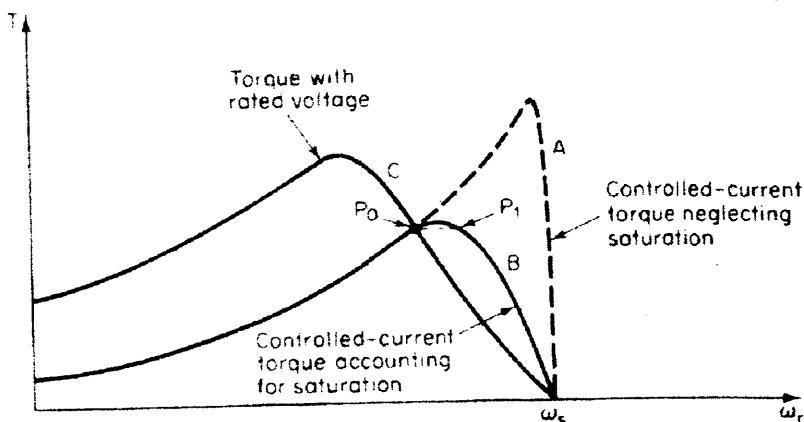
Figure 3.8 Torque speed curves for voltage and current control [3.1]

In figure 3.8 the graph of the torque speed characteristic of voltage controlled and current controlled inverter. At the low range of speed as the flux is below the rated value and the torque due to current control is lower than the corresponding torque obtained by rated voltage control. [3.1]

3.6 Cycloconverter drive

A cycloconverter is a direct frequency changer that converts ac power directly from one frequency level to another. No dc link is required for a cycloconverter. Normally cycloconverter has an output frequency range of zero to one third of the input

frequency. A cycloconverter is capable of producing variable frequency output suitable for induction motor drives. Cycloconverter drives are used in large horsepower applications up to 20000 hp. The system can provide reverse operation and regeneration. [3.1]

3.7 Regulation of slip power

Speed control can be achieved in a wound rotor induction motor by inserting a passive external resistance in the rotor circuit. Speed control using external resistance involves channelling portion of the air gap power at slip frequency into the resistor, which is dissipated as heat. In this speed control, efficiency is sacrificed to attain the required goal. [3.1]

By introduction of new power semiconductor devices and system technology it became possible to reliable control speed by regulation of slip power with less cost and size.

3.7.1 Static Kramer drives

A conventional Kramer drive used an auxiliary machine connected to the rotor circuit of a wound rotor induction motor to convert a portion of the power of the rotor circuit from slip frequency to supply frequency and then feeding it to the supply. A static Kramer drives employs a diode rectifier connected to the rotor circuit to convert a portion of slip frequency power to dc, which then converts to ac at supply frequency using a commutated inverter. [3.1]

3.7.2 Static Scherbius drives

The static Kramer drive permits flow of slip power only from the rotor circuit to the supply lines, and operation is therefore restricted to speed in sub-synchronous range. In a Scherbius drive, speed can therefore be controlled in both the sub-synchronous region and super-synchronous region. In the later case, power at slip frequency is injected in to the rotor circuit. A line commutated phase controlled cycloconverter can be used in place of the dc link converter in a sophisticated static Scherbius drive. [3.1]

3.8 Inverters

The ac induction motor is widely used in a number of variable-speed or torque control applications. Predominant applications are in variable speed ac drives, where the rotor speed is controlled through the supply frequency, and the machine flux through the supply voltage. For these applications dc-to-ac switch-mode inverters are used to produce a sinusoidal ac output whose magnitude and frequency can be controlled independently. Power semiconductor switches produce temporary connections at high repetition rates between the dc terminals and the ac drive motor, one example is a three-phase ac motor drive shown in figure 3.9 [3.2] [3.3].
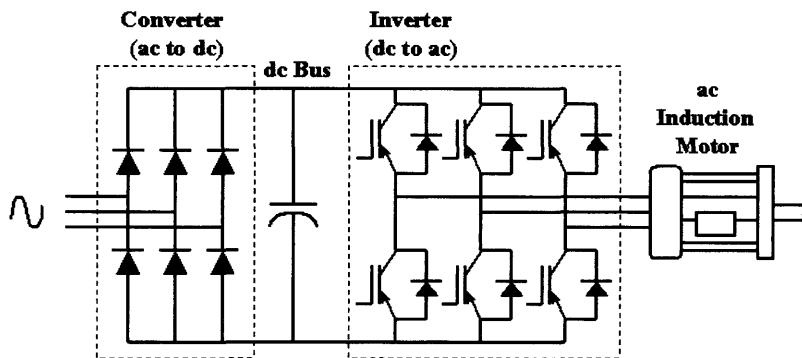
Figure 3.9 Three-phase ac motor drive [3.3]

There are two types of inverters, which are classified according to their dc input, the voltage-source inverters (VSI) and the current-source inverters (CSI). The voltage-source inverters can be further divided into three general categories, pulse-width modulation type (PWM), square-wave type (also known as six-step inverters) and single-phase inverters with voltage cancellation [3.4-3.5].

In pulse-width modulated (PWM) inverters, the input dc voltage is essentially constant in magnitude and the ac output voltage has controlled magnitude and frequency. There are various schemes to pulse-width modulate the inverter switches in order to shape the output ac voltages to be close to that of a sine wave [3.4].

For square-wave inverters, the input dc voltage is controlled in order to adjust the magnitude of the output ac voltage, therefore the inverter has to control only the frequency of the output voltage. The output ac voltage has a waveform similar to that of a square wave [3.4].

In a single-phase inverter with voltage cancellation, it is possible to control the magnitude and the frequency of the inverter output voltage with a constant dc input voltage for a different switch mode that is not pulse width modulated. The inverter output voltage waveform is similar to a square wave. This technique works only with single-phase inverters [3.4].

3.9 Pulse-Width Modulated (PWM) schemes

The ideal requirement for sinusoidal motor voltages can be closely approximated by the synthesis of voltage waveforms using the pulse width modulation technique, characterised by the generation of constant amplitude pulses with the pulse duration modulated to obtain a specific waveform. The fundamental component can be controlled in magnitude and frequency. The harmonic content can be made low and the harmonic order higher than those obtained with the six-step method [3.6].

The waveforms of modulated voltages can be created by modulating a triangular carrier wave with amplitude v_c and frequency f_c, by means of an adjustable direct voltage square-wave, figure 3.10. The fundamental frequency component of the output (modulated) wave is equal to the frequency of the modulating wave. This technique was often used because of its easy implementation by analogue electronics but now the modern design technique involving digital electronics and microprocessor permit the use of more suitable modulation waveforms [3.6].
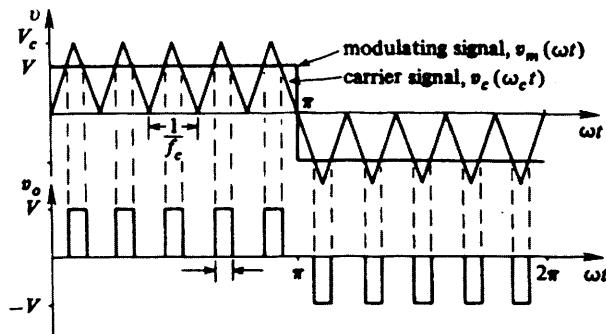
Figure 3.10 Multiple-pulses voltage waveform (v_o) obtained from a triangular carrier wave with square-wave modulation [3.6]

Sinusoidal PWM is the most basic pulse-width-modulation technique used as standard for ac waveform creation. Third-harmonic PWM, $60°$ PWM, and space vector modulation (SVM) are increasing in popularity because they utilise more of the available dc bus voltage. Sinusoidal PWM, third-harmonic PWM, and $60°$ PWM share a common implementation scheme. SVM and six-step modulation have different calculation and implementation requirements [3.3].

In order to produce a sinusoidal output voltage waveform at a desired frequency, a sinusoidal control signal at the desired frequency is compared with a triangular waveform as shown in figure 3.11. This particular type of multiple-pulse PWM is referred to as sinusoidal pulse width modulation (SPWM) [3.3].
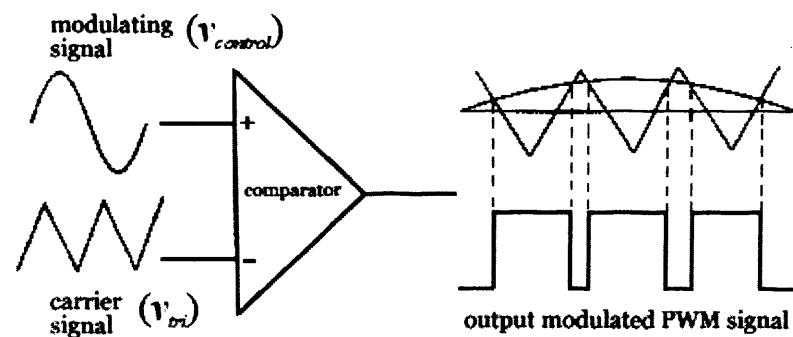
Figure 3.11 Pulse width modulating PWM waveform produced by comparison between sinusoidal control signal and a carrier (triangular) signal

The frequency of the triangular waveform v_{tri} establishes the inverter switching frequency and it is generally kept constant along with its amplitude $\hat{V}_{tri}$. The control signal $v_{control}$ is used to modulate the switch duty ratio and has a frequency f_1, which is the desired fundamental frequency of the inverter voltage output, recognising that the inverter output voltage will not be a perfect sine wave and will contain voltage components at harmonic frequencies of f_1 [3.4].

The adjustment of the ac output voltage of the inverter is achieved by adjusting the amplitude modulation ratio (or modulation index) m_a, defined in equation 1, where $\hat{V}_{control}$ is the peak amplitude of the control signal and $\hat{V}_{tri}$ is the amplitude of the triangular.

$$m_a = \frac{\hat{V}_{control}}{\hat{V}_{tri}} \qquad (1)$$

The frequency modulation ratio m_f defines the frequencies at which the harmonics occur and it is defined by equation 2, where f_s is the switching frequency and f_1 is the fundamental frequency.

$$m_f = \frac{f_s}{f_1} \qquad (2)$$

Theoretically, the frequencies where the harmonics occur can be defined by equation 3 [5.3], where the harmonic order h corresponds to the kth sideband of j times the frequency modulation ratio m_f.

$$f_h = (jm_f \pm k)f_1 \qquad (3)$$

An integer mf results in synchronous PWM where the triangular-waveform signal and the control signal should be synchronised. The reason for using the synchronous PWM is that the asynchronous PWM (where m_f is not integer) results in sub-harmonics of the fundamental frequency that are very undesirable in most

applications. The frequency-modulation ratio m_f should be an odd integer except in single-phase inverters with PWM unipolar voltage switching. Choosing mf as an odd integer results in odd symmetry [f (-t) = -f (t)] as well as a half-wave symmetry [f (t) = -f (t+Ts/2)] with the time origin. Therefore, only odd harmonics are presented and the even harmonics disappear from the waveform [3.4].

In inverters, the switches are controlled based on the comparison of $v_{control}$ and v_{tri}, and the output voltage will depend of the circuit configuration of the inverter, i.e., single-phase half-bridge, single-phase full-bridge or three-phase.

3.10 Single-phase inverters

There are two circuit topologies commonly used for single-phase inverter, the half-bridge and the full-bridge. For certain low power applications, the half-bridge may suffice but the full bridge is more convenient for adjustment of the output voltage by pulse width modulation techniques [3.4].

The half-bridge inverter has two controlled static switching elements, which are controlled based on the comparison of $v_{control}$ and v_{tri}. The output-voltage waveform v_{A0}, shown in figure 3.12, results in

$$v_{Ao} = \frac{V_d}{2} \text{ if } v_{control} > v_{tri} \text{ or } v_{Ao} = -\frac{V_d}{2} \text{ if } v_{control} < v_{tri}.$$

where V_d is the dc bus voltage value in the input of the inverter.

The full-bridge topology has four switching blocks. In the PWM with bipolar voltage switching, the diagonally opposite switches are switched as switch-pairs 1 and 2, respectively. The inverter output v_o is shown in figure 3.13 and it can be observed that the voltage switches between $-V_d$ and $+V_d$ voltage levels.

$V_{control}$ V_{tri}

0 t

$\left(\dfrac{1}{f_s}\right)$

(a)

v_{Ao}

$v_{Ao,\ fundamental} = (v_{Ao})_1$

0 t

$\dfrac{V_d}{2}$

$-\dfrac{V_d}{2}$

$t = 0$

$\left\{\begin{array}{l} v_{control} < v_{tri} \\ T_{A-}:\ \text{on},\ T_{A+}:\ \text{off} \end{array}\right\}$

$\left\{\begin{array}{l} v_{control} > v_{tri} \\ T_{A+}:\ \text{on},\ T_{A-}:\ \text{off} \end{array}\right\}$

(b)

$\dfrac{(\hat{V}_{Ao})_h}{V_d/2}$

1.2
1.0
0.8
0.6
0.4
0.2
0.0

$m_a = 0.8,\ m_f = 15$

1   m_f $2m_f$ $3m_f$

$(m_f + 2)$ $(2m_f + 1)$ $(3m_f + 2)$

Harmonics h of f_1 ⟶

(c)
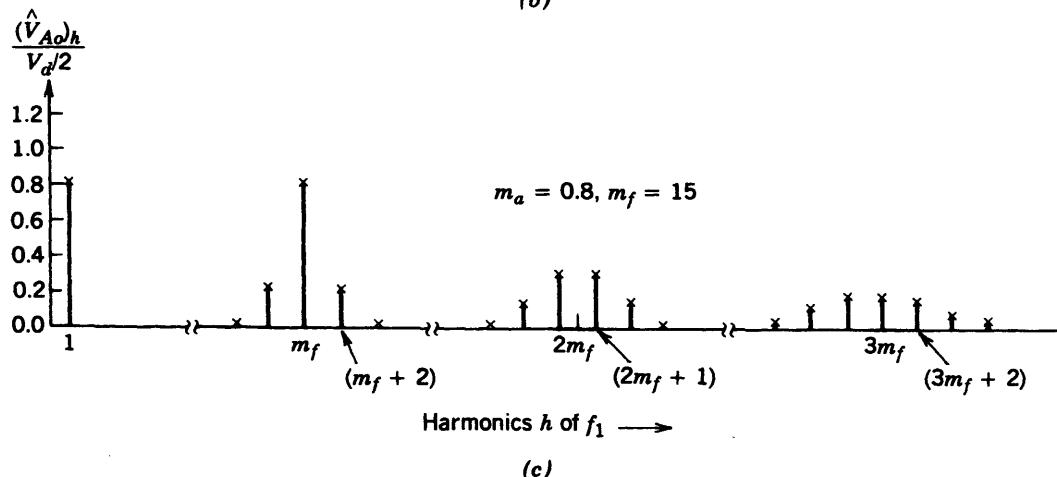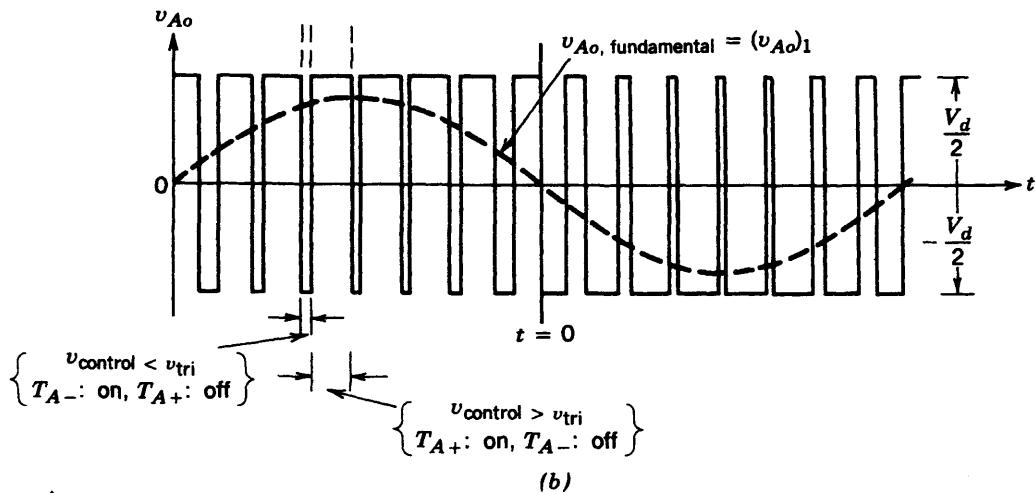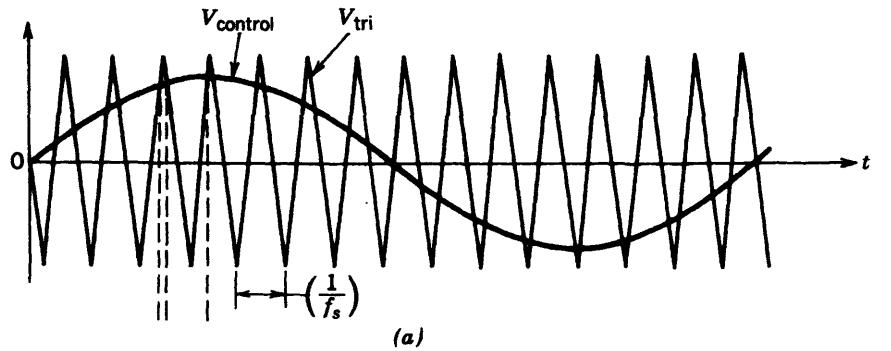
* **Figure 3.12 (a) Switching mode, (b) output voltage modulated PWM signal and (c) harmonic spectrum of a single-phase half-bridge inverter**
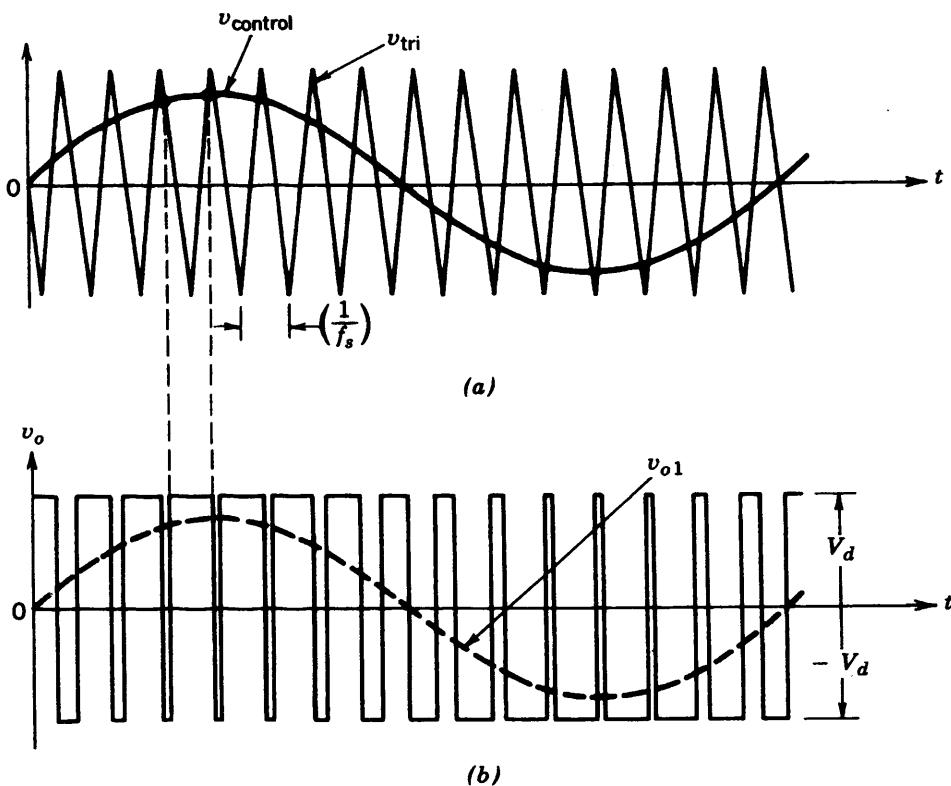
Figure 3.13 (a) Switching mode and (b) output voltage modulated PWM (bipolar) signal of a single-phase full-bridge inverter

In PWM with unipolar voltage switching, the switches of the full-bridge inverter are not switched simultaneously, as in the bipolar scheme. Here the legs of the full-bridge inverter are controlled separately by comparing v_{tri} with $v_{control}$ and $-v_{control}$, respectively. As shown in figure 3.14, in this type of PWM scheme, when switching occurs, the output voltages change between 0 and $+V_d$ or between 0 and $-V_d$ voltage levels. For this reason, this scheme is called pulse-width modulation with unipolar voltage switching and has the advantage of effectively doubling the switching frequency as far as the output harmonics are concerned, compared to the bipolar voltage switching scheme. The harmonic spectrum of the output voltage appears as sidebands of twice the switching frequency. Therefore, the frequency modulation mf is even in a single-phase inverter with unipolar voltage switching.
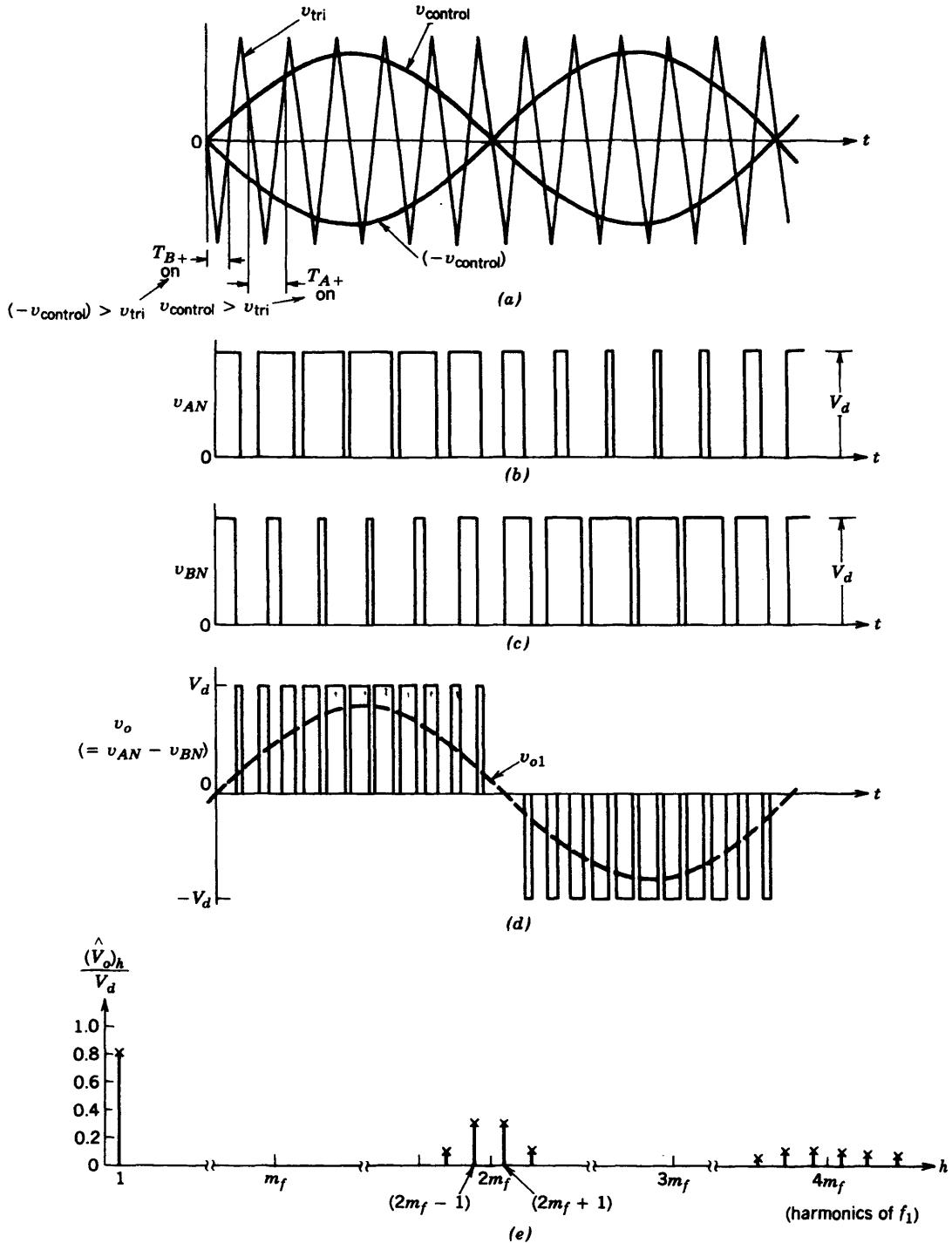
Figure 3.14 (a) Switching mode, (b) (c) output voltage of inverter leg (A and B) with respect to the negative dc bus N and (d) output voltage modulated PWM (unipolar) signal and (e) harmonic spectrum of a single-phase full-bridge inverter

3.11 Three-phase inverter

As with the single-phase inverter, the object of a pulse-width modulated three-phase system is to shape and control three-phase output voltages in magnitude and frequency with an essentially constant input voltage. To obtain balanced three-phase output voltages in a three-phase pulse-width modulated (PWM) inverter, the same triangular voltage waveform is compared with three sinusoidal control voltages, which are 120o out of phase, as shown in figure 3.15.
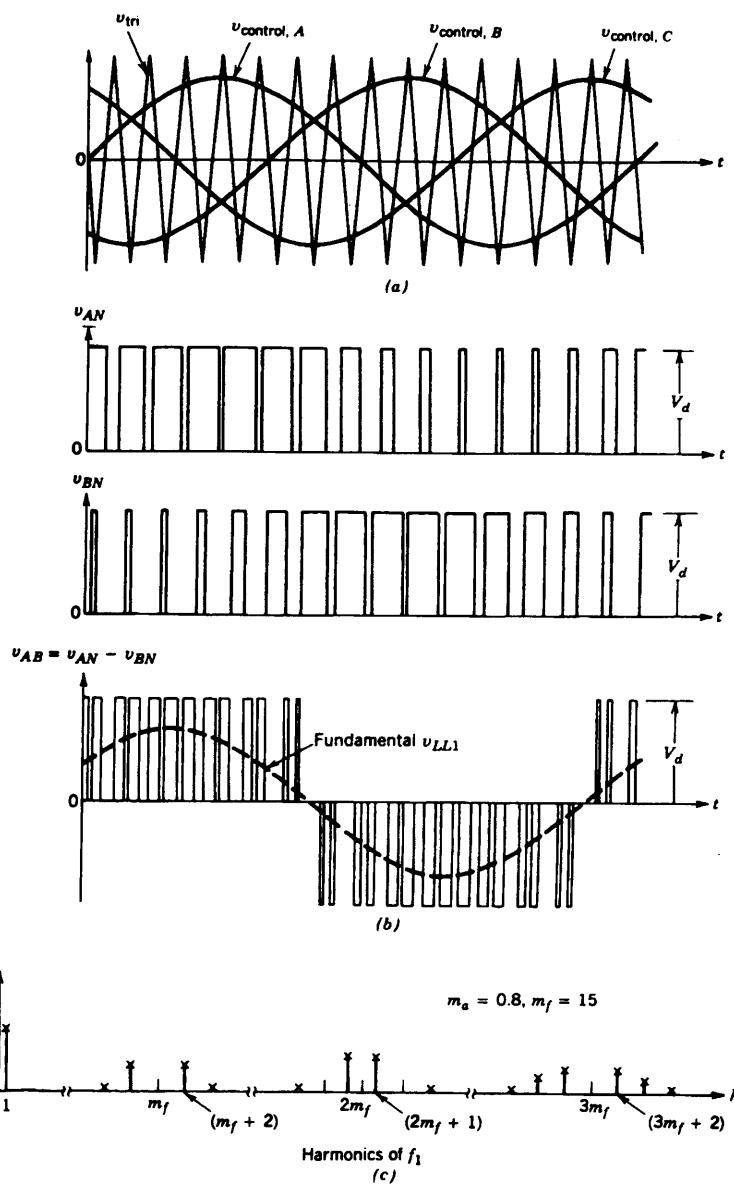
Figure 3.15 (a) Switching mode, (b) output voltage modulated PWM signal and (c) harmonic spectrum of a three-phase inverter.

3.12 Linear modulation and over-modulation

In the linear region ($m_a \leq 1.0$), the fundamental frequency component in the output voltage varies linearly with the amplitude-modulation ratio m_a. In PWM over-modulation ($m_a > 1.0$), the peaks of the control voltages are allowed to exceed the peak of the triangular wave. Unlike in the linear region, during this mode of operation the fundamental frequency voltage magnitude does not increase proportionally with m_a. Figure 3.16 shows the *rms* value of the fundamental frequency line-to-line voltage V_{LL1} plotted as a function of m_a. As with the single-phase PWM, for sufficiently large value of m_a, the PWM degenerates into a square-wave inverter waveform.
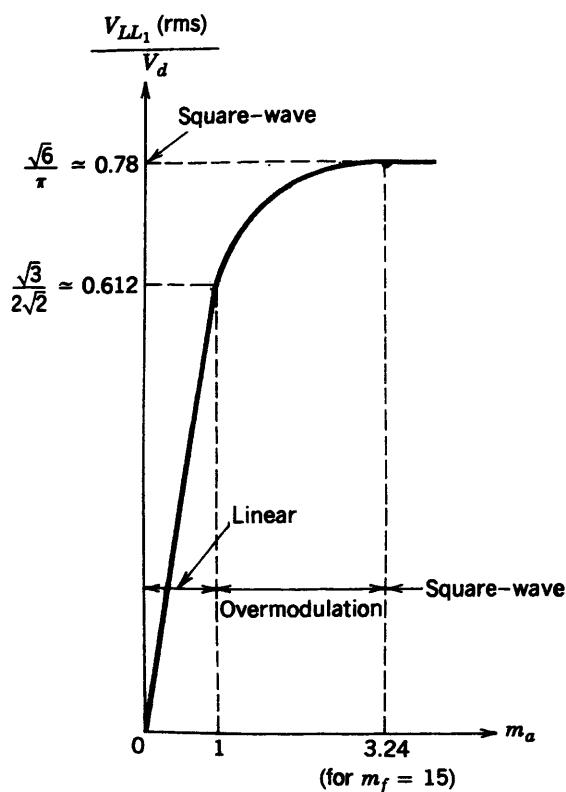
Figure 3.16 Three-phase inverter V_{LL1}/V_d ratio as a function of ma, where V_{LL1} is fundamental frequency line-to-line voltage and V_d is the dc bus voltage [3.4]

REFERENCES FOR CHAPTER 3

[3.1] M. E. El-Hawary, "Principles of machines with power electronics applications", Prentice-Hall, 1986

[3.2] J. Holtz, "Pulse with modulation for electronic power conversion", Proceedings of the IEEE, vol.82, No.8, Aug.1994, pp. 1994-1214

[3.3] R. Valentine, "Motor control electronics handbook", Mc Graw-Hill Handbooks, 1998

[3.4] Mohan, Undeland, Robbins, "Power electronics: converters, applications and design", John Wiley and Sons, 1989

[3.5] A. Boglietti, P. Ferraris, M. Lazzari, M. Pastorelli, "Iron loss measurement with inverter supply: a first discussion to define a standard methodology", IEEE Transaction on Magnetics, vol.31, no.6, November 1995, pp 4006-4008.

[3.6] W. Shepherd, L.N. Hulley, D.T.W. Liang, "Power electronics and motor control", Cambridge University Press, 2nd edition, 1995

CHAPTER 4

THEORY OF STATOR WINDINGS

4.1 Introduction

The winding of a motor conveys electrical energy to the stator, and is concerned with emf induction and the development of magneto-motive force (mmf). The ac armature winding develops emfs in a number of phases when associated with a heteropolar magnetic field. The emfs are normally equal in magnitude and correctly displaced in a time-phase relationship. The winding is compose of conductors in slots spaced around the periphery of the air gap, connected together at the ends, and grouped to form separate phase windings. When excited the phase winding combination should produce an mmf that is, as far as possible, sinusoidally distributed in the air gap. [4.1]

The operation of a polyphase induction motor depends upon the creation of a rotating magnetic field. This is accomplished by matching the number of winding phases and their phase displacements of currents. This implies that the two phases will have two winding phases that are displaced by 90 electrical degrees and that a three-phase motor will have three winding phases that are displaced in space by 120 electrical degrees. [4.2]

It is significant that a polyphase squirrel cage motor may be designed to operate on either two standard voltages sources, one twice the other. This is readily accomplished by merely connecting the winding properly to correspond with the available line voltage, such as 460 or 230 volts. Manufacturers generally take advantage of this well-established practice by bringing out the required number of terminal leads for interconnection, a practice that makes it possible to reduce the number of stock motor and minimize design and service problem. It is, in fact, often simple matter to reconnect the winding of a given motor to fulfil one or more combination of voltages, frequency and speed. [4.2]

Coils used for polyphase induction motor windings are for the most part similar to that of dc armature; they are moreover, installed, though are not connected in much the same way for the both types of machines. Also, since slotted cores are always used for ac windings, it is imperative that there be a proper number of slots for the phase-pole combination of the motor. For symmetrically placed windings the number of core slots is a multiple of pole× phase. Interconnection between the coils then follow definite patterns which, when clearly understood, simplify practical winding procedure. [4.2]

Figure 4.1 shows the stator lamination cross section of an induction motor. The windings are embedded in the slots of the stator core.
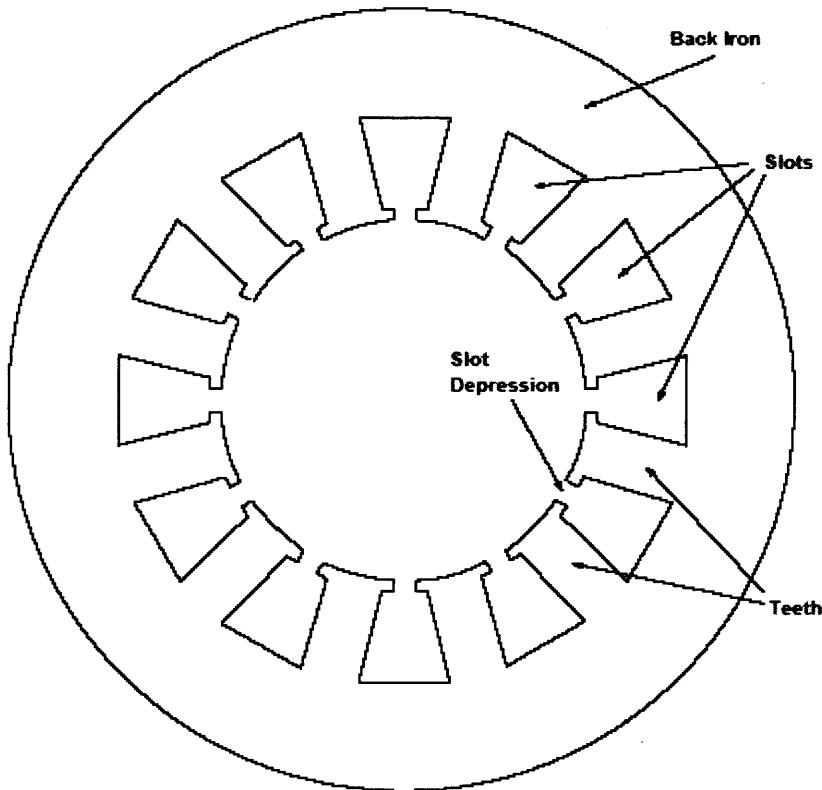
Figure 4.1 Stator lamination cross-section

4.2 The stator coils

A coil of an induction motor is as shown in figure 4.2.
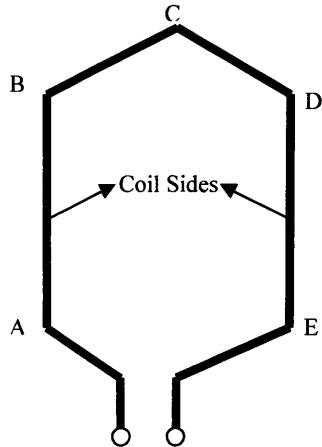
Figure 4.2 Coils in Induction motor
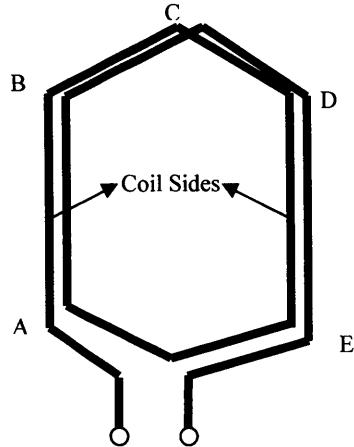
Figure 4.3 Two Turn Coil

One turn consists to two conductors. In figure 4.2, the two conductors are AB and DE. One coil may consist of any number of turns; example in figure 4.2 one coil has one turn, in figure 4.3 once coil has two turns. The number of turns in any particular coil decides the designation, example a coil having one turn is called single turn coil. Similarly the coil may designated as 2-turn coil, 3-turn coil or N-turn coil depending upon weather it has two turns, three turns or N-turns respectively. A multi turn (N-turn) coil is one, which has more than one turn.

4.3 Pole pitch and coil pitch

The term pitch indicates a particular method of measurement in terms of coil sides, teeth etc. A pole pitch is defined as peripheral distance between identical points on two adjacent poles, see figure 4.4a and figure 4.4b. Pole pitch is always equal to 180° electrical.
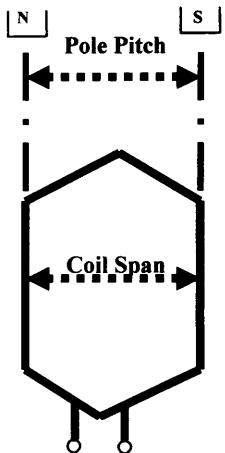
Figure 4.4a Full Pole Pitch   **Figure 4.4b Short pitched coil**
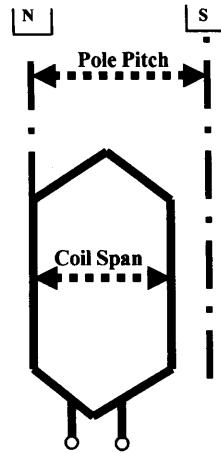
The distance between the two coil-sides of a coil is called coil-span or coil-pitch. It is expressed in terms of teeth, slots or electrical degrees. [4.3]

4.4 Open-circuit winding

All winding used in the polyphase induction motor are open circuited; this means that the ends of each phase of two of three phase winding are, in effect, free and are closed only when connected to the source of supply. The fact that the polyphase ac windings do not close is not always apparent, because the individual phases are interconnected and often, as in the delta connection, each phase is actually closed through other two. When each winding phase is considered independent of the others, however, the open-circuit designation is correct. [4.2]

4.5 Types of winding

Three general coil constructions are employed for polyphase induction motor. They are designated as lap, wave, and concentric coils and, when suitably interconnected, are called, respectively, lap, wave, and concentric coil windings. Figure 4.5 shows the lap and wave coil windings. The difference between them is only the manner in which the coil ends are connected. The leads emerging in lap windings are bent inwards and that of the wave windings are outwards. In concentric winding the coil concentricity is maintained as shown in figure 4.6. [4.2]

——Coils   — — — Interconnections
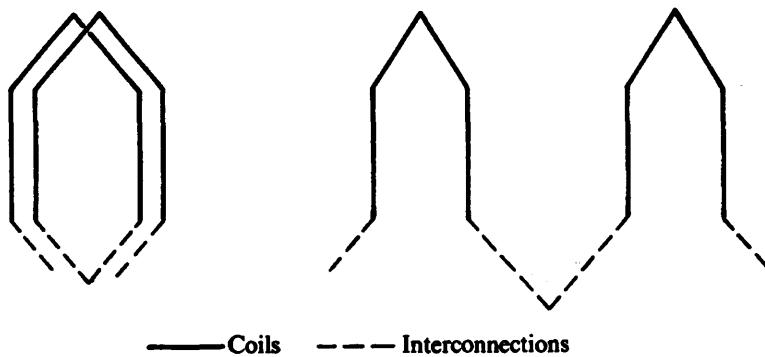
Figure 4.5 Lap and Wave connection
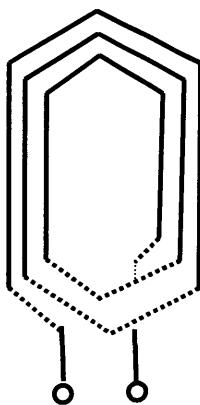
Figure 4.6 Concentric Winding

The lap winding is most frequently used on stators, while the wave winding is usually preferred for rotors of wound-rotor machines. The concentric winding has limited use in practice, although it is widely used in single phase motor and some large diameter ac generators.

All the coils of a lap or wave winding are identical, although those employed for concentric coil winding have several shapes and sizes. The coils are, however, placed in the slots of the core with complete regularity.

4.6 Single layer and double layer winding

According to the number of coil side occupancy of the slots, the windings are divided into single layer and double layer types. In the single layer winding one coil side occupies one slot of the stator and in double layer winding two coil sides occupy one stator slot.

The main difference between single layer and double layer windings is in the arrangement of their overhang. In the single layer winding the coils sides are arranged in groups. This is possible only by having individual coil groups of different size and shapes from the other sets. This means that the single layer winding requires coils of differing shape and size. All this adds to cost of single-layer windings. Single-layer windings are usually only used in very small machines.

For double layer windings to be mechanically and electromagnetically symmetrical, it is obviously necessary that the same sides of all coil occupy the upper halves of the slots and that the corresponding other sides be placed in the lower halves of the slots. To fulfil this important requirement, it is necessary to form the coils with 'knuckle' bends at the front and rear. This is clearly seen in the form-wound coil of figure 4.7.
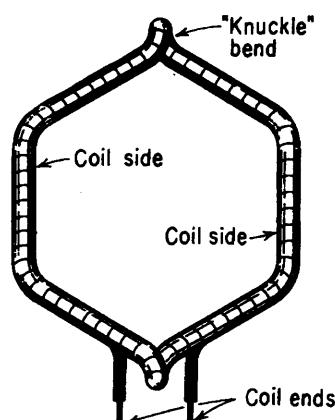
Figure 4.7 Coil assembled for double layer winding

The armature-winding techniques for this kind construction are well established and used. An important point in this connection is that all coils are identical and occupy exactly similar positions, top and bottom, in the slot to provide an excellent degree of uniformity.

The fact that lap and wave windings for poly-phase induction are double-layer means that the total number of coils will always be exactly the same as the number of core slots. A sketch of multi turn lap coil and the position of the coil sides in the slots of a double layer winding are illustrated in figure 4.8. [4.2]
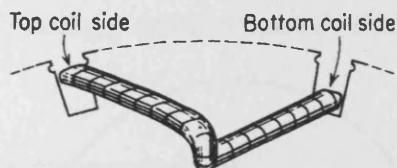
Figure 4.8 Position of two coil sides in double layer winding

The advantages of double-layer winding over single-layer winding are as follows:

    (a) Easier to manufacture and lower cost of the coils

    (b) Fractional-slot winding (slot per pole per phase is not an integer) can be used

    (c) Lower leakage reactance and, therefore, better performance of the machine

    (d) Better emf waveform.

4.7 Connecting the three-phase motor with double layer winding

All three-phase motors are usually wound with as many coils as slots. These coils are so connected as to produce three separate windings called phases. The number of coils in each phase must be one third of total number of coil in the stator. Therefore, if for example a three-phase motor has 36 coils, each phase will have 12 coils. These phases will have 12 coils. [4.4]

All the three-phase motors have their phases arrangement in either a star (**Y**) connection or delta (Δ) connection. A star-connected three-phase motor is one in which one end of each phase are joined together as shown in figure 4.9. [4.4]
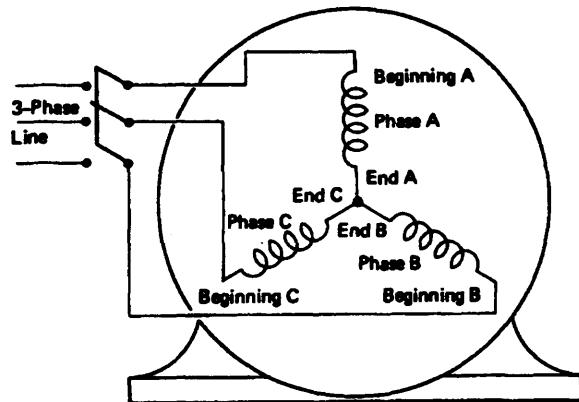
Figure 4.9 Star connected three-phase induction motor stator winding

Figure 4.10 shows a correspondingly delta connected winding.
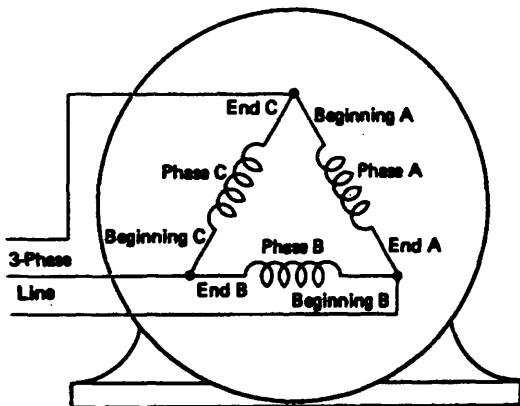
Figure 4.10 Delta connected three-phase induction motor stator winding

4.8 Poles

In the motor under discussion, the coils are connected to produce four poles. Thus in 36-coil four pole motor each pole consists of nine coils as shown in figure 4.11.
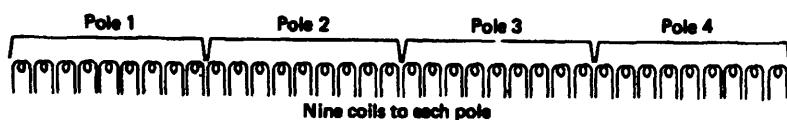
Figure 4.11 A 36-coil, three-phase motor with coils divided into poles

The arrangement showed in figure 4.11 is shown in more detailed in figure 4.12 for a lap winding. To the eye the coils appear as shown in figure 4.12. To simplify the connection process, each coil can be eliminated from the drawing so that only two leads if the coils are shown. Figure 4.13 is such a simplified diagram. [4.4]
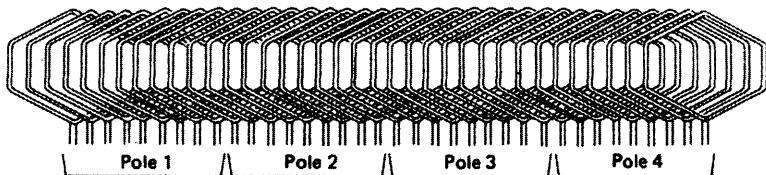
Figure 4.12 True shape of coils divided into poles
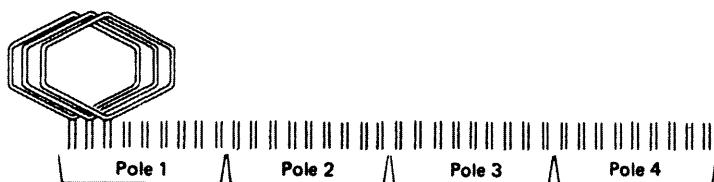
Figure 4.13 A simplified diagram of coils in a three-phase, four-pole motor

4.9 Group

A group is defined number of adjacent coils connected in series. In all three-phase motor there are always three groups in each pole, one of each phase. This section of three coils is often called as pole-phase group. Three groups in one pole are shown in figure 4.14. Another view of same connection is shown in figure 4.15.
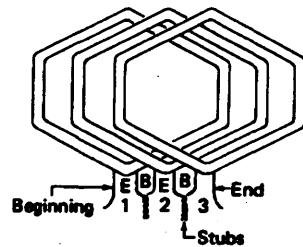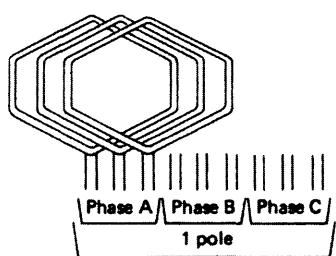
Figure 4.14 Three groups in one pole   **Figure 4.15 Coils connected in series for a group**

Coils are connected in a group when they are individually wound. When coils are group-wound, the group are automatically formed by the method shown in figure 4.16. Most motor are group wound. [4.4]

Group removed from form
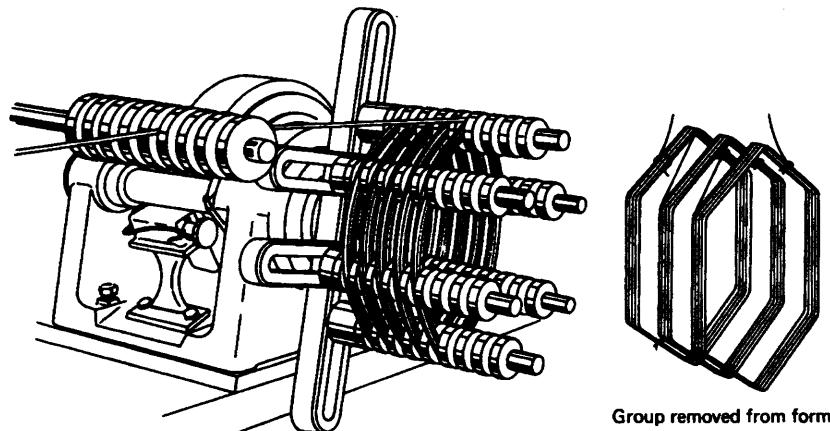
Figure 4.16 Method of winding coils in groups [4]

4.10 Connecting the coils into groups and phases

When the number of coils in each group is known, the coils can be connected into groups shown in figure 4.14 and figure 4.15, or they can be wound into groups, as shown in figure 4.16, thereby eliminating connections between coils. The coils are then connected in star or delta form and the direction of current are shown in the figure 4.17 and figure 4.18 respectively.
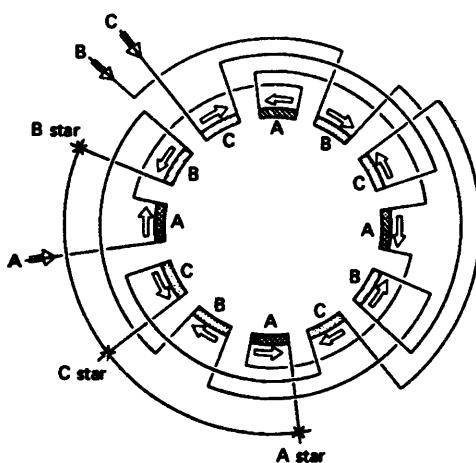
Figure 4.17 Circular diagram for current flow in star connected three-phase winding [4.4]
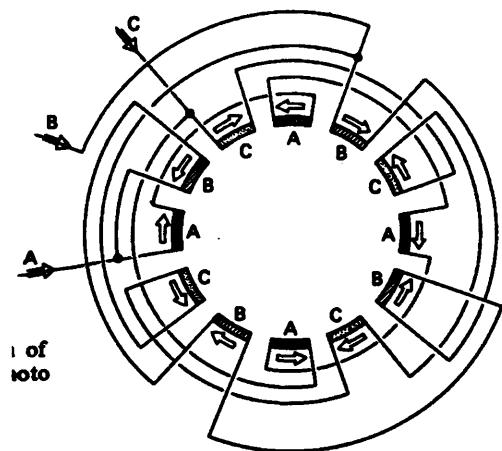
Figure 4.18 Circular diagram four-pole, three-phase delta connected motor [4.4]

REFERENCES FOR CHAPTER 4

[4.1] M. G. Say, "Alternating current machine", Longman Scientific and Technical, fifth edition, 1983

[4.2] C. S. Siskind, "Induction Motor, Single-phase and Poly-phase", Mc Graw-Hill, 1958

[4.3] P. S. Bimbra, "Electrical Machinery", Khanna Publications, fifth edition, 1997

[4.4] R Rosenberg, "Electric Motor Repair", Rinehart Press, San Francisco, 1970

CHAPTER 5

PREVIOUS WORK ON INDUCTION MOTOR LOSSES AND HARMONIC COMPENSATION OPERATION WITH NON-SINUSOIDAL SUPPLY WAVEFORMS

5.1 Introduction

Prior to the advent of solid-state controllers for the speed control of induction machines, the supply voltage was sinusoidal in nature, being practically free from time harmonics. The standard integral slot winding, having a similar pattern of conductors in each phase winding, has been used with the machine giving reasonably good performance. At the present time, induction motors are widely supplied with several types of solid state adjustable voltage- frequency controllers with a wide range of operating features. However, in many case, the motor has to be derated because of the harmonic effect due to the non-sinusoidal nature of voltage supply. The magnitude and distribution of additional losses and the related motor derating, in steady state, depends on the harmonic contents of the applied voltage and on the motor design.

The output voltage of present day static controllers deviates substantially from sinusoidal form and contains a wide spectrum of time harmonics of which lower order components predominate in general, having frequency closer to the wanted output frequency and the sub-harmonics in particular, are found potentially objectionable in practice and are at the same time difficult to filter them out. Besides directly reducing the rating of the machine, these time harmonics produce other undesirable effects on the performance.

Attempts have, however, been constantly made to modify the design of controller circuit for improving the waveform of the output voltage and to modify the motor design itself to reduce the harmonic effect on the performance. The success has been achieved to a limited extend at the cost of added complications, which has reduced the reliability and increase the cost of controller unit besides causing an increase in switching losses.

This chapter gives a state-of-art-discussion of the performance of induction motors operating on non-sinusoidal supply waveforms, highlighting the analytical and technical considerations as well as various issues addressed in the literature towards the practical realization of this technology for better drive stability with improvement in performance. A number of publications are reviewed and classified into four sub sections.

5.2.1 Modelling and analysis

The basic paper for induction machine analysis has been prepared by Stanley [5.1]. Later on, many researchers made contributions to the basis of the machine model given by Stanley with some modifications.

Hughes and Alderd [5.2] have suggested a general model for transient and unbalanced operation of two and three-phase induction machines. The machine equations are expressed with respect to αß–dq coordinates. The model is simulated using an analogue computer and the obtained results are compared with practical values.

Sarkar and Berg [5.3] have presented a direct three-phase model using phase variables and a two axis models for the three-phase induction machine. The models are simulated using a digital computer. The machine performance under a rectangular waveform supply is also included.

Jacobides [5.4] has reported the model of a drive consisting of a three-phase induction motor fed from a full bridge cycloconverter. The model based on phase variables and the Gaussian elimination method is used to reduce the order of the connecting matrix.

Murthy and Berg [5.5] have presented a dynamic model based on instantaneous symmetrical component theory. The model is used to obtain the transient behaviour of thyristor-controlled three-phase induction motors. The model covers most of the operating modes and the analysis is done without reference to the rotor position.

Krause and Lipo [5.6] [5.7] [5.8] [5.9] and many other researchers have reported different analytical techniques based on phase variables and reference frame transformations for three-phase induction machine. Various machine and supply conditions have been included.

Ueda et al. [5.10] have studied the effect of supplying the machine from a variable frequency source from the point of view of stability. The effect of machine parameter variation on the machine stability has been discussed and clarifies that for non zero stator resistance, the motor become unstable, however the existence of transient inductance works to suppress the instability and stabilize of the motor. The analysis of the induction motor verifies that the unstable range can be determined analytically.

Neto et al. [5.11] have presented a mathematical model of a three-phase induction motor using phase variables. The model is based on the harmonic impedance concept and accordingly the voltage and torque equations are derived from which the time and space harmonics can be studied. Two cases are included in the analysis, supplying the machine from a sinusoidal supply and from non-sinusoidal supplies using PWM inverters. It is also shown that the torque oscillations in steady state are higher with a sinusoidal source than with the PWM inverter.

Toliyat et al. [5.12] [5.13] have developed an analytical method for modelling the multiphase cage induction motor. The model considers the mmf harmonics using the winding function approach. It is based on the geometry of induction machine and the physical layout of all the windings. This model can simulate the transient and steady state performance of induction motors, including the effect of static rotor eccentricity. The only drawback of this model is that the effect of stator and rotor slots is not taken into account. The model is used effectively to simulate various types of machine faults such as asymmetry in the stator winding, air gap eccentricity and rotor bar faults.

Joksimovic and Penman [5.14] have presented an induction motor model based on a winding function approach to investigate the relation between machine faults and the current harmonics. One of the common methods used to simulate the supply faults and unbalance in stator and rotor circuit is the symmetrical component method [5.35].

Result shows that the frequency components at 150 Hz (3rd harmonic) increase under the action of inter-turn short-circuit conditions. It is also demonstrated that under short circuit conditions, a significant increase in rotor slot harmonic occurs.

Oguchi [5.15] has reported a closed-form, analytical solution for the current and torque waveform for a three-phase induction motor, supplied with a multiple phase-shifted voltage source inverter system. Motor performance, such as the torque ripple factor and the peak stator current ratio, has been calculated for the inverter output voltage waveform with 6–48 steps. A guideline for the design of multiple inverter systems has been given and a comparison between motor performance of multi-stepped voltage-fed and a PWM voltage-fed designs has been made.

Bonnet [5.16] has reported the analysis of the impact of the PWM inverter voltage waveforms on ac induction motors. The effects of the maximum voltage, rate of rise of voltage (dv/dt), switching frequency, capacitors, resonance and harmonics have been considered in the study. But this study doesn't take into account the distortion on the line side of the adjustable speed drive, only the load side.

Wang and Liu [5.17] have discussed the steady state harmonic modelling and simulation of a cycloconverter drive system (CSD). The operation and control of a cycloconverter drive and a synchronous motor load were modelled in the time domain. The theme of this paper is to understand harmonic problem associated with a CDS from an integrated point of view, with special attention given to harmonic filtering and cancellation effect of converter coupling transformers. The study showed that the zigzag connection of a transformer, which cancels the current harmonic, didn't show a significant effect when compared to the other types of connections used in the experiment. It also showed that delta-star connection is less preferable for a CSD application as it injects more harmonics into the power system. Results also suggested that the amount of harmonic does not change much at rated speed or above but become large below the rated speed of the motor.

Dell'Aquilla et al. [5.18] have presented an analytical method to model and calculate the line side currents produced by variable speed induction motor drives. The authors say that the function of the d.c link capacitor in the inverter is not only to limit the

ripple in the inverter input voltage but also to prevent a large part of the input inverter harmonic current from flowing in the line. The authors claim that the method has the great advantage of being suitable for every type of variable speed drive with a diode bridge rectifier and a d.c. link filter. They also state that this method gives correct evaluation of the line currents for every set of parameter and every PWM modulation technique for VSI inverter.

5.2.2 Induction motor losses on non-sinusoidal supply

Doggett and Queer [5.19] for first time in 1929 have presented the preliminary investigation of an induction motor operation with non-sinusoidal impressed voltages and suggested that for a known pattern of non-sinusoidal supplies, the voltage profile can be analyzed into a fundamental component and a series of time harmonics. If magnetic saturation is neglected, a motor operating on such a supply system may be regarded as a linear device and the principle of superposition can be applied. The overall response to the non-sinusoidal voltage is then obtained as an aggregation of responses to the individual components. Klingshirn and Jordan showed the performance of a three-phase induction motor performance under a non-sinusoidal voltage source [5.20]. In 1968, Chalmer and Sarkar studied the induction motor losses due to non-sinusoidal supply waveforms [5.21]. In 1972 and 1979, Linders investigated the effects of poor quality power sources on ac motors and suggested the hidden costs and containment due to the distorted waveforms [5.22] [5.23]. Raphael (1977) discussed the additional losses and torque pulsations in PWM inverter-fed squirrel-cage induction motors [5.24]. In 1986, Cummings simplified the harmonic equivalent circuit and proposed a method to estimate motor loss and temperature rise [5.25]. In 1987, Fuchs et al. investigated the sensitivity of electrical appliances to the harmonics [5.26].

Sen and Landa in 1990, proposed the derating operation under waveform distortion [5.27] according to the enclosure of an induction motor. They used derived loss equation to develop the computer programme for loss calculation. Two types of motor enclosures were used with three cases of 5% voltage distortion. Results shows that the 2nd harmonic in a non sinusoidal supply has a most pronounced effect on the temperature rise and so the restriction of the second harmonic should be included in

the harmonic established by IEEE Standard 519 and in some cases the derating should be considered less than 5%. They also conclude that the efficiency plays an important role in derating of a motor and suggest that smaller machines (less than 5 hp) are affected more by the harmonic than larger machines. But this paper does not consider skewing and the analysis is limited to a full load study.

In 1993, Wagner et al., presented a summary of the state-of-knowledge of the effects of harmonics on power system equipment and load [5.28]. They suggested that the losses in an electrical machine are dependent on the frequency spectrum of the applied voltage. The core and stray losses become more significant in an induction motor driven by an inverter producing high harmonic frequencies.

Lee and Lee in 1999 reported the effects of non-sinusoidal voltage on the operating performance of a three-phase induction motor [5.29]. They used a load test to investigate the performance of a three-phase induction motor under different voltage distortion factors. They used voltage waveform of voltage distortion factor (VDF) 5%, 10% and 15%. Results shows that the lower order harmonics result in low motor efficiency, and a larger VDF causes lower efficiency. The experimental results show that the difference between the largest and the smallest harmonics is 3% when VDF=10%. At 10% VDF it has been noticed that the lower order harmonic below five affect the performance of the induction motor more severely than the harmonic order above five. They conclude that when studying the impact of the harmonic on a three phase induction motor, one must consider both odd and even order harmonics particularly harmonic order below five. If the arrangement of transformers in a distribution system cannot eliminate the zero-sequence harmonic completely the effect of zero-sequence harmonics on induction motors must be considered.

There have been many studies of iron losses in induction machines. The equivalent circuit has been modified in various ways to improve the accuracy of the loss estimate for wide ranges of operating conditions. In the case of a distorted voltage waveform supply, it is not possible to use, in general, such a model due to the non-linear behaviour of the material and the complexity of the phenomena involved. One such modification of the standard equivalent circuit representation of the motor for the kth harmonic of the voltage waveform proposed by Vamvakari et al. [5.30] is shown in

figure 5.1. In this figure, Vk denotes the voltage harmonic of order k, Rs the stator winding resistance, Rrk the corresponding rotor resistance, Xls, Xlr the stator and rotor leakage reactances and Xm is the magnetizing reactance at fundamental frequency. Rmk is the core loss resistance. Rl_{sk} and Rl_{rk} are resistors representing harmonic iron losses associated with stator and rotor leakage fluxes, respectively, placed in parallel with corresponding leakage reactance terms. This has been tested by supplying the voltage waveform with non negligible low order higher harmonics of 5% of third harmonic and 5% of 5th harmonic. It can be been seen that the modified equivalent circuit motor representation provides a good predetermination of the induction motor current peak value when supplied by a distorted voltage waveform. However, it introduces a slight phase lead with respect to the current estimated which indicates model limitation for harmonic loss predetermination.
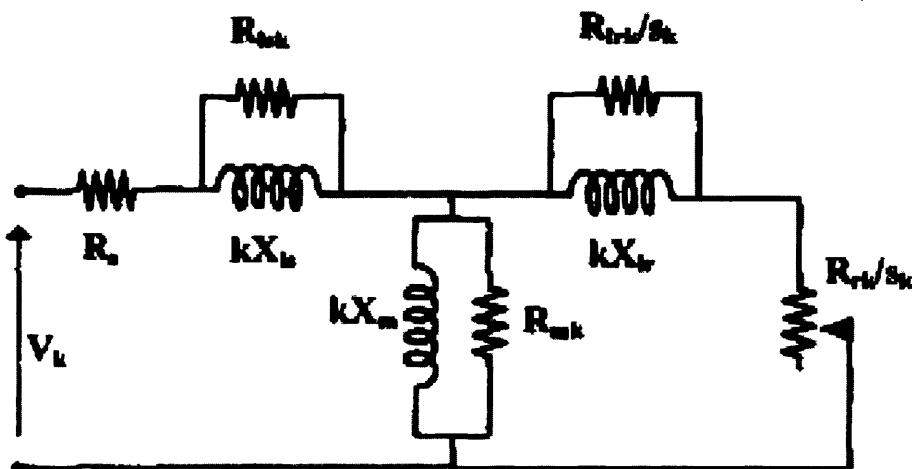
Figure 5.1 Modified equivalent circuit of an induction motor for the kth order voltage harmonic component [5.30]

Iron loss models suitable for use in dq-models of the induction machine have also been studied [5.31] [5.32]. These lumped models of iron loss are useful but do not allow the details of iron losses to be studied.

Some studies have specifically addressed losses arising from inverter supplies [5.33] [5.34] but are limited in nature. There are models for iron loss in thin laminations [5.30] [5.31] [5.35]. These models provide loss density results for a localized flux density expressed as a function of time.

Boglietti et al. [5.36] have reported the effect of inverter characteristics on the iron loss increment in induction motors fed by PWM-controlled converters. The inverter parameters such as modulation index, modulation waveform and switching frequency are considered in the study. The result shows that in order to reduce the iron losses it is better to operate the inverter with highest allowed modulation index as can be inferred from figure 5.2.

The switching frequency is not so important from the iron loss point of view. The modulation waveform is not so important factor for the increase in the iron loss. However this study was not about the iron loss in a practical working condition of the induction motor with an inverter, on load.
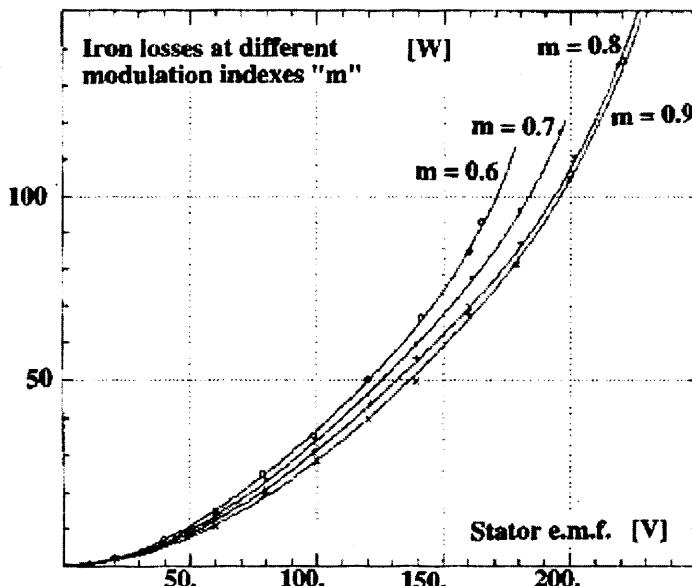
Figure 5.2 Variation of iron loss with fundamental component of output voltage V with different modulation indices [5.36]

In another study Boglietti [5.37] has given a method for evaluation of the steady state loss in medium power industrial induction motors supplied by PWM inverters. The method is based on the no-load and a short circuit test with a PWM supply and is quite simple to realize. This technique is similar to the standard no-load and short circuit tests used with a sinusoidal voltage supply. The method is based on some simple hypothesis that has been verified during the experimental tests by means of mathematical models. It is possible to compare the no-load and the short circuit tests under sinusoidal and PWM inverter supplies considering the same rms fundamental

voltage. The method has been applied to a 7.5 kW induction motor supplied by a prototype PWM Voltage Source Inverter (VSI) modulated with a ramp comparison technique at a 1 kHz switching frequency. The author claims that the results could be utilized in order to define some design criteria and the derating for standard induction motors supplied by PWM inverters.

Gerlando and Perini [5.38] have reported a methodology for the calculation of the extra iron losses occurring in the core of the inverter-fed electromagnetic devices. The results show that with increasing frequency ratio m_f, the extra iron losses due to the PWM inverter supply decreases because the eddy current losses decrease due to the reducing effect of coefficient k_{fe}. The behaviour of eddy current losses when the modulation ratio m_a increases is similar to that of the first harmonic contribution i.e. similar to that of sinusoidal operation. The authors did not explain which modulation technique is used for this modelling and the results are not experimentally proved.

Boglietti and co-workers [5.39] have presented results on grain-oriented steel and amorphous alloy wound core samples tested under sinusoidal, six-step and a PWM inverter supply at 50 Hz. For the PWM waveform, where the modulation technique and parameter were not clearly defined, a 42% increase of iron losses was measured in the case of the amorphous material and about 100% in the case of grain-oriented material which was attributed to the high eddy-current increase linked to the very particular waveform of this supply. The loss comparison was made at the same peak value of the first harmonic of the flux density. In the PWM case, where it was not possible to calculate the relationship between the first harmonic of the output voltage and the total rms output voltage, the peak value of the first harmonic of the flux density had been obtained using the output waveform of an analog integrator circuit and a digital scope (figure 5.3). It is not clear if the peak flux density of the first harmonic was used or just the peak flux density since it is necessary for a spectrum analyser to check the amplitude of the harmonic component of the induced voltages or the integrated signal (from the analog integrator).
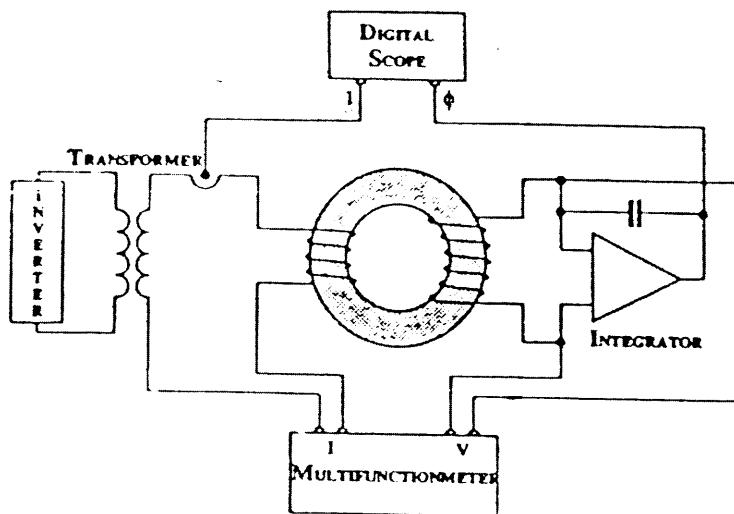
Figure 5.3 Measurement system used by Boglietti and co-workers in [5.39]

In a recent study [5.40], authors have presented a methodology for a convenient modification of induction motor equivalent circuit parameters, taking into consideration switching frequency iron losses in the case of inverter supply. The authors have also presented a modified two axes equivalent circuit as shown in figure 5.4. The methodology adopted was based on a high fidelity transient model of an induction motor simulated on a stationary reference frame, fed by an appropriately designed voltage source sinusoidal pulse-width modulated inverter, serving as a variable voltage variable frequency three phase power supply. The model includes the harmonic iron loss representation as well as the motor equivalent circuit parameter variation. The d-q transformation is used in this modelling to give the advantage of a fast convergence and to provide sufficient accuracy for greater time steps during extended transient phenomenon. The method validity has been checked by measurement on a 20 kW cage induction motor drive system.
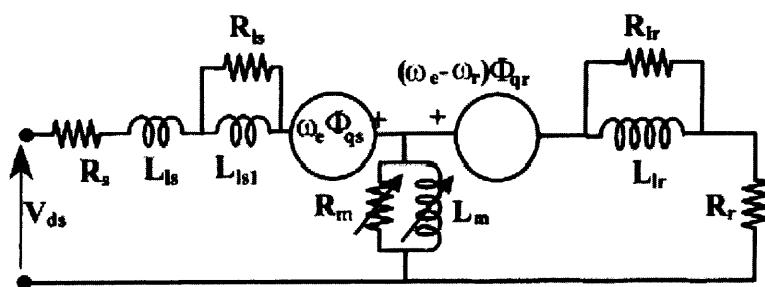
(a)
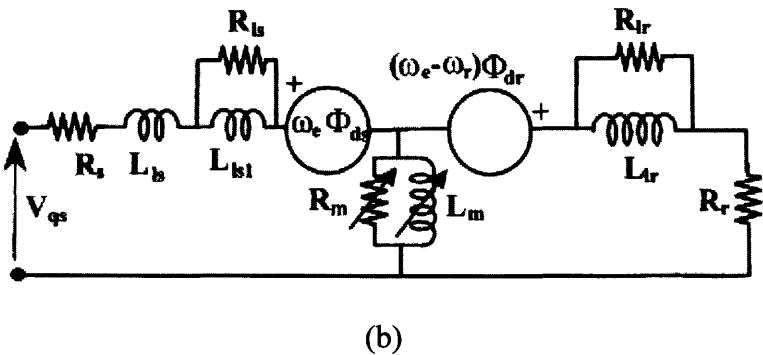
(b)

Figure 5.4 Modified equivalent circuit for the induction motor dynamic model: (a) d-axis equivalent circuit (b) q-axis equivalent circuit [5.40]

One of the recent studies by Ekram and Sarkar [5.41] discussed the effect of harmonics on inverter fed induction motors. In this study they have shown through simulation that if the number of pulses at the PWM inverter output is either small or very large then the magnitudes of the harmonic vary accordingly. In this study via simulation using C++ and Matlab it has been seen that when the number of pulses, m, is five then the lower order harmonics have significant magnitude and as m is increased between 17 and 35 then the lower order harmonics significantly reduce whereas when m is equal to 71 the lower order harmonics increased. But the magnitude of the fundamental component also has been reduced. The study is related to a 500 hp induction motor, the authors did not made clear if this applies to low rating machines.

DeWinter and Wu [5.42] presented their review on the medium voltage motor harmonic heating, torques and voltage stress when applied on variable frequency drives (VFD). The authors suggest that it is important to know the torque and the additional heating as a function of a specific motor rather than based on a hypothetical ideal motor. Generic data provided by a drive manufacturer as to the harmonic losses and the torque is of little value unless the specific motor parameters are known because motor inductance plays such a large role. They also suggest that generally technology is available to reduce the amount of harmonic heating and the torque produced by a motor linked to more sophisticated drives to less than the amount experienced as a result of normal voltage imbalance.

Emanuel [5.43] estimated the effect of the harmonic voltage fluctuations on the temperature rise of squirrel cage induction motors. In his study he suggested that the capability of a squirrel cage motor to tolerate the fluctuating harmonics with the total harmonic distortion, THD_{max}, in excess of the recommended 5% is a function of the equivalent thermal time constant of the rotor, the time integral during which the distortion voltage reaches and remains at the maximum and the frequency distribution function characterising the occurrences of distortion. The calculation provided by the author indicates that for the rotor with a thermal time constant of 60 minutes, it is possible to tolerate a total voltage distortion, THD of 4% and THD_{max} of 10% provided the duration of maximum distortion lasts for less than 36 seconds. However, the author did not measure the temperature rise under different non-sinusoidal waveforms and have not provided the background information of the theoretical modelling.

Hanna [5.44] presented the characteristic of harmonics produced by an adjustable speed drive systems, the method of reducing them, and installation examples. The author suggests that theoretically the magnitude of the harmonic in a motor depends on the stator winding configuration i.e. three-phase (connected to six-pulse system) or six-phase (connected to twelve pulse system), the harmonic reactance and the rotor damping effect. He showed in the tables (figure 5.5), the space harmonic produced in three-phase and six-phase winding arrangements. It can be seen from the figure that more space harmonics are suppressed in the six-phase winding than in the three-phase winding. So the heating in the six-phase winding is lower than the other. To understand the presence of harmonics in adjustable speed drives (ASD) he presented the two installations of a six-pulse system and a twelve-pulse system. In the first installation it is clearly seen that the current waveform is distorted and the major harmonic components are the 5th, 7th, 11th and 13th. Due to this the temperature rise under inverter supply was in excess of 150° C. This temperature rise is reduced by design modification of the rotor such as adding damper bars in the pole face, decreasing the air gap or improving airflow by replacing cooling fans. In the second case as the 5th and 7th harmonics exist and not suppressed. This is due to the variation in the voltage, difference in thyristor's firing pulse angle between multi-pulse circuits. So the authors suggest that drive design should be carefully taken into account to reduce harmonics.

Order of Space Harmonic h	Order of Time Harmonic n					
	1	3	5	7	11	13
1	$+1$		-5	$+7$	-11	$+13$
3		±1				
5	$-1/5$		$+1$	$-7/5$	$+\frac{11}{5}$	$-\frac{13}{5}$
7	$+\frac{1}{7}$		$-\frac{5}{7}$	$+1$	$-\frac{11}{7}$	$+\frac{13}{7}$
9		$\pm\frac{1}{3}$				
11	$-\frac{1}{11}$		$+\frac{5}{11}$	$-\frac{7}{11}$	$+1$	$-\frac{13}{11}$
13	$+\frac{1}{13}$		$-\frac{5}{13}$	$+\frac{7}{13}$	$-\frac{11}{13}$	$+1$

* Synchronous speed is obtained when n = 1, h = 1.

Figure 5.5a The speed and the direction of rotation of the components of the stator MMF of a three-phase winding [5.44]

Order of Space Harmonic h	Order of Time Harmonic n				
	1	5	7	11	13
1	$+1$			$-\frac{11}{7}$	$+\frac{13}{7}$
3					
5		$+1$	$-\frac{7}{5}$		
7		$-\frac{5}{7}$	$+1$		
9					
11	$-\frac{1}{11}$			$+1$	$-\frac{13}{11}$
13	$+\frac{1}{13}$			$-\frac{11}{13}$	$+1$

* Synchronous speed when n = 1, h = 1.

Figure 5.5b The speed and the direction of rotation of the components of the stator MMF of a six phase winding [5.44]

Lumyong and Chat-Uthai [5.45] proposed the technique, which allows the effect of harmonics on the performance of three-phase induction motors to be studied by using a non-sinusoidal voltage source obtained from the brushless synchronous reluctance generator. The technique is particularly suitable for testing the impact of the

harmonics on three-phase induction motors since the frequency and the amplitude of the kth order harmonic can be independently controlled. Several models of a non-sinusoidal voltage source having the fundamental with various orders of harmonics and % VDF are presented. The test results indicates that increase of % VDF, the fundamental with lower order harmonics will have an influence on the increase of input current, power and loss more than those with the higher order harmonics. At the same % VDF, fundamental with lower order harmonic will result in higher input current, power and loss than those with high order harmonics. Negative sequence harmonics will cause slightly higher power loss than positive sequence harmonics, however this effect is not significant because of the low amplitude of negative electromagnetic torque. Increasing motor load has a slight effect on the power loss of the kth order harmonic.

The various studies [5.46] [5.47] [5.48] [5.49] made on harmonic losses reveal that:

• The presence of the harmonic currents in the stator winding causes an increased copper loss. When skin effect is negligible, the stator copper loss when a non-sinusoidal supply is used is proportional to the square of the total rms current.

• The presence of harmonics also increases the fundamental component of the current slightly, due to an increased magnetizing current.

• The assumption of a constant resistance at harmonic frequencies is reasonably justified for the stator windings of the wire-wound machines. For large ac motors, there is an increase in stator resistance with frequency, which depends on the shape, size and disposition of the conductor in the stator slots.

• The skin effect is much more pronounced in the cage rotor, which exhibits a significant increase in resistance at harmonic frequencies, particularly in the case of deep bar rotors. Since the rotor resistance is a function of the harmonic frequency, the rotor copper loss is calculated independently for each harmonic.

• It is appropriate to use a reduced value of per unit reactance because the rotor leakage inductance is reduced significantly as a result of skin effect.

• The core loss in the machine is also increased by the presence of harmonics in the supply voltage and current.

• The core loss due to the space harmonic air gap flux is negligible, but the end-leakage and skew-leakage fluxes, which normally contribute to the stray load loss, may produce an appreciable core loss at harmonic frequencies. Consequently, these

effects must be taken into consideration for a motor operation on non-sinusoidal supply.

• The magnitude of harmonic loss obviously depends on the harmonic content of the motor voltage and current. Large harmonic voltages at low-harmonic frequencies cause a significant increase in machine loss and reduce efficiency.

• The higher order harmonic currents usually have small magnitudes. For such waveforms, the reduction in full load motor efficiency is not excessive.

5.2.3 Control scheme for loss minimization in induction motor drives

Selection of the level of flux in the induction motors remains an open problem from the perspective of maximizing motor efficiency and many researchers continue to work on this problem. Numerous operation schemes have been proposed by many researchers concerning the optimal choice of the excitation current or the flux level for a given operating point [5.50-5.57]. The techniques aimed at giving an improvement to the efficiency can be divided into two categories. The first category is the so-called loss model-based approach [5.50] [5.51] [5.52], which consists of computing losses by using the machine model and selecting a flux level that minimizes these losses. The second category is the power-measure-based approach, also known as the search controllers (SCs) [5.53–5.57], in which the flux (or its equivalent variables) is decreased until the electrical input power settles down to the lowest value for a given torque and speed.

Lorenz and Yang [5.50] took the copper loss and the iron loss into account to formulate the loss model. Dynamic programming is used to minimize the loss of a field oriented controlled induction motor drive during closed cycle operation. Constraints on the input current, input voltage, maximum velocity and the rotor flux are taken into account for the problem formulation. Using an objective function that depends on the drive's loss and includes constraints, they calculated the optimal flux trajectories for the vector control online. The authors conclude that acceleration (storing of kinetic energy to be consumed by the process work function) has greatest loss potential and thus, optimization should concentrate on this interval. The efficiency of the dynamically optimised (varying flux) trajectories for the whole cycle

is better than the optimal constant flux by 10% to 20% or more unless a very short interval is used.

Garcia et al. [5.51] obtained a loss model after simplifying the induction motor's equivalent circuit by deleting leakage inductance in d–q coordinates. This model is based on the theory that when the induction motor is used for adjustable speed drives it operates far from the rated conditions and so there is imbalance between the iron and the copper losses, which cause the drop in efficiency. This balance can be achieved by controlling the magnetic flux. The loss model consists of resistors reflecting iron loss, rotor and stator copper losses as a function of stator current i_{ds} stator field current and i_{qs} stator torque current in the d–q frame. This model allows an equation to be established to quantify the copper and the iron losses. Based on this equation, a loss minimization algorithm was proposed and simulated to show the possibility of energy saving.

Kioskeridis and Margaris [5.52] developed a loss model controller (LMC) for determining the optimal air-gap flux that minimise the losses of the scalar controlled induction motor adjustable speed drive. The authors suggested that although this method is based on the induction motor loss model, its implementation does not require the knowledge of the loss model. They calculated the total iron loss, copper loss and the stray loss and derived an optimal flux level that minimizes the total loss. They also said that the model can be easily implemented both for analogue and digital techniques but only the stator current measurement is required which contradicts the above statement suggesting that the loss model knowledge is not required.

In the model-based loss-minimization algorithms, the leakage inductance of the stator and rotor are usually neglected to simplify the loss model and minimization algorithm [5.51] [5.52]. However, with this simplified model, the loss minimization cannot be achieved, especially for the high-speed operation of motors, since a large voltage drop across the leakage inductance is neglected.

Kirschen et al. [5.53] proposed a solution of minimizing the input power by decreasing the flux command in steps. This is a very simple technique, but torque pulsation is unavoidable. Sousa et al. [5.54] improved the work of Kirschen et al.

[5.53] by adaptively reducing the reference flux current with the aid of fuzzy logic. They solved the torque pulsation problem by applying feed forward compensation. This method for efficiency optimization of a vector control drive uses a fuzzy controller to adjust adaptively the magnetising current based on the drive measured input power, thus yielding the true optimum operation efficiency with a fast convergence. The proposed method can be incorporated into an existing vector drive system. However, extra hardware needs to be added to the existing drive system.

Kim et al. [5.55] adjusted the squared rotor flux according to a minimum power algorithm based on the Fibonacci search method. The torque ripple is not generated in this configuration, since the speed and rotor flux are decoupled by means of non-linear control. For maximum power efficiency, the square root flux is adjusted until the measured power input reached a minimum. This method doesn't need the information of stator inductance and stator resistance. The major advantage of this modelling was that it doesn't need a voltage sensor for the identification of rotor resistance.

Moreira et al. [5.56] used the information of third harmonic components of the air gap flux to reduce the d-axis current. This signal is used to determine the resulting instantaneous position of the fundamental component of air gap flux and consequently the torque and the flux producing components of the stator current. In addition the third harmonic component is used to determine the rotor speed. So the output power of the machine can be calculated with only a single sensing wire attached to the neutral point of the stator winding. The flux producing component is adjusted to produce the minimum input power for a given output power.

Sul and Park [5.57] proposed an efficiency-maximizing technique by defining an optimal slip. The optimal slip is firstly searched for by trial and error, and stored in a microprocessor memory. Then, the control system is forced to track the optimum slip presented in a lookup table.

5.2.4 Harmonic reduction techniques

The increasing application of power electronic equipment, especially adjustable-speed drives (ASDs) in the industrial environment has led to a growing concern for harmonic distortion and the resulting impacts on system equipment and operation. Possible problems include transformer overheating, motor failures, fuse blowing, capacitor failures and malfunctioning of control. Harmonic currents are generated by the operation of non-linear loads and equipment on the power system. Voltage distortion results from the interaction of these currents with the system impedance versus frequency characteristics. The characteristics of the input current for adjustable speed drives depend on the drive type, drive loading and characteristics of the system supplying the drive. The harmonic distortion in these currents can vary over a wide range.

In the last two decades, major focus has been on harmonic reduction techniques. Some summaries on three-phase harmonic reduction technique can be found in references [5.58] to [5.69].

Domijan et al. [5.58] discussed various techniques for harmonic reduction in adjustable speed drives. They summarised the important techniques in six categories namely:

1) Phase Multiplication
2) Passive filters
3) Active filters
4) Harmonic injections
5) Harmonic mitigation technique with PWM
6) Wye-Delta transformer connection

They also suggested that the trend among researchers seems to be towards increasing utilisation of pulse width modulation (PWM) as a part of their mitigation technique, especially the ones that use current injection for the reduction or elimination of harmonics. However when the problem arises in the industry due to harmonic distortion, field engineers to a large extent use conventional filtering method.

Rastogi et al. [5.59] presented the comparative evaluation of a harmonic reduction technique, which satisfies the current harmonic limit, specified by the IEEE standard 519, and at the same time provided a regulated dc output voltage. The technique considered included the active and hybrid filters and various current wave-shaping approaches for the three-phase utility interface. They divided the harmonic reduction techniques as show in figure 5.6.
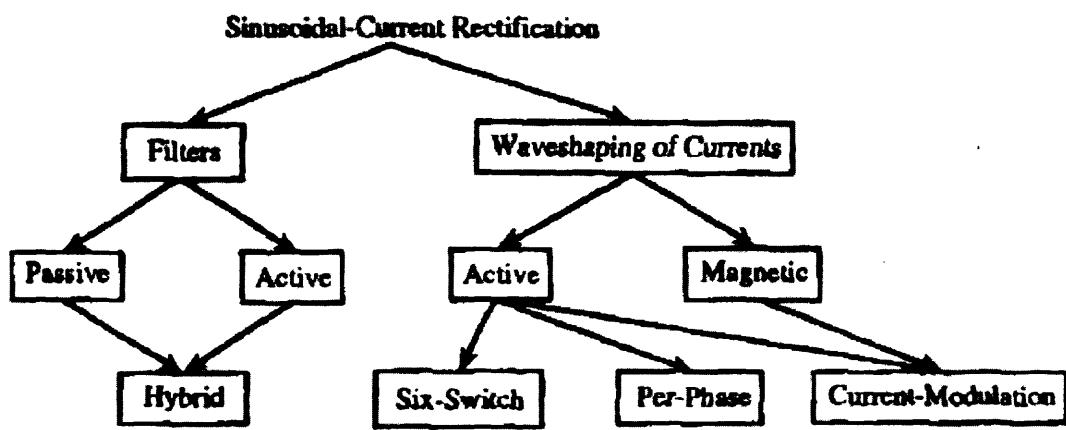

Figure 5.6 Classification of the harmonic reduction technique [5.59]

Salmon et al. [5.60] presented numerous circuit topologies, which can be used in PWM boost rectifiers. Circuit performances are highly in terms of the switch count, cost, conduction losses, the PWM waveform characteristics and the bi directional power flow capability. Three-phase topologies exist that lower the per-unit current rating of the active switching networks and lower the electrical stress on the switches. Operation of the rectifiers with low current distortion is possible with an output dc voltage as low as 1.35 times the line-to-line voltage.

The method of harmonic cancellation by mixing nonlinear single-phase and three-phase loads was presented by Hansen et al. [5.61]. The reason for mixing is that the fifth and seventh harmonic currents of a single and a three phase non-linear loads often are in counter phase. This method doesn't increase the current THD in transformer but actually lowers the THD and thereby, lowers the losses. They also suggest that care should be taken for when setting the strict limit to harmonic current

emission for the three-phase diode rectifier because of their harmful effect. Reduction of harmonics due to cancellation is shown in figure 5.7.


(a)
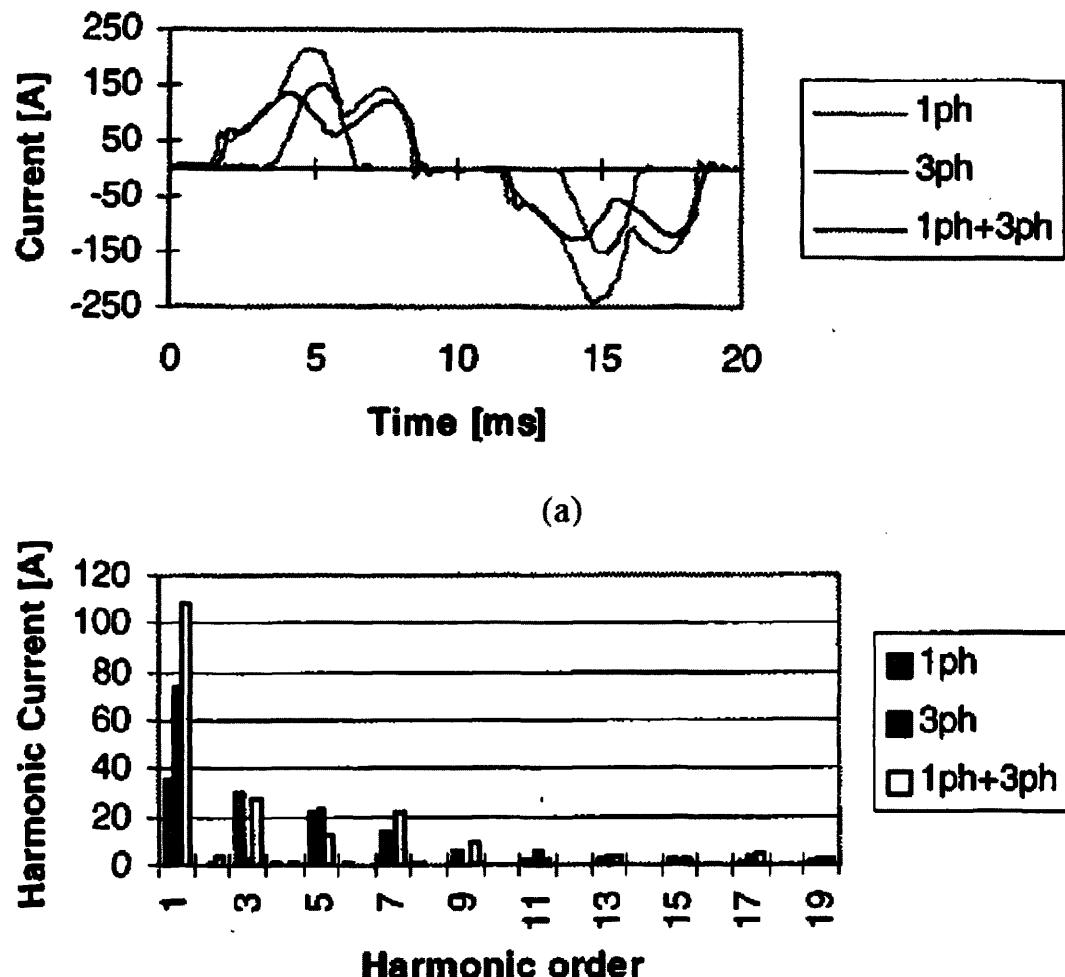
Figure 5.7 (a) Measurement of single phase, three-phase and the sum of both currents. (b) Harmonic spectrum of single phase, three-phase and the sum of both currents [5.61]

Third harmonic injection schemes for the three-phase diode rectifier for reducing the harmonic currents have produced some promising results presented by Mohan [5.62]. An approach to achieve nearly sinusoidal line current rectification of a three phase utility voltage is presented by the author. The scheme incorporates two dc-dc converters to modulate current at third harmonic frequency and then circulated through the ac-side of a diode bridge rectifier, using a zigzag transformer as shown in

figure 5.8. This interface draws input current with a harmonic distortion of less than 5% and provides regulated dc voltage at the output.
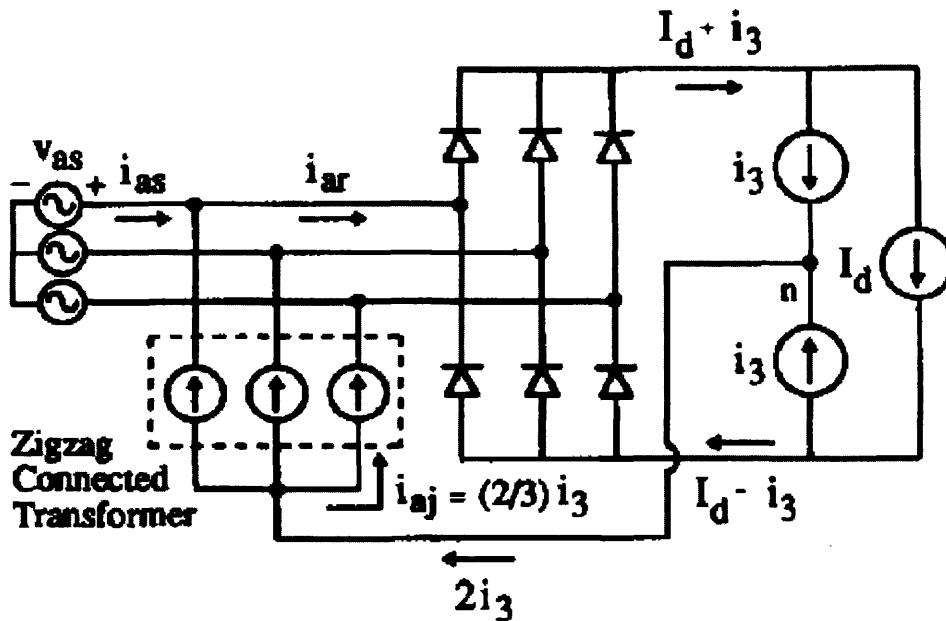

Figure 5.8 Third harmonic injection scheme [5.62]

In a study by Lee et al [5.63], a robust three-phase active power-factor-correction (PFC) and the harmonic reduction scheme suitable for the higher power applications is proposed. The system is a unique combination of a low-kilovolt ampere 12-pulse rectifier system with a single-phase boost PFC scheme to shape the input current to a near sinusoidal wave shape. It has been shown that by injecting a low kilovolt ampere (0.05Po) active current source Ix into the AIPT (active interface transformer), sinusoidal currents with 1% THD can be obtained. Further more an active PWM inverter is not directly exposed to line transients. In the event of failure of active PWM control, the proposed system reverts to 12- pulse operation with fifth and seventh harmonic cancellation in the input utility line current.

Hansen et al. [5.64] have proposed an integrated single-switch approach to improve the harmonic performance of a standard pulse width modulation adjustable-speed drive. The approach is essentially an add-on solution to a standard ASD topology and is based on circulating a third harmonic current to reduce the harmonics in the line current. The dynamic braking chopper was used to control the amplitude of the third harmonic circulating current. Input current distortion well below 15% is obtained.

Alexa and Sirbu [5.65] have presented a thorough analysis of the operation for a combined filtering system consisting of a passive filter with diodes connected in parallel with capacitors and a low-power inverter. The diode limits the voltage across the capacitor and the inverter starts to work when disturbances occur in the three-phase network, sending back to the network the excess energy taken by the capacitors from the network during these disturbances. The authors also discussed the advantages and shortcomings of the passive, active and combined filtering systems and have suggested essential modifications. The volume of the capacitors used in the case of proposed version is 25%-30% of the volume of the ac capacitors used in classical versions of passive filters with LC series circuits. It also proves that the values of the harmonic current injected into a power system can be maintained within the limit imposed by harmonic standards.

Mohapatra et al. [5.66], present harmonic elimination and suppression scheme for a dual-inverter-fed open-end winding induction motor drive shown in figure 5.9. Two isolated dc link source with voltage ratio of approximately 1:0.366 are used and this link feeding two inverter to drive the open-end winding induction motor eliminates the triplen harmonic currents from the motor phase. The PWM scheme proposed enables the cancellation of all the 5th and the 7th harmonic voltage and suppresses the 11th and 13th harmonic voltage amplitude in the motor voltage phase, in all modulation ranges. The scheme is experimentally verified for a 1-hp induction motor drive. The carrier wave of frequency of 12 times the frequency of modulating wave is used experimentally for v/f control for the entire speed range. The authors claims that the smooth and linear transition to the over modulation range is possible with this method. They also suggest that by properly choosing the frequency modulation ratio (12, 24, 48) at different speed ranges (0-50Hz) in the proposed scheme, the switching frequency of both inverters can be kept within 600 Hz and also the harmonic current amplitude can be controlled within an acceptable limit for variable speed application.

INVERTER - 1   INVERTER - 2
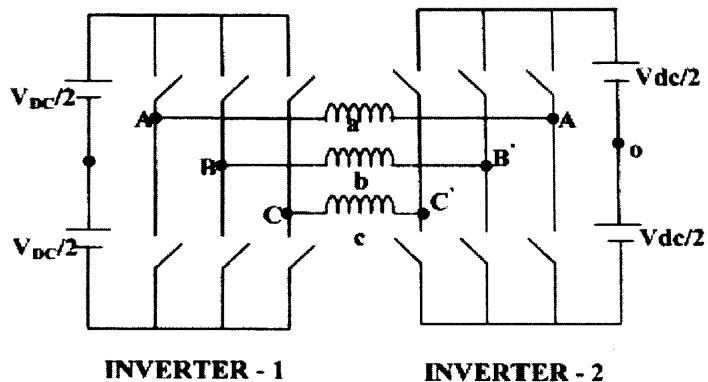
Figure 5.9 Power circuit for the harmonic elimination and suppression scheme [5.66]

In a recent study [5.67], Sundareswara and Kumar have reported a voltage harmonic elimination technique in PWM ac/ac voltage converter using a genetic algorithm (GA). The circuit of the PWM ac chopper and output voltage is shown in figure 5.10. The output voltage of the ac chopper with k pulses per half cycle is written in terms of the switching angle using a Fourier series, and the best switching angles are identified with the dual objective of the harmonic elimination and output voltage regulation. For performance comparison of the GA, other optimisation method such as Rosenbrock's rotating coordinate method and Newton Raphson method are also applied to the problems. Comparison showed that the GA method is on a par with conventional optimisation methods.
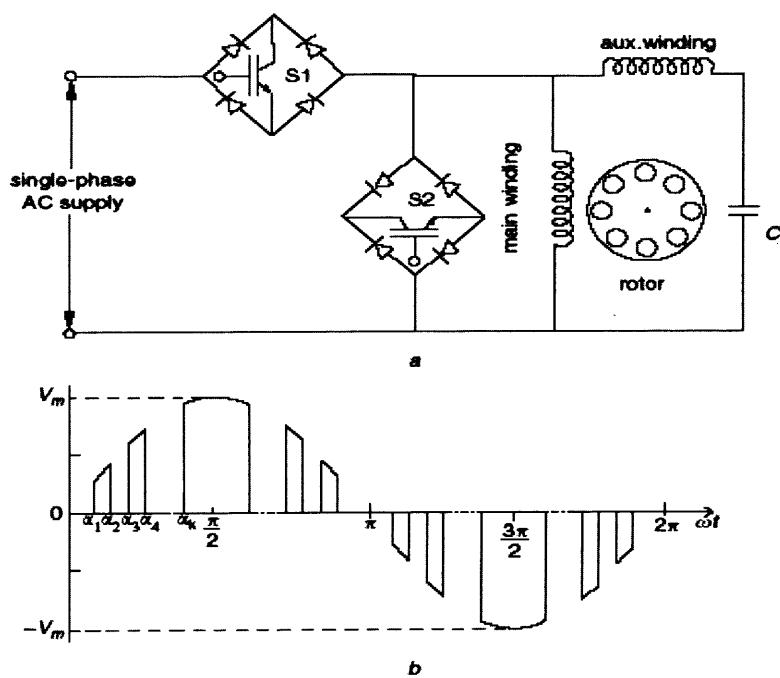
Figure 5.10 (a) Circuit of PWM ac chopper, (b) Output Voltage [5.67]

A review of harmonics in rotating machine is presented by Wakileh [5.68]. In this paper author discussed the impact of harmonics on the losses of induction motor and the formulae for the induced emf, pitch factor and distribution factor are extended to include the effect of harmonics thus allowing the computation of voltage harmonic distortion. The author extended formulae for hysteresis loss due to harmonics to

$$P_{hpu} = \sum_{h=1} h^{1-n} E^{n}_{hpu} \qquad (5.1)$$

Where P_{hpu} is the total per unit Hysteresis loss, h is the harmonic order, E_{hpu} is the hth harmonic rms generated in per unit.

The author discussed the elimination of harmonics in rotating machine by chording the stator coil and thus he worked out numerically the waveform of full pitch and chorded winding as shown in figure 5.11.
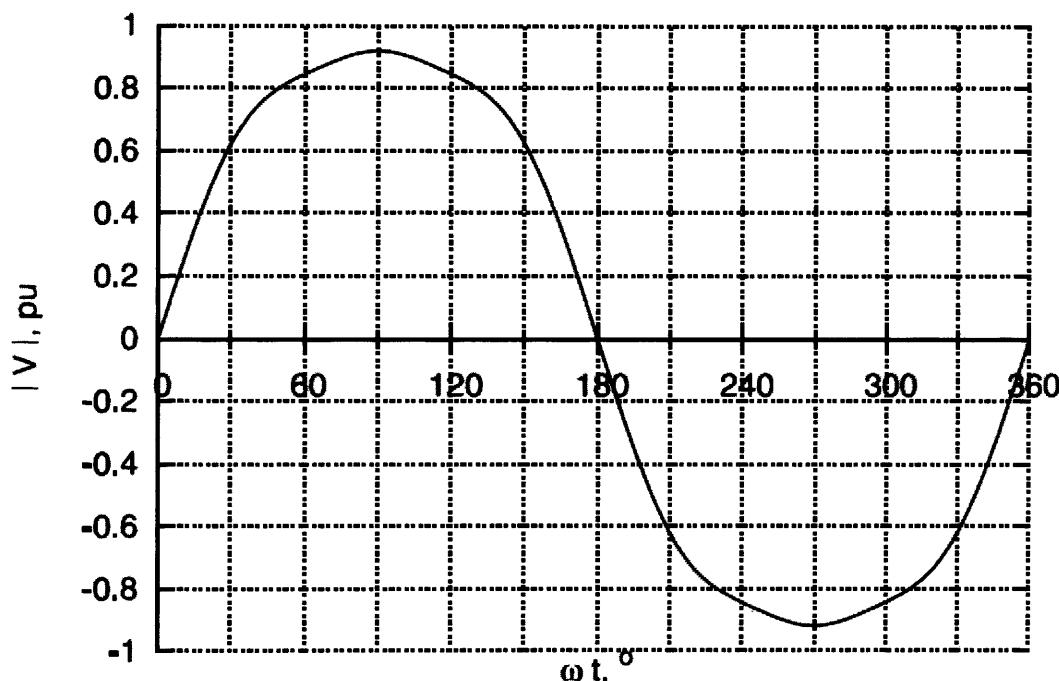

Figure 5.11 (a) Phase voltage waveform, full pitch
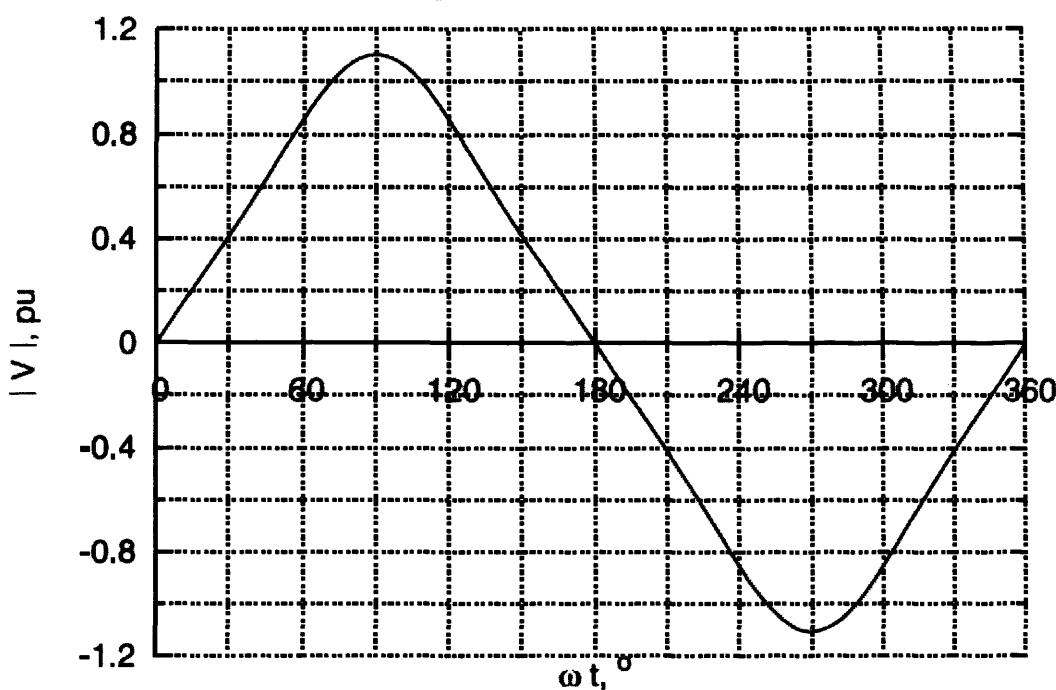
Figure 5.11 (b) Phase voltage waveform, short pitched [5.68]

The author conclude that in rotating machines chording reduces the fundamental component of the induced emf, yet it has an advantage of reducing harmonic voltage thus resulting in an improved voltage waveform. A coil span chosen to give a pitch factor of zero at a certain harmonic results in complete suppression of that harmonic. This was presented on a numerical basis experimental verification has not been reported.

Chen and Chen [5.69] designed a new winding for an ac three-phase machine, which has low harmonic content and high winding coefficient. The new winding designed using this principle is not bound to the basic unit of 60°-phase belt (per pole per phase) and has a short pitch coil span. The new winding doesn't have coil groups but has the coil side group. In this method there are two types of mixed connection one is start-delta in parallel and another is star-delta in series as shown in figure 5.12, for 4 pole 36 slot stator winding. The new winding increased the efficiency of the induction motor by 3% and odd harmonics are suppressed.
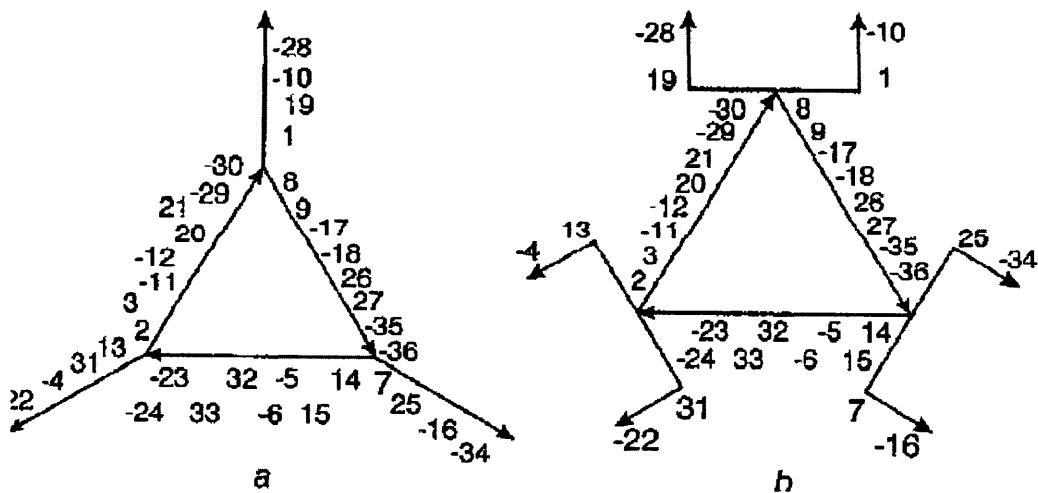
Figure 5.12 Star-Delta mixed connections in series [5.69]

Based on all the above findings of the study from section 5.2.4, it is found that:

• The simplest method to provide some level of harmonic control and also accomplish power factor correction requirement is to add the power factor correction in the form of tuned capacitor banks. This prevents magnification of any characteristic harmonic components from the drives.

• A significant harmonic reduction can be obtained from PWM type adjustable-speed drives simply by adding a choke inductance at the input. Some drives manufacturers include this choke inductance in the dc link of the drive.

• Two isolated dc link sources with voltage ratio of approximately 1:0.366 feeding an open-end induction motor are capable of eliminating triplen harmonic currents from the motor phase.

• A reduction of harmonic content by increasing the pulse number does not necessarily offer a substantial improvement. The application of a PWM inverter within a broad time-fundamental frequency range thus offers disadvantages, unless it is possible and intended to filter the output.

• Fixed frequency or on/off PWM current-controlled techniques can provide a high-quality, controlled-current source.

• A high-carrier ratio improves waveform quality by raising the order of the principle harmonics. At low fundamental frequencies, very large carrier ratios are feasible and resulting in near-sinusoidal output current waveforms account for one of the main

attributes of the sine wave PWM inverter drive-the extremely smooth rotation at low speeds.

• Harmonics can be reduced by chording the stator winding.

REFERENCES FOR CHAPTER 5

[5.1] H. C. Stanley, 'An analysis of the induction machine', AIEE Transaction, vol. 57 pp.751–757, 1938

[5.2] F. M. Hughes, A.S. Alderd, 'Transient characteristics and simulation of induction motors', IEE Proceeding, vol. 111, issue 12, pp. 2041–2050, 1964

[5.3] A. K. Sarkar, G.J. Berg, 'Digital simulation of three phase induction motors', IEEE Transactions on Power Apparatus and System issue, vol. 89, issue 6, pp 1031–1036, 1970

[5.4] L. J. Jacobides, 'Analysis of a cycloconverter-induction motor drive system allowing for stator current discontinuities', IEEE Transactions Industry Application, vol. 9, issue 2, pp. 206–215, 1973

[5.5] S. S. Murthy, G. J. Berg, 'A new approach to dynamic modelling and transient analysis of SCR-controlled induction motors', IEEE Transactions Power Apparatus and System, vol. 101, issue 9, pp. 3141–3150, 1982

[5.6] P. C. Krause, C. H. Thomas, 'Simulation of symmetrical induction machinery', IEEE Transactions Power Apparatus and System, vol. 84, pp 1038–1053, 1965

[5.7] P. C. Krause, 'Method of multiple reference frame applied to the analysis of symmetrical induction machinery', IEEE Transactions Power Apparatus and System, vol. 87, issue 1, pp. 218–227, 1968

[5.8] P. C. Krause, 'Analysis of Electric Machinery', McGraw-Hill, 1986

[5.9] T. A. Lipo, P. C. Krause, Stability analysis of a rectifier inverter induction motor drive, IEEE Transactions Power Apparatus and System, vol. 88, issue 1, pp. 55–66, 1969

[5.10] R. Ueda, T. Sonoda, K. Koga, M. Ichikawa, 'Stability analysis in induction motor driven by v/f controlled general purpose inverter', IEEE Transactions Industry Application, vol. 28, issue 2, pp. 472–481, 1992

[5.11] L. M. Neto, J. R. Camacho, C. H. Salemo, 'Analysis of a three-phase induction machine including time and space harmonic effects: the ABC reference frame', IEEE Transactions Energy Conversion, vol. 14, issue 1. pp. 80–85, 1999

[5.12] H. A. Toliyat, T. A. Lipo, 'Transient analysis of cage induction machines under stator rotor bar and end ring faults', IEEE Transactions Energy Conversion, vol. 10, issue 2, pp. 241–247, 1995

[5.13] H. A. Toliyat, M. S. Arefeen, A. G. Parlos, 'A method for dynamic simulation of air-gap eccentricity in induction machines', IEEE Transactions Industry Application, vol. 32, issue 4, pp. 910–917, 1996

[5.14] G. M. Joksimovic, J. Penman, 'The detection of inter-turn short circuit in the stator windings of operating motors', IEEE Transactions Industrial Electronics, vol. 47, issue 5, pp. 1078–1084, 2000

[5.15] K. Oguchi, 'Time domain analysis of a multiple phase-shifted voltage source inverter-fed induction motor', Electric Power Component and System, vol. 11, pp. 13–23, 1986

[5.16] A. H. Bonnet, 'Analysis of the impact of pulse-width modulated inverter voltage waveforms on ac induction motors', IEEE Transactions Industry Application, vol. 32, issue 2, pp. 386–392, 1996

[5.17] Z. Wang, Y. Liu, 'Modeling and simulation of a cycloconverter drive systems for harmonic studies', IEEE Transactions Industrial Electronics, vol. 47, issue 3, pp. 533–541, 2000

[5.18] A. Dell'Aquilla, A. Lassandro, P. Zanchette, 'Modelling of line side harmonic currents produced by variable speed induction motor drives', IEEE Transactions Energy Conversion, vol. 13, issue 3, pp. 263–269, 1998

[5.19] L. A. Doggett, E. R. Queer, 'Induction motor operation with non-sinusoidal impressed voltages', AIEE Transactions, vol. 48, pp. 1217–1223, 1929

[5.20] E. A. Klingshirn, H. E. Jordan, 'Polyphase induction motor performance and losses on non-sinusoidal voltage sources', IEEE Transactions Power Apparatus and System, vol. 87, issue 3, pp. 624–631, 1968

[5.21] B. J. Chalmer, B. R. Sarkar, 'Induction motor losses due to non-sinusoidal supply waveforms', IEE Proceeding, vol. 115, issue12, pp.1777–1782, 1968

[5.22] J. R. Linders, 'Effects of power supply variations on ac motor characteristics', IEEE Transactions Industry Application, vol.15, pp. 383–400, 1972

[5.23] J. R. Linders, 'Electric wave distortion: their hidden costs and containment', IEEE Transactions Industry Application, vol.8, issue 5, pp. 458–471, 1979

[5.24] H. Raphael, 'Additional losses in PWM inverter-fed squirrel cage motors', Proceedings of IEEE Industrial Applications Society, Annual Meeting, vol. 1, pp. 632–636, 1977

[5.25] P. G. Cummings, 'Estimating effect of system harmonics on losses and temperature rise of squirrel cage motors', IEEE Transactions Industry Application, vol. 22, issue 6, pp. 1121–1126, 1986

[5.26] E. F. Fuchs, D. J. Roesler, F. S. Alashhab, 'Sensitivity of electrical appliances to harmonics and fractional harmonics of the power systems voltage part I: transformer and induction motors', IEEE Transactions Power Delivery, vol. 2, issue 2, pp. 437–444, 1987.

[5.27] P. K. Sen, H. A. Landa, 'Derating of induction motors due to waveform distortion', IEEE Transactions Industry Application, 26, vol. 6, pp. 1102–1107, 1990

[5.28] V.E. Wagner, et al., 'Effects of harmonics on equipments', IEEE Transactions Power Delivery, vol. 8, issue 2, pp. 672–680, 1993

[5.29] C. Y. Lee, W. J. Lee, 'Effects of non-sinusoidal voltage on the operation performance of a three-phase induction motor', IEEE Transactions Energy Conversion, vol. 14, issue 2, pp. 193–201, 1999

[5.30] A. Vamvakari, A. Kandianis, A. Kladas, S. Manias, J. Tegopoulos, 'Analysis of supply voltage distortion effects on induction motor operation', IEEE Transactions Energy Conversion, vol. 16, issue 3, pp. 209–213, 2001

[5.31] R. C. Healy, S. Williamson, A. Smith, 'Improved cage rotor models for vector controlled induction motors', IEEE Transactions Industry Application, vol. 31, pp. 812–822, 1995

[5.32] E. Levi, 'Impact of iron loss on behaviour of vector controlled induction machines', IEEE Transactions Industry Application, vol. 31, pp. 1287–1296 1995

[5.33] N. E. Hilderbrand, H. Roehrdanz, 'Losses in three-phase induction machine fed by PWM converter', IEEE Transactions Energy Conversion, vol. 16, pp. 228–233, 2001

[5.34] H. Rapp, 'Examination of additional rotor losses in inverter fed induction machine', in: Proceedings of International Conference on Industrial Electronics, Control and Instrumentation, vol. 2, pp. 881–886, 1993

[5.35] W. Prescott, D. G. Watterson, M. Bradford, M. Lockwood, 'Computational methods for the steady-state performance prediction of cage induction motors fed from non-sinusoidal supplies, in: Proceedings of IEE Conference on Electric Machines and Drives, pp. 271–274, 1989

[5.36] A. Boglietti, P. Ferraris, M. Lazzari, M. Pastorelli, 'Influence of inverter characteristics on the iron losses in PWM inverter fed induction motors', IEEE Transactions Industry Application, vol. 32, issue 5, pp. 1190–1194, 1996

[5.37] A. Boglietti, 'PWM Inverter Fed Induction Motor Losses Evaluation', Electric Machines and Power Systems, vol. 22, USA, pp. 439–449, 1994

[5.38] A. D. Gerlando, R. Perini, 'Evaluation of the effects of the voltage harmonics on the extra iron losses in the inverter fed electromagnetic devices', IEEE Transactions Energy Conversion, vol. 14. issue 1, pp. 57–64, 1999

[5.39] A. Boglietti, P. Ferraris, M. Lazzary, F. Profumo, 'Loss Items Evaluation in Induction Motors fed by Six-Step VSI', Electric Machines and Power Systems, USA, vol. 19, pp. 513–526, 1991

[5.40] Z. K. Papazacharopoulos, K. V. Tatis, A. G. Kladas, S.N. Manias, 'Dynamic model for harmonic induction motor analysis determined by finite elements', IEEE Transactions Energy Conversion, vol.19, issue 1, pp. 102–108, 2004

[5.41] S. Ekram, B. Sarkar, Effects of harmonics on PWM fed induction machines', Electrical Engineering Journal, IIT India, vol. 85, pp.1-12, 2004

[5.42] F. A. DeWinter, B. Wu, 'Medium voltage harmonic heating, torques and voltage stress when applied on VDFs', IEEE Industry Application, Conference Proceeding, vol. 43, pp. 131-139, 1996

[5.43] A. E. Emanuel, 'Estimating the effect of harmonic voltage fluctuation on the temperature raise of squirrel-cage motor', IEEE Transactions on Energy Conversion, vol. 6, issue1, pp. 162-169, 1991

[5.44] R. A. Hanna, 'Harmonics and technical barriers in adjustable speed drives', IEEE Transactions on Industry Application, vol. 5, issue 25, pp. 894-900, 1989

[5.45] P. Lumyong, C. Chat-Uthai, 'A study of harmonic effect on the performance of three-phase induction motor using BSRG', in: Proceedings of IEEE Power System Technology, vol. 2, pp. 1190-1194, 2002

[5.46] V. B. Honsinger, 'Induction motors operating from inverters', in: Conference of Rec. IEEE Industrial Applications Society Annual Meeting, pp. 1276–1285, 1980

[5.47] J. M. D. Murphy, V. B. Honsinger, 'Efficiency optimization of inverter-fed induction motor drives', in: Conference of Rec. IEEE Industrial Applications Society Annual Meeting, pp. 544–552, 1982

[5.48] A. C. Williamson, 'The effects of system harmonics upon machines', International Journal of Electrical Engineering Education, vol.19, pp.145–155, 1982

[5.49] T. V. Avadhanly, 'Derating factors of three-phase induction motors', Journal of Industrial Engineering, India, vol. 54, pp. 113–117, 1974

[5.50] R. D. Lorenz, S. M. Yang, 'Efficiency-optimized flux trajectories for closed-cycle operation of field-orientation induction machine drives', IEEE Transactions Industrial Application, vol. 28, issue 3, pp. 574–580, 1992

[5.51] G. O. Garcia, J. C. M. Luic, R. M. Stephan, E. H. Watanabe, 'An efficient controller for an adjustable-speed induction motor drive', IEEE Transactions Industrial Electronics, vol. 41, issue 5, pp. 533–539, 1994

[5.52] I. Kioskeridis, N. Margaris, 'Loss minimization in induction motor adjustable-speed drives', IEEE Transactions Industrial Electronics, vol. 43, issue 1, pp. 226–231, 1993

[5.53] D. S. Kirschen, D. W. Novotny, T. A. Lipo, 'Online efficiency optimization of a variable frequency induction motor drive', IEEE Transactions Industrial Application, vol. 21, issue 4, pp. 610–615, 1985

[5.54] G. C. D. Sousa, B. K. Bose, J. G. Cleland, 'A fuzzy logic based online efficiency optimization control of an indirect vector-controlled induction motor drive', IEEE Transactions Industrial Electronics, vol. 42, issue 2, pp.192–198, 1995

[5.55] G. K. Kim, I. J. Ha, M. S. Ko, 'Control of induction motors for both high dynamic performance and high power efficiency', IEEE Transactions Industrial Electronics, vol. 39, issue 4, pp.323–333, 1992

[5.56] J. C. Moreira, T. A. Lipo, V. Blasko, 'Simple efficiency maximizer for an adjustable frequency induction motor drive', IEEE Transactions Industry Application, vol. 27, issue 5, pp. 940–946, 1991

[5.57] S. K. Sul, M. H. Park, 'A novel technique for optimal efficiency control of a current-source inverter-fed induction motor', IEEE Transactions Power Electronics, vol. 3, issue 2, pp. 192–198, 1988

[5.58] A. Domijan, E. Embriz-Santander, 'A summary and evaluation of recent developments on harmonic mitigation techniques useful to adjustable speed drives', IEEE Transactions Energy Conversions, vol. 7, pp. 64–71, 1992

[5.59] M. Rastogi, N. Rajendra, N. Mohan, 'A comparative evaluation of harmonic reduction techniques in three-phase utility interface of power electronic loads', IEEE Transactions Industry Application, vol. 30, pp.1149–1155, 1994

[5.60] J. D. Salmon, 'Circuit topologies for PWM boost rectifiers operated from 1-phase and three-phase supplies using either single or split dc rail voltage outputs', in: Proceedings of IEEE APEC95, pp. 463–470, 1995

[5.61] S. Hansen, P. Nielsen, F. Blaabjerg, 'Harmonic cancellation by mixing nonlinear single-phase and three-phase loads, 'IEEE Transactions Industry Application, vol. 36, issue 1, pp. 152–159, 2000

[5.62] R. Naik, M. Rastogi, N. Mohan, ' Third harmonic modulated power electronics interface with three-phase utility to provide a regulated DC output and to minimize the line current harmonics', IEEE Transactions on Industry Application, vol. 31, issue 3, pp. 598-602, 1995

[5.63] B. S. Lee, J. Hahn, P. N. Enjeti, I. J. Pitel, 'A robust three-phase active power-factor-correction and harmonic reduction scheme for high power', IEEE Transactions Industry Application, vol. 46, issue 3, pp. 483–494, 1999

[5.64] S. Hansen, P. N. Enjeti, J. H. Hahn, F. Blaabjerg, 'An integrated single-switch approach to improve harmonic performance of standard PWM adjustable-speed drives', IEEE Transactions Industry Application, vol. 36, issue 4, pp. 1189–1196, 2000

[5.65] D. Alexa, A. Sirbu, 'Optimized combined harmonic filtering system, IEEE Transactions Industrial Electronics, vol. 48, issue 6, pp. 1210–1218, 2001

[5.66] K. K. Mohapatra, K. Gopakumar, V. T. Somasekhar, L. Umanand, 'A harmonic elimination and suppression scheme for an open-end winding induction motor drive', IEEE Transactions Industrial Electronics, vol. 50, issue 6, pp. 187–1198 2003

[5.67] K. Sundareswara, A. P. Kumar, 'Voltage harmonic elimination in PWM ac chopper using genetic algorithm', IEE Proceedings Electrical Power Application, vol. 151, issue 1, pp. 26–31, 2004

[5.68] G. J. Wakileh, 'Harmonics in rotating machines', Electric Power System Research, vol. 66, issue 1, pp. 31-37, 2003

[5.69] J. Y. Chen, C. Z. Chen, 'Investigation of a new AC electrical machine winding', Proceedings of IEE Electric Power Application, vol. 145, issue 2, pp. 125-132, 1998

CHAPTER 6

EXPERIMENTAL MOTOR WINDING DESIGN

6.1 Introduction

Four, three-phase, four pole commercial squirrel cage induction motors were purchased and redesigned to obtain stator short pitch windings. All the motors were initially concentrically wound. The windings were stripped out and re-wound.

6.2 Motor specifications

The specification of the commercial motors is as follows;

1) Power output: 1 Horse Power (746 watts)
2) Phase Voltage: 230 Volts
3) Rated Speed: 1420 rpm
4) Phases: Three-phase
5) Rated Current: 3.4 Amperes
6) Insulation Class: B
7) Number of stator slots: 36
8) Number of stator teeth: 36
9) Winding type: Concentric
10) Connection type: Delta
11) Wire diameter: 0.6 mm
12) Layers of coil side in each slot: Single
13) Number of turns in each coil: 78
14) Slot type: Semi-enclosed

The new winding designed specifications are as follows:

1) Wire thickness: 0.6 mm
2) Coil insulation type: Class-H
3) Layers of coil side in each slot: Double
4) Type of winding: Lap
5) Number of turns in each coil: 39
6) Connection type: Delta

The coil insulation type is changed from Class-B which has maximum temperature resistance of 130° C to Class-H which has maximum temperature resistance of 180° C as there was a possibility of increase in the temperature while motor was on load due to change of the standard winding design. The type of winding was changed to lap as it gives advantage of easy manual rewinding. To take advantage of the better emf, lower cost of coils and better performance of the motor the double layer winding is used.

In the above specifications the number of turns per coil in the motor before rewinding is 79. The type of winding is single layer winding. In the re-wound motor it can be noticed that the number of turns in each coil is 39 this is because the re-wounded motors is double layer winding so as to maintain equal amount of turns in each slot the number of turns are reduced from 78 to 39. So for the re-wounded motors one stator slot has two coil sides, which consist of $2 \times 39 = 78$ turns.

6.3.1 Design of motor M1 (Full pitched)

A symmetrical m phase winding is defined as one in which the starts of the phases are displaced around the periphery of

$$\frac{2\pi}{m} = \frac{360°}{m} \text{ Electrical degrees}$$

In this case *m= 3,* as it is a three-phase motor. So it is given as

$$\frac{360°}{3} = 120°$$

Each pole-pitch corresponds to π electrical radians or 180 electrical degrees.

If the number of poles are 4, number of slots, S, are 36. So each pole P, the number of slots per pole is given by

$$Slots \ per \ pole = \frac{36}{4} = 9$$

So the coil span of 9 slots will cover 180° electrical; more over, the number of electrical degrees between adjacent slots i.e. slot pitch is given by equation

$$slot \ pitch = \frac{180°}{9} = 20°$$

One motor was wound with a full pitch winding. The motor is of four poles and the pole pitch '*p*' is 180° electrical or nine slots. The winding position of a single coil is shown in figure 6.1. The three phase winding distribution relative to two poles is shown in figure 6.2. In the figure **a, b, c** are the three phases and the *a* and *a'* positive and negative direction of the currents respectively. The detailed layout of the winding is shown in figure 6.3.
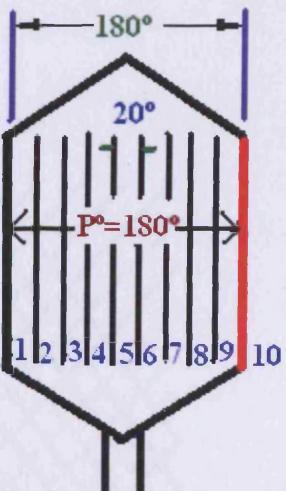
Figure 6.1 Winding design for single coil of 180° Coil pitch Motor (full pitch motor)
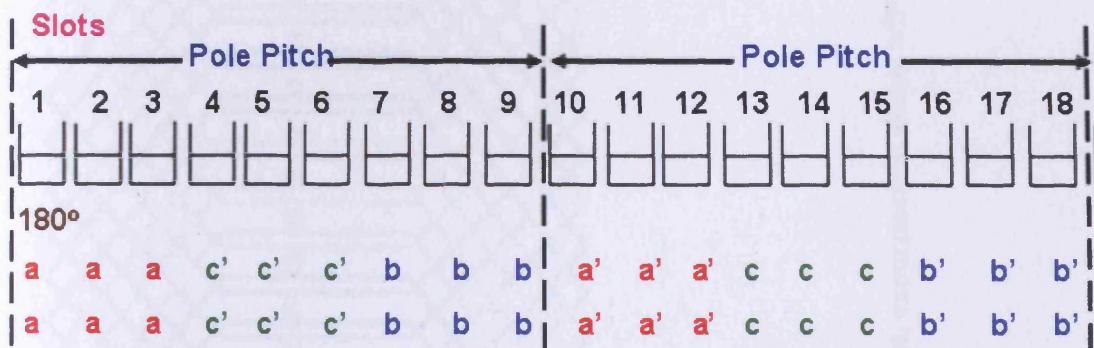

**Figure 6.2 Phase distribution and current direction relative to two poles (180° coil-pitch motor)**
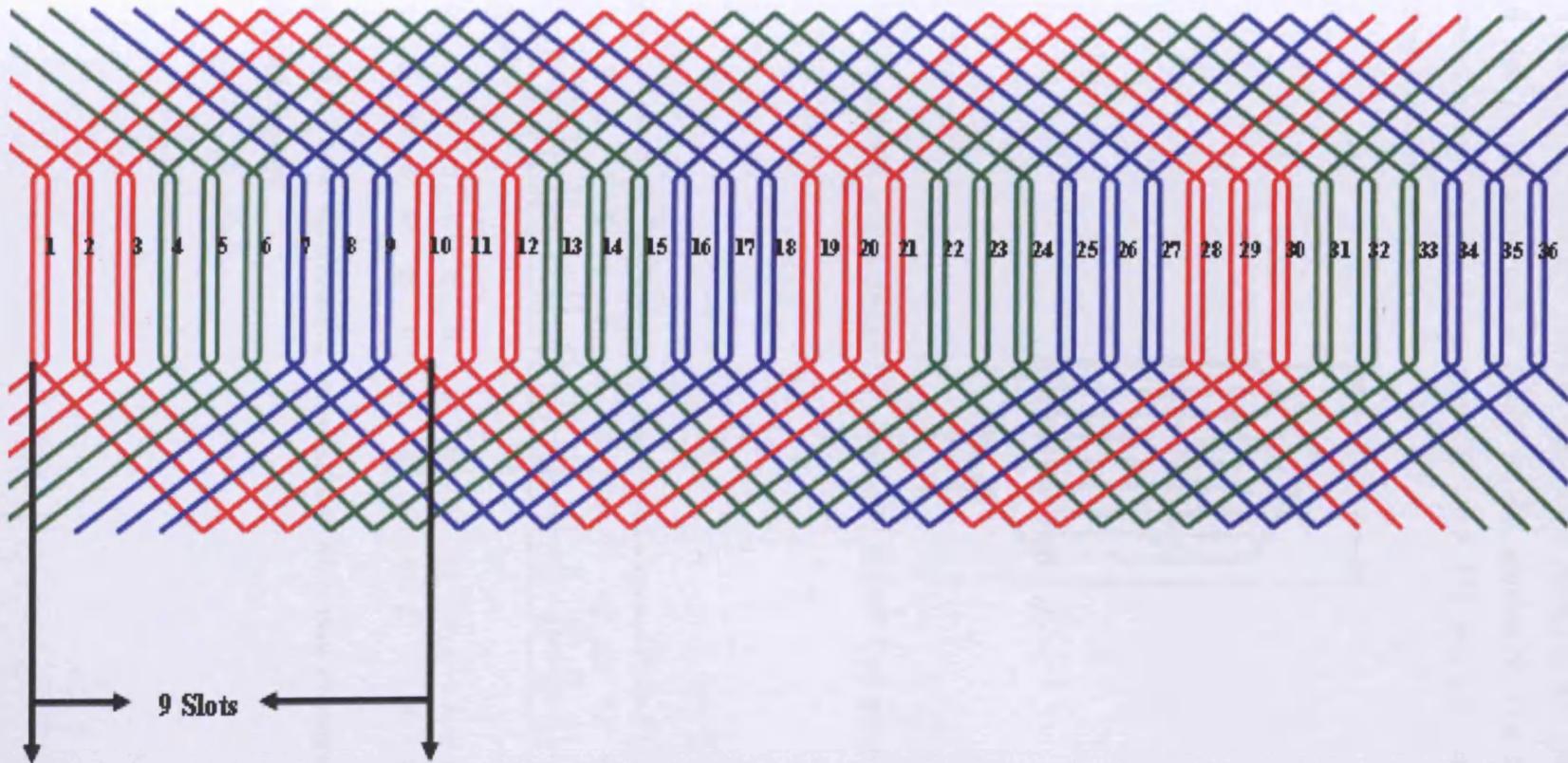
Figure 6.3 Detailed winding of the 180° coil pitch, 36 slot, experimental stator winding

6.3.2 Design of motor M2 (160° Coil Pitch)

Motor M2 is designed such that the coil pitch is 160°. The winding design for a single coil is shown in figure 6.4. The first coil-side is placed in slot number 1 and the other coil side of the same coil is placed in slot number 9. The three phase winding distribution in two poles is shown in figure 6.5. The detailed winding for 36 slots for 160° is shown in figure 6.6.
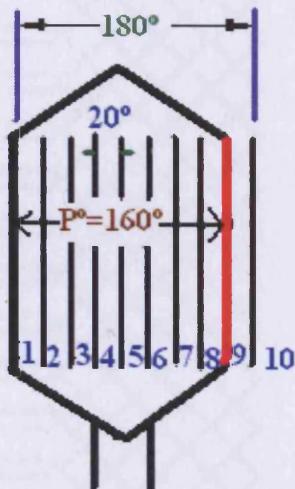

**Figure 6.4 Winding design for single coil of 160° Coil pitch Motor**
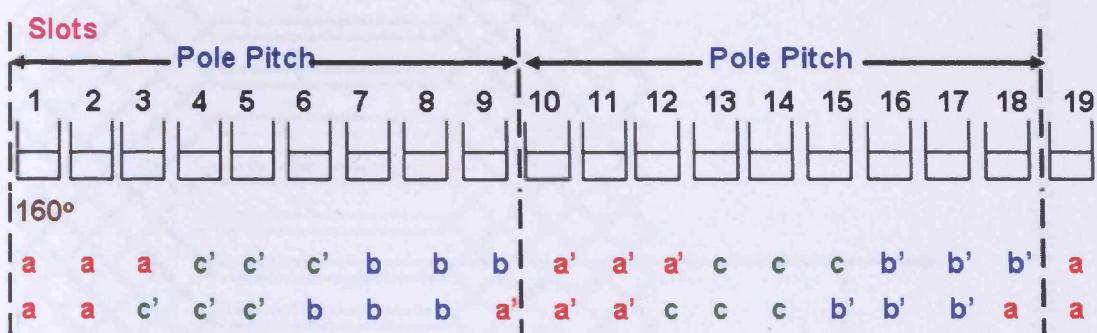
Figure 6.5 Phase distribution and current direction relative to two poles (160° coil-pitch motor)
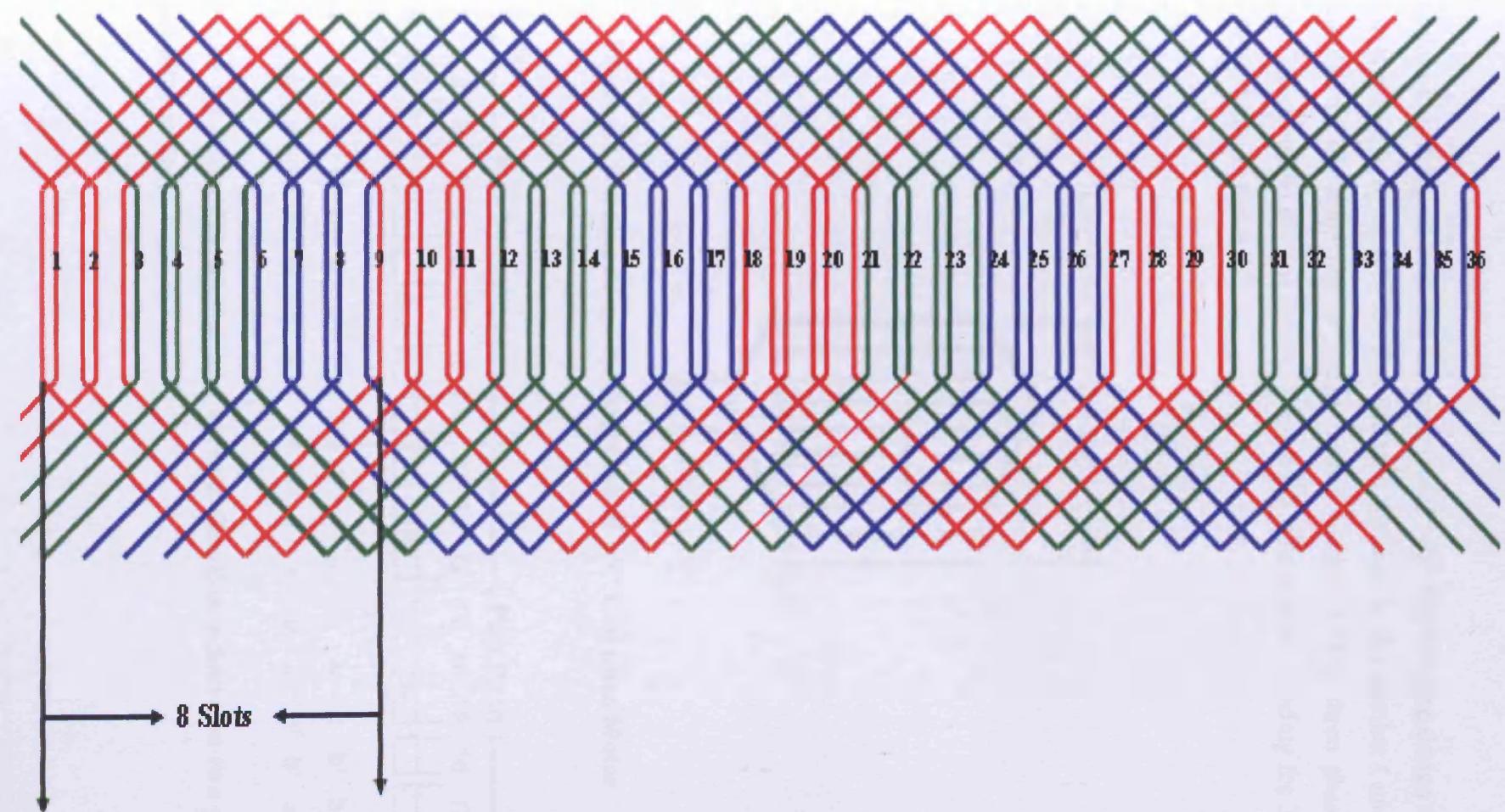
Figure 6.6 Detailed winding of the 160° coil pitch, 36 slot, experimental stator winding

6.3.3 Design of motor M3 (140° Coil Pitch)

Motor M3 is designed such that the coil pitch is 140°. The winding design for a single coil is shown in figure 6.7. The first coil side is placed in slot number 1 and the other coil-side of the same coil is placed in slot number 8. The three phase winding distribution in two poles is shown in figure 6.8. The detailed winding for 36 slots for 140° is shown in figure 6.9.
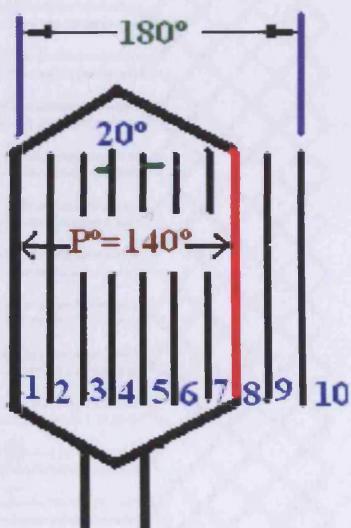
Figure 6.7 Winding design for single coil of 140° Coil pitch Motor
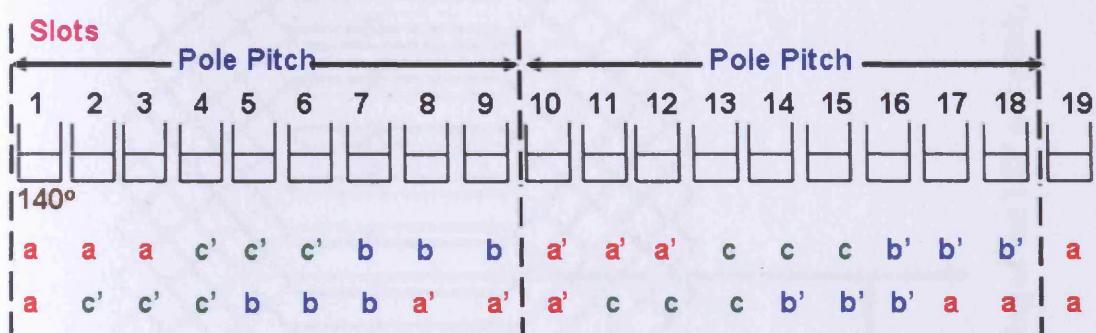
Figure 6.8 Phase distribution and current direction relative to two poles (140° coil-pitch motor)
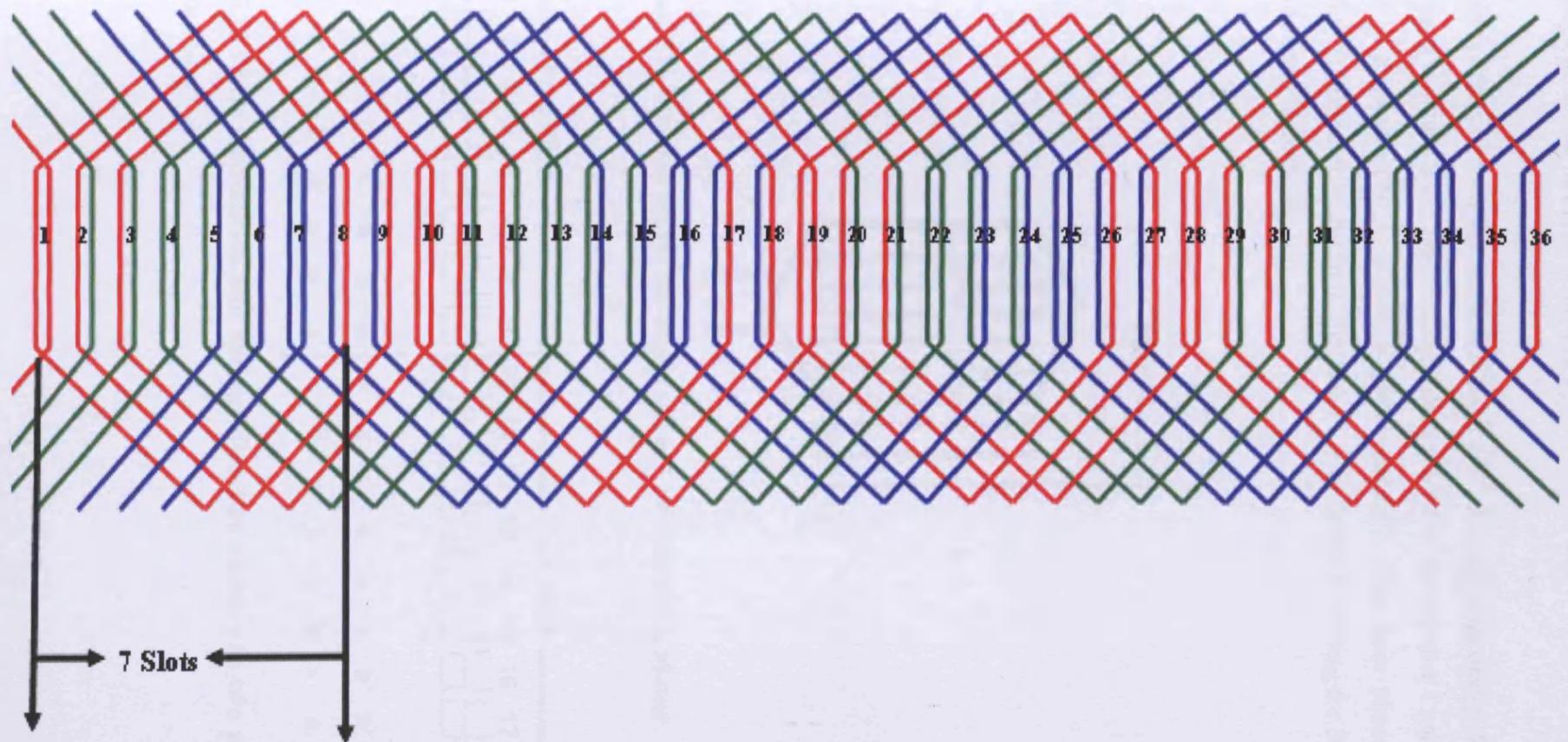
Figure 6.9 Detailed winding of the 140° coil pitch, 36 slot, experimental stator winding

6.3.4 Design of motor M4 (120° Coil Pitch)

Motor M4 is designed such that the coil pitch is 120°. The winding design for a single coil is shown in figure 6.10. The first coil side is placed in slot number 1 and the other coil-side of the same coil is placed in slot number 7. The three phase winding distribution in two poles is shown in figure 6.11. The detailed winding for 36 slots for 120° is shown in figure 6.12.
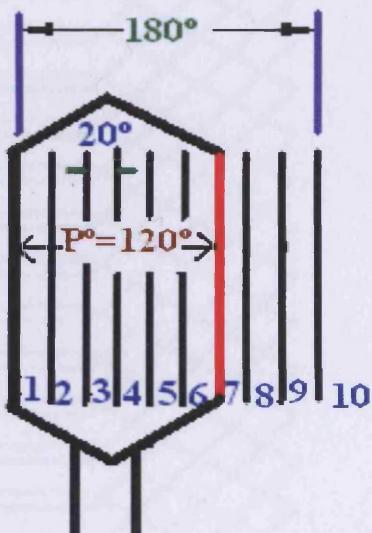

**Figure 6.10 Winding design for single coil of 120° Coil pitch Motor**
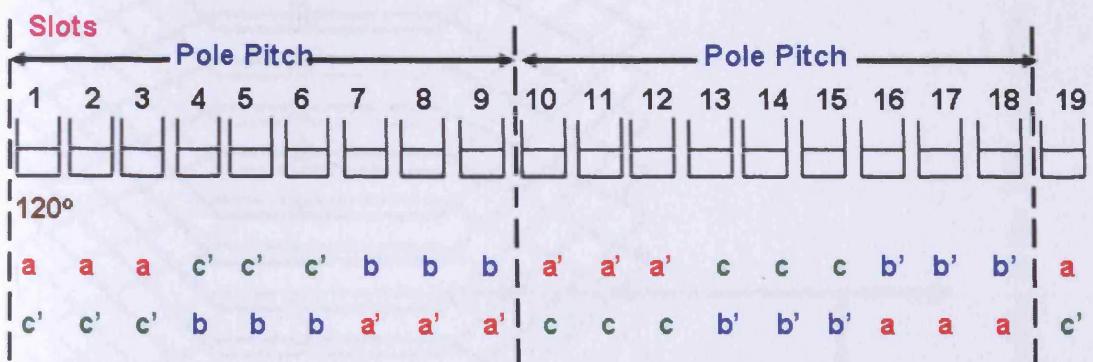
Figure 6.11 Phase distribution and current direction relative to two poles (120° coil-pitch motor)
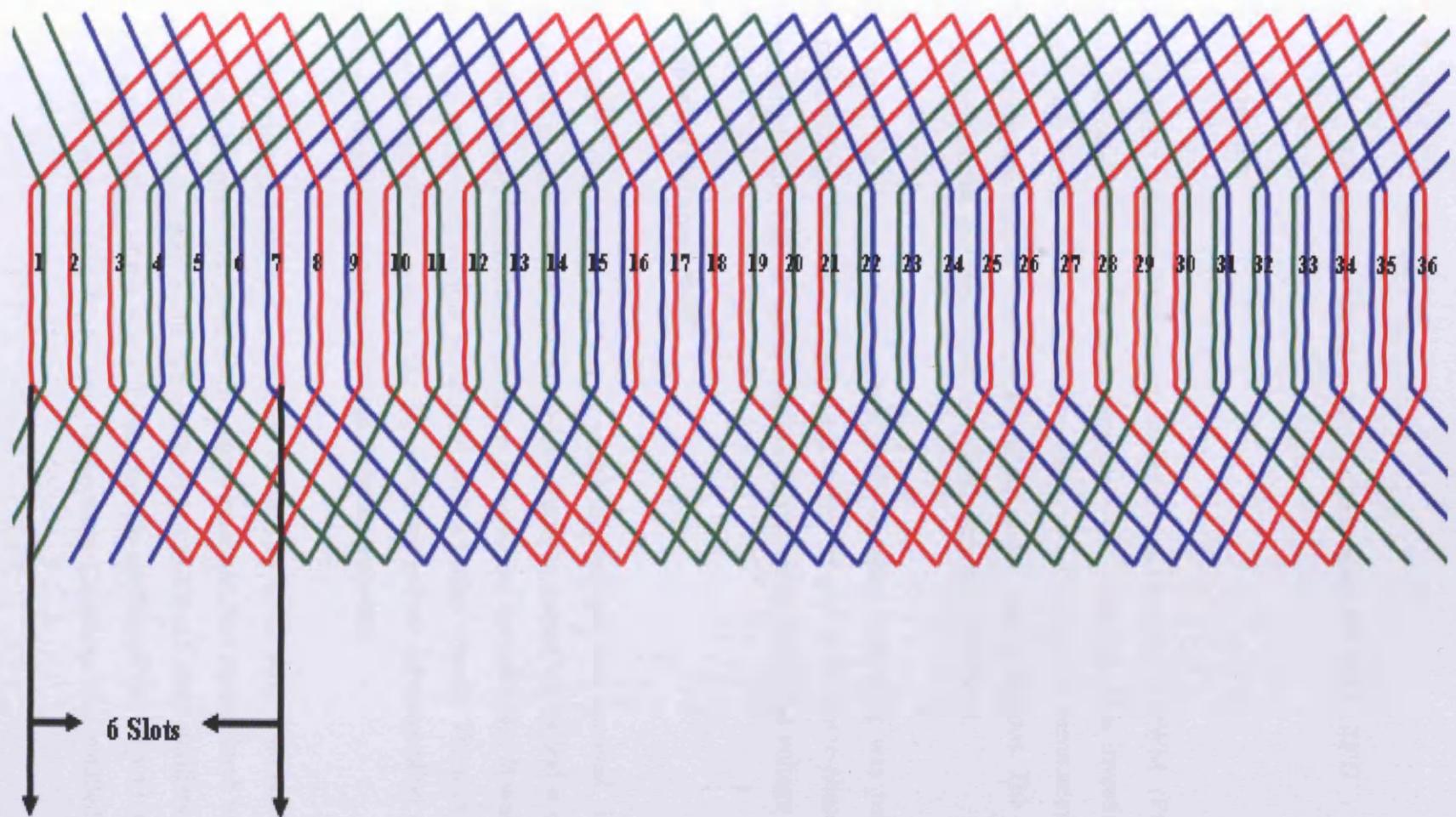
Figure 6.12 Detailed winding of the 120° coil pitch, 36 slot, experimental stator winding

CHAPTER 7

EXPERIMENTAL APPARATUS AND MODELLING

7.1 Introduction

The efficiency of the three-phase induction motors under PWM (Pulse width modulation) and sinusoidal voltage supplies were measured. This investigation also includes the stator voltage harmonic measurements, torque measurement, speed measurement and output power measurement under load conditions. The speed, rms voltage, rms current and rms power at no load were also measured.

Apart from the above measurements, finite element modelling was performed to assess the voltage harmonics component in the air-gap of the three-phase induction motor using OPERA 2D Rotating machine model under sinusoidal voltage supply.

7.2 Experimental equipment

This system consists of a test bed on which the machine was mounted. The test bed consists of an eddy current brake, NEMA frame to mount motor and a cooling fan. The motor was mounted on the platform by adjusting the rail bolts. It was aligned to the height of the eddy current brake shaft with a ratchet wrench. The motor shaft was coupled to the eddy current brake by using the rubber drive-coupling spider. The motor was slid into position and locked down by tee joints.

The eddy current brake was connected to the 110 V, 20 Amp load controller. This controller has the smooth slide main control knob and fine control knob to control the applied load on the shaft of the motor. There is a 110 V, 15 Amp auxiliary cooling fan to assist the cooling of the brake. To display the reading of the output torque, speed, power at the shaft the 100 V, 15 Amp Horsepower Computer was installed.

The torque on the shaft was measured by using a strain gauge. The surface of a shaft under torque would experience compression and tension. The strain gauge elements were mounted in pairs at 90 degrees to each other on the shaft. One was mounted parallel to the length of the shaft, the other perpendicular to it. A Wheatstone bridge was used to measure the changes in the compression and tension and thus measuring torque. The speed sensor installed to measure the speed at the shaft uses a magnetic pulse system. The output power at the shaft is calculated by multiplying shaft torque by the corresponding angular speed.

To measure the input parameter Yokogawa WT1600 Digital Power Meter was used. It measures three-phase rms current, rms voltage, power, harmonic voltages, voltage harmonic distortion, total harmonic distortion, rms fundamental frequency and switching frequency.

To supply the motor with the PWM supply an ABB three-phase inverter was used. The modulation frequencies and the switching frequencies could be varied from the front control panel. Inverter allows the switching frequency of 4 kHz, 8 kHz and 16 kHz. The sinusoidal supply was supplied from a three-phase source.

The complete set-up is as shown in figure 7.1.
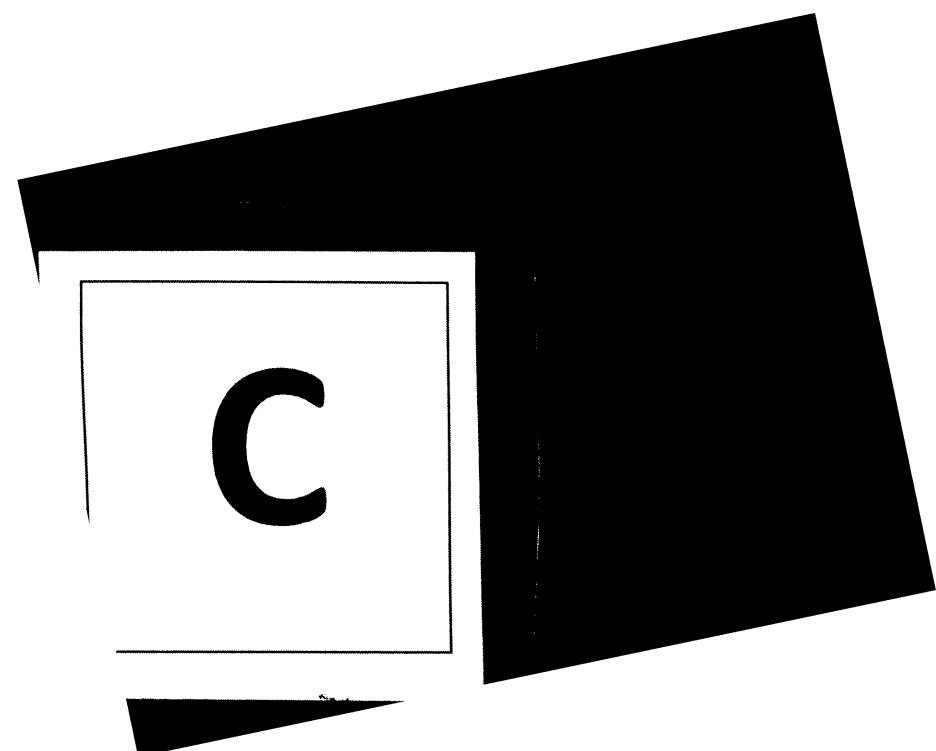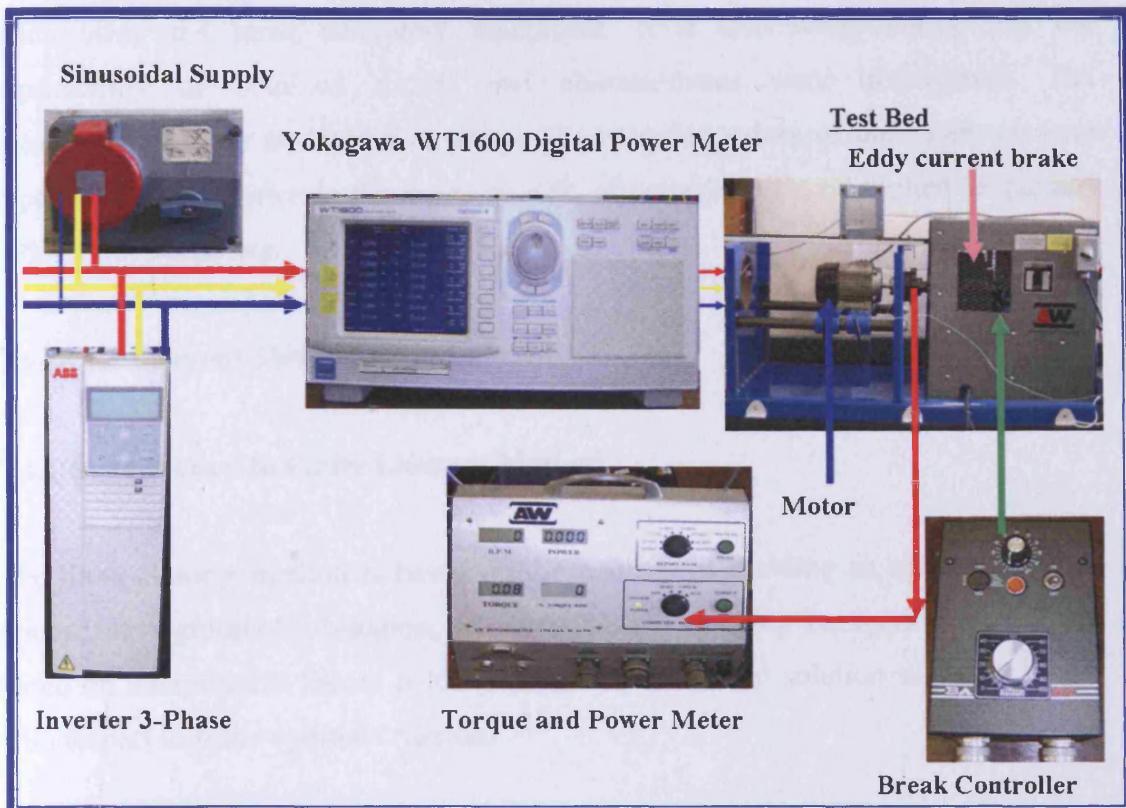
Figure 7.1 Experimental -Setup

7.3 Experiment procedure

The motor was installed on the test bed and energised by the three-phase sinusoidal voltage. The motor was made to run for 5 minutes so that the speed was properly settled down. The torque was applied on the shaft by brake controller. The torque is varied from 1.5 N-m to 7.5 N-m. At each step of applied torque, the input voltage, input current, input power and supply frequency are noted from the digital power meter. The harmonic voltages at every instant of load were captured and were saved in the digital power meter so that the all the harmonics could be measured at same time. The output power, torque and speed are measured in the horsepower computer. This is repeated with all the four motors with stator coil pitch 120°, 140°, 160° and 180°.

The same test was performed with the inverter supply by changing the switching and modulation frequencies of the inverter. All the test results carried out were expected to have the same percentage instrument error as the test were carried out on the same

setup using the same laboratory equipment. It is also worth noting that the repeatability of obtained results and characteristics were investigated. The measurements were repeated five times. The recorded values of measurement were repeatable with an error in the limits of ±2% of voltages, ±3% of applied torque and ±2% of out put power.

7.4 Finite Element Method and Modelling

7.4.1 Introduction to Finite Element Method

The finite element method is based on the concept of dividing an original problem region, into a group of sub-region, the elements, and applying a numerical formulation based on interpolation theory to the element. A numerical solution was then sought with respect to some optimal criterion.

The finite-element method (FEM) originated from the needs for solving complex elasticity, structural analysis problems in civil engineering and aeronautical engineering. Its development can be traced back to the work by A. Hrennikoff [7.1] and R. Courant. While the approaches used by these pioneers are dramatically different, they share one essential characteristic: mesh discretization of a continuous domain into a set of discrete sub-domains. Hrennikoff's work discretizes the domain by using lattice analogy while Courant's approach divides the domain into finite triangular subregions for solution of second order elliptic partial differential equations (PDEs), which arise from the problem of torsion of a cylinder. In 1970, an article by Silvester and Chari entitled "finite element solution of saturable magnetic field problem", in which they proposed a formulation capable of dealing with complex geometry and problem of magnetic non-linearity, signalled the beginning of the new era in the field of applied electromagnetism [7.2]. They made major contribution to the development of the method and made it so widely applied today in electrical engineering.

The finite element method is in fact a numerical technique for solving large scale, complex problem, using a simple and flexible data structure. In order to discretise a problem region, it is necessary to choose elements of a given shape. Several element

shapes are used and the principle ones are: the triangle, the quadrilateral, and curvilinear shapes [7.2]. Elements are defined in terms of their shape and the order of polynomial interpolation of the trial function (the function that describe the variation of the solution parameter with in an element in terms of the element's nodal values).

7.4.2 Potentials and energy minimality

The analysis of the electromagnetic field problem is facilitated by using potential rather than field vectors and the earlier was used in this modelling. Poisson's and Laplace's equations are derived from Maxwell's equations and solved under specified boundary conditions stated in terms of potentials [7.4]. Example of partial differential equations describing electrostatic and magnetostatic problems are respectively:

$$\nabla^2 V = -\frac{\rho}{\varepsilon} \tag{7.1}$$

and

$$\nabla^2 P = 0 \tag{7.2}$$

Where V is the electrostatic potential, ρ is the electric charge density, ε is the permittivity, and P is the magnetic scalar potential.

The stored energy for electrostatic and magnetostatic problems, W_E and W_M respectively, may also be expressed in terms of the potentials as follow:

$$W_E = \frac{\varepsilon}{2} \int_{vol} (\nabla V)^2 dv \tag{7.3}$$

and

$$W_M = \frac{\mu}{2} \int (\nabla P)^2 dv \tag{7.4}$$

Where μ is the permeability of the material, it is important to notice that both energies are expressed in terms of the squared values of the field gradient, a feature that can be exploited to obtain solution in terms of potentials. This is because the principles of the minimisation of the system's energy will lead to an approximation to the solution.

The potentials in the above equations are the functions of the position. For example, in a two dimensional problem modelled in the Cartesian coordinates, one can write:

$$V = V(x, y) \tag{7.5}$$

and

$$P = P(x, y) \tag{7.6}$$

The energy associated with each potential distribution is a function of the potentials, which themselves are expressed in terms of position. The energy is therefore expressed by a composite function to a functional [7.5, 7.6].

The minimisation of the magnetic energy function over a set of elements (the mesh) leads to a matrix equation that has to be solved for the magnetic vector potential. It is in fact the minimisation of the potential through the mesh [7.6, 7.7].

7.4.3 Boundary conditions

In some electromagnetic devices, for example electrical machines, the field is mainly confined to the region of the device or else it decays very rapidly with distance. An outer boundary is specified and the potential constraints defined on this boundary. The boundary conditions are used in two ways. Firstly, they can provide a way of reducing the size of the finite element representation of symmetrical problems. Secondly, they are used to approximate the magnetic field at large distances from the problem. In electrical machines, three main types of boundary are widely used [7.7].

7.4.4 Tangential magnetic

This boundary requires the magnetic vector potential (A), at a particular point to take a prescribed value:

$$\vec{A} = m \tag{7.7}$$

where m is specified value. This boundary forces the flux lines to be parallel to the boundary's angle [7.8]. In two dimensional problems, a flux line is a line of $\vec{A}$ =constant. By using the boundary condition $\overline{A} = 0$, the flux lines are forced to follow the boundary. For example, the outer edge of the stator lamination could be assigned to a tangential boundary. This is a simplification to neglect all the flux which would extend beyond the stator. The high relative permeability of stator lamination ensures that most of the flux remains within the laminations and in most electrical machines designs this is a good simplification to make.

7.4.5 Normal magnetic

This boundary conditions requires the normal derivative of the magnetic vector potential be zero:

$$\frac{\partial \overline{A}}{\partial n} = 0 \tag{7.8}$$

This condition implies that flux lines enter the boundary at right angles; the boundary thus represents a line of symmetry.

7.4.6 Periodic boundary

If a device is a symmetrical structure where the geometry and the field repeat at intervals, for example in electrical machines, then it is only necessary to model the smallest symmetrical part. The potential on one line of symmetry were related to the potentials on the other line of symmetry. For example, if one pole pitch of a motor is modelled, then the potentials on one line of symmetry are equal and opposite to the potentials on the other line. This condition is specified by defining constraint between each corresponding pair of nodes.

7.5 Electromagnetic CAD systems

The use of the finite element technique for the numerically solving the electromagnetic field equation is nowadays accomplished by fast, powerful and general-purpose software packages. Most of these packages are developed to solve general electromagnetic system rather than problem oriented programs. These systems are known as electromagnetic CAD system, and CAD refers to computer-aided design, a terminology that stress the importance of these systems in the design. Electromagnetic field simulators or simply finite element package are other popular forms of these systems. There are three main factors are contributed to the development of these systems:

1. The advent of digital computer power.
2. The development of interactive computer graphics.
3. The advances in numerical analysis, allowing both the topology and the equations to be represented in a discretised form.

Most of the CAD systems for the numerical analysis of the electromagnetic problems are based on the finite element method (FEM). The method has proved to be flexible, reliable and effective. [7.4, 7.7, 7.9].

The finite element packages are powerful tools in research, development and design. By using only personal computer, it is possible to analyse a number of different

geometries and operating conditions. Also, the numerical simulation provides, in most cases, reliable and accurate information about device's behaviour irrespective of geometric complexity and material non-linearity. For example, in induction motors, the FEM can analyse accurately various shapes and materials. There is no need to calculate reluctances, leakage factors or operating point.

Most finite element packages have three main elements:

1. A pre-processor, which enables the user to define the problem's geometry and specify boundary conditions and sources. Mesh generation is conceptually a pre-processing operation, and at this stage, the number of sub-divisions of a model and tolerances are set and material properties are specified.

2. A solver, for constructing the system of algebraic equations, which model the physical situation mathematically, and produce solutions. These solutions are usually given as a set of nodal potentials. There are three main solver types covering most of the power frequency. Those are:

(i)- The magnetostatic solver: This solver is used for analysing the magnetic field in and around a specified current distribution region of a model with magnetic material that may be linear or non-linear. The solved field equations are time invariant where the source field is constant with no induced current. It is widely used in the analysis of permanent magnet devices. In electrical machines, it is used to model at specific excitation, such as to calculate the torque of the motor at specified stator currents.

(ii)- The time-harmonic solver: This solver is applicable for devices with sinusoidal excitation with eddy current taking the skin depth into account. The source and fields are assumed to be time harmonic at one specific frequency, and they are represented by complex function. This solver is used to simulate eddy-current problem in conductive regions, for example it is used to calculate the locked rotor parameter of an induction motor [7.10]. If the model is non-linear the equivalent reluctivity (reciprocal of the relative permeability) of the material is used. Permanent magnet and non-sinusoidal quantities cannot to be taken into account.

(c)- The transient solver: This is a time dependent solver that solves eddy current problems where the driving source in changing with time in a predetermined way. It

can analyse the response to multiple drive functions including a dc background field, skin effect, non-linear materials and permanent magnet. However, it is expensive in terms of computing time, since it solves the model at each time-step throughout the excitation cycle.

3. Post-processing, that allows the analysis of result. In this stage, it is possible to visualise and manipulate the fields. In addition, important design parameters such as force, torque, inductance and losses may be calculated.

Most FEM packages incorporate in the pre and post-processors, both interactive and batch operations. The solver may be regarded as the principal part of the system, but its operation usually does not require user interaction. On the other hand, the modelling of the problem normally involves a number of issues related to the magnetic field. The planning of the model may be seen as relevant step even at the choice of the appropriate solver, its sequence of solutions and the corresponding convergence criteria.

OPERA 2D rotating motion solver was the software package used in this project.

7.6 Problem modelling

When dealing with the problem involving complex geometries, it is important to plan the finite element model, especially in its aspect concerned with mesh construction and specification of the boundary conditions. This will allow extra flexibility for altering material properties, defining sequence of similar problems and facilitating the analysis of the results.

Some of the practical issues usually considered during planning of the finite element models are:

a) Percentage of entire problem to be examined.

b) Modelling for rotating machine solver

c) Short pitching design

d) Harmonics measurement.

These points are discussed as they are applied to the modelling of the three-phase induction motor. Figure 7.2 illustrates a sketch of a one-quarter 2D model of an motor.
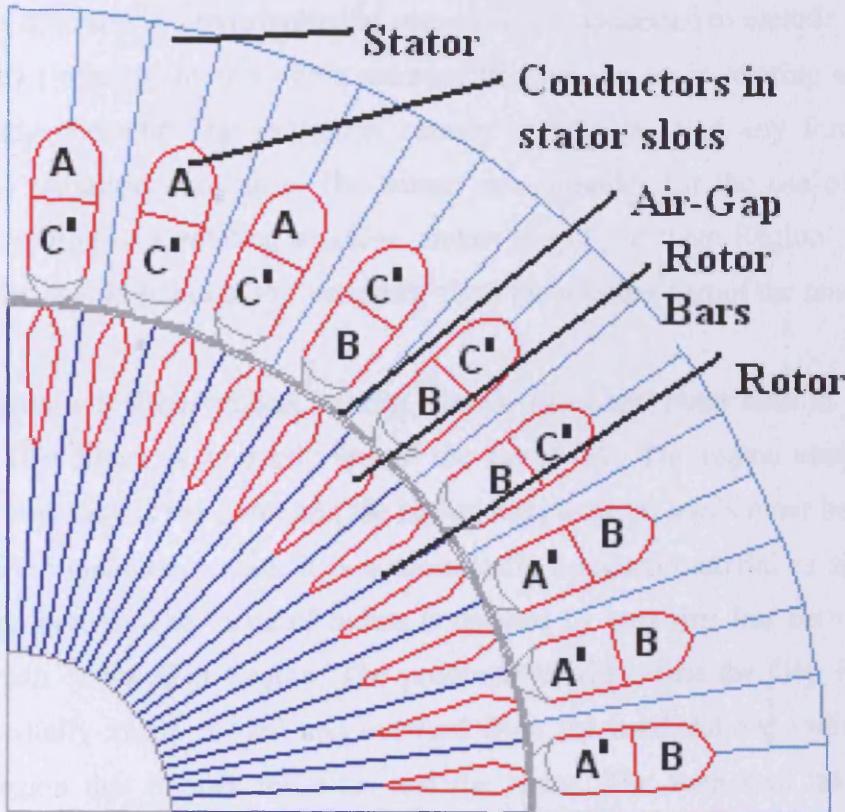
Figure 7.2 One-quarter model of an induction motor in 2D

7.6.1 Inspection of the symmetry

The analysis of the entire structure is computationally expensive and a great deal of time can be saved by analysing only a part of the structure. For electrical machines, the analysis can be readily identified for such a problem. This inspection usually consists of, firstly, enforcing a flux-line boundary along the shaft edge and along the outer periphery of the machine and, secondly, specifying periodicity condition for two lateral, radial edges, separated by one pole pitch. It is also convenient to place the model such that it is symmetrical with respect to one of the coordinate axes. The OPERA 2D rotating machine supports fixed potential boundary condition but does not cater for the periodic boundaries.

7.6.2 Modelling for rotating machine solver

The OPERA 2D rotating machine programme is used to solve the model in this project. This software is a transient eddy current solver, extended to include the effect of rigid body (rotating) motion. This assumes that the device is rotating and hence inducing eddy currents. The excitation current or voltage is of any form that is described by variation over time. The solver also provides for the use of external circuits. Modelling of a rotating machine makes use of the 'Gap Region', which is defined by the user to separate the stationary from the rotating part of the model.

The gap region is a single region, having circular inner and outer radii as shown in figure 7.3. This figure is zoomed view of the figure 7.2. The region above the air gap's outer boundary is the stator and the region below the air gap's inner boundary is the rotor of the induction motor. It is automatically assigned material as air with its respective properties. The value of radius is defined by user that lies between inner and outer radii of the Gap Region. The programme will create the Gap Region by extending radially inside inward and outward from the used defined radius until it finds the region that defines the rotor and the stator. The snap shot taken of the rotating motion of the three-phase induction motor is as shown in the figure 7.4.
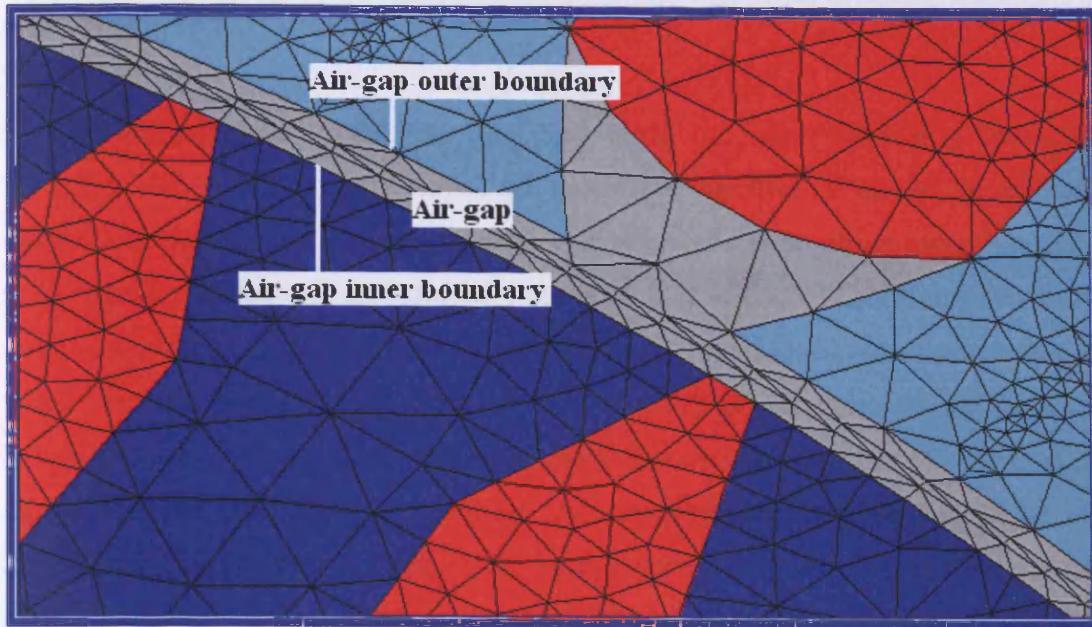
Figure 7.3 Air-gap in the induction motor 2D model
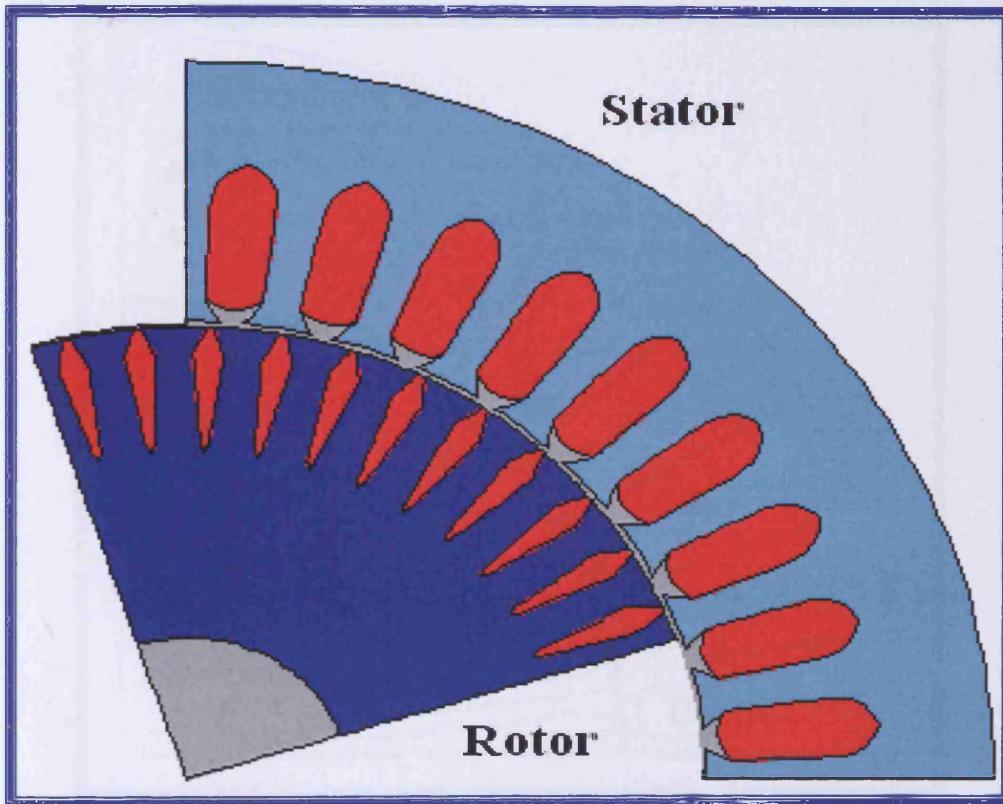
Figure 7.4 Snapshot of the rotating motion of three-phase induction motor

7.6.3 Short pitching design

The rotating machine model was designed using the same dimension, excitation voltage, number of stator coil turns, and material properties of that of the practical motors used for experimentation. The short pitch of the three-phase induction motor stator winding is done by changing the phases and direction of the conductors in the stator slots. Initially the stator slots were divided into two halves as the motor consists of a double layer winding. For the 180° coil pitch motor, the upper half and the lower half of a stator slot conductor had same phase and current direction as shown in the figure 7.5. The 160° coil pitch motor was designed by changing the phase and direction of current in upper and lower half of the stator slot conductor for the one pole as shown in figure 7.6. Similarly, the 140° and 120° coil pitch were designed by changing the phase and directions of currents in the two and three stator slot conductors respectively in one pole pitch as shown in the figure 7.7 and figure 7.8.
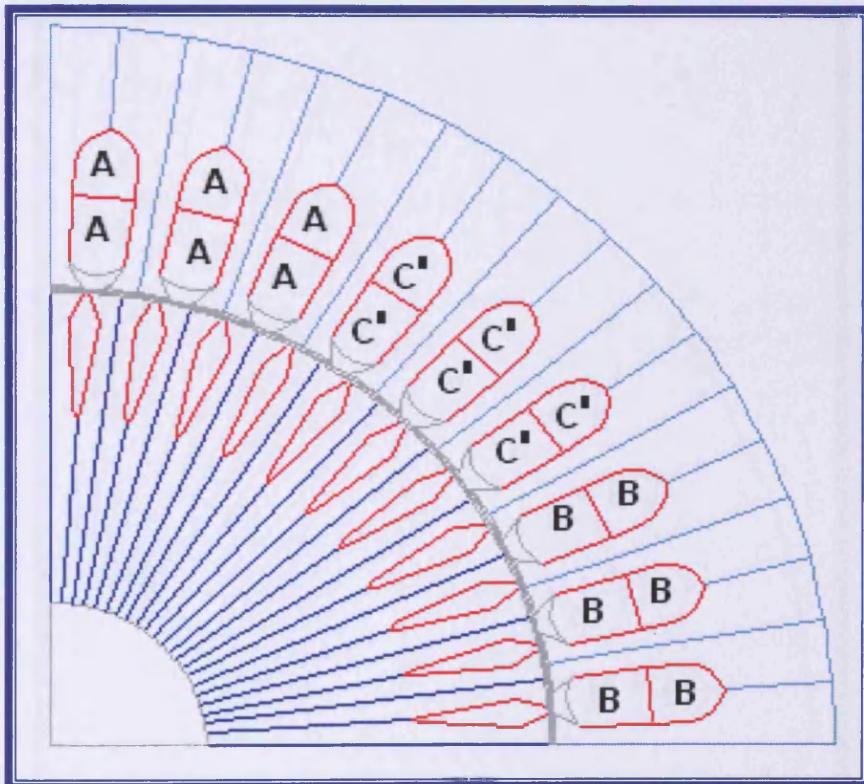
Figure 7.5 Stator winding layout of the 180° coil pitch motor
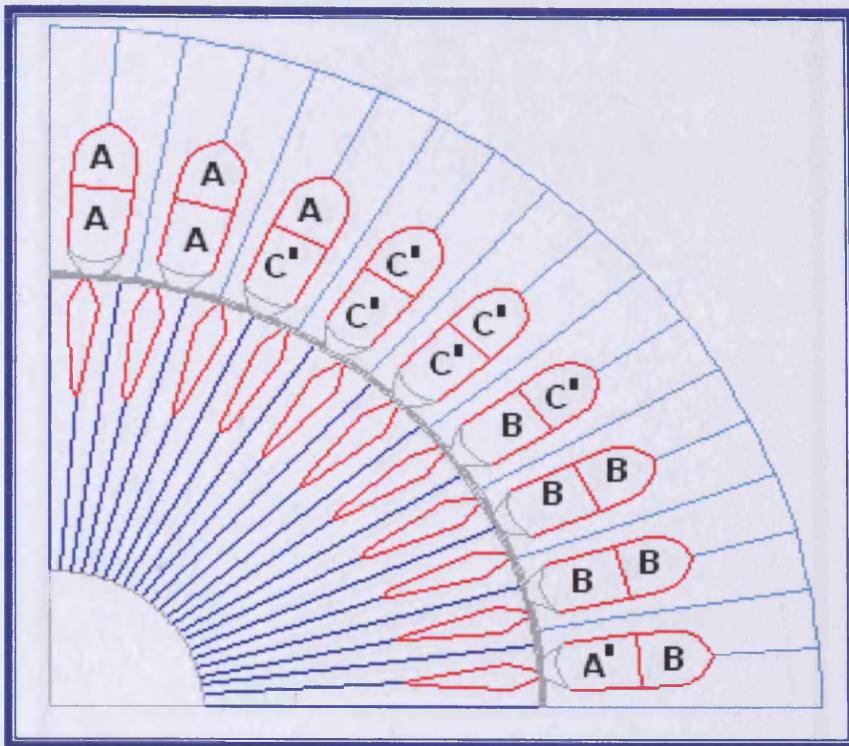
**Figure 7.6 Stator winding layout of the 160° coil pitch motor**
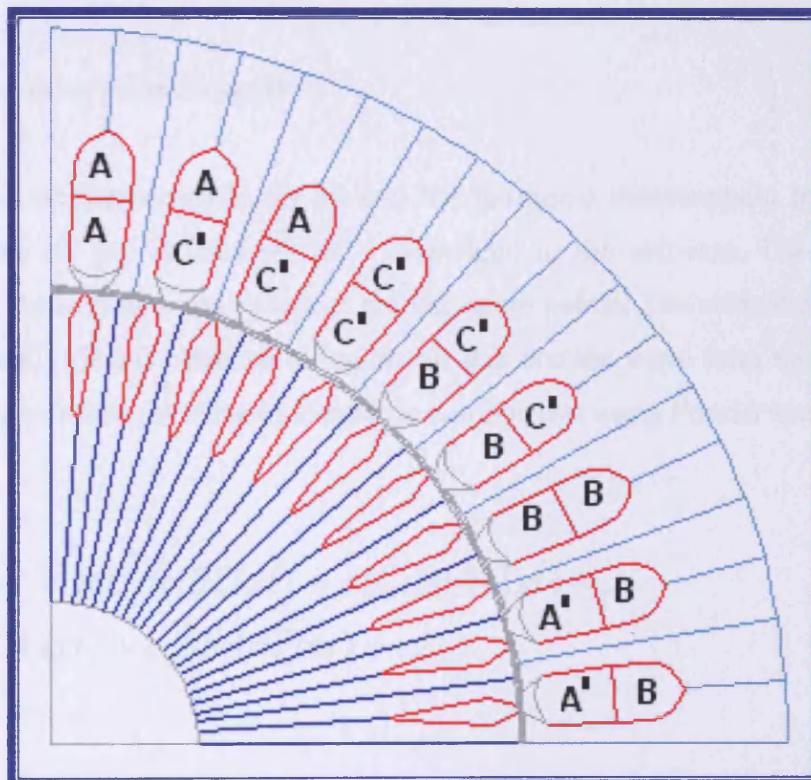
Figure 7.7 Stator winding layout of the 140° coil pitch motor
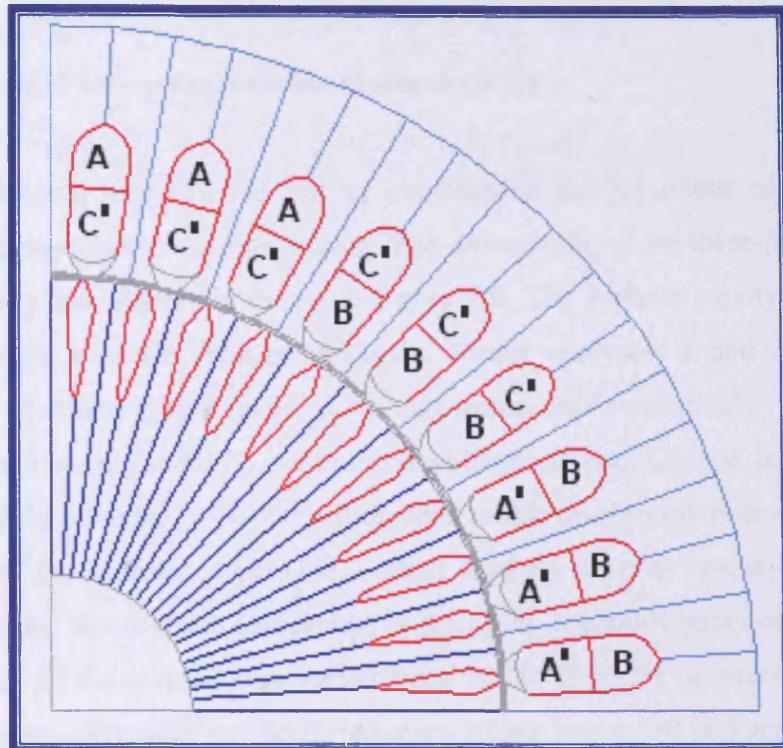
Figure 7.8 Stator winding layout of the 120° coil pitch motor

7.6.4 Harmonics measurement

To measure the harmonics in the air-gap the harmonic measurement tool along the centre of the air gap is used which is embedded in the software. The curvature is defined by the start and end values of the curvature points. The normal component of the flux density (B_n) is obtained along the air-gap and the wave form thus obtained is analysed by software itself for its harmonic components using Fourier series described by

$$F(x) = a_o + a_1 Cos(2\Pi xt) + a_2 Cos(4\Pi xt) + ...$$
$$+ b_1 Sin(2\Pi xt) + b_2 Sin(4\Pi xt) + ...$$

(7.9)

This analysis is done by software itself and the harmonic components obtained are plotted in the chapter 8.

7.7 Experimental set-up for inverter characteristics

The measurements were carried out to characterise the behaviour of the inverter feeding the three-phase induction motor. The connection of the three-phase inverter with measuring instruments is shown in figure 7.9. The 3-phase supply is fed to the inverter through a circuit breaker as shown. Power analysers 1 and 2 are used to measure the input and output currents, voltage and power respectively. To obtain the waveforms of the output PWM current and voltage, an oscilloscope is connected at the output of the inverter. A 3-phase induction motor on no load is connected at the output side of the inverter to provide a small load for inverter operation. The rated frequency of the motor (base frequency) is set up by a control panel of the inverter. The frequency of the inverter was varied from 10 Hz to 60 Hz in intervals of 10 Hz, which was compatible with the rated frequency of the motor (50 Hz) and with a fixed switching frequency of 3 kHz. For completeness, the speed of the motor indicated on inverter control panel was recorded. The stator current represents the magnetizing current in the motor at no-load. At nominal frequency this current gives the desired flux, which gives the desired air gap magnetic induction.
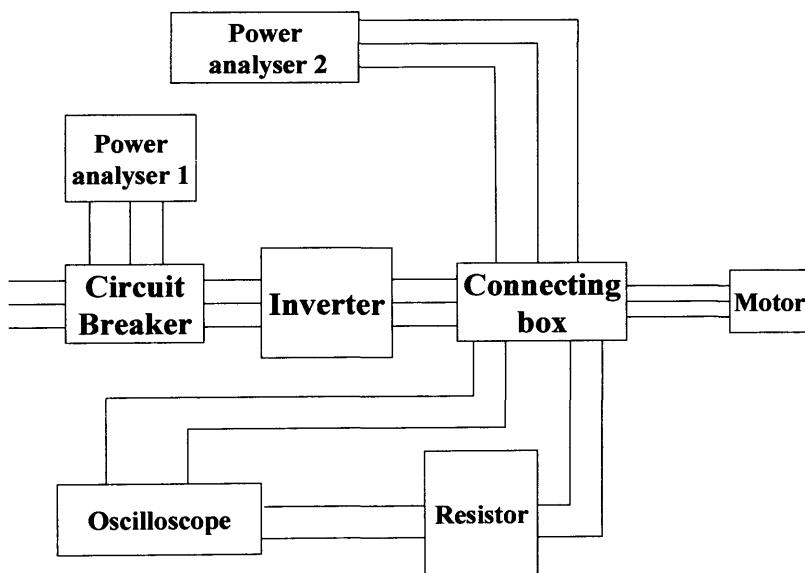
Figure 7.9 Experimental set-up to measure the efficiency of the PWM inverter and to record the output current and voltage waveforms.

REFERENCES FOR CHAPTER 7

[7.1] A. Hrennikoff, "Solution of problems of elasticity by the frame-work method", ASME J. Appl. Mech. Vol. 8, pp. A619–A715, 1941

[7.2] P Silvester, M Chari, "Finite element solution of saturable magnetic problems", IEEE Trans. Power Apparatus Syst., Vol. 89, No. 7, pp. 1642-1650, 1970

[7.3] O. Zienkiewiez, "The finite element method in engineering science", McGraw-Hill, London, 1977

[7.4] I. Nathan, J. Basto, "Electromagnetics and calculation of fields", Spinger-Verlag, New York, 1997

[7.5] C. Towbridge, "An introduction to computer-aided electromagnetic analysis", Wessex Press Ltd., Oxon, England, 1990

[7.6] K. Riley, "Mathematical methods for the physical sciences", Cambridge University Press, 1974

[7.7] P. Silvester, R. Ferrari, "Finite element for electrical engineering", Second Edition, Cambridge University Press, 1990

[7.8] E. Freeman, "The MagNet user Guide", Infolytica, March 1991

[7.9] D. Lowther, P Silvester, "Computer-aided design in magnetics", Springer-Verlag, New York, 1986

[7.10] S. Fu, "Review and future application of finite element method in induction motors", Electrical machines and power systems, Vol. 26, pp. 111-125, 1998

CHAPTER 8

RESULTS BASED ON EXPERIMENTS AND SIMULATIONS

8.1 Introduction

The measurements were carried out for the four, three-phase squirrel cage induction motors with stator winding coil pitches of 180°, 160°, 140° and 120°. The first sets of measurements were taken under sinusoidal voltage supply and the other set of measurement were under PWM voltage, supplied by a PWM inverter. The switching frequency and the modulation frequency of the inverter were varied. Simulations were carried using OPERA 2D software, rotating machine model under sinusoidal voltage supplies.

8.2 Measurements under sinusoidal voltage supplies

All four motors were tested for their efficiencies, voltage harmonic distortion and lower level harmonic contents under a sinusoidal voltage supply. The supply voltage was 230V, 3.5A. The measurements were carried out at 1 N-m, 2.5 N-m, 3.5 N-m, 4.5 N-m, 5.5 N-m and 6.5 N-m torques applied to the shaft using eddy current brake. Graphs were plotted for lower order harmonics, total harmonic distortion (THD) and efficiency against each re-wound motor under sinusoidal supply. The graphs plotted in figure 8.1 to figure 8.5 are under a sinusoidal voltage supply.
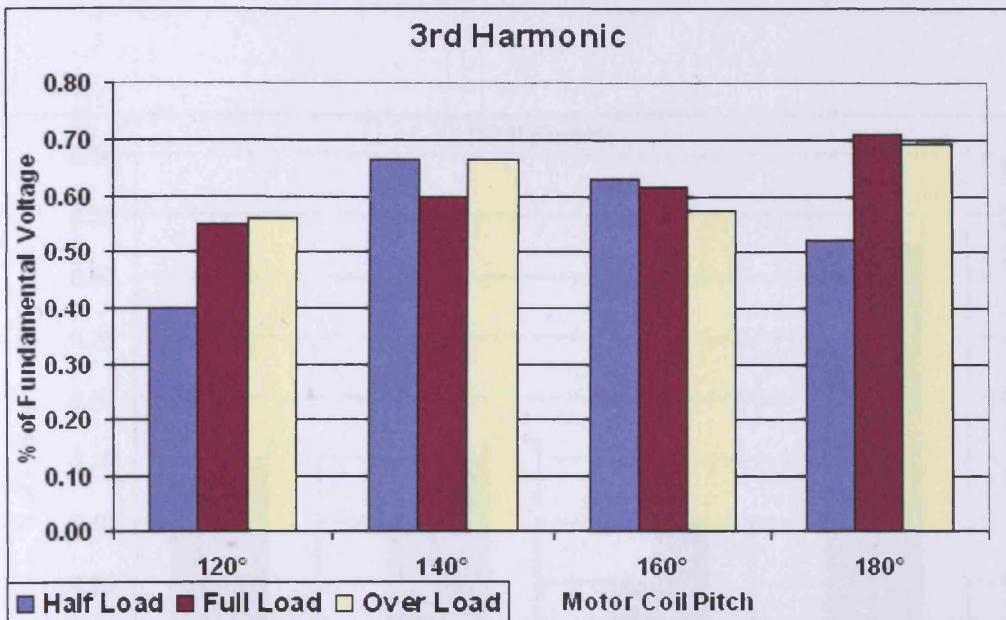
Figure 8.1 Third harmonic voltages as percentages of the fundamental voltage for the 120°, 140°, 160° and 180° coil pitch motors at half load, full load and overload under sinusoidal supply voltage.
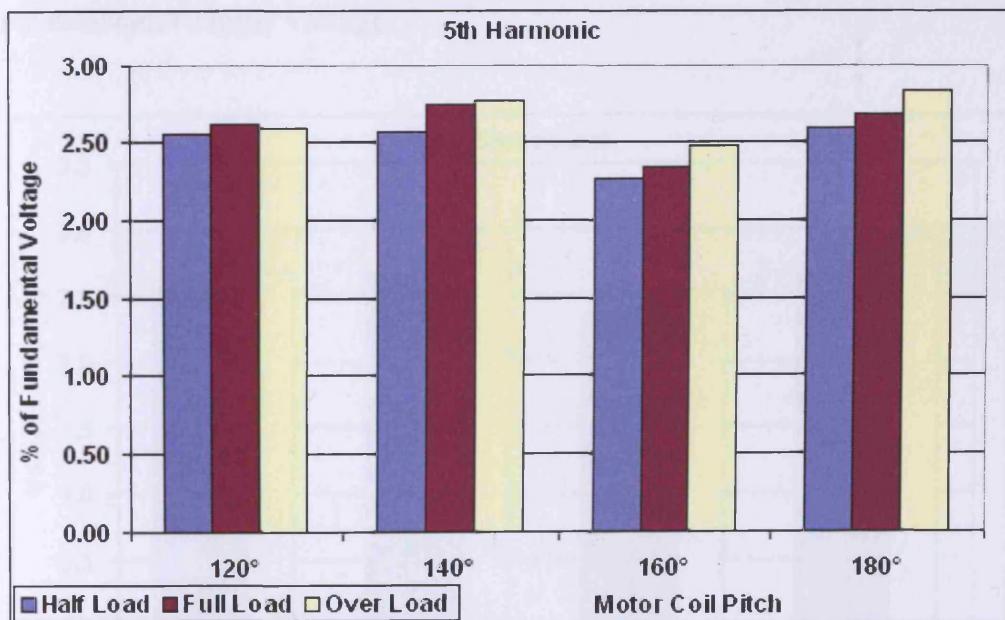

Figure 8.2 Fifth harmonic voltages as percentages of the fundamental voltage for the 120°, 140°, 160° and 180° coil pitch motors at half load, full load and overload under sinusoidal supply voltage.
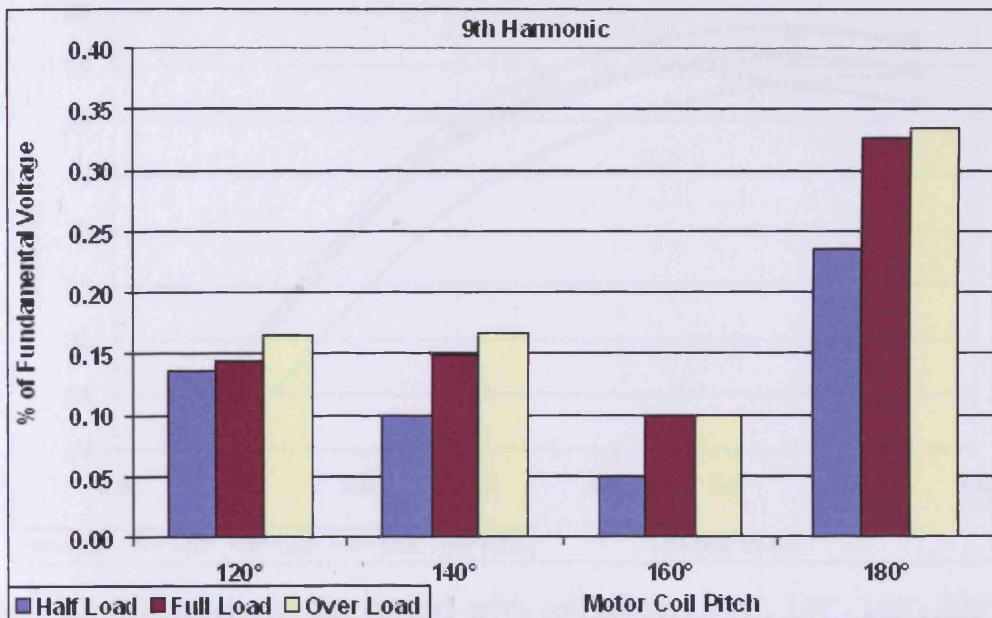
Figure 8.3 Ninth harmonic voltages as percentages of the fundamental voltage of the 120°, 140°, 160° and 180° coil pitch motors at half load, full load and overload under sinusoidal supply voltage.
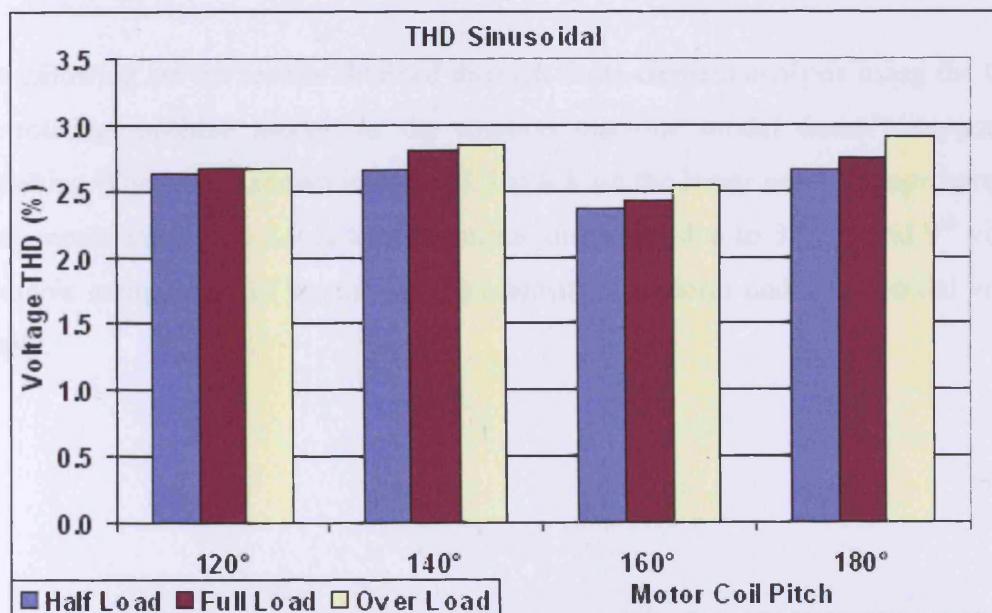
Figure 8.4 Total harmonic distortion voltages due to 3rd, 5th and 9th harmonic voltages as percentages of the fundamental voltage for the 120°, 140°, 160° and 180° coil pitch motors at half load, full load and overload under sinusoidal supply voltage.
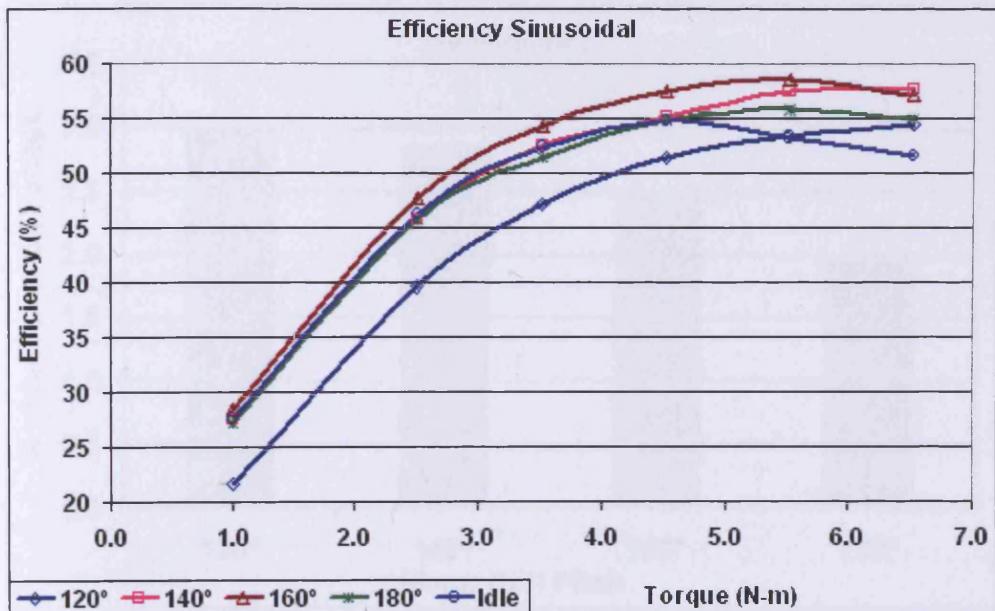
Figure 8.5 Efficiencies of the motors with coil pitches 120°, 140°, 160°, 180° and the motor before rewinding at different torques under sinusoidal voltage supply.

8.3 Finite Element Analysis under sinusoidal voltage supplies

The following are the results obtained through finite element analysis using the Opera 2D rotating machine model, as the rotation machine model doesn't support 3D modelling. The results shown in figure 8.6 to 8.8 are the lower order voltage harmonic components and figure 8.9 is total harmonic distortion due to 3rd, 5th and 9th voltage harmonic components of the air-gap flux density waveform under sinusoidal voltage supply.
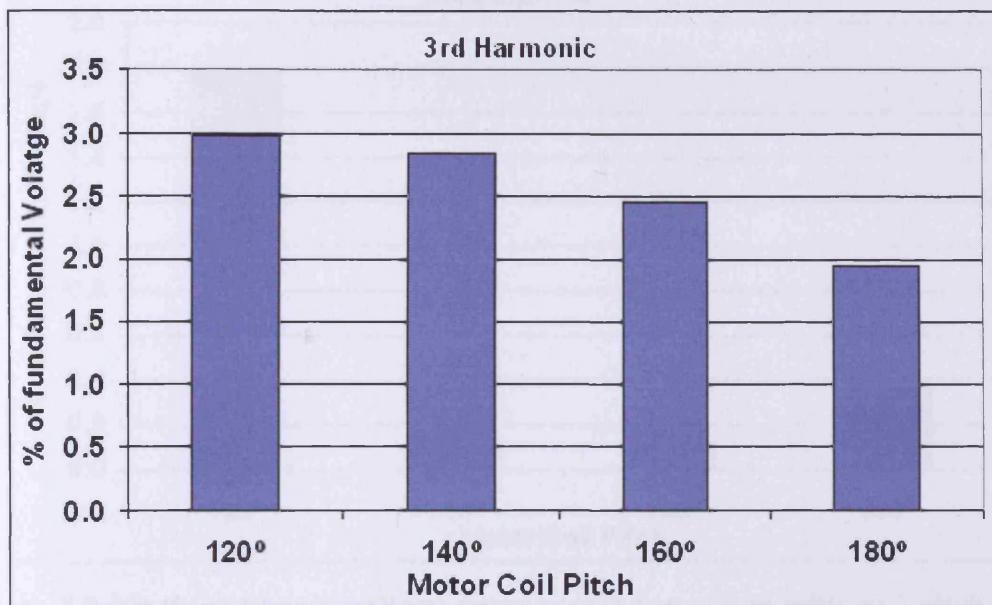
Figure 8.6 **Third harmonic voltage components for motor with coil pitch 120°, 140°, 160° and 180° under sinusoidal voltage supply using finite element analysis, rotating machine model**
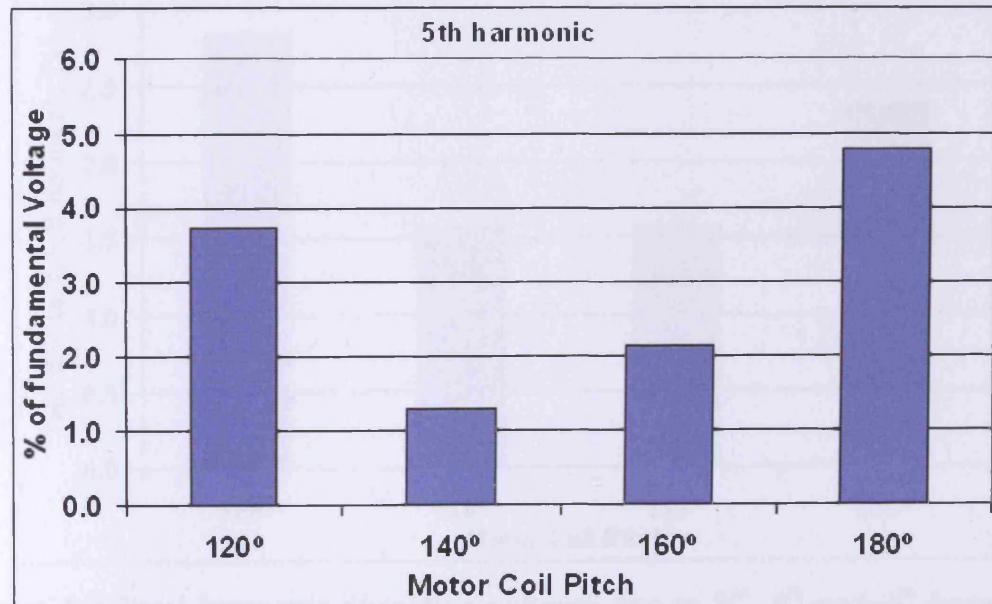

Figure 8.7 **Fifth harmonic voltage components for motor with coil pitch 120°, 140°, 160° and 180° under sinusoidal voltage supply using finite element analysis, rotating machine model**
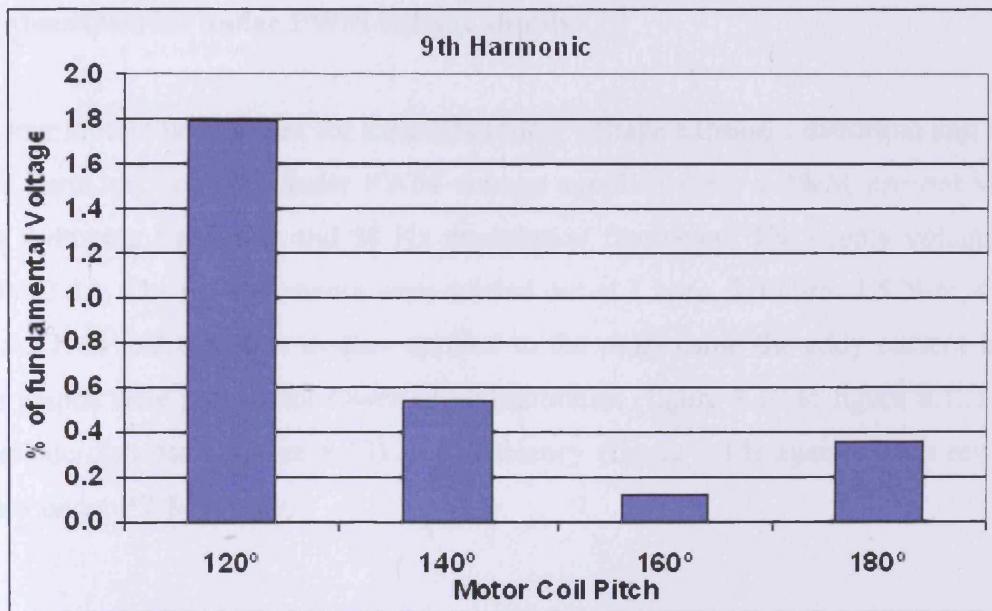
Figure 8.8 Ninth harmonic voltage components for motor with coil pitch 120°, 140°, 160° and 180° under sinusoidal voltage supply using finite element analysis, rotating machine model
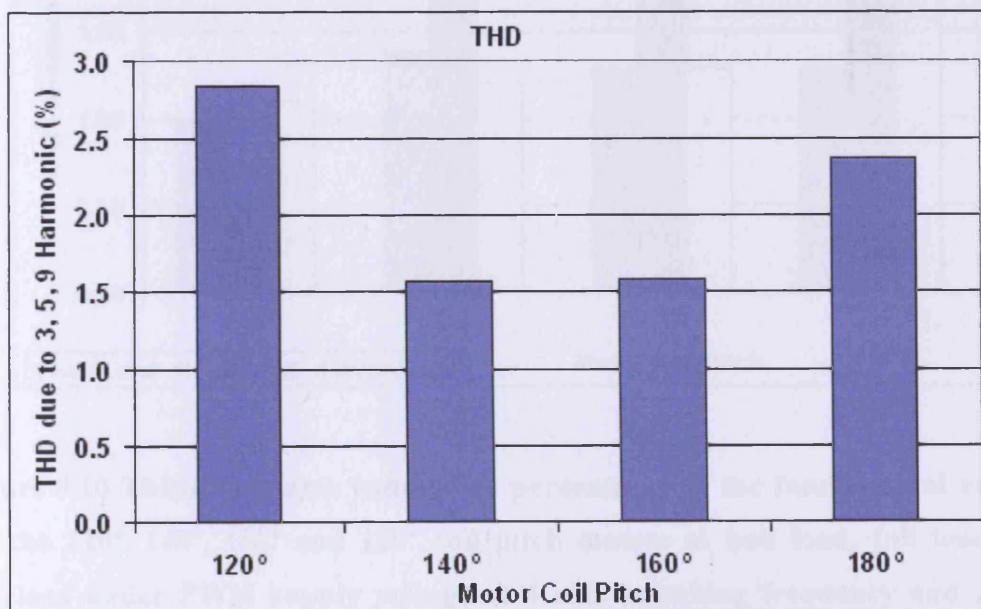

Figure 8.9 Total harmonic distortion voltages due to 3rd, 5th and 9th harmonic voltages in percentages of fundamental voltage for the 120°, 140°, 160° and 180° coil pitch motors under sinusoidal supply voltage using finite element analysis, rotating machine model

8.4 Measurement under PWM voltage supply

All four motors were tested for their efficiency, voltage harmonic distortion and lower level harmonic contents under PWM voltage supplied from a PWM inverter with 4 kHz switching frequency and 50 Hz modulation frequency. The supply voltage was 230V, 3.5A. The measurements were carried out at 1 N-m, 2.5 N-m, 3.5 N-m, 4.5 N-m, 5.5 N-m and 6.5 N-m torques applied to the shaft using the eddy current brake. The graphs were plotted for lower order harmonics (figure 8.10 to figure 8.12), total harmonic distortion (figure 8.13) and efficiency (figure 8.14) against each rewound motor under PWM supply.
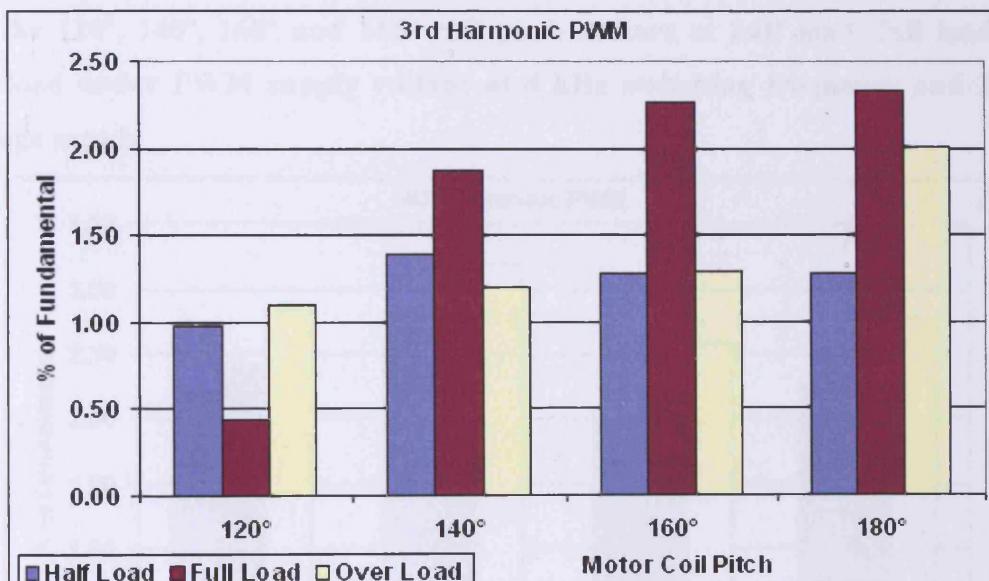
Figure 8.10 Third harmonic voltages as percentages of the fundamental voltage for the 120°, 140°, 160° and 180° coil pitch motors at half load, full load and overload under PWM supply voltage at 4 kHz switching frequency and 230 V voltage supply
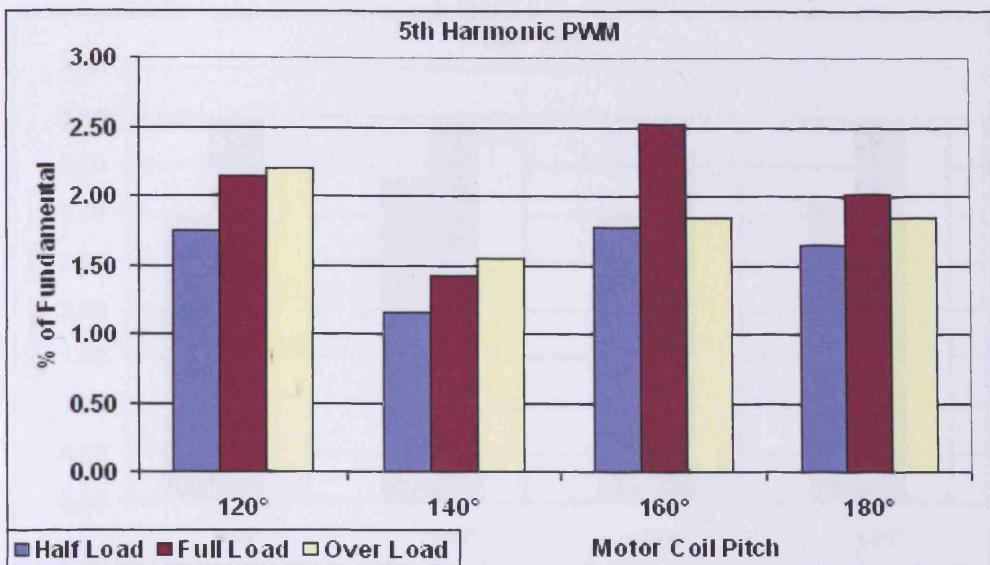
Figure 8.11 Fifth harmonic voltages as percentages of the fundamental voltage for the 120°, 140°, 160° and 180° coil pitch motors at half load, full load and overload under PWM supply voltage at 4 kHz switching frequency and 230 V voltage supply
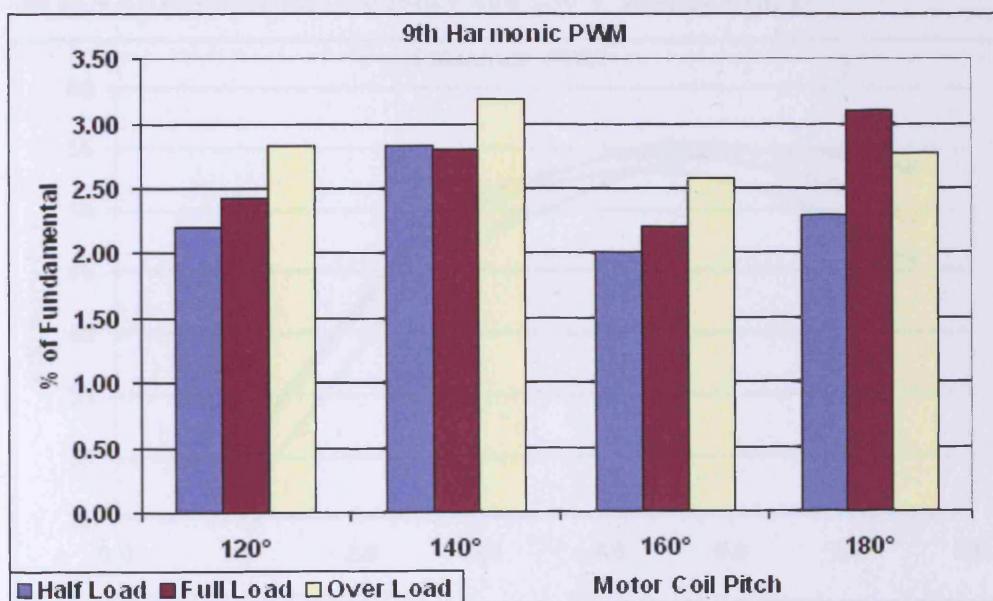

Figure 8.12 Ninth harmonic voltages as percentages of the fundamental voltage for the 120°, 140°, 160° and 180° coil pitch motors at half load, full load and overload under PWM supply voltage at 4 kHz switching frequency and 230 V voltage supply
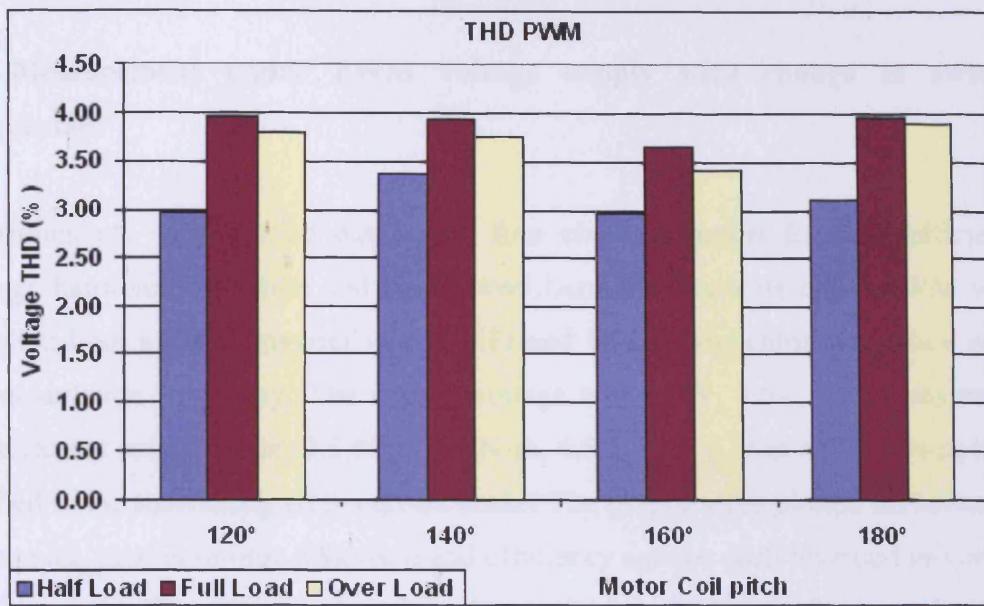
Figure 8.13 Total harmonic distortion voltages due to 3rd, 5th and 9th harmonic voltages as percentages of the fundamental voltage for the 120°, 140°, 160° and 180° coil pitch motors at half load, full load and overload under PWM supply voltage at 4 kHz switching frequency and 230 V voltage supply
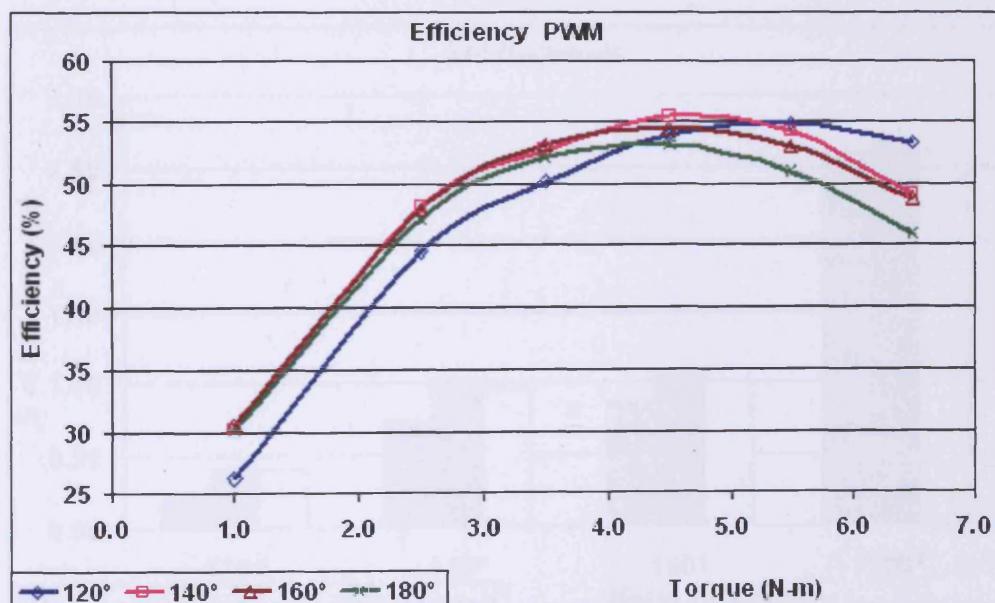

Figure 8.14 Efficiencies of the motors with coil pitches 120°, 140°, 160°, 180° and the motor before rewinding at different torques under PWM supply voltage at 4 kHz switching frequency and 230 V voltage supply

8.5 Measurement under PWM voltage supply with change in switching frequencies

Measurements were carried out for all four chorded motors for their efficiencies, voltage harmonic distortion and lower level harmonic contents under PWM voltage supplied from a PWM inverter with 8 kHz and 16 kHz switching frequency with 50 Hz modulation frequency. The supply voltage was 230V, 3.5A. The measurements were carried out at 1 N-m, 2.5 N-m, 3.5 N-m, 4.5 N-m, 5.5 N-m and 6.5 N-m torques applied to the shaft using eddy current brake. The graphs were plotted for lower order harmonics, total harmonic distortion and efficiency against each rewound motor under PWM supply. The graphs plotted in figure 8.15 to figure 8.19 are under 8 kHz switching frequency and figure 8.20 to figure 8.24 are under 16 kHz switching frequency.
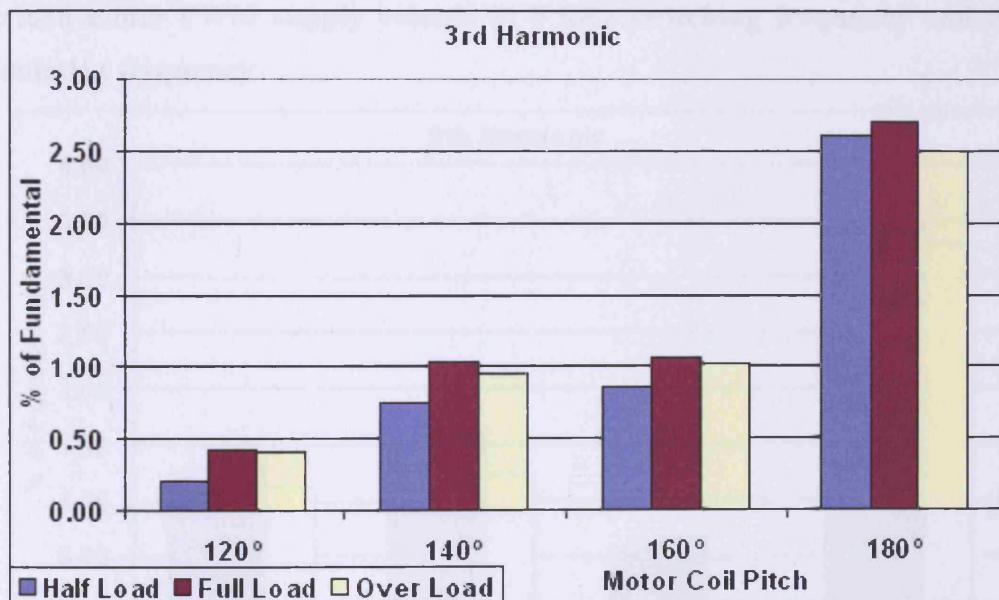
Figure 8.15 Third harmonic voltages as percentages of the fundamental voltage for the 120°, 140°, 160° and 180° coil pitch motors at half load, full load and overload under PWM supply voltage at 8 kHz switching frequency and 50 Hz modulation frequency
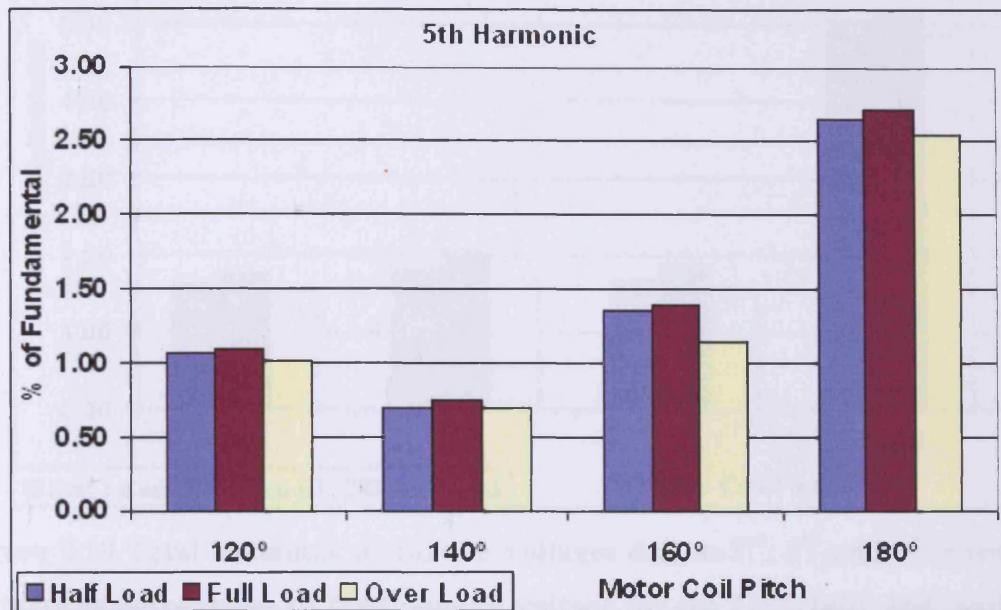
Figure 8.16 Fifth harmonic voltages as percentages of the fundamental voltage for the 120°, 140°, 160° and 180° coil pitch motors at half load, full load and overload under PWM supply voltage at 8 kHz switching frequency and 50 Hz modulation frequency
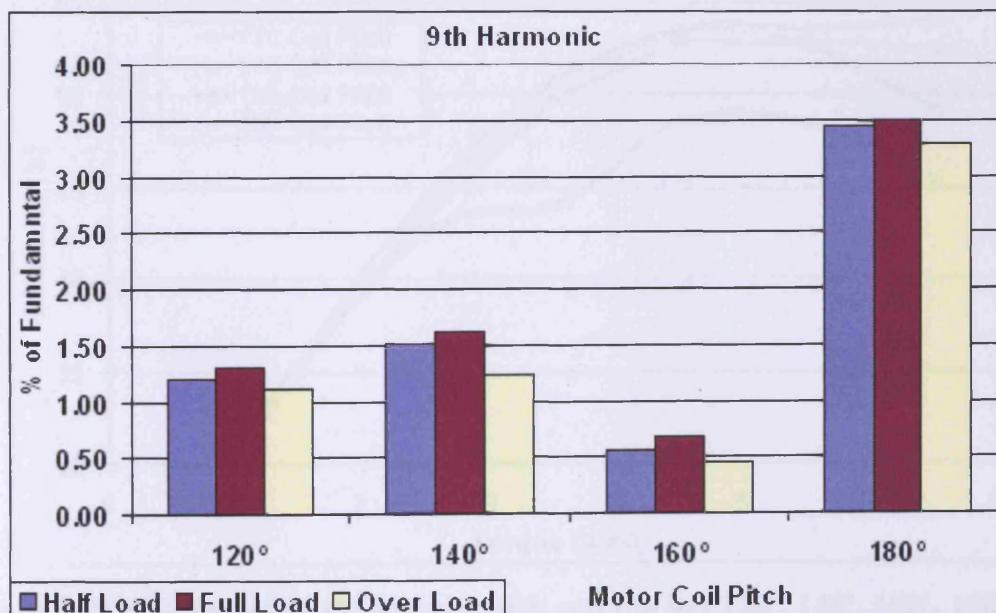
Figure 8.17 Ninth harmonic voltages as percentages of the fundamental voltage for the 120°, 140°, 160° and 180° coil pitch motors at half load, full load and overload under PWM supply voltage at 8 kHz switching frequency and 50 Hz modulation frequency
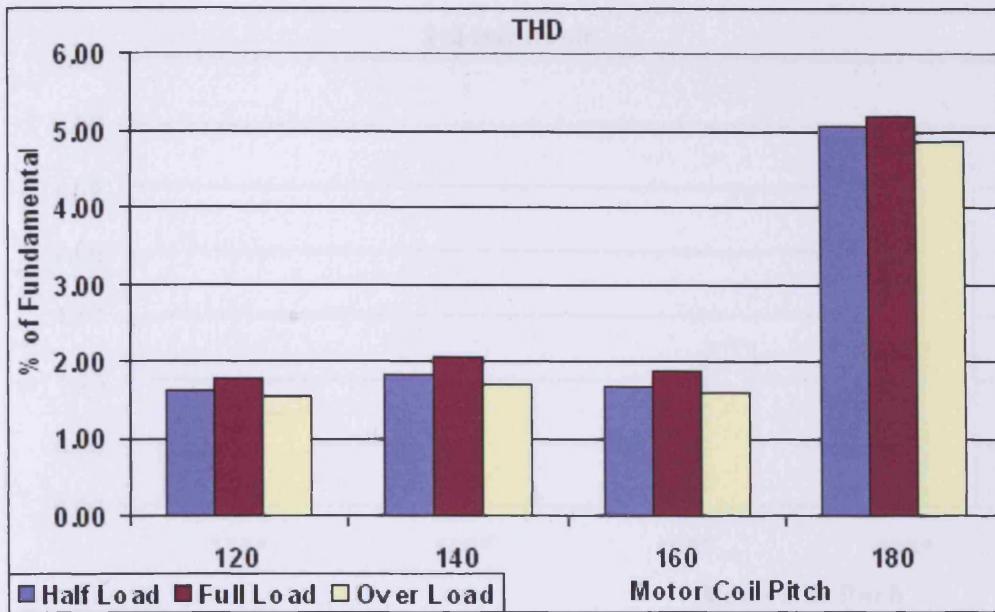
Figure 8.18 Total harmonic distortion voltages due to 3rd, 5th and 9th harmonic voltages as percentages of fundamental voltage for the 120°, 140°, 160° and 180° coil pitch motors at half load, full load and overload under PWM supply voltage at 8 kHz switching frequency and 50 Hz modulation frequency
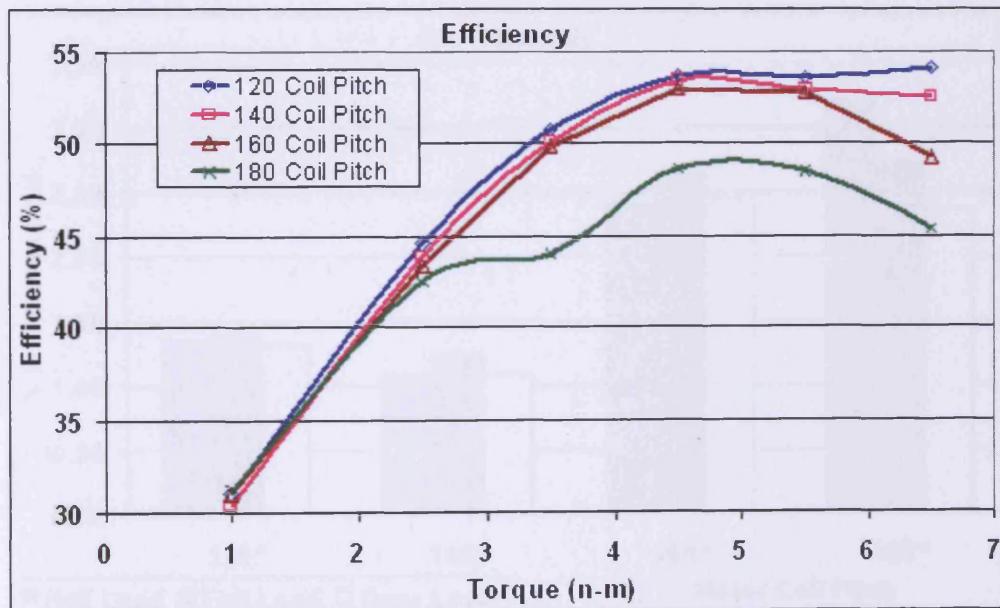

Figure 8.19 Efficiencies of the motors with coil pitches 120°, 140°, 160°, 180° and the motor before rewinding at different torques under PWM supply voltage at 8 kHz switching frequency and 50 Hz modulation frequency
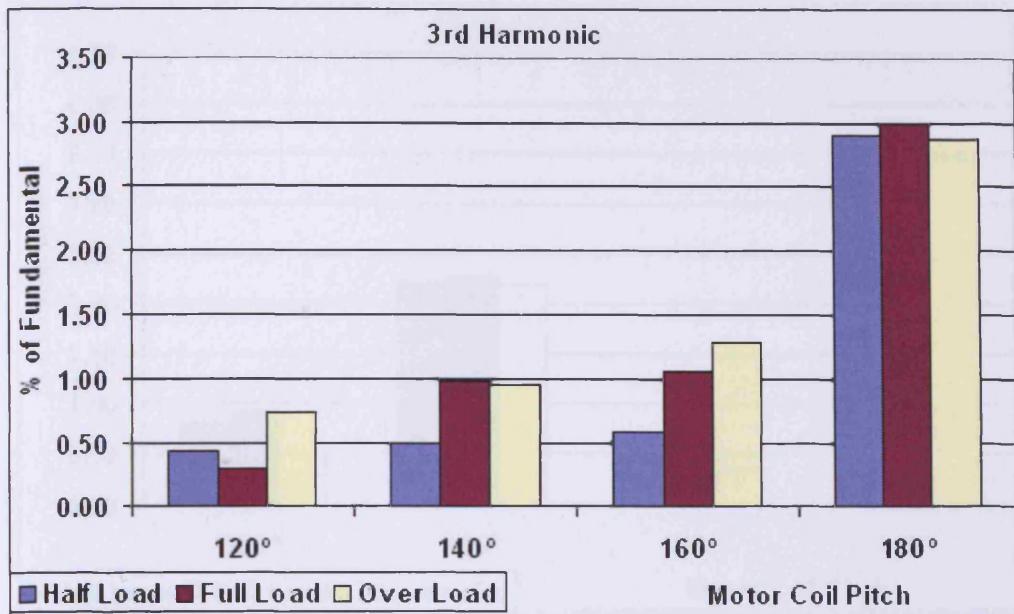
Figure 8.20 Third harmonic voltages as percentages of the fundamental voltage for the 120°, 140°, 160° and 180° coil pitch motors at half load, full load and overload under PWM supply voltage at 16 kHz switching frequency and 50 Hz modulation frequency
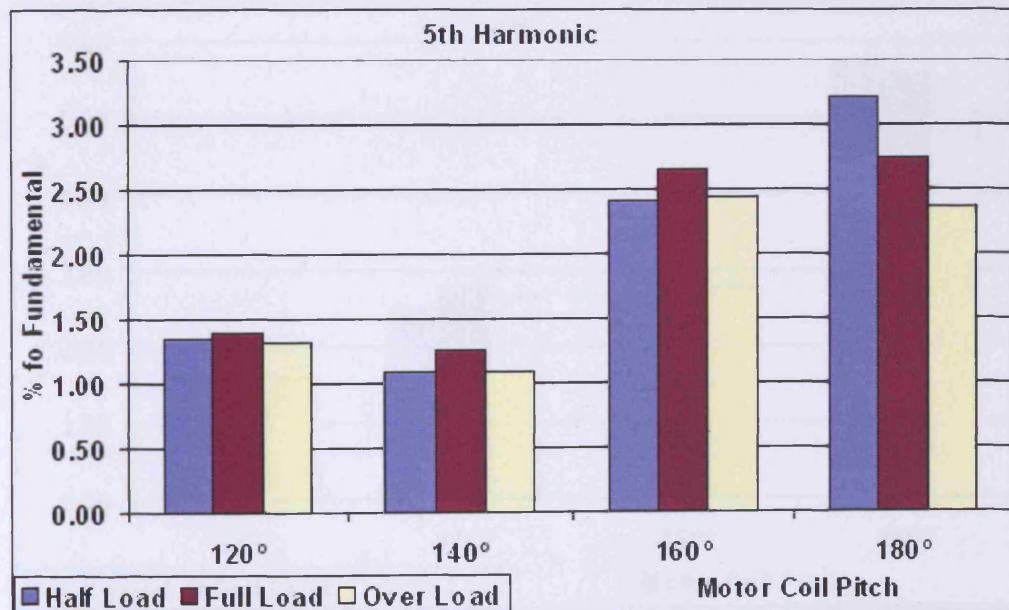

Figure 8.21 Fifth harmonic voltages as percentages of the fundamental voltage for the 120°, 140°, 160° and 180° coil pitch motors at half load, full load and overload under PWM supply voltage at 16 kHz switching frequency and 50 Hz modulation frequency
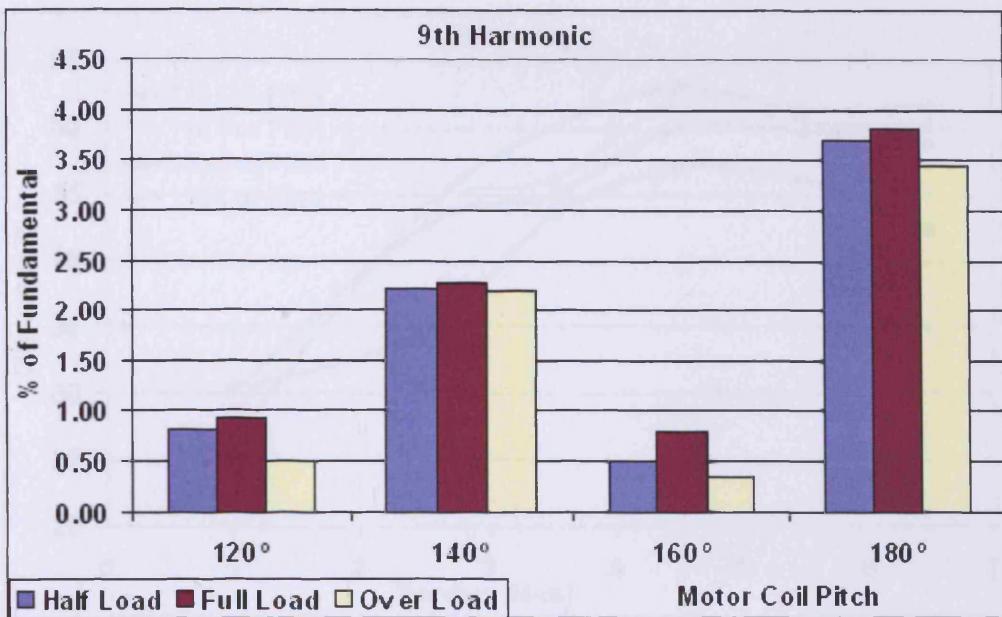
Figure 8.22 Ninth harmonic voltages as percentages of the fundamental voltage for the 120°, 140°, 160° and 180° coil pitch motors at half load, full load and overload under PWM supply voltage at 16 kHz switching frequency and 50 Hz modulation frequency
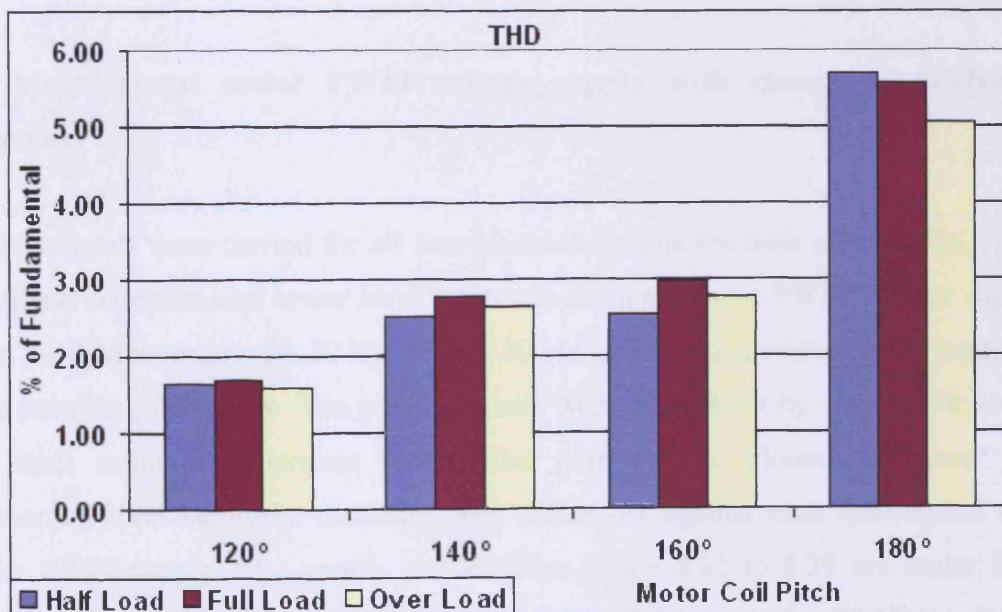
Figure 8.23 Total harmonic distortion voltages due to 3rd, 5th and 9th harmonic voltages as percentages of the fundamental voltage for 120°, 140°, 160° and 180° coil pitch motors at half load, full load and overload under PWM supply voltage at 16 kHz switching frequency and 50 Hz modulation frequency
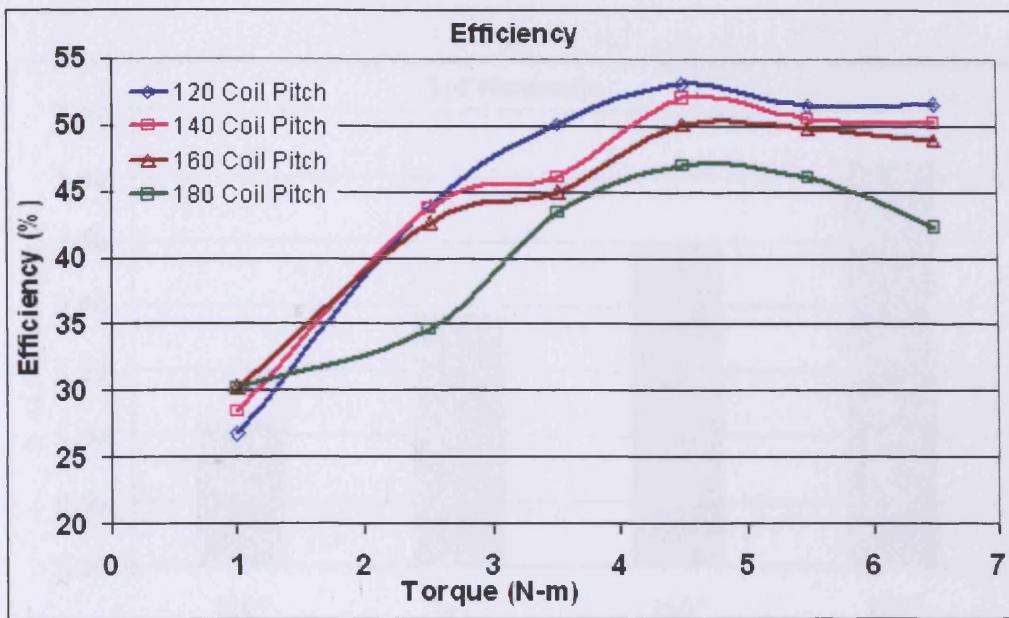
Figure 8.24 Efficiencies of the motors with coil pitches 120°, 140°, 160°, 180° and the motor before rewinding at different torques under PWM supply voltage at 16 kHz switching frequency and 50 Hz modulation frequency

8.6 Measurement under PWM voltage supply with change in modulation frequency

Measurements were carried for all four chorded motors for their efficiencies, voltage harmonic distortion and lower level harmonic contents under PWM voltage supplied from a PWM inverter with 30 Hz, 40 Hz, 50 Hz and 60 Hz modulation frequency at 4 kHz switching frequency. The measurements were carried out by varying the load on the shaft using eddy current brake. The graphs were plotted for lower order harmonics, total harmonic distortion and efficiency against each rewounded motor under PWM supply. The graphs plotted from figure 8.25 to 8.29 are under 30 Hz modulation frequency, from figure 8.30 to figure 8.34 are under 40 Hz modulation frequency, from figure 8.35 to figure 8.39 are under 50 Hz modulation frequency and from figure 8.40 to 8.44 are under 60 Hz modulation frequency.
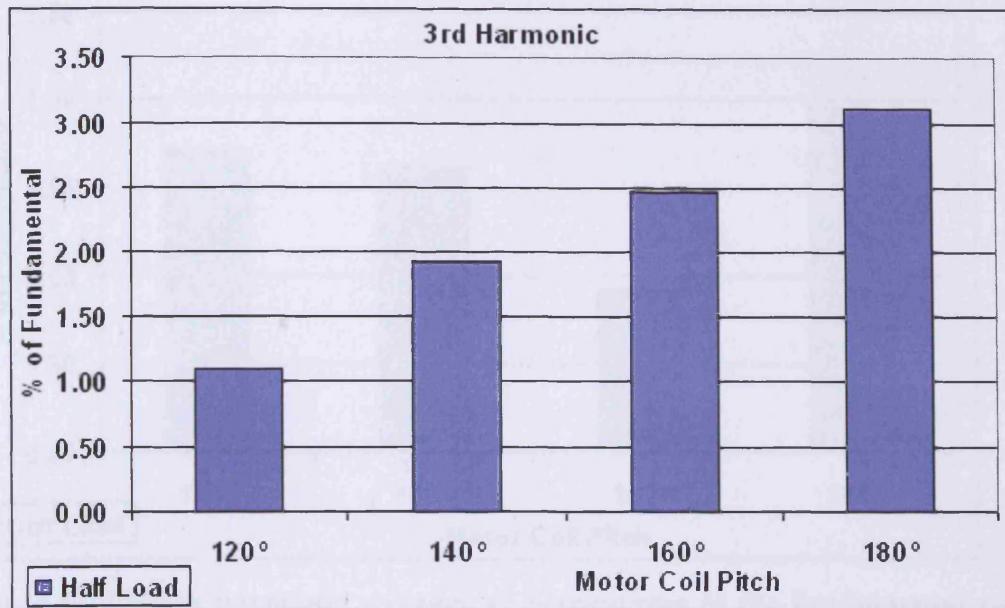
Figure 8.25 Third harmonic voltages as percentages of the fundamental voltage for the 120°, 140°, 160° and 180° coil pitch motors at half load under PWM supply voltage at 30 Hz modulation frequency and 4 kHz switching frequency. (Experimentally measured)
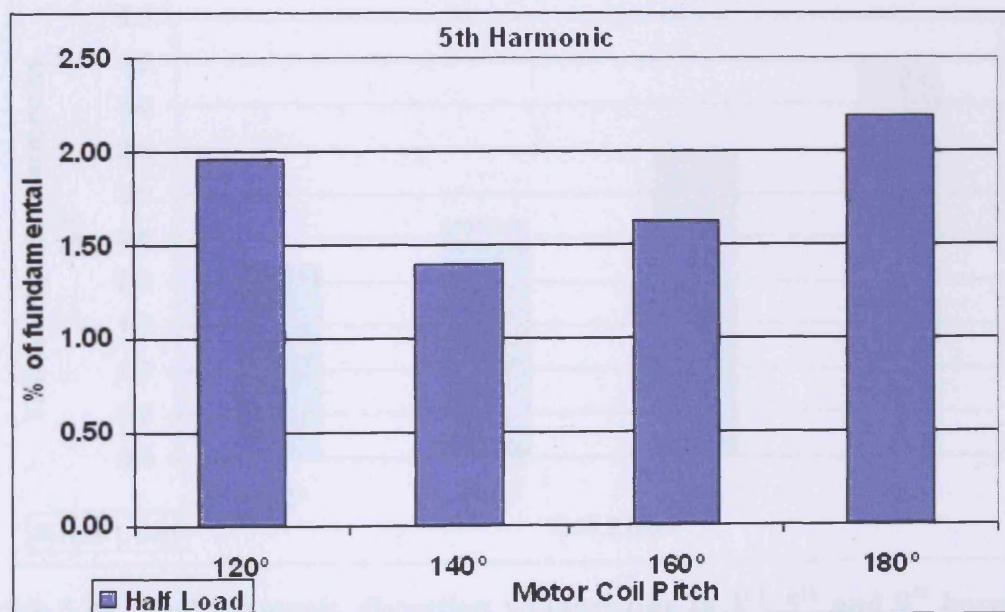
Figure 8.26 Fifth harmonic voltages as percentages of the fundamental voltage for the 120°, 140°, 160° and 180° coil pitch motors at half load under PWM supply voltage at 30 Hz modulation frequency and 4 kHz switching frequency (Experimentally measured)
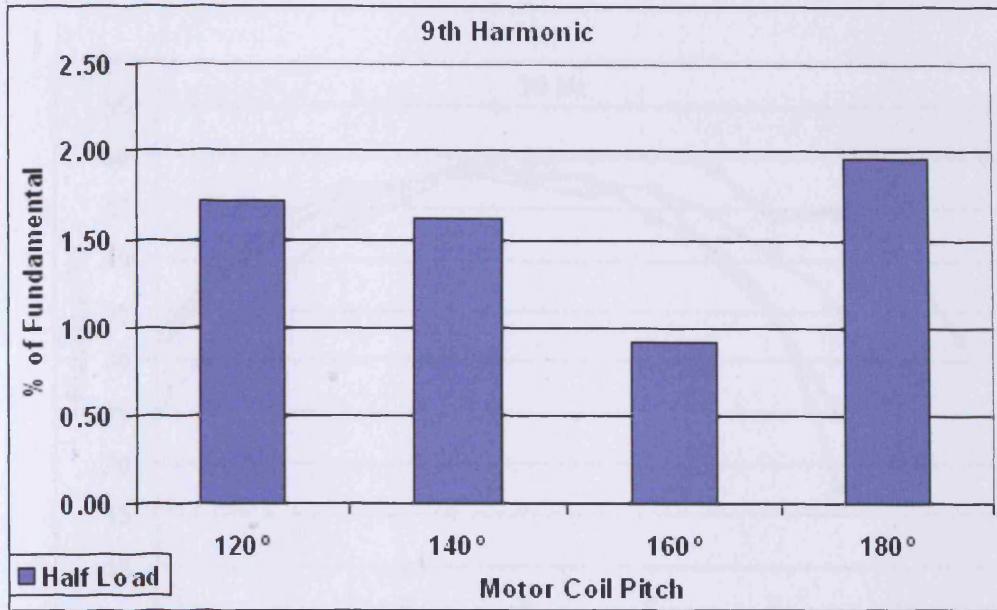
Figure 8.27 Ninth harmonic voltages as percentages of the fundamental voltage for the 120°, 140°, 160° and 180° coil pitch motors at half load under PWM supply voltage at 30 Hz modulation frequency and 4 kHz switching frequency (Experimentally measured)
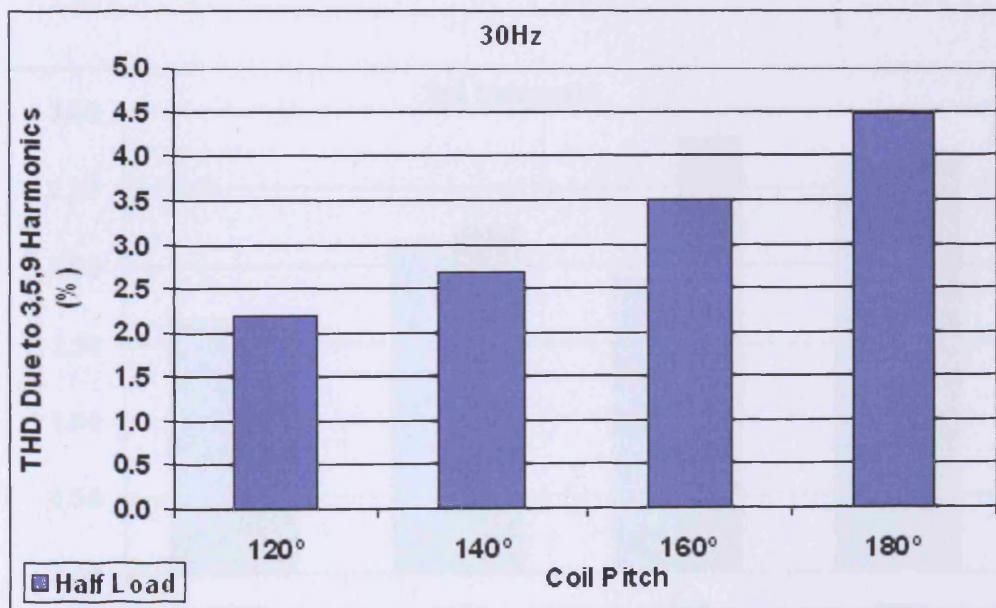
Figure 8.28 Total harmonic distortion voltages due to 3rd, 5th and 9th harmonic voltages as percentages of the fundamental voltage for the 120°, 140°, 160° and 180° coil pitch motors at half load under PWM supply voltage at 30 Hz modulation frequency and 4 kHz switching frequency (Experimentally measured)
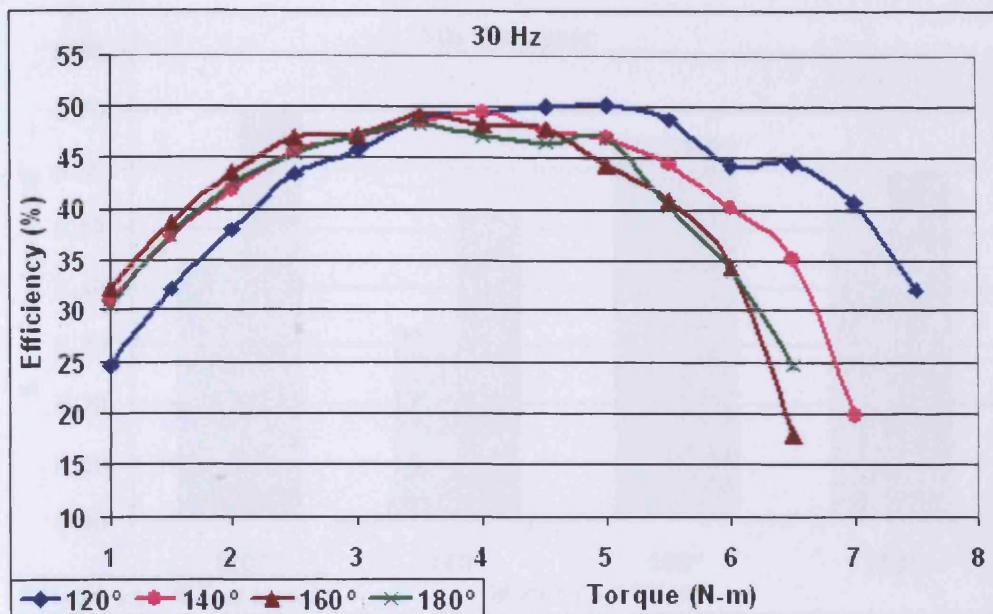
Figure 8.29 Efficiencies of the motors with coil pitches 120°, 140°, 160°, 180° at different torques under PWM supply voltage at 30 Hz modulation frequency and 4 kHz switching frequency
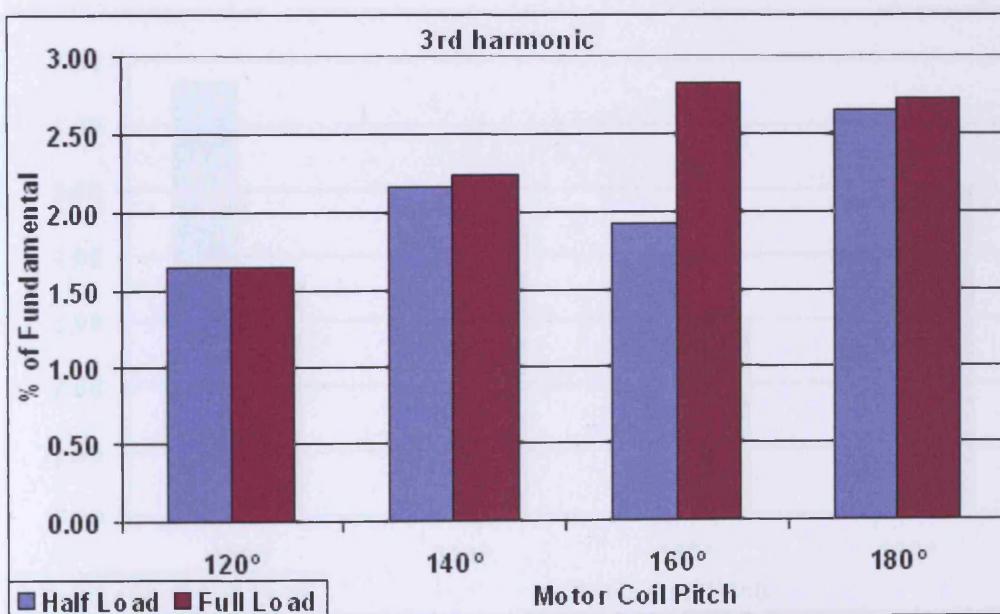
Figure 8.30 Third harmonic voltages as percentages of the fundamental voltage for the 120°, 140°, 160° and 180° coil pitch motors at half load and full load under PWM supply voltage at 40 Hz modulation frequency and 4 kHz switching frequency
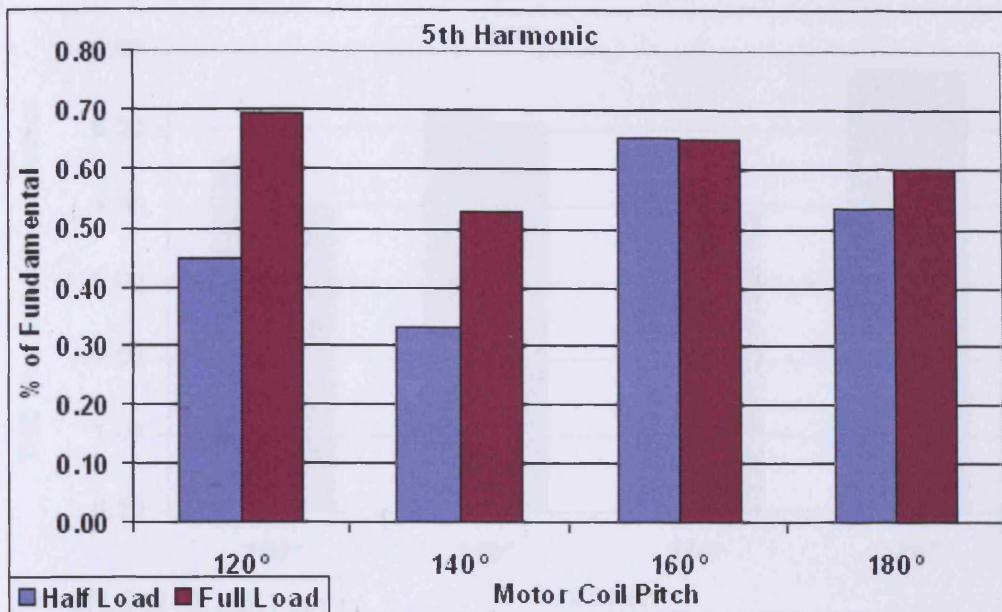
Figure 8.31 Fifth harmonic voltages as percentages of the fundamental voltage for the 120°, 140°, 160° and 180° coil pitch motors at half load and full load under PWM supply voltage at 40 Hz modulation frequency and 4 kHz switching frequency
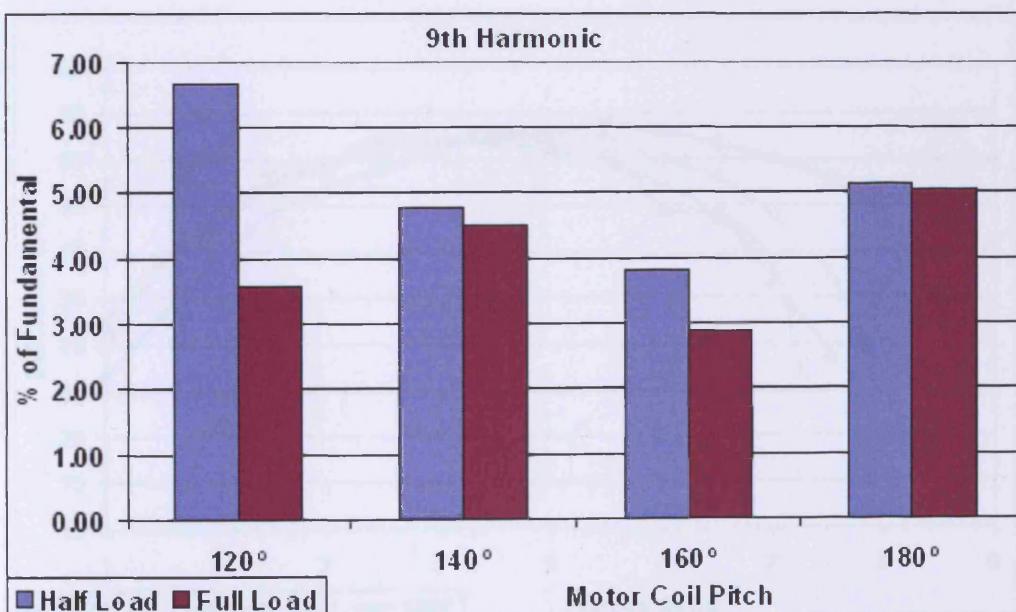

Figure 8.32 Ninth harmonic voltages as percentages of the fundamental voltage for the 120°, 140°, 160° and 180° coil pitch motors at half load and full load under PWM supply voltage at 40 Hz modulation frequency and 4 kHz switching frequency
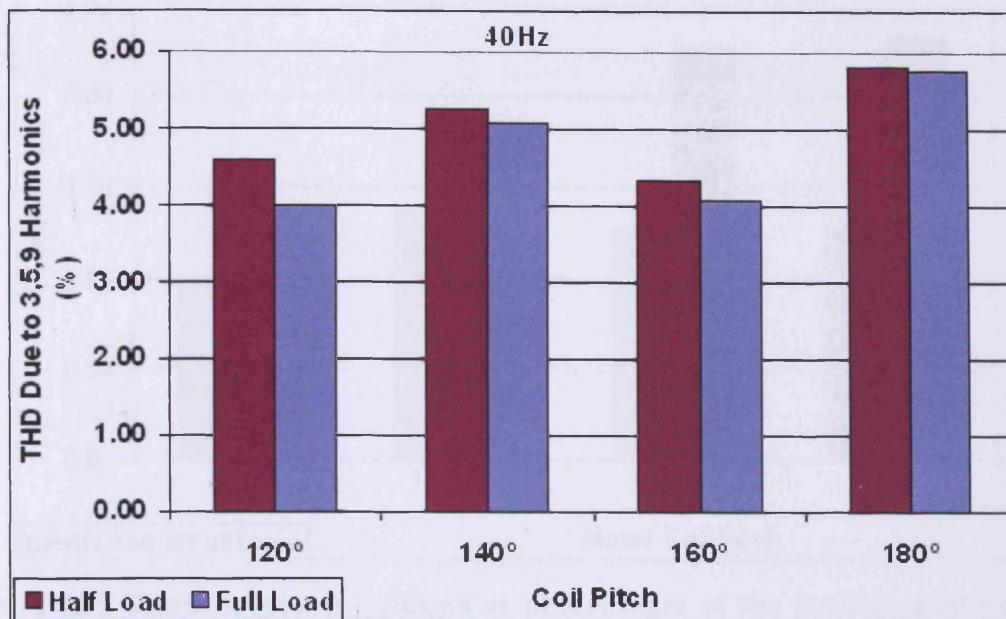
Figure 8.33 Total harmonic distortion voltages due to 3rd, 5th and 9th harmonic voltages as percentages of the fundamental voltage for the 120°, 140°, 160° and 180° coil pitch motors at half load and full load under PWM supply voltage at 40 Hz modulation frequency and 4 kHz switching frequency
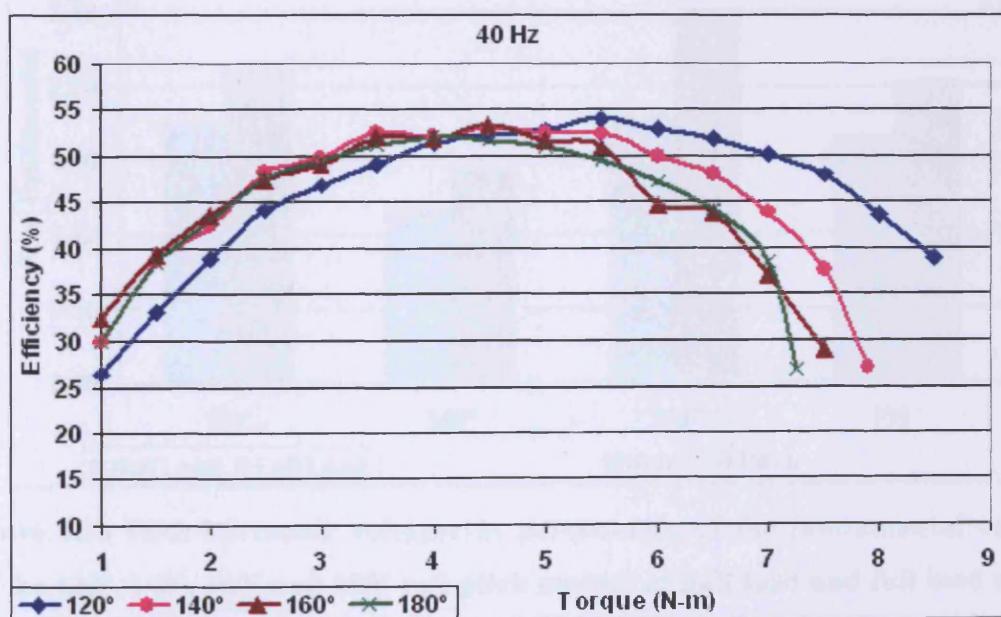
Figure 8.34 Efficiencies of the motors with coil pitches 120°, 140°, 160°, 180° at different torques under PWM supply voltage at 40 Hz modulation frequency and 4 kHz switching frequency
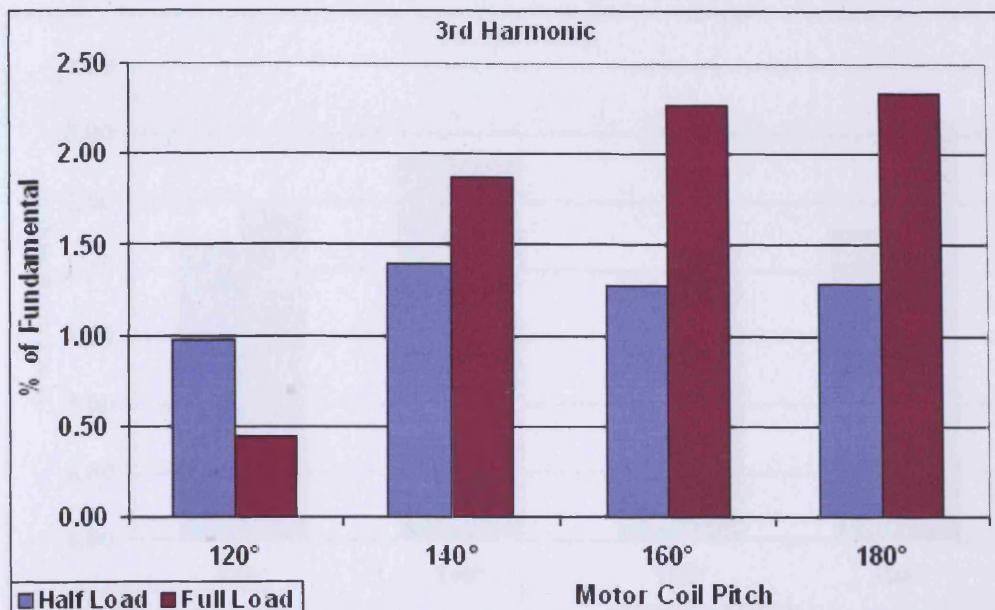
Figure 8.35 Third harmonic voltages as percentages of the fundamental voltage for the 120°, 140°, 160° and 180° coil pitch motors at half load and full load under PWM supply voltage at 50 Hz modulation frequency and 4 kHz switching frequency
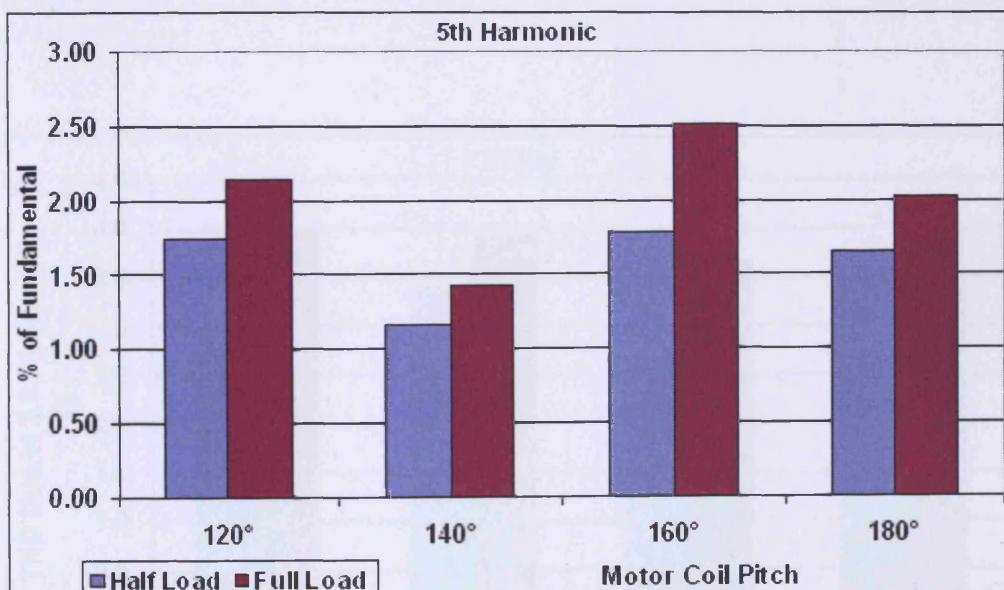
Figure 8.36 Fifth harmonic voltages as percentages of the fundamental voltage for the 120°, 140°, 160° and 180° coil pitch motors at half load and full load under PWM supply voltage at 50 Hz modulation frequency and 4 kHz switching frequency
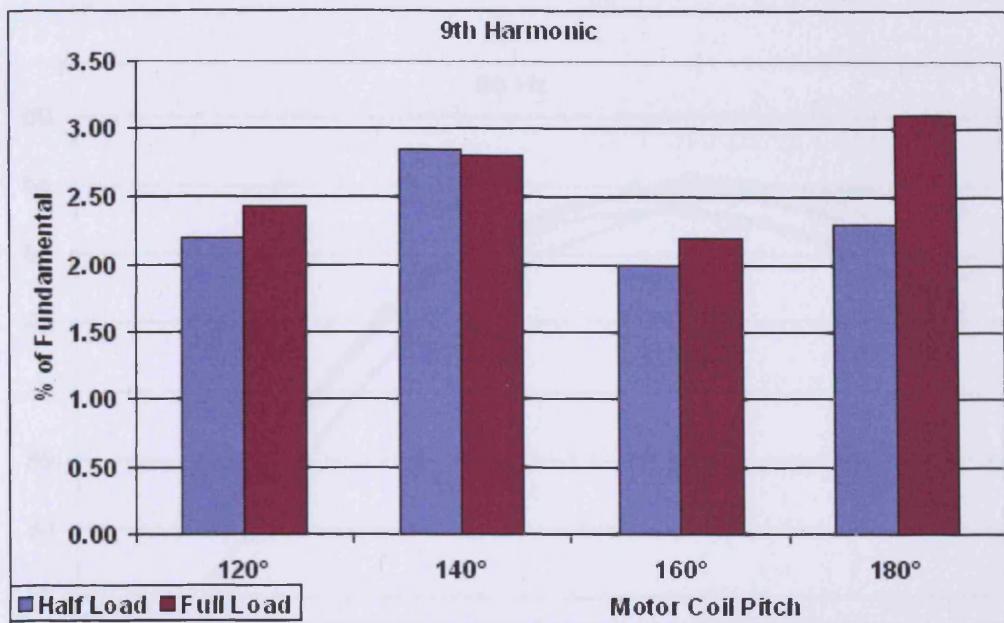
Figure 8.37 Ninth harmonic voltages as percentages of the fundamental voltage for the 120°, 140°, 160° and 180° coil pitch motors at half load and full load under PWM supply voltage at 50 Hz modulation frequency and 4 kHz switching frequency
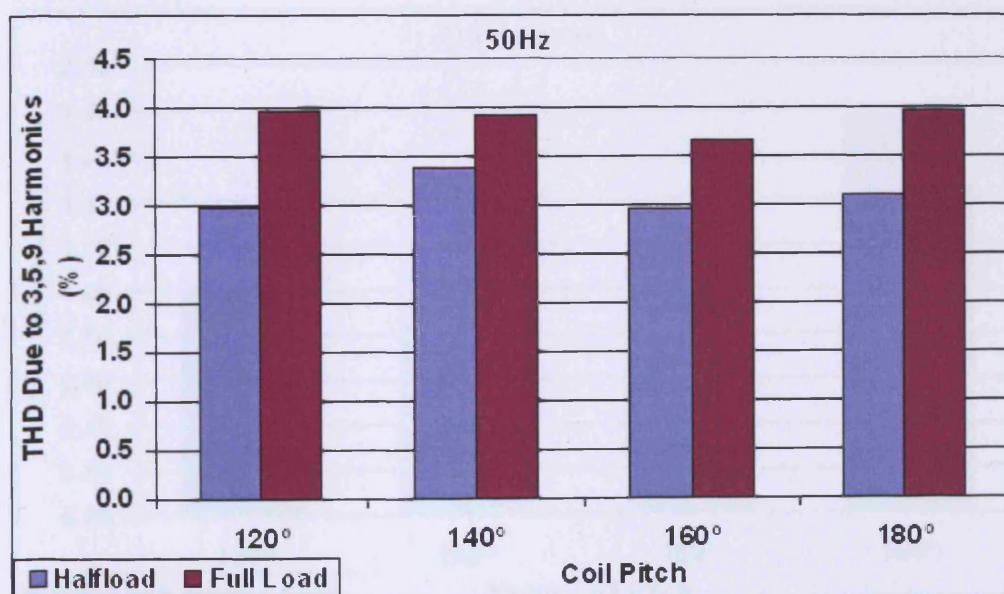

Figure 8.38 Total harmonic distortion voltages due to 3rd, 5th and 9th harmonic voltages as percentages of fundamental voltage for the 120°, 140°, 160° and 180° coil pitch motors at half load and full load under PWM supply voltage at 50 Hz modulation frequency and 4 kHz switching frequency
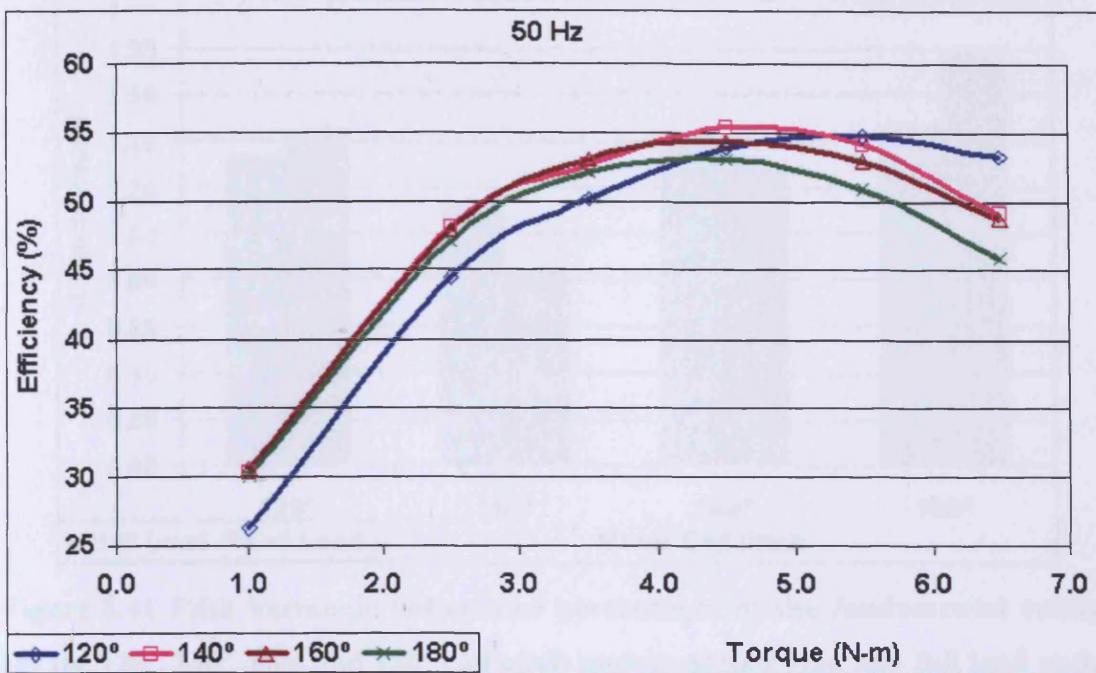
Figure 8.39 Efficiencies of the motors with coil pitches 120°, 140°, 160°, 180° at different torques under PWM supply voltage at 50 Hz modulation frequency and 4 kHz switching frequency
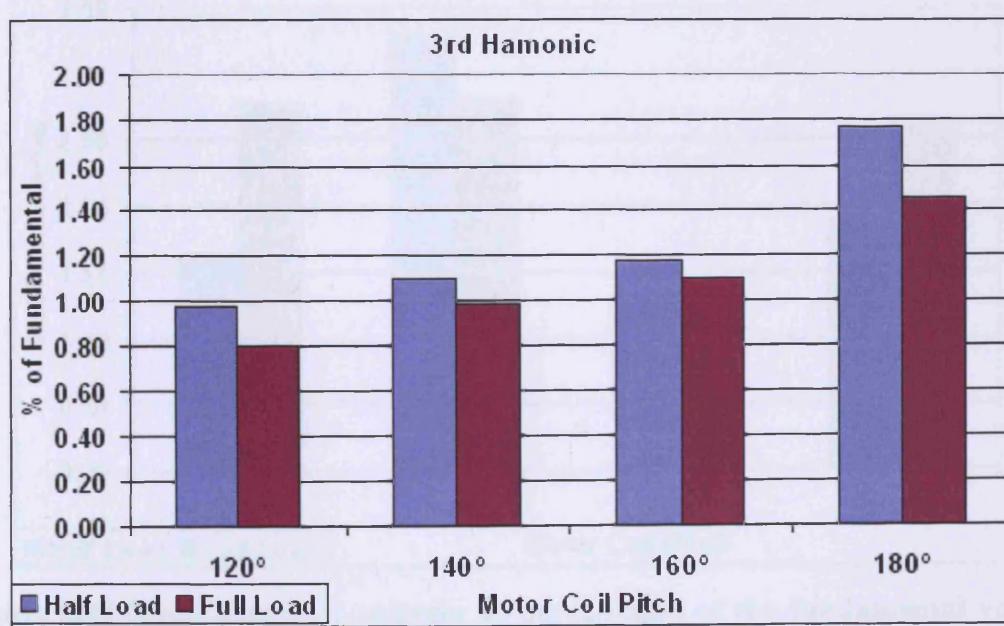

Figure 8.40 Third harmonic voltages as percentages of the fundamental voltage for the 120°, 140°, 160° and 180° coil pitch motors at half load and full load under PWM supply voltage at 60 Hz modulation frequency and 4 kHz switching frequency
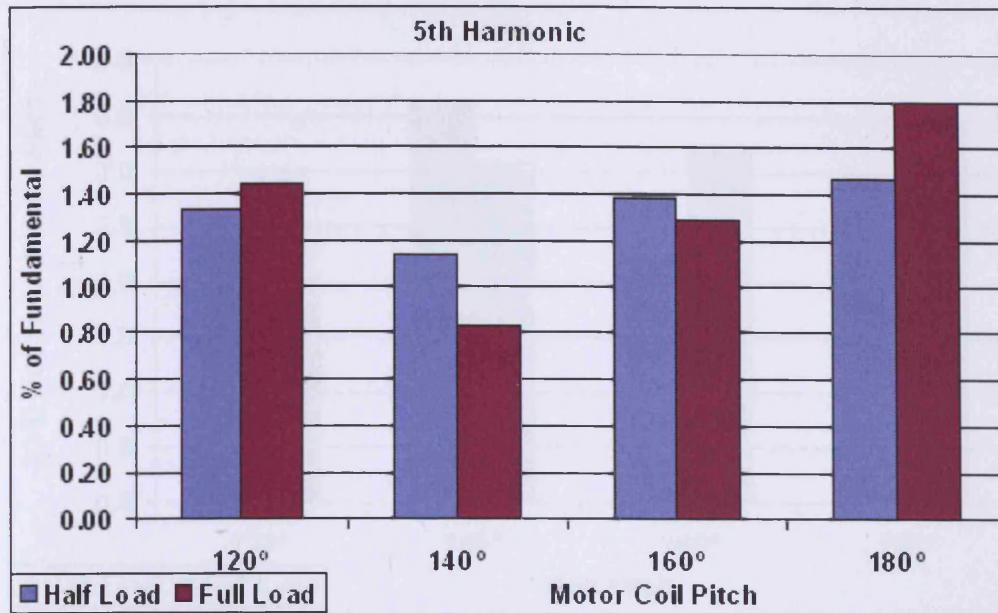
Figure 8.41 Fifth harmonic voltages as percentages of the fundamental voltage for the 120°, 140°, 160° and 180° coil pitch motors at half load and full load under PWM supply voltage at 60 Hz modulation frequency and 4 kHz switching frequency
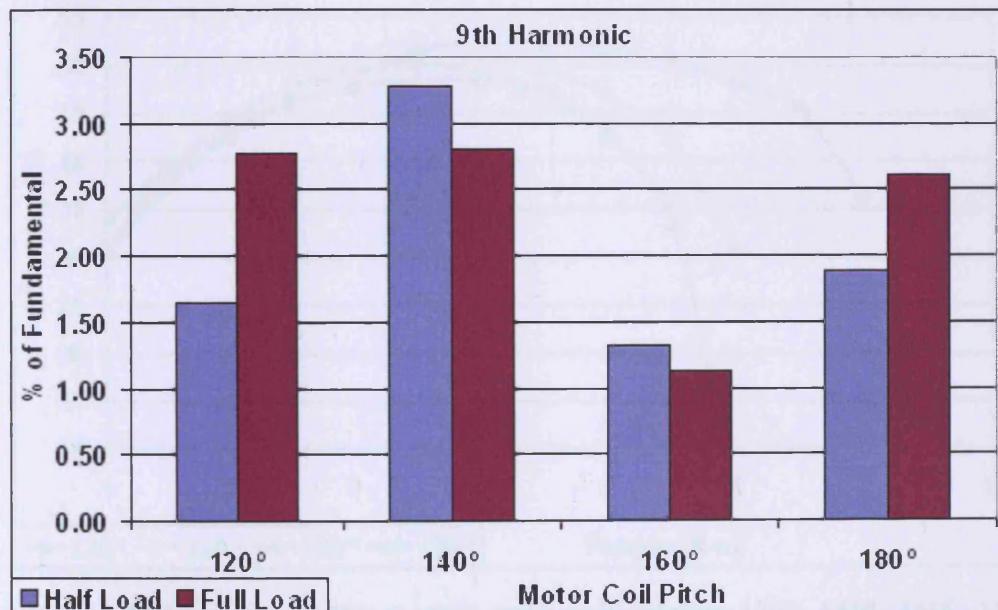

Figure 8.42 Ninth harmonic voltages as percentages of the fundamental voltage for the 120°, 140°, 160° and 180° coil pitch motors at half load and full load under PWM supply voltage at 60 Hz modulation frequency and 4 kHz switching frequency
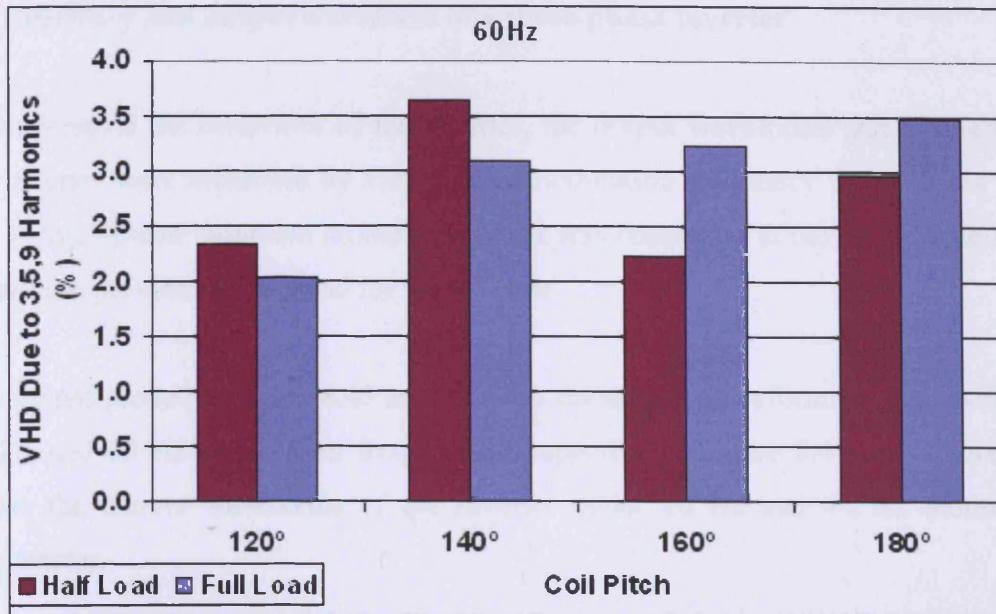
Figure 8.43 Total harmonic distortion voltages due to 3rd, 5th and 9th harmonic voltages as percentages of the fundamental voltage for the 120°, 140°, 160° and 180° coil pitch motors at half load and full load under PWM supply voltage at 60 Hz modulation frequency and 4 kHz switching frequency
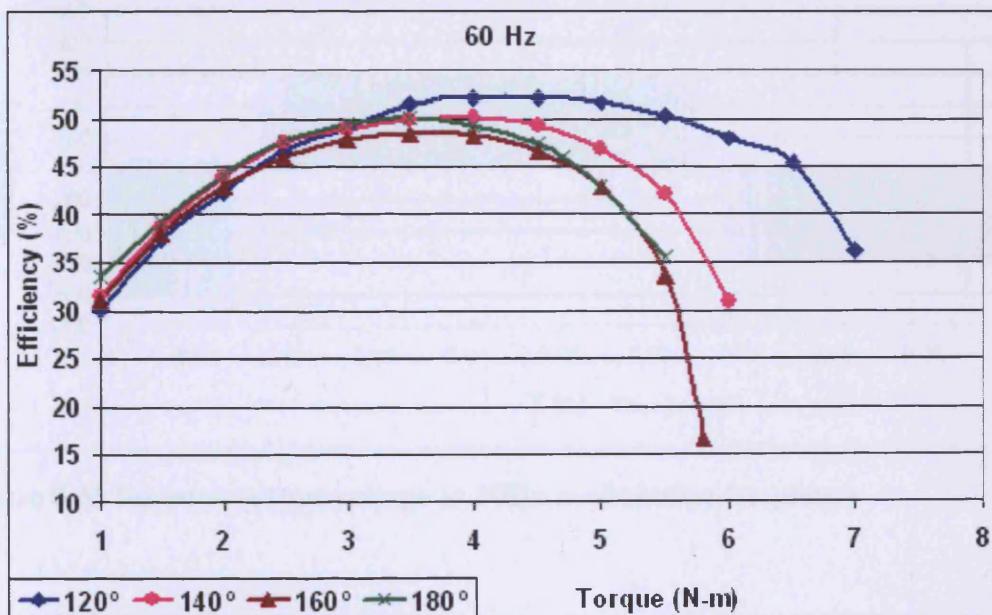

Figure 8.44 Efficiencies of the motors with coil pitches 120°, 140°, 160°, 180° at different torques under PWM supply voltage at 60 Hz modulation frequency and 4 kHz switching frequency

8.7 Efficiency and output waveform of a three-phase inverter

To understand the behaviour of the inverter, the output waveforms and efficiency of the inverter were measured by varying the modulating frequency from 10 Hz to 60 Hz. A three-phase induction motor on no load was connected at the output side of the inverter to provide a small load for the inverter.

The graphs plotted in figure 8.45 and 8.46 are the output waveforms of the inverter at 10 Hz and 60 Hz modulation frequencies respectively. Figure 8.47 and figure 8.48 shows the current waveforms of the inverter under 20 Hz and 40 Hz modulation frequencies.
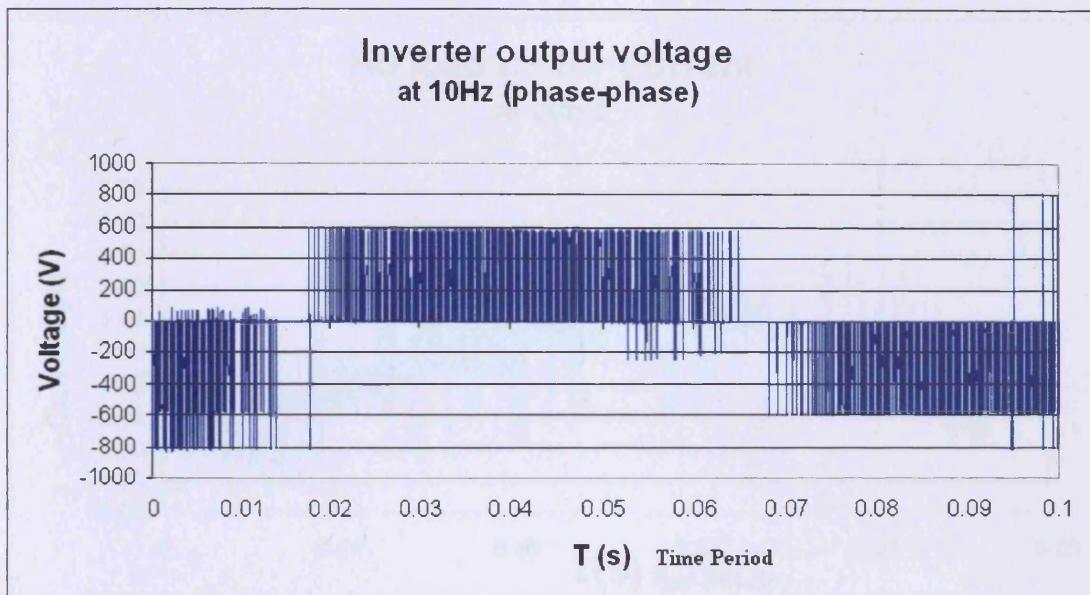
Figure 8.45 Inverter output voltage at 10Hz modulation frequency
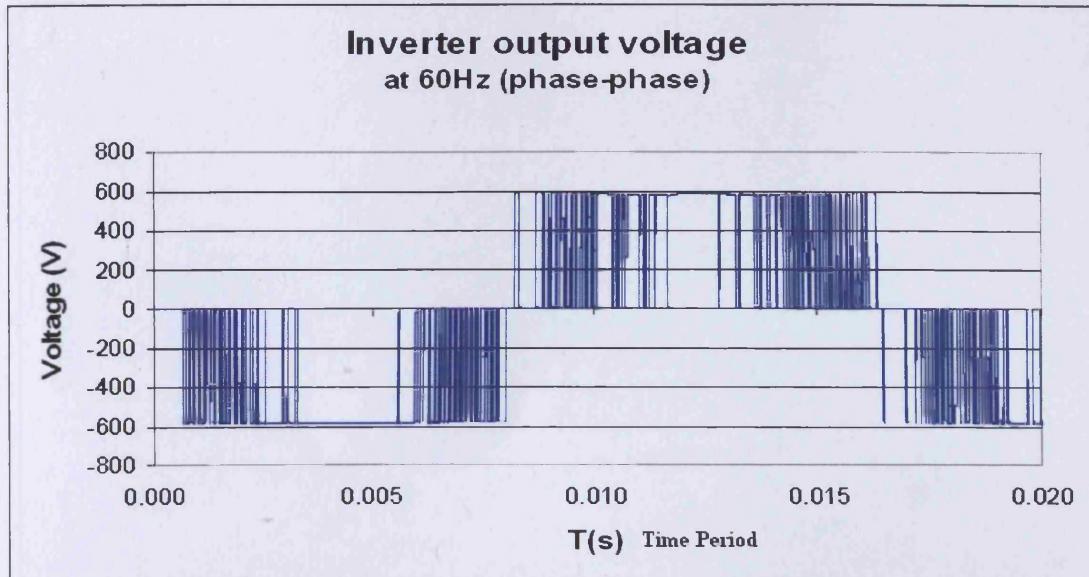
Figure 8.46 Inverter output voltage at 60Hz modulation frequency
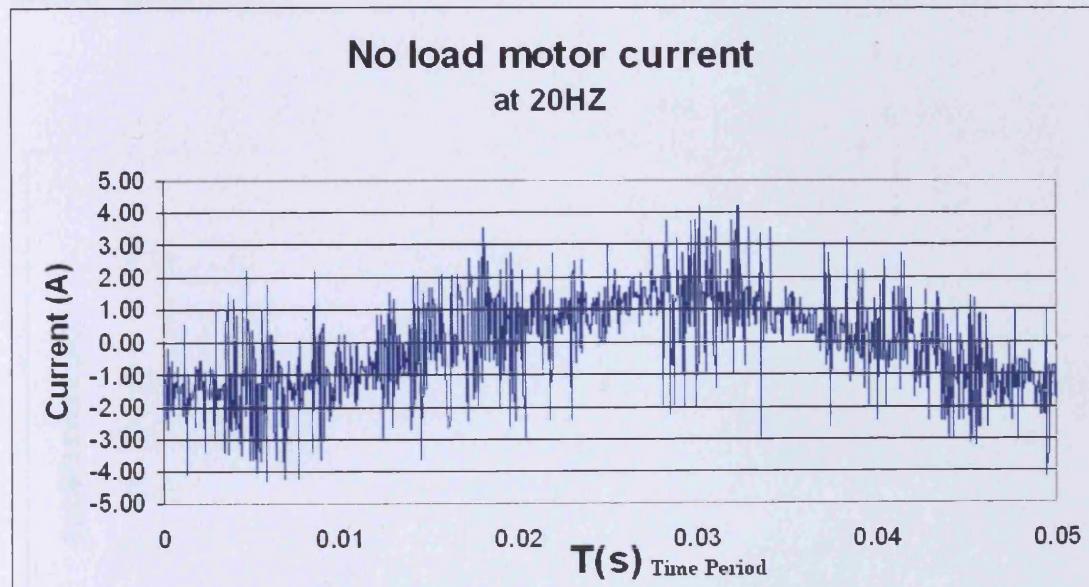
Figure 8.47 Variation of instantaneous no-load motor current at 20Hz over one cycle of magnetisation

No load motor current at 40Hz
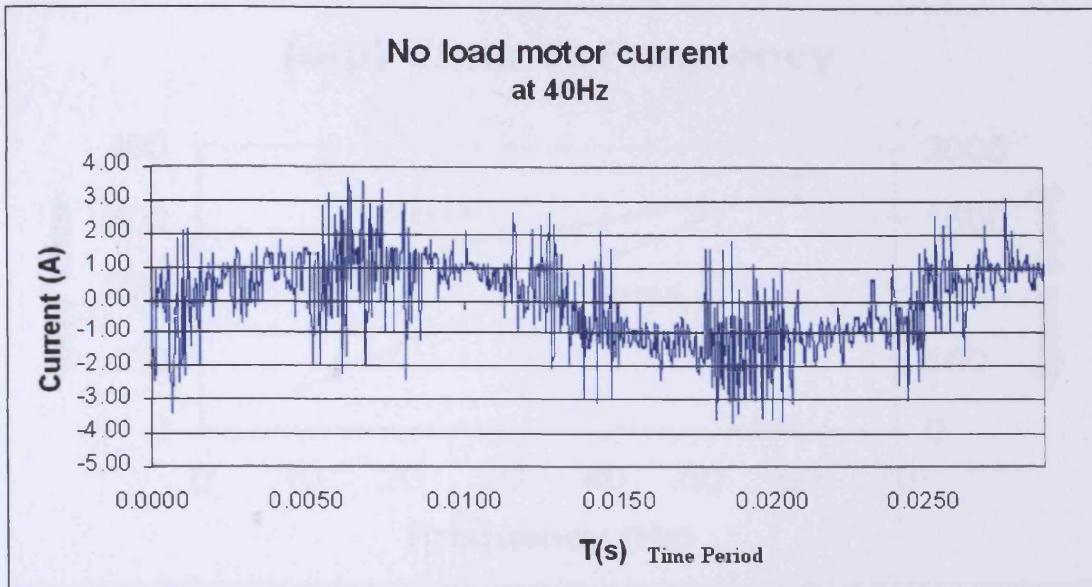
Figure 8.48 Variation of instantaneous no-load motor current at 40Hz over one cycle of magnetisation
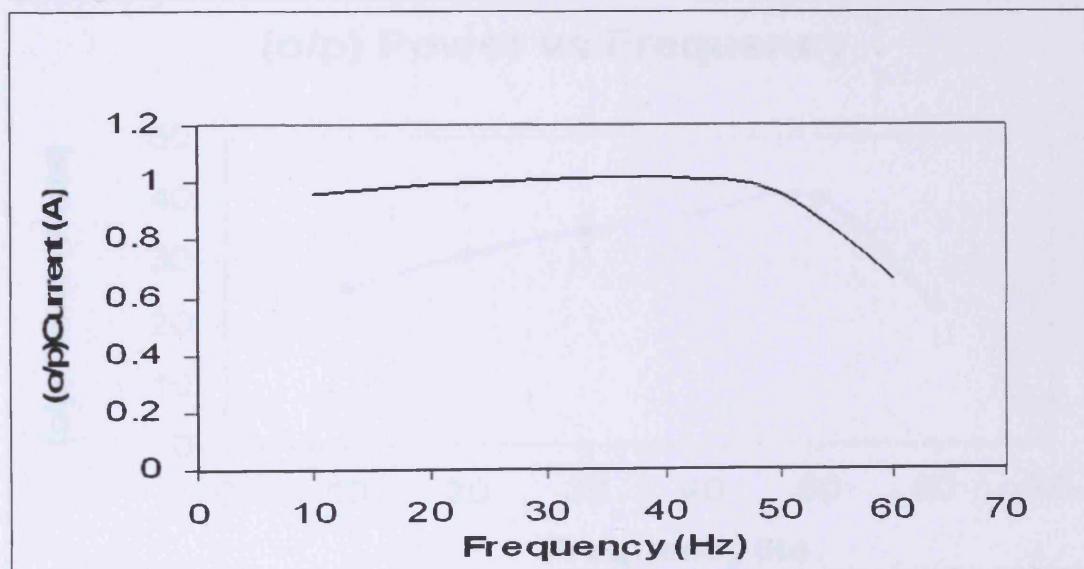
Figure 8.49 Variation of output rms current with fundamental frequency

(o/p) Vrms vs Frequency
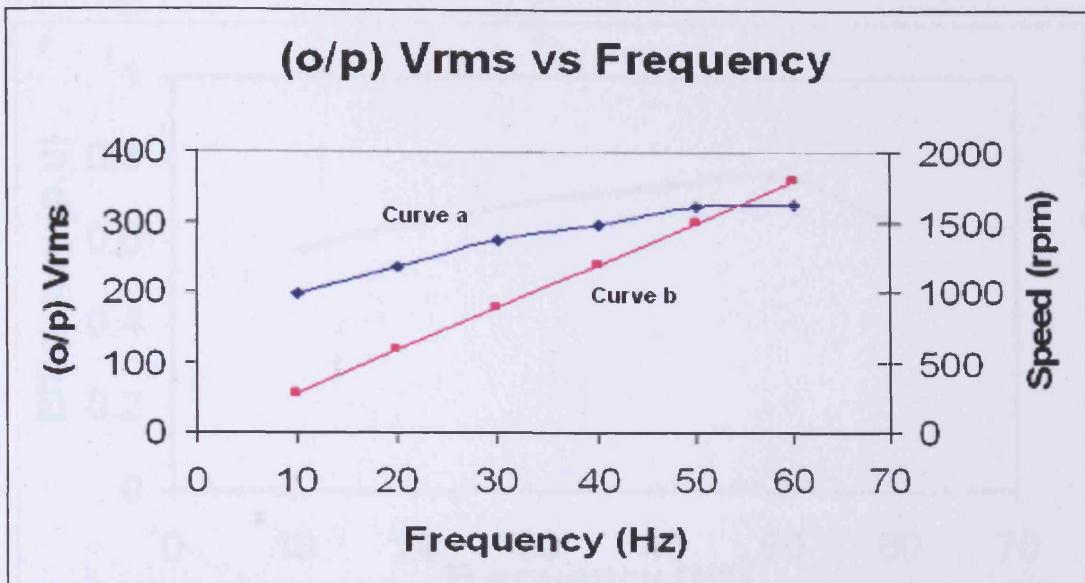
Figure 8.50 Variation of (a) output rms voltage (V) and (b) the speed (rpm) with fundamental frequency

(o/p) Power vs Frequency
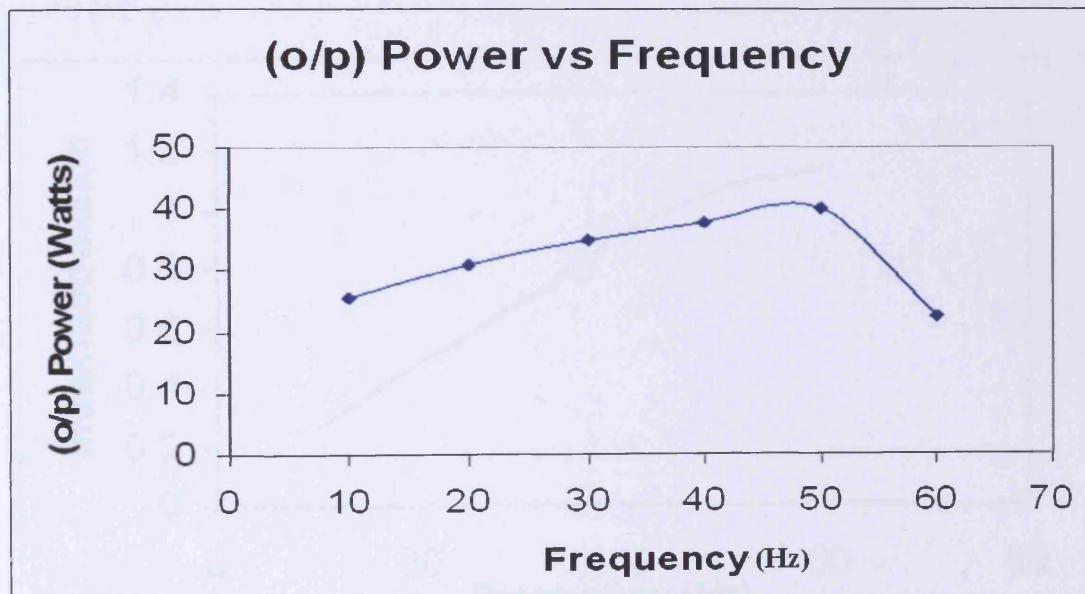
Figure 8.51 Variation of output power of the inverter (motor input power) with fundamental frequency
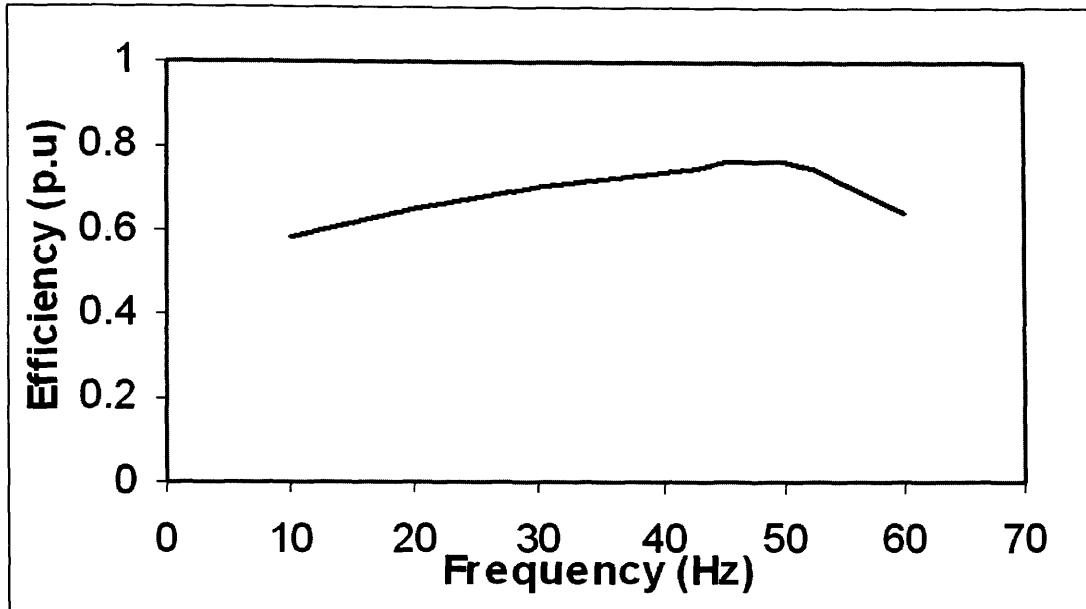
Figure 8.52 Variation of the inverter efficiency with fundamental frequency
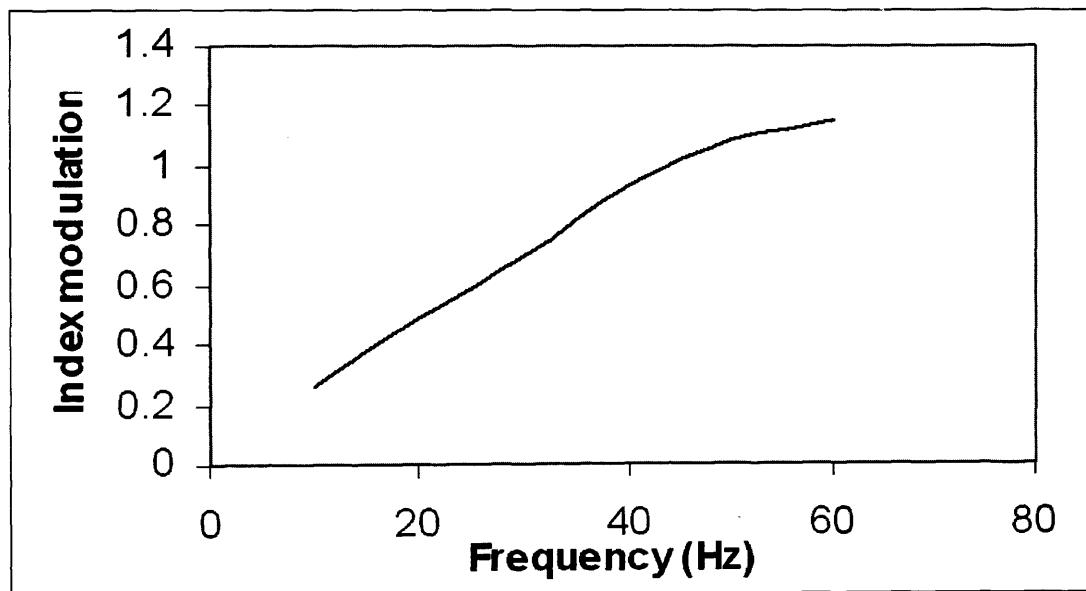
Figure 8.53 Variation of index modulation with fundamental frequency

The analysis and discussion for this chapter is presented in the chapter 9.

CHAPTER 9

DISCUSSION

9.1 General discussion

Most industries use three phase induction motors with inverters to control the speed. The stator winding of these motors are more often full pitched or short pitched to $160°$ for a three-phase induction motor with 36 slots. A short-pitched motor of $160°$ is the classical design for use with a sinusoidal voltage supply. After the introduction of inverters with PWM supplies, there were no steps taken to estimate the dynamic performance of induction motors with short pitching of less than $160°$. Four short pitched, three phase induction motors were tested for lower-order harmonic content, total harmonic distortion factor and efficiency. The results obtained by short pitching these motors shows that the one with $120°$ coil pitch is the most efficient with a PWM voltage supply. An attempt has been made in this chapter to analyse the measurements carried out on four re-wound induction motors supplied with both sinusoidal and PWM voltage sources.

9.2 Sinusoidal voltage supply

All four motors were tested with a sinusoidal voltage supply with varying load conditions. Figure 8.1 shows the third harmonic voltages as a percentage of the fundamental voltage for the $120°$, $140°$, $160°$ and $180°$ coil-pitch motors at half load, full load and overload under a sinusoidal voltage supply. It has been seen, that in the motor with $120°$ coil pitch, the third voltage harmonic is reduced by 23%, 22% and 19% when compared to the full-pitch motor at half load, full load and overload respectively. It can be seen that due to short pitching, this phenomenal increase in the magnitude of voltage harmonic components is much reduced.

Figure 8.2 shows the fifth harmonic voltages as percentages of the fundamental voltage for the 120°, 140°, 160° and 180° coil-pitch motors at half load, full load and overload under a sinusoidal supply voltage. It has been observed that the motor with a coil pitch of 160° has a reduced fifth harmonic component magnitude when compared to the full-pitch motor. This reduction is 13%, 13% and 12% respectively at half load, full load and 20% overload respectively.

It can be observed from the figure 8.3 that for the motor with a 160° coil pitch, the 9th harmonic is reduced by 79%, 69% and 70% respectively when compared to a full-pitch motor. It has also been observed that the 9th harmonic is significantly reduced for the other short-pitched motors and this reduction was found to be 54% and 56% for 140° and 120° coil-pitch motors respectively at full load.

All the above reductions in the harmonic components are due to the short pitching of the motor. It is generally observed that if the motor coil-pitch is reduced by $1/n^{th}$ of the pole pitch then the nth harmonic is suppressed [9.1]. The pole pitch is 180° or 9 slots. So, for the 160° coil-pitch motor the coil pitch is reduced by 20° i.e. reduced by one slot, which is $1/9^{th}$ of the pole pitch, therefore the ninth harmonic should be suppressed. If the motor coil-pitch is reduced by 36° ($1/5^{th}$ of 180°) then the fifth harmonic is expected to be reduced. As a pole pitch has nine slots, then the coil would have to have a span of between seven and eight slots to achieve this condition. This is not possible in current configurations but a coil span of seven was chosen as a coil span of eight was already used as mentioned above. So, a coil span of seven represents a motor with a 140° coil pitch in which the coil pitch has been reduced by 40° i.e. reduced between the $1/4^{th}$ and $1/5^{th}$ of the pole pitch, so the fifth harmonic should be suppressed. In the 120° coil-pitch motor the coil pitch is reduced by 60° i.e. it has a coil span of six and the coil pitch is reduced by $1/3^{rd}$ of the pole pitch, so the third harmonic should be suppressed. The same phenomenon is seen in 120° and 160° coil-pitch motors. However, these reduction phenomena were not observed for the fifth harmonic in the motor with a coil pitch of 140 °.

The total harmonic distortion due to the 3rd, 5th and 9th harmonic voltages, as percentages for the 120°, 140°, 160° and 180° coil-pitch motors at half load, full load and overload under sinusoidal supply voltage can be seen in figure 8.4. Low-order

voltage harmonics have a larger impact on three-phase induction motors than that caused by high-order harmonics [9.2]. Only the third, fifth and ninth harmonic components are taken into account for the total harmonic distortion due to lower order harmonics. This is because of the significant reduction in these (third, fifth and ninth) lower order harmonics due to the short pitching of these motors, particularly following the $1/n^{th}$ rule mentioned above. In this work, experimental motors were designed using this rule. So, the seventh and other harmonic components are not considered whilst estimating the total harmonic distortion due to lower order harmonic components.

It is seen from figure 8.4 that the total harmonic distortion due to lower order harmonics (third, fifth and ninth) is reduced by 1.5%, 3% and 8% at half load, full load and overload for the 120° coil-pitch motor. This reduction is significant for the 160° coil pitch motor and is 11.5%, 12% and 13% at half load, full load and 20% overload respectively.

Figure 9.1 shows the winding layout of all four motors. In this figure **a, b, c** are the three phases and a indicates the current in the positive direction and a' indicates the current flow in the negative direction for phase a. The same is repeated for the phases b and c. It can be seen that for the motor with a 180° coil pitch the upper and lower coils in each slot have the same phase and current directions. However, for the motor with a 160° coil pitch, slot numbers three, six and nine have conductors carrying phases with opposite currents, thus overlapping between adjacent phase bands benefits the air-gap flux patterns by cancelling out the harmonics [9.3]. This overlapping is higher in the motor with 140° coil pitch and higher again in the motor with coil pitch 120°. Hence, there are greater possibilities for harmonic cancellation in motors with 140° and 120° coil pitches.

Slots

			Pole Pitch											Pole Pitch					
1	2	3	4	5	6	7	8	9	10	11	12	13	14	15	16	17	18	19

180°

a	a	a	c'	c'	c'	b	b	b	a'	a'	a'	c	c	c	b'	b'	b'	a
a	a	a	c'	c'	c'	b	b	b	a'	a'	a'	c	c	c	b'	b'	b'	a

160°

a	a	a	c'	c'	c'	b	b	b	a'	a'	a'	c	c	c	b'	b'	b'	a
a	a	c'	c'	c'	b	b	b	a'	a'	a'	c	c	c	b'	b'	b'	a	a

140°

a	a	a	c'	c'	c'	b	b	b	a'	a'	a'	c	c	c	b'	b'	b'	a
a	c'	c'	c'	b	b	b	a'	a'	a'	c	c	c	b'	b'	b'	a	a	a

120°

a	a	a	c'	c'	c'	b	b	b	a'	a'	a'	c	c	c	b'	b'	b'	a
c'	c'	c'	b	b	b	a'	a'	a'	c	c	c	b'	b'	b'	a	a	a	c'
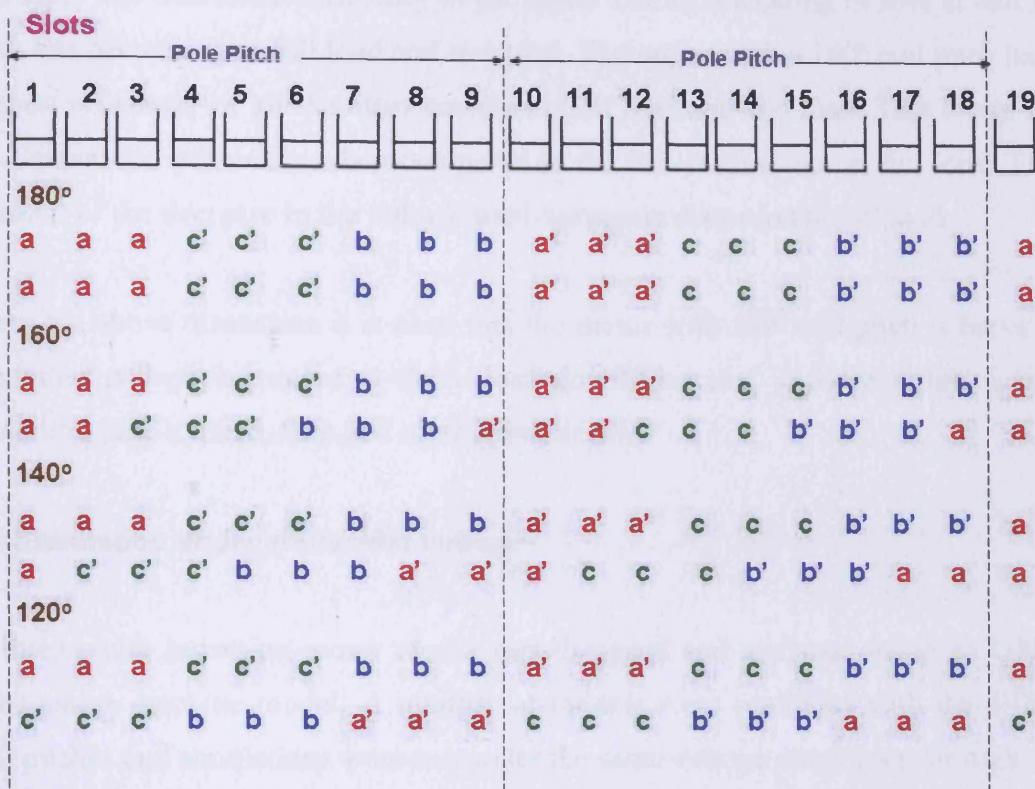
Figure 9.1 Three- phase double layer winding configuration in the stator slots

However, from figure 8.4 for motors with a total harmonic distortion due to the third, fifth and ninth harmonics at different loads, the motor with 160° coil pitch had a lower total harmonic distortion than the other motors under sinusoidal excitation. This was as a result of the boosting of the lower-order harmonics (third, fifth and ninth) due to the overlapping of the MMF wave caused by short pitching of the coil. For example; the boosting of the fifth and ninth harmonics is more than the suppression of the third harmonic in a 120° coil-pitch motor, due to amplitude of harmonic voltage.

The efficiencies of motors with coil pitches of 120°, 140°, 160°, 180° and the motor before rewinding, at different applied torques under a sinusoidal voltage supply, is shown in figure 8.5. The half load, full load and over load were attained at 2.5 N-m, 4.5 N-m and 6.5 N-m torques respectively. The maximum efficiencies of all the motors before and after rewinding were found to be not more than 60%. This is because the motors used in this project are commercially available units purchased from 'off the shelf' and are of 1 HP, which usually have low efficiencies [9.4]. It is clear that the motor with a 120° coil pitch has the lowest efficiency at half load and

full load. The maximum efficiency of the motor before rewinding is 55% at half load, with this decreasing at full load and overload. The motor with a 160° coil pitch has the highest efficiency of all the other motors at half load and full load. This motor has a 5% increase in efficiency when compared to the full-pitch motor at full load. This is because of the decrease in the voltage total-harmonic distortion at full load.

From the above discussion it is clear that the motor with 160° coil pitch is better than the other coil-pitch motors at these load conditions due to lower total harmonic distortion (due to third, fifth and ninth harmonics).

8.3 Simulation under sinusoidal voltage

A three phase induction-motor model was designed and analysed using an OPERA 2D rotating machine model. A number of models were produced with the different coil pitches and simulations were run under the same voltage conditions for each.

It has been seen in simulations that the short pitching does not show its harmonic reduction effect for the motor with a 120° coil pitch as shown in figure 8.6. Rather, it has been seen that the full-pitch motor has the lowest third-harmonic voltage component. The 120° coil-pitch motor third harmonic voltage was increased by 46% when compared with a full-pitch motor.

When the fifth harmonics are compared for the four motors then the motor with 140° has the lowest fifth harmonic as shown in the figure 8.7. This reduction in 140° coil pitch motor is 72% when compared with a full pitch motor.

Figure 8.8 shows the ninth harmonic voltage components for the motor with coil pitch 120°, 140°, 160° and 180° under sinusoidal voltage supply and its seen that the ninth harmonic is suppressed for the motor with coil pitch 160°. This reduction is 65% when compared with the full pitch motor. But interestingly the 120° coil pitch motor's ninth harmonic is increased drastically by 500%. It was concluded that the finite element analysis (OPERA 2D) results does not match the harmonic suppression phenomenon for the 120° coil pitch motor.

If the total harmonic distortion due to third, fifth and ninth voltage harmonics is seen for all the motors from figure 8.9, it is clearly seen that motor with 140° and 160° motor has the lowest values due to short pitching of the stator coils.

When these simulation results are compared with the experimental results the magnitude of the harmonic components differs for all the motors. This is due to the fact that under simulation, pure sinusoidal voltage waveforms are used, whereas in practical experiment the input voltage supply waveform is distorted due to harmonics in the voltage supply.

It is worth nothing that only the pattern of harmonic suppression is compared for simulation and experiment but not the magnitude of harmonic suppression. It has been observed under simulation and experimental results that the motors with 140° and 160° coil pitch have the same harmonic suppression. But the motor with 120° coil pitch doesn't have the same harmonic suppression pattern under simulation and the experimental conditions. It is clearly understood that the motor with 160° coil pitch was the most efficient motor with sinusoidal excitation in the course of simulation and experimentation.

9.4 PWM voltage supply

All four re-wound motors with coil pitch 120°, 140°, 160° and 180° were tested under a PWM voltage supply with 4 kHz switching frequency and 230V voltage supply.

Motors were loaded with various torques; half load, full load and over load were achieved at 2.5 N-m, 5.5 N-m and 6.5 N-m, respectively. The input voltage was 230 V rms. The fundamental voltage components were 206 V, 205 V, 204 V and 203 V rms for 180 °, 160 °, 140 ° and 120° coil pitch motors respectively. So it is clearly seen that as the coil pitch decreases the fundamental voltage component decreases.

Figure 8.10 shows the third harmonic voltages as a percentage of the fundamental voltage for the 120°, 140°, 160° and 180° coil pitch motors at half load, full load and at 20% overload under PWM excitation. It can be seen that third harmonic voltage component is suppressed compared to all the other motors. This reduction is 81%

when compared with the full pitch motor. This reduction is very high when compared with a sinusoidal voltage supply. This is because the amplitude of the third harmonic voltage component in the PWM voltage supply is three times higher when compared to sinusoidal supply for the full pitch motor so there is a higher possibility of suppression in harmonic when short pitched.

It can be seen from figure 8.11 that the fifth voltage harmonic component is suppressed in the motor with 140° coil pitch motor at all loads under PWM excitation. This reduction is 30% when compared with full pitch motor at half load and full load. This reduction was not seen under sinusoidal excitation for the same reason; the amplitude of the fifth voltage harmonic component is higher in PWM voltage supply, which increases the probability of the suppression of higher harmonics.

The motor with 160° coil pitch has the lowest ninth harmonic voltage component when compared with the other motors under PWM excitation at all loads as shown in figure 8.12. This suppression is 12%, 29% and 7% compared to that of the full pitch motor at half load, full load and overload respectively.

When the total voltage harmonic distortion is observed for the third, fifth and ninth voltage harmonic component for all the coil pitch motors it is seen that the motor with 160° coil pitch has the lowest values at the three loads as shown in figure 8.13. This decrease in total voltage harmonic distortion is 5%, 8% and 12% at half load full load and over load respectively when compared with the full pitch motor. It can be seen that that total voltage harmonic distortion due to the third, fifth and ninth harmonic components when supplied with sinusoidal supply is less when compared with PWM voltage supply as the amplitude of the third and ninth harmonics voltage components are less under sinusoidal excitation.

The efficiencies of the four motors can be seen in figure 8.14. The efficiencies of all motors before rewinding at full load were between 49% and 50%. It is very clear that the efficiency of the shortest pitched coil motor (120° coil pitch) is lowest below half load. The efficiency of the shortest pitched motor starts rising from half load and becomes maximum at full load and is highest at full load when compared to all other motors. It is 7.5% and 16% more efficient than the full pitch motor at full load and

overload. The full pitch motor efficiency is lowest of all motors at full load and overload. At overload the shortest pitched motor has the highest efficiency compared to the other motors.

From the above discussion it is very clear that the motor with 120° coil pitch is the best motor which can be used for the PWM voltage supplies at full load and over load.

9.5 Change in switching frequency

The switching frequency of the inverter was varied up to 8 kHz with the modulating frequency being the same as the 50 Hz and measurements were carried out on the four re-wound motors and the load was varied using eddy current brake.

The third voltage harmonic component is reduced by 92%, 84% and 84% when compared with the full pitch motor at half load, full load and 20% of overload respectively as shown in figure 8.15. It can be seen in figure 8.16 that the fifth voltage harmonic component is reduced by 74%, 72% and 73% when compared with the full pitch motor at half load, full load and overload respectively. The ninth voltage harmonic reduction at 8 kHz switching frequency can be seen from figure 8.17. It is reduced by 84%, 81% and 86% when compared with the full pitch motor at half load, full load and overload respectively. The lower voltage harmonic reduction phenomenon is also followed under 8 kHz switching frequency.

The third fifth and ninth voltage harmonics are increased for the full pitch motor at 8 kHz switching frequency when compared to 4 kHz switching frequency. It can be observed that the reduction of the harmonics is increased when compared with the full pitch motor as the switching frequency is increased from 4 kHz to 8 kHz. This is because as the switching frequency increases, the number of pulses increases, hence the amplitude of lower order harmonics rises [9.5] for the full-pitch motor and with short pitching the suppression of harmonics related to the coil pitches (third, fifth and ninth) increases.

The total harmonic distortion voltages due to third fifth and ninth harmonic voltages as percentages for the 120°, 140°, 160° and 180° coil pitch motors at half load, full

load and overload under PWM supply voltage at 8 kHz switching frequency and 50 Hz modulation frequency can be seen from figure 8.18. In all the short pitched motors the total voltage distortion due to the lower-order harmonic is reduced significantly. This reduction when compared to the full pitch motor is as shown in table 9.1.

Reduction in THD (%) when compared to 180° coil pitch motor			
Loads	120° Coil Pitch Motor	140° Coil Pitch Motor	160° Coil Pitch Motor
Half load	68%	64%	66%
Full Load	66%	60%	63%
Overload	68%	64%	67%

Table 9.1 Percentage reduction of the total harmonic distortion voltage due to third, fifth and ninth harmonic distortion of short pitched motors when compared with fully pitched motor at 8 kHz switching frequency and 50 Hz modulation frequency

The 120° coil pitch motor has the lowest total harmonic distortion voltage. This is because of the increase in suppression of the third, fifth and ninth harmonics in the motor 120° coil pitch was more significant when compared with the other short-pitched motors.

The efficiencies of the four motors at 8 kHz switching frequency shows that from minimum load to maximum load range the motor with 120° coil pitch is more efficient than the other motors. The increase in efficiency from half load, full load and overload is 5%, 11% and 19% respectively under 8 kHz switching frequency when compared with the full pitch motor. This increase in the efficiency of 120° coil pitched motor can be easily correlated with the reduction in total voltage harmonic distortion with 8 kHz switching frequency supply. As the short pitching is increased the efficiencies also increased due to the cancellation of the lower order harmonics. The graph also signifies that as the switching frequencies increases the efficiency dependence on lower order harmonics also increases. The increase of the efficiency

of the short-pitched motors when compared with full pitch motor is shown in table 9.2.

Increase in efficiency compared to 180° coil pitch motor			
Loads	120° Coil Pitch Motor	140° Coil Pitch Motor	160° Coil Pitch Motor
Half load	5%	3%	2%
Full Load	11%	9%	9%
Overload	19%	16%	9%

Table 9.2 Increase in efficiency of short pitched motors when compared with the fully pitched motor at 8 kHz switching frequency and 50Hz modulating frequency

All motors were supplied with PWM voltage of 16 kHz switching frequency at 50 Hz modulating frequency. The suppression of third voltage harmonic can be seen in figure 8.20. The motor with 120° coil pitch has the highest third voltage harmonic suppression. This suppression is 85%, 90% and 74% at full load, half load and overload respectively when compared with the full pitch motor. Figure 8.21 shows the reduction of the fifth voltage harmonic and the motor with 140° coil pitch has a higher reduction than the other motors. This reduction is 66%, 55% and 53% at full load, half load and overload respectively when compared to the full pitch motor. Similarly, the motor with 160° coil pitch has the lowest ninth voltage harmonic component and is 86%, 79% and 90% when compared to the fully pitched motor as shown in figure 8.22. Interestingly, the motor with 120° coil pitch followed the lower voltage harmonic component sequence of the fifth and ninth voltage harmonic component of the motor with 140° and 160° coil pitched motor respectively. This reduction is shown in table 9.3.

120° Coil pitch motor voltage harmonic reduction when compared with fully pitched motor		
Loads	5th Harmonic	9th Harmonic
Half load	58%	78%
Full Load	49%	76%
Overload	44%	86%

Table 9.3 Suppression of fifth and ninth voltage harmonic component in the motor with 120° coil pitch motor compared with the fully pitched motor at 16 kHz switching frequency and 50 Hz modulating frequency

The total voltage harmonic distortion due to third fifth and ninth harmonic voltage is shown in figure 8.23. The motor with 120° coil pitch has the lowest total voltage harmonic distortion. This is because the motor with a 120° coil pitch has the lowest third voltage harmonic component and has the additional advantage of possessing the second-lowest fifth and ninth voltage harmonic components following to the motor with 140° and 160° coil pitch respectively. These advantages were not there in the 140° and 160° coil pitch motor. The reduction in the total voltage harmonic distortion for all three short-pitched motor when compared with the full-pitched motor is shown in table 9.4.

Reduction in THD (%) when compared to 180° coil pitch motor			
Loads	120° Coil Pitch Motor	140° Coil Pitch Motor	160° Coil Pitch Motor
Half load	71%	56%	56%
Full Load	70%	50%	47%
Overload	69%	48%	45%

Table 9.4 Reduction in total voltage harmonic distortion due to third, fifth and ninth harmonic for the short pitched motors compared with the fully pitched motor 16 kHz switching frequency and 50 Hz modulation frequency

The efficiencies of the motors with coil pitches 120°, 140°, 160°, 180° and the motor before rewind at different applied torques under PWM supply voltage at 16 kHz switching frequency and 50 Hz modulation frequency is shown in figure 8.24. Again the motor with 120° coil pitch motor has the highest efficiency compared to other motors. This increase in efficiency is more significant when compared with the full pitch motor. The dependence of efficiency on the lower order voltage harmonic is again seen. This increase in efficiency for all the chorded motor when compared with the full-pitched motor can be seen in table 9.5.

Increase in efficiency compared to 180° coil pitch motor			
Loads	120° Coil Pitch Motor	140° Coil Pitch Motor	160° Coil Pitch Motor
Half load	27%	26%	23%
Full Load	12%	10%	8%
Overload	22%	19%	16%

Table 9.5 Increase in efficiency of the short pitched motors compared with the fully pitched motor at 16 kHz switching frequency and 50Hz modulating frequency

The efficiencies of motor with 180° coil pitch and 120° coil pitch motor are shown in figure 9.2. It can be seen that as the switching frequency increases, the overall efficiency at full load decreases. In figure 9.2, the motor with 180° coil pitch at 4 kHz switching frequency has almost the same efficiency as the motor with 120° coil pitch motor under 16 kHz switching frequency at full load. It can be concluded that the same efficiency of a motor can be maintained with increase of switching frequency with chording a motor from 180° to 120°. So the performance of the motor will remain the same at higher switching frequency with chording.

When compared with a 180° coil-pitch motor, an increase in the switching frequency applied to a 120° coil-pitch motor causes less of a decrease in efficiency at full load.

It is also seen that the efficiencies of the motor with 120° coil pitch from full load to over load is almost constant and if the full pitch motor is considered there is a steep fall in the efficiency from full load to over load. So, the motor with 120° coil pitch can be utilised for the over load band under a good efficiency condition.
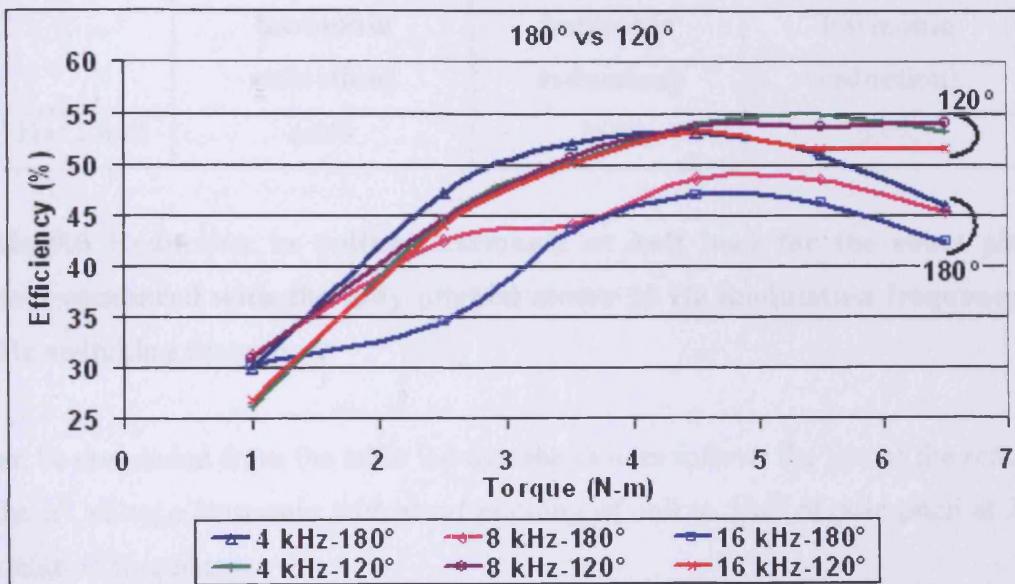
Figure 9.2 Efficiencies of the 180° and 120° coil pitch motor with PWM voltage supply at 4 kHz, 8 kHz and 16 kHz switching frequency and 50 Hz modulating frequency.

8.6 Change in modulation frequency

The modulation frequency of the inverter was set to 30 Hz, 40 Hz, 50 Hz and 60 Hz in a series of test runs. All four motors were tested keeping the switching frequency at 4 kHz, 230 V PWM voltages and the load at the shaft of the motor was varied using an eddy current brake.

Voltage harmonic reduction compared to 180° coil pitch motor			
Load	120° Coil Pitch Motor (Third voltage harmonic reduction)	140° Coil Pitch Motor (Fifth voltage harmonic reduction)	160° Coil Pitch Motor (Ninth voltage harmonic reduction)
Hal Load	65%	36%	53%

Table 9.6 Reduction in voltage harmonic at half load for the short pitched motors compared with the fully pitched motor 30 Hz modulation frequency and 4 kHz switching frequency

It can be concluded from the table 9.6 that the motors follows the law of the reduction of the nth voltage harmonic with short pitching of coil to $1/n^{th}$ of pole pitch at 30 Hz modulation frequency.

Total harmonic distortion voltages due to third, fifth and ninth harmonic voltages as percentages for the 120°, 140°, 160° and 180° coil pitch motors at half load under PWM supply voltage at 30 Hz modulation frequency and 4 kHz switching frequency can be seen from figure 8.28. The 120° coil pitch motor has the lowest total harmonic distortion voltage and was reduced by 51% at half load when compared to the full pitch motor. The harmonic reduction for all the chorded motor when compared to the full pitch motor is as shown in table 9.7.

Reduction in THD (%) when compared to 180° coil pitch motor			
Loads	120° Coil Pitch Motor	140° Coil Pitch Motor	160° Coil Pitch Motor
Half Load	51%	40%	22%

Table 9.7 Reduction in total voltage harmonic distortion due to third, fifth and ninth harmonic for the short pitched motors compared with the fully pitched motor at 30 Hz modulation frequency and 4 kHz switching frequency

The efficiencies of the four motors at different applied torques under PWM supply voltage at 30 Hz modulation frequency and 4 kHz switching frequency are shown in figure 8.29. It can be noticed that at 1 N-m applied torque the efficiency of the motor with the 120° coil pitch is lowest of all the motors. The efficiency then starts to rise from one third of full load and reaches maximum at half load for this motor. The maximum efficiency of the motor is 50% then it maintains nearly constant efficiency till two third of full load and then starts dropping.

The maximum efficiency for the other motors is also below 50%. This is because at 30 Hz modulating frequency the modulation index is 0.6. At this modulation index the voltage output waveform from the inverter is distorted by harmonic components, which increase the motor losses [9.6].

Interestingly, the maximum efficiencies of the four motors occurred nearly at half load and were at 4.5 N-m torque. The maximum efficiencies of all motors are shown in table 9.8. Full load power is not achieved by any motor. This is because at 30 Hz modulation frequency the speed of motor is low and with increase in applied torque the speed drops and reaches the unstable region. The motor with 120° coil pitch has maximum output and was 505 Watts at 7 N-m torque.

120° Coil pitch motor	140° Coil pitch motor	160° Coil pitch motor	180° Coil pitch motor
50%	49%	47%	47%

Table 9.8 Maximum efficiency reached by each motor at 30 Hz modulating frequency

Voltage harmonic reduction compared to 180° coil pitch motor			
Loads	120° Coil Pitch Motor (Third voltage harmonic reduction)	140° Coil Pitch Motor (Fifth voltage harmonic reduction)	160° Coil Pitch Motor (Ninth voltage harmonic reduction)
Half load	38%	38%	26%
Full Load	40%	12%	43%

Table 9.9 Reduction in voltage harmonic at half load for the short pitched motors compared with the fully pitched motor 40 Hz modulation frequency and 4 kHz switching frequency

Table 9.9 shows that the harmonic suppression is followed by all the chorded motor at 40 Hz modulating frequency.

The third and fifth voltage harmonics as percentage of fundamental voltage component for all the motors are decreasing for the 40 Hz modulating frequency compared to the 30 Hz modulating frequency due to reduction in the amplitude of the voltage harmonic components.

The total harmonic distortion voltages due to the third, fifth and ninth harmonic voltages in percentages for the 120°, 140°, 160° and 180° coil pitch motors at half load and full load under PWM supply voltage at 40 Hz modulation frequency and 4 kHz switching frequency is shown in figure 8.33. At this modulating frequency the 160°

coil pitched motor has the lowest total voltage harmonic distortion at half load and the 120° coil pitched motor has the lowest at full load. This reduction is 26% for the 160° coil pitch motor at half load and 30% for the 120° coil pitch motor at full load compared to the full pitch motor.

A similar pattern is followed by the 120° coil pitch motor at 40 Hz modulating frequency for the starting efficiency when compared with the 30 Hz modulating frequency as shown in figure 8.34. However, the maximum efficiency reached in this case by the 120° coil pitched motor is 54% and is 4% increase when compared with maximum efficiency reached by the full pitch motor. This is achieved at 83% of applied full load.

It is again noticed that 120° coil pitched motor has the highest efficiency of the four motors at 40 Hz modulation frequency from three quarter of full load and is maintained up to over load. The maximum efficiency reached by the other motors is shown in the table 9.10. At this modulation frequency the 120° coil pitch motor has reached the full load and over load mark. All the other motors have not reached the full load point. The 140° coil pitched motor, 160° coil pitched and full pitch motor have reached up to the 92%, 84% and 81% of full load respectively and then it goes towards unstable region. This happened because as the chording increases the speed of the motor at constant applied torque increases and the stable operating region increases. It has also been seen that the half load is achieved at 3 N-m torque for all the motors.

120° Coil pitch motor	140° Coil pitch motor	160° Coil pitch motor	180° Coil pitch motor
54%	53%	53%	52%

Table 9.10 Maximum efficiency reached by each motor at 40 Hz modulating frequency

The third harmonic voltage reduction in the 120° coil pitch motor under 50 Hz modulating frequency is shown in figure 8.35. This reduction is 81% at full load when compared to the full pitch motor. Similarly, the fifth harmonic voltage for the 140° coil pitch motor and ninth harmonic voltage reduction for the 160° coil pitch motor can be seen in figure 8.36 and figure 8.37 respectively. This reduction of the fifth harmonic voltage is 30% for the 140° coil pitch motor and the ninth harmonic is 29% for the 160° coil pitch motor. We can see that the reduction phenomenon is successfully continuing for the 50 Hz modulating frequency supply.

The total voltage harmonic distortion due to the third, fifth and ninth voltage harmonics at 50 Hz modulating frequency for the 120°, 140°, 160° and 180° coil pitch motors can be seen in figure 8.38. It can be observed that the 160° coil pitch motor has lowest harmonic distortion than all other motors. This decrease in total voltage harmonic is 5% and 8% compared with the full pitch motor at half load and full load respectively. It has also been seen that when 50 Hz modulation frequency is applied to all four motors, the total voltage harmonic distortion at full load is higher than other modulation frequencies.

The efficiencies of all the motors at 50 Hz modulation frequency and at 4 kHz switching frequency are shown in figure 8.39. The motor with 120° coil pitch motor is not highest until above half load and increases from half load to full load and overload. It is 7.5% higher than the full pitch motor at full load. At over load the shortest pitch motor is the motor with the highest efficiency. The maximum efficiencies reached by all the motor at full load are shown in table 9.11.

120° Coil pitch motor	140° Coil pitch motor	160° Coil pitch motor	180° Coil pitch motor
55%	54%	54.5%	52%

Table 9.11 Maximum efficiency reached by each motor at 50 Hz modulating frequency at full load

Voltage harmonic reduction compared to 180° coil pitch motor			
Loads	120° Coil Pitch Motor (Third voltage harmonic reduction)	140° Coil Pitch Motor (Fifth voltage harmonic reduction)	160° Coil Pitch Motor (Ninth voltage harmonic reduction)
Half load	45%	22%	30%
Full Load	50%	53%	57%

Table 9.12 Reduction in voltage harmonic at half load for the short pitched motors compared with the fully pitched motor 60 Hz modulation frequency and 4 kHz switching frequency

Interestingly, the harmonic suppression at full load is more than at half load for all the motors as show in table 9.12.

The total voltage harmonic suppression due to the third, fifth and ninth voltage harmonic for all the motors at 60 Hz modulating frequency is shown in figure 8.43. It can be observed that the motor with the 120° coil pitch has the lowest total voltage harmonic distortion and is 42% and 22% at full load and half load respectively when compared to the full pitch motor. Again the full load total voltage harmonic distortion is less.

Figure 8.44 shows the efficiencies of all the motors at 60 Hz modulating frequency and 4 kHz switching frequency. This modulating frequency generates over

modulation. It has been observed that half load occurs at 2 N-m torque for all the motors, which is at a much lower applied torque than under the other modulating frequencies. The full load occurs at 4.5 N-m torque. It has been seen again that the stable operating region for the 120° coil pitch motor is highest than any other motor.

The maximum efficiency reached by each motor is given in table 9.13. The efficiency of the 120° coil pitch motor is higher than that of any of the other motors. But these efficiencies are lower than those observed with a 50 Hz modulating frequency. The increase in the efficiency of the 120° coil pitch motor was 13% compared to the full pitch motor at full load under over modulation (60 Hz modulating frequency) where as this increase was 10% under 50 Hz modulation frequency.

120° Coil pitch motor	140° Coil pitch motor	160° Coil pitch motor	180° Coil pitch motor
52.2%	50.2%	48.4%	50%

Table 9.13 Maximum efficiency reached by each motor at 60 Hz modulating frequency

The efficiency of all the motors under over modulation was decreased compared to the 50 Hz modulation frequency. This decrease in efficiency was related to the inverter efficiency and output waveform supplied by inverter to the motor. To understand the effect of the inverter's behaviour on the motor's efficiency, the output waveforms and efficiency of the inverter were studied.

Figure 8.45 and figure 8.46 show the inverter output voltage at 10 Hz and 60 Hz. The number of pulses per cycle at 10 Hz and 60 Hz are 300 and 50 respectively. As the frequency increases, the number of pulses per cycle decreases and disturbances in the voltage waveform decreases. This is because the modulation index increases with increasing frequency and the total harmonic distortion also decreases. Figure 8.46 shows the over modulation case at 60Hz where the pulses are skipped in the waveform.

It can be observed that as the frequency increases the harmonic component in the current waveform decreases as shown in figure 8.47 and 8.48. It is seen from figure 8.47 that at 20 Hz the spikes are greater than 4 Amps and from figure 8.48 that at 40 Hz the spikes are less than 4 Amps. The harmonic components at higher frequencies are less and are affected by the motor behavior. The observed effects also indicate that the magnetic losses of the motor at partial load are more influenced by the harmonic contributions of the inverter current.

Figure 8.49 shows the variation of output rms current with the fundamental frequency when the fundamental frequency was varied from 10 Hz to 60 Hz in steps of 10 Hz. The speed of the motor at no load was also increased as the frequency increased as shown in curve (b) of figure 8.50. It is seen that as the fundamental frequency increases the current remains almost constant up to the rated frequency of the motor, after that it drops. It is well known that the voltage/frequency ratio should be constant to maintain constant current (constant air gap induction) in the motor, but it can be seen in curve (a) of figure 8.50 that the voltage is almost constant in the over modulation region, so as the fundamental frequency increases the inductive reactance increases therefore to maintain constant voltage the current drops. This is the typical behaviour of an asynchronous motor, where the maximum value of the voltage occurs at the nominal frequency. Increasing the frequency, the amplitude of the air gap induction consequently decreases.

Curve (a) of figure 8.50 shows the variation of output PWM rms voltage with fundamental frequency. It is seen that as the fundamental frequency increases the output PWM rms voltage increases almost linearly up to the rated frequency of the motor then it becomes constant due to over modulation. Over modulation (m≥1) causes the output voltage to contain many more side band harmonics than in the linear range (m<1). The harmonics dominant in the linear range are not so prominent during over modulation. More significantly, when over modulated the amplitude of the fundamental frequency component does not vary linearly with amplitude modulation ratio.

Figure 8.51 shows the variation of no load output power of the inverter with fundamental frequency. It can be seen that as the fundamental frequency increases the output power increases up to the rated frequency of the motor then it falls. This is because the iron losses increases in the motor core as the frequency increases up to base frequency (50 Hz) [9.7], so the power required by the motor to cater for this loss increases and the output power of inverter increases. Above the base frequency the iron losses in the motor decrease [9.7], so the power required by the motor decreases, hence the output power of the inverter decreases.

Figure 8.52 shows the variation of the efficiency of the inverter with fundamental frequency. It is seen that as the fundamental frequency increases the efficiency of the inverter increases up to the rated frequency of the motor then it drops because the output power falls when (m>1) as explained above. Obviously, the inverter output is very low compared to its rated value so the efficiency is not representative of normal load conditions. The inverter efficiency varied from 60% to 78% but this was at around 2% of its rated output so a low efficiency is not surprising since the switching losses predominate. Figure 8.53 shows that as the fundamental frequency increases the index modulation also increase linearly up to over modulation then it increases nonlinearly. If the frequency were increased further then the index modulation would tend to become constant.

9.7 Speed torque characteristics

Figure 9.3 to figure 9.6 shows the speed-torque curved of all the motors at 30 Hz, 40 Hz, 50 Hz and 60 Hz modulating frequency at 4 kHz switching frequency.
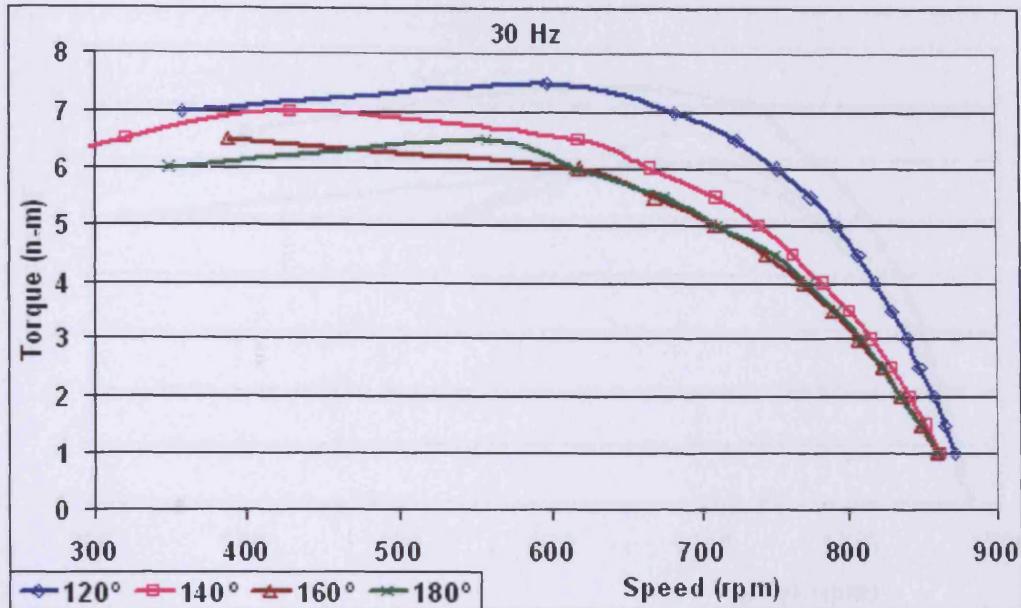
Figure 9.3 Speed torque curves of the motors with coil pitches 120°, 140°, 160°, 180° at different torques under PWM supply voltage at 30 Hz modulation frequency and 4 kHz switching frequency
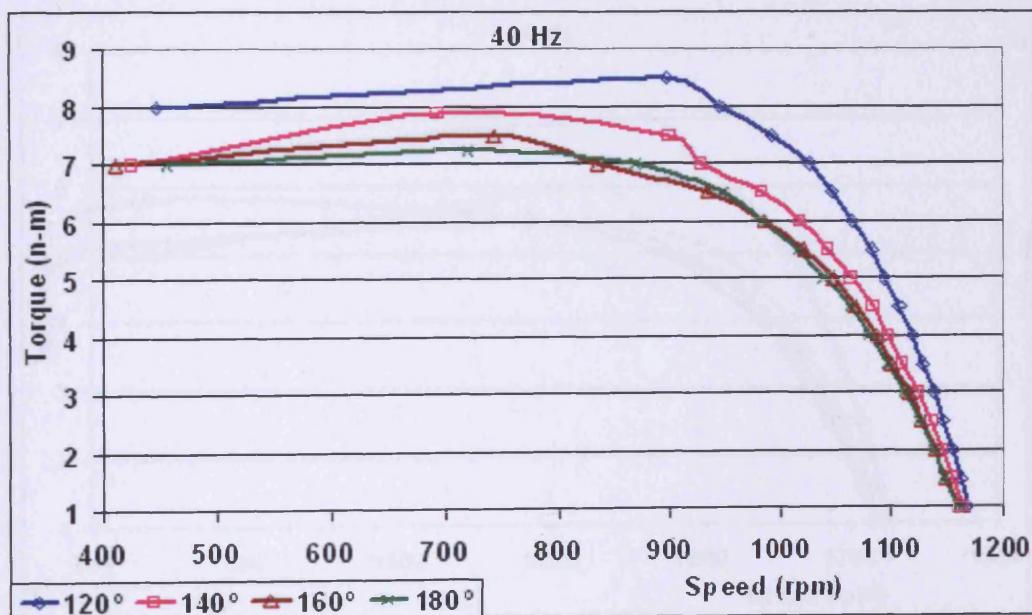
Figure 9.4 Speed torque curves of the motors with coil pitches 120°, 140°, 160°, 180° at different torques under PWM supply voltage at 40 Hz modulation frequency and 4 kHz switching frequency
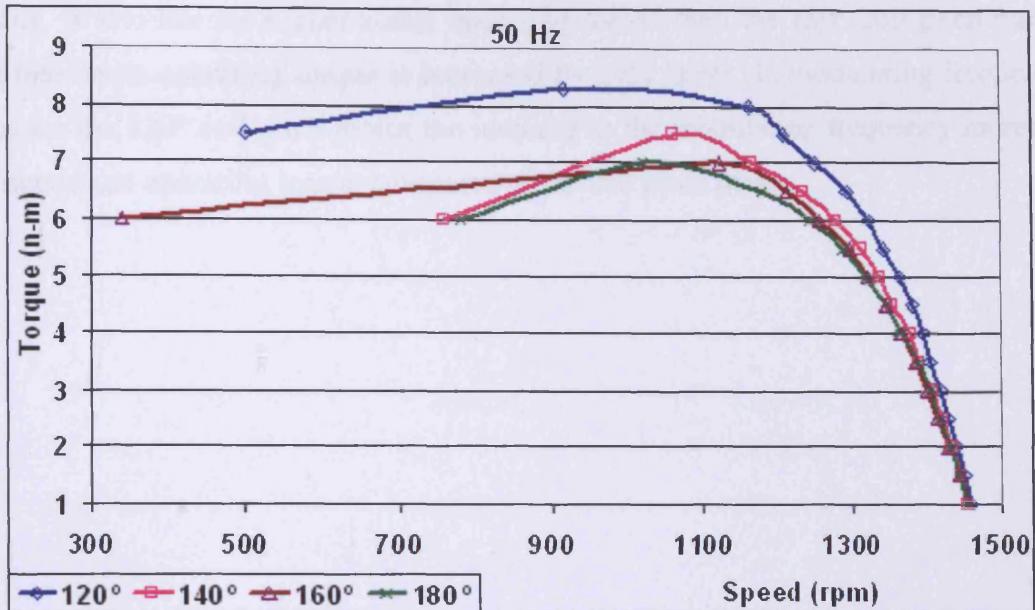
Figure 9.5 Speed torque curves of the motors with coil pitches 120°, 140°, 160°, 180° at different torques under PWM supply voltage at 50 Hz modulation frequency and 4 kHz switching frequency
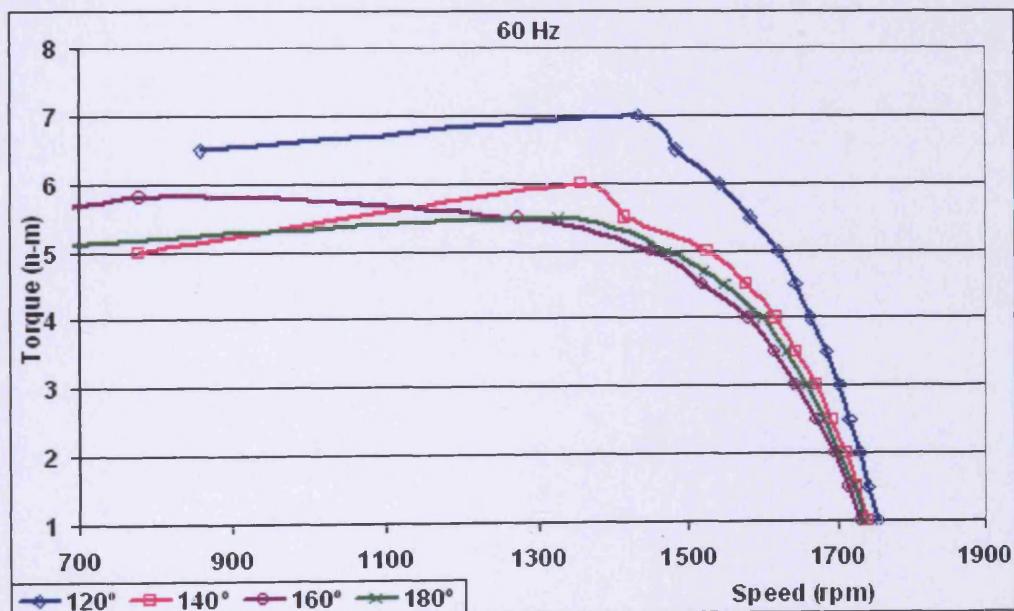

Figure 9.6 Speed torque curves of the motors with coil pitches 120°, 140°, 160°, 180° at different torques under PWM supply voltage at 60 Hz modulation frequency and 4 kHz switching frequency

From the above figures it can be seen that at all the modulating frequencies the motor with 120° has the improved speed-torque characteristics when compared to other

motors. It also has the higher stable operating region than the 180° coil pitch motor. The maximum operating torque is increased by 27% at 60 Hz modulating frequency. Thus for the 120° coil pitch motor the increase in the modulating frequency increases the maximum operating torque compared to the full pitch motor.

REFERENCES FOR CHAPTER 9

[9.1] M. G. Say, "Alternating currents machines", 5th edition, Longman Scientific & Technical Publishers, p.95-98, 1983

[9.2] C.Y. Lee, W.J. Lee, Y.N. Wang, J.C. Gu, "Effect of voltage harmonics on the electrical and mechanical performance of a three-phase induction motor", Industrial and Commercial Power Systems Technical Conference, Atlanta, Canada IEEE p.88-94, 1998.

[9.3] AEMT Good practice guide, "The repair of induction motor", Association of electrical and Mechanical trade Publishers, p.30-33, 1998

[9.4] ABB Catalogue BU/M2BA FI 99-03, 1999.

[9.5] S. Ekram, B. Sarkar, "Effect of harmonics on PWM inverter fed induction machines", Journal of Institute of Engineers, India, pt EL, Vol. 85, p.12, June 2004.

[9.6] Deshmukh R., Moses A.J., Anayi F., Schneider J., 'Efficiency and output waveform of 3-phase inverter driving an a.c. motor at no load', Proc. of Soft Magnetic Materials 16, Stahleisen, Düsseldorf, PP 879-883, 2004.

[9.7] Hodowanec M.M., IEEE Industy Applications Magazine, pp.40-46, 2000

CHAPTER 10

CONCLUSION AND FUTURE WORK

10.1 Conclusion

Low order harmonics in the stator voltage of three-phase induction motors fed by a sinusoidal voltage source can be reduced by short pitching the stator winding. The phenomenon of chording of the stator winding of a three phase induction motor by $1/n^{th}$ of the pole pitch to partially suppress the nth harmonic voltage was followed by all the chorded motors except the 140° coil pitch motor under sinusoidal voltage supply.

This suppression of harmonics due to chording is also followed under PWM voltage supply by all the chorded motors. Particularly, the 120° coil pitch motor follows the above law most significantly by suppressing the third harmonic by 81% at full load. These suppressions are followed by all the chorded motors under the 4 kHz, 8 kHz and 16 kHz switching frequencies and under the 30 Hz, 40 Hz, 50 Hz and 60 Hz modulating frequencies.

The 160° coil pitch motor has the lowest total harmonic distortion (THD) voltage due to the third, fifth and ninth harmonic voltages under sinusoidal voltage supply and under PWM voltage supply at 4 kHz switching frequency. The phenomenon of attenuation of lower-order voltage THD due to chording improves with an increase in switching frequency and so the 120° coil pitch has the lowest THD under 16 kHz switching frequency.

Simulation using OPERA 2D rotating machine model also followed the suppression rule all the short pitched motor except for the 120° coil pitch motor under sinusoidal voltage supply. The 160° coil pitch motor having the lowest THD was agreed by the simulation and experimental results under sinusoidal supply.

The efficiency of the motor depends on the lower order voltage harmonics. The motor with a coil pitch 160° is considered efficient under sinusoidal voltage supply and has 5% increase when compared with fully pitched motor due to reduction of THD. The motor with 120° coil pitch is considered most efficient under PWM voltage supply and the increase is 12% when compared to fully pitch motor at full load.

The same efficiency of a motor can be maintained with increase of switching frequency with chording a motor from 180° to 120°. The 120° coil pitch motor is most efficient at all modulating frequencies. Its efficiency increased by 13% at full load under over modulation and this motor's performance is best under 50 Hz and 40 Hz modulating frequencies.

There is a significant beneficial effect of chording under PWM and sinusoidal supplies for the low-power three-phase induction motors.

10.2 Future work

The present investigation has given rise to the need for obtaining the behavior of the motor with different winding designs other than the one used in this project. The winding design can be changed to one that is over pitched and the effects on the harmonics, the total voltage harmonic distortions and the efficiencies can be assessed.

Similar measurements as mentioned in the present work can be assessed for three phase induction motors with higher power ratings. Consequently, the effects on the motors, such as total iron losses, core losses etc can be studied to give a better understanding of the influence of the coil-pitch winding on the loss distribution.

An investigation of the overall effect of the change in winding design of stator on the efficiency of the total system, which includes motor and inverter, can be carried out.

APPENDIX A

PUBLICATIONS/PRESENTATIONS

- Deshmukh R., Moses A.J., Anayi F., Schneider J., 'Efficiency and output waveform of 3-Phase inverter driving an A.C. motor at no load', Proc. of Soft Magnetic Materials 16, Stahleisen, Düsseldorf, pp. 879-883, 2004.

- Deshmukh R., Moses A.J., Anayi F., 'Voltage Harmonic Variation in Three Phase Induction Motors with Different Coil Pitches', *Journal of Magnetism and Magnetic materials*, Vol. 304, Issue 2, pp. e801-e812. Sep. 2006.
  (Poster presentation in the Soft Magnetic Materials Conference 17, September 2005, Bratislava-Slovakia)

- Deshmukh R., Moses A.J., Anayi F., 'Behaviour of Three-Phase Induction Motor with Variable in Stator Coil Winding Pitch', *Journal of Applied Physics*, Vol. 99, Issue 8, pp. 08R310-08R313, April 2006.
  (Poster presentation in the 50th Magnetism and Magnetic Materials Conference, November 2005, San Jose-USA)

- Deshmukh R., Moses A. J. Anayi. F., 'Improvement in Performance of Short Chorded Three-Phase Induction Motors With Variable in PWM Switching Frequency', *IEEE Transaction on Magnetics,* Vol. 42, Issue 10, pp. 3452-3454, October 2006.
  (Poster presentation in the IEEE International Magnetics Conference, May 2006, San Diego-USA)